The role of the X chromosome in embryonic and postnatal growth

Daniel Mark Snell

A dissertation submitted in partial fulfillment

of the requirements for the degree of

Doctor of Philosophy

of

University College London.

Francis Crick Institute/Medical Research Council National Institute for Medical Research

University College London

January 28, 2018

I, Daniel Mark Snell, confirm that the work presented in this thesis is my own. Where information has been derived from other sources, I confirm that this has been indicated in the work.

Abstract

Women born with only a single X chromosome (XO) have Turner syndrome (TS); and they are invariably of short stature. XO female mice are also small: during embryogenesis, female mice with a paternally-inherited X chromosome (X^PO) are smaller than XX littermates; whereas during early postnatal life, both X^PO and X^MO (maternal) mice are smaller than their XX siblings. Here I look to further understand the genetic bases of these phenotypes, and potentially inform areas of future investigation into TS.

Mouse pre-implantation embryos preferentially silence the X^P via the non-coding RNA *Xist*. X^PO embryos are smaller than XX littermates at embryonic day (E) 10.5, whereas X^MO embryos are not. Two possible hypotheses explain this observation. Inappropriate expression of *Xist* in X^PO embryos may cause transcriptional silencing of the single X chromosome and result in embryos nullizygous for X gene products. Alternatively, there could be imprinted genes on the X chromosome that impact on growth and manifest in growth retarded X^PO embryos. In contrast, during the first three weeks of postnatal development, both X^PO and X^MO mice show a growth deficit when compared with XX littermates. This deficit is not observed in the presence of a second sex chromosome - i.e. in normal XX female mice, or in females with a Y chromosome that lacks *Sry* - suggesting haploinsufficiency of genes with homologues present on, and expressed from, both sex chromosomes as a cause.

In this thesis I have investigated the role of *Xist* in X^PO embryonic growth retardation; and utilised mouse stem cells to perform an *in vitro* screen to identify X-linked imprinted genes. To characterise postnatal haploinsufficiency, I identify four candidate genes and, utilising CRISPR-Cas genome editing, delineate the role of each in the growth deficit phenotype. I further use these X-linked mutants to investigate the functional divergence of the X and Y chromosomes in the context of postnatal survival.

Acknowledgements

"There is nothing like looking, if you want to find something. You certainly usually find something, if you look, but it is not always quite the something you were after."
J.R.R. Tolkien, *The Hobbit*, 1937

Whilst this thesis bears my name, undoubtedly I couldn't have finished it without the generous support, advice and encouragement of many colleagues and friends. Firstly, thanks to my supervisor, James, for agreeing to take a punt on me, probably somewhat unexpectedly, after our initial meeting. I am particularly appreciative of your input during the writing process, during which my ability to construct short, logical, umambiguous sentences has improved immeasurably...

Thanks to the whole Turner lab, past and present, for collectively making it a pleasure to come to work: Andrew, Alex, Ben, Bryony, Charlotte, Elias, Shantha, Taka, and Valdone. I pay particular thanks to Fanny, without whose patient teaching and timely words of encouragement I would not be half the molecular biologist (and person) I am today. I am also grateful to Mahesh for analysing the RNA-seq data, and for helpful discussions regarding data interpretation, and likewise to Jasmin. Many thanks to Oana, who is likely the most conscientious and hard working BSc and MSc project student anyone could ever wish for.

The writing of this thesis has coincided with the lab migration from an old, characterful asylum in Mill Hill to "Sir Paul's Cathedral" in central London. I'd like to thank Kathy and the Niakan lab for providing me space to work during the migration

and beyond. I'm particularly indebted to Sissy for many fascinating, wide-ranging conversations, both scientific and philosophical.

Thanks to the former Developmental Genetics Division for their scientific advise and weekly cake; and in particular to Christophe for motivational words at key times (and for having very slightly less hair than me at all times).

None of the work presented here would have been possible without the support of the Biological Research Facility. In chronological order, thanks to Hannah, Sue, Pete, and Pat for providing excellent husbandry over many years. I'm also majorly indebted to the former Procedural Services Section from Mill Hill: almost without exception, Sophie expertly carried out all of the microinjection work for my projects, as well as tolerating my occasional moans when things didn't go to plan. Thanks must also be extended to Sarah, Marta, Nicolle, and Katharine.

From UCL, I will be forever grateful to (now) Emeritus Professor Gordon Stewart for giving me the opportunity to pursue the slightly different MBPhD academic track during medicine. I appreciate the input of my Thesis Committee, Alex Gould, Vivian Li, and Robin Lovell-Badge; and thanks to both Rosetrees Trust and Medical Research Council for funding my work.

Thanks to my friends - Jack, Lara, Charlie, Ben, and Saba - for showing great understanding when I've either been late or not made it to things because I was in the lab. I can't promise I've quite got the balance right just yet, but I'm making progress. This progress is indisputably the result of the influence of Daria. Thank you for helping me to realise the need to live outside of work, and for encouraging me to do things I never imagined I would a year ago. Thank you for being there, unquestioning; and thank you for tolerating me.

Saving the final, biggest acknowledgment until last, I thank my parents, Liz and Mark, for their unconditional love, support, and understanding; not only during the past four years, but the past 32 years. Here is, undoubtedly, the most expensive book you'll never read. This thesis is dedicated to you both.

Contents

List of Figures

List of Tables

Nomenclature

3C	Chromosome conformation capture
ALL	Acute lymphocytic leukaemia
ARID	AT rich interacting domain
ASF	Advanced sequencing facility
BAC	Bacterial artificial chromosome
BCA	Bicinchoninic acid
bHLH	Basic helix loop helix
BSA	Bovine serum albumin
ccRCC	Clear cell renal cell carcinoma
cDNA	Complimentary DNA
ChIP-seq	Chromatin immunoprecipitation sequencing
CML	Chronic myeloid leukaemia
CpG	Cytosine phosphate guanine
CRISPR	Clustered regularly interspaced short palindromic repeats
CTA	Cancer testis antigen
DAPI	4',6-diamidino-2-phenylindole
DE	Differentially expressed
DGE	Differential gene expression
DMSO	Dimethyl sulphoxide
DTT	Dithiothreitol
dUTP	Dexoyuridine triphosphate

ECL	Enhanced chemiluminescence
EDTA	Ethylenediaminetetraacetic acid
EGFP	Enhanced green fluorescent protein
EPC	Ectoplacental cone
EtOH	Ethanol
ExE	Extraembryonic ectoderm
FACS	Fluorescence activated cell sorting
FDR	False discovery rate
FHM	Follicle holding medium
FISH	Fluorescence *in situ* hybridisation
gDMR	Germline differentially methylayted region
gDNA	Genomic DNA
GO	Gene ontology
Gy	Gray
HCC	Hepatocellular carcinoma
HCV	Hepatitis C virus
HIV	Human immunodeficiency virus
HLA	Human leukocyte antigen
ICM	Inner cell mass
IF	Immunofluorescence
iPSC	Induced pluripotent stem cell
IUGR	Intrauterine growth restriction
iXCI	Imprinted X chromosome inactivation
KEGG	Kyoto encylopaedia of genes and genomes
KS	Kabuki syndrome
KSOM	Potassium supplemented simplex optimised medium
LB	Luria broth
LIF	Leukaemia inhibitory factor
LINE	Long interspersed nuclear element

lncRNA	Long non coding RNA
MA	Methanol:acetic acid
MAPK	Mitogen activated protein kinase
MDS	Multidimensional scaling
MEF	Mouse embryonic fibroblast
Meg	Maternally expressed gene
mEpiLC	Mouse epiblast like cell
mESC	Mouse embryonic stem cell
MHC	Major histocompatibility complex
mRNA	Messenger RNA
MSCI	Meiotic sex chromosome inactivation
mTSC	Mouse trophoblast stem cell
MWD	Mean weighted difference
mXEN	Mouse extraembryonic endoderm
MYA	Million years ago
ORA	Over representation analysis
PAM	Protospacer adjacent motif
PAR	Pseudoautosomal region
PBS	Phosphate buffered saline
PCR	Polymerase chain reaction
PE	Primitive endoderm
Peg	Paternally expressed gene
PGC	Primordial germ cell
PRC	Polycomb repressor complex
qRT-PCR	Quantitative real time polymerase chain reaction
RCC	Renal cell carcinoma
RFLP	Restriction fragment length polymorphism
RIN	RNA integrity number
RIPA	Radioimmunoprecipitation assay

RNA-seq	RNA sequencing
RNAi	RNA interference
RT-PCR	Reverse transcription polymerase chain reaction
rXCI	Random X chromosome inactivation
s-TGC	Sinusoidal trophoblast giant cell
SDS PAGE	Sodium dodecyl sulphate polyacrylamide gel electrophoresis
sgRNA	Small guide RNA
siRNA	Small interfering RNA
SNP	Single nucleotide polymorphism
SPRI	Solid phase reversible immobilisation
SSC	Saline sodium citrate
SWI/SNF	SWItch/sucrose non-fermentable
Syn	Syncytiotrophoblast
t-SNE	T-distributed stochastic neighbour embedding
TAD	Topologically associating domain
TBS-T	Tris-buffered saline Tween
TDF	Testis determining factor
TE	Trophectoderm
TGC	Trophoblast giant cell
TPM	Transcripts per million
TPR	Tetratricopeptide repeat
TS	Turner syndrome
UHC	Unsupervised hierarchical clustering
X^M	Maternally inherited X chromosome
X^P	Paternally inherited X chromosome
XAR	X added region
XCI	X chromosome inactivation
XLID	X linked intellectual disability
XUR	X upregulation

YAR	Y added region

Chapter 1

Introduction

Fundamental differences exist between males and females, encompassing areas including anatomy, physiology, and behaviour. Such differences undoubtedly play a part in the well documented, yet poorly understood, disparity in disease susceptibility between the sexes. Although traditionally attributed to differences in sex hormone levels, recent work has begun to shed more light on the contribution of genetics - and in particular the sex chromosomes - to this sexual dimorphism. This chapter begins with an overview of sex chromosome evolution, before focusing on topics most pertinent to this thesis, including dosage compensation, aneuploidy, and growth.

1.1 Sex

Sexual reproduction - meiotic recombination and the subsequent production and fusion of gametes - is widespread throughout the eukaryotic kingdom. This encompasses all mammals and birds, most reptiles, fish and amphibia, and about 99.9% of flowering plant species (Charlesworth, 2006). Whilst many plant species combine male and female sex organs within individuals as hermaphrodites, most animals have, through the evolution of anisogamy, segregated these organs into different individuals, thus resulting in two sexes (Bachtrog et al., 2014). During development, these sexes must be accurately differentiated. Evolution has resulted in multiple

solutions to this sex determination problem, which can be broadly grouped into environmental and genotypic. Environmental sex determination is exemplified by external stimuli - such as social factors or temperature - determining the sex of the offspring. Such a mechanism has been shown to be favoured over a genetic mechanism when specific environments benefit one sex. Conversely, genetic sex determination is found when the environment is either unpredictable or not varied enough, and is mediated by elements ranging in size from genes through chromosomes to entire genomes (Bachtrog et al., 2014). Mammalian sex determination is a primary example of this mechanism.

1.1.1 Sex determination and the evolution of the mammalian sex chromosomes

Hermann Muller posited the first theory of sex chromosome evolution following observations that at least one gene could be linked to each of the *Drosophila* autosomes but not the Y chromosome (Muller, 1914). He hypothesised that the X and Y chromosomes evolved from an ordinary pair of autosomes. The Y chromosome subsequently accumulated deleterious mutations that, due to a lack of recombination, could not be repaired, leading to the dearth of reported Y linked genes. This was consistent with observations from human genetics: whilst multiple traits were mapped to the X chromosome, everything attributed to the Y was publicly discredited (Stern, 1957). Following the development of karyotyping techniques in the 1950s, a role for the Y chromosome in sex determination was firmly established. It was shown that individuals with only a single X chromosome are phenotypically female (XO; Turner syndrome(TS)), whereas those with an XXY karyotype are male (Klinefelter syndrome, Ford et al., 1959a; Jacobs and Strong, 1959). Ohno built on this work, and that of Muller, in arguing that a spontaneous mutation producing a proto sex determining gene (see section 1.2.1) had arisen on one of the ancestral vertebrate autosomes to create a pair of heteromorphic sex chromosomes (Ohno, 1967). He went on to suggest that a pericentric inversion containing this proto sex determining gene would suppress crossing over between the nascent sex chromo-

somes. The resulting pair of heteromorphic sex chromosomes would in turn cause isolation of the sex specific chromosome, thereby facilitating divergence through either innovation or degeneration.

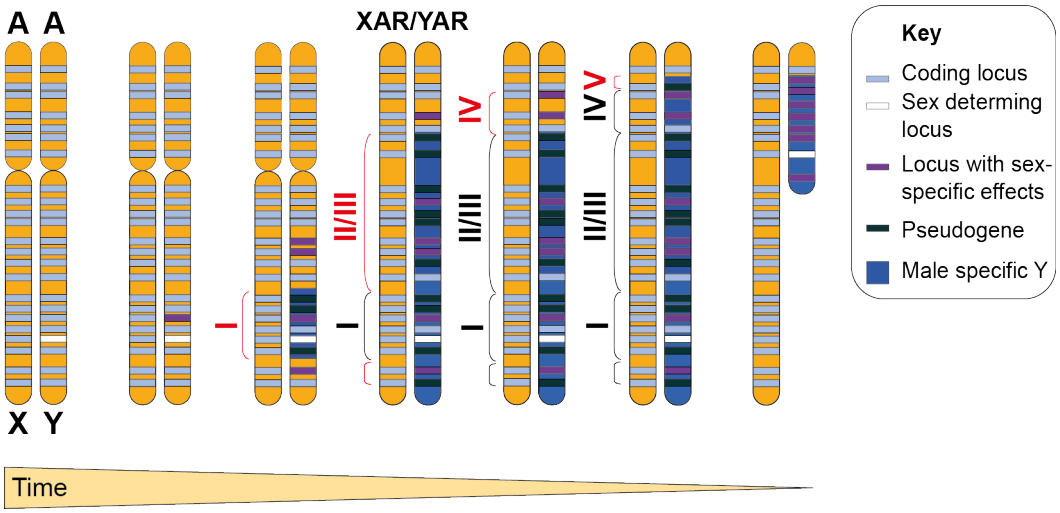

Figure 1.1: Evolution of the mammalian sex chromosomes from autosomes. A sex determining locus (white) was acquired around 180-200 million years ago (mya). Sexually antagonistic alleles (purple) then evolved at nearby loci, selecting for recombination suppression between the X and Y chromosomes, and resulting in the first X chromosome evolutionary stratum (I), and the so called male specific Y. Following the end of recombination in a given region, genes without sex specific benefits often become pseudogenes (dark blue). The appearance and selection for sexually antagonistic alleles, followed by further recombination suppression, then becomes iterative and, as the non recombining region expands, further strata appear (II-V). Between the evolution of strata I and II/III, a fusion event took place between the sex chromosomes and a pair of autosomes, resulting in the expansion of both sex chromosomes in the X added region (XAR) and Y added region (YAR). Over evolutionary time, the lack of recombination leads to the accrual of repetitive DNA sequences and a short term increase in the size of the chromosomes; though this eventually results in large deletions and explains the relatively diminutive size of the Y chromosome in most mammals.

Innovation in sequencing technology provided the first sequences of the human sex chromosomes. These sequences added weight to the theory of a common evolutionary origin, which was based on nucleotide divergence patterns (Lahn and Page, 1999). By comparing nucleotide divergence between Y linked and X linked gene copies, Lahn and Page highlighted a strong correlation with the position of the X linked gene. X-Y gene pairs were shown to be present in at least four groups of increasing divergence, from the short to the long arm of the X chromosome. Thus, the authors posited the existence of distinct evolutionary strata (Lahn and Page,

1999). These strata represent genes isolated by the same recombination event (see Figure 1.1), and are likely the physical evidence for Ohno's inversion hypothesis (Ohno, 1967). Subsequent work supports these conclusions, and further extends the data across eutherians and into metatherians, monotremes, and birds, where similar strata have also be identified (Bellott et al., 2014; Cortez et al., 2014).

1.2 The mammalian Y chromosome

As previously highlighted, the Y mammalian chromosome contains the sex determining gene, and genes that have survived the process of Y degeneration (X degenerate, Bellott and Page, 2009) in the strata identified by X-Y divergence. Additionally, the Y chromosome also harbours genes that have been transposed from the X chromosome later in history, and genes that have become ampliconic (Skaletsky et al., 2003; Bellott et al., 2014; Cortez et al., 2014).

1.2.1 The Testis Determining Factor: *Sry*

Following on from the confirmation that presence of a Y chromosome genetically determines maleness in humans (Ford et al., 1959a; Jacobs and Strong, 1959), the identity of a specific locus was sought. This search for a testis determining factor (*TDF*) utilised sex reversed patients, i.e. XX males and XY females, hoping to isolate the smallest fragment of Y chromosome required for a male phenotype. Sex determining region on the Y chromosome, or *SRY*, was identified first in human and mouse, then shown to be present in a "Noah's Ark" (Gubbay et al., 1990; Sinclair et al., 1990) of mammals. This conservation extends across eutherians, and the sequence is present in therians and prototherians (Cortez et al., 2014), though whether it retains a role in sex determination in these clades remains an open question.

Sry is expressed for a brief period at E11.5 in XY mouse embryonic gonads, preceding the morphological differentiation of the testes (Gubbay et al., 1990). A 14kb transgene containing the *Sry* open reading frame (ORF), along with 8kb of upstream

and 5 kb of downstream sequence, has been shown sufficient to induce testis formation (though not spermatogenesis) in XX mice (Koopman et al., 1991).

1.2.2 Transposed and ampliconic genes

The first resolved examples of ampliconic genes were found on the human Y chromosome, where there are nine multicopy gene families. Two of these families originated on the pre-degenerate Y, and seven have been transposed from autosomes (Skaletsky et al., 2003). More recently, sequencing of the mouse Y chromosome has identified massively ampliconic sequence comprising >95% of the euchromatin and containing three protein coding gene families with significant homology to autosomal genes (Soh et al., 2014). Ampliconic genes on the Y chromosome were originally thought to be important in intrachromosomal recombination and gene conversion to slow degeneration of the Y (Rozen et al., 2003). It was later hypothesised that the high copy number inherent to these ampliconic genes might also facilitate high levels of protein expression, specifically in the testis (Mueller et al., 2013). An alternative explanation cites the presence of the same gene families amplified on the mouse X chromosome (Mueller et al., 2013), and suggests that genomic conflict between the two sex chromosomes during spermatogenesis to increase transmission is the driving force behind amplification (Bachtrog, 2014). The latter hypothesis serves to contradict the hypothesis often popularised in the press that the Y chromosome will lose all protein coding genes within the next 10 million years (Aitken and Graves, 2002).

1.2.3 X degenerate genes

Following the publication of the first complete sequence of the human Y chromosome in 2003 (Skaletsky et al., 2003), it became clear that only around 3% of ancestral genes survived 200 million years of sex chromosome evolution on the human Y, in stark contrast to 98% on the X chromosome (Mueller et al., 2013). This decay has been observed in the sex specific chromosomes across therian mammals.

It is especially true of the mouse Y chromosome, which has fewer ancestral genes than most other mammals studied. Given this extensive loss of genes from mammalian Y chromosomes, are the survivors simply lucky, or do they carry biological importance?

The evolutionary significance of the X degenerate genes lies in their convergent survival and longevity across not only primates (Hughes et al., 2005, 2010, 2012), but also eutherians and the wider therian subclass (Bellott et al., 2014; Cortez et al., 2014). This convergent survival is exemplified by *KDM5D* and *UBE1Y*. The stratum containing both genes evolved independently in eutherian and metatherian lineages, containing a combined 184 shared genes. The former lineage has retained three Y linked genes, and in the latter nine survived on the Y chromosome. Remarkably, *KDM5D* and *UBE1Y* are still present in both lineages, an event unlikely to happen under the assumption of random genetic decay (Bellott et al., 2014).

1.3 The mammalian X chromosome

Ohno (1967) hypothesised that dosage compensation keeps the X chromosome constant in terms of gene content. This prediction was initially borne out by sequencing data, as high conservation was noted within eutherians at the gene level (Carver and Stubbs, 1997; Ross et al., 2005), and fewer interchromosomal translocations were uncovered than on the mammalian autosomes (Carver and Stubbs, 1997). Changes have, however, undoubtedly taken place. The rate of global X chromosome expression adjusted quickly during early sex chromosome evolution, perhaps in order to enact faster functional adaptation (Brawand et al., 2011). Moreover, events such as translocations from the pseudoautosomal region (PAR, see section 1.3.2) to the autosomes in mouse have served to reshape the gene content of the X chromosome towards enrichment for specific physiological functions (Palmer et al., 1997; Carver and Stubbs, 1997; Rugarli et al., 1995).

1.3.1 Sexual antagonism drives X chromosome evolution

The X chromosome spends two thirds of its time in females, and one third in males (Fisher, 1931; Rice, 1984). Therefore if a mutation arises with significant fitness effect on heterozygous carriers that benefits females and is deleterious in males, it will be subject to positive selection more often than negative selection, and will increase in frequency. A recessive, or partially recessive, mutation that is beneficial to males and deleterious to females can spread by virtue of positive selection in male carriers, and masking in female carriers (Vicoso and Charlesworth, 2006). These theoretical examples of sexual antagonism explain the accumulation of either male or female biased genes on the X chromosome relative to the autosomes, via processes such as retrotransposition and gene duplication.

Reverse transcription and integration via a mature mRNA intermediate - retrotransposition - has generated and recruited a disproportionately high number of functional genes from and to the X chromosome relative to the autosomes (Emerson et al., 2004). A significant number of X to autosome transposition events involved genes with testis biased expression (Emerson et al., 2004). This bias has been explained by both mutational bias and natural selection for expression in germ cells, possibly resulting from need to maintain gene expression during meiotic sex chromosome inactivation (MSCI, Turner, 2007).

A further driver of enrichment for testis biased genes has been noted in the form of gene duplication events on the X chromosome. Duplication of existing genes has created vast swathes of ampliconic sequence which, in human, often take the form of cancer testis antigens (CTAs, Warburton et al., 2004). CTA genes exist in families that have expanded independently in both primate and rodent lineages, in a somewhat similar manner to the expansion of ampliconic sequence on the mammalian Y chromosome (Chomez et al., 2001; Birtle et al., 2005; Ross et al., 2005). They are usually expressed only in male germ cells, but also aberrantly in certain cancers (Simpson et al., 2005).

In addition to enrichment for genes expressed in testis, the human and mouse X chromosomes show over representation of genes expressed in brain; and a correlation has been reported between patterns of X linked gene expression in these two tissues (Guo et al., 2003, 2005). It has been suggested that this relates to females selecting more intelligent males (Zechner et al., 2001). A more likely explanation puts forward that genes involved in cognition and fertility are especially important in the evolution of mammals, and are therefore more likely to experience positive selection (Vicoso and Charlesworth, 2006). Finally, the X chromosome also shows specific enrichment for genes expressed in the ovary (Khil et al., 2004), and the placenta (Hemberger, 2002).

1.3.2 Pseudoautosomal region (PAR)

The PAR is the only region of continuous sequence homology between the two heteromorphic mammalian sex chromosomes, where evolutionary divergence has not taken hold. This conservation enables pairing, synapsis, and recombination during meiosis (Koller and Darlington, 1934; Moses et al., 1975; Solari, 1974), as also takes place on the autosomes, hence the derivation of the name PAR (Burgoyne, 1982). The state of diploidy with reference to loci located within the PAR also means that there is no requirement for dosage compensation by XCI (Ellis and Goodfellow, 1989; Ross et al., 2005). The PAR is, therefore, also subject to the effects of aneuploidy (see section 1.5).

As all eutherian pseudoautosomal genes are autosomal in metatherians, it is thought that the PAR evolved following a large autosome to sex chromosome translocation between 80 and 130 MYA (Park et al., 2005; Waters et al., 2007). PAR evolution has since proceeded at significantly different rates in mammalian species. Humans are the only known eutherian species to have two PARs, with 25 genes annotated in PAR1 and four genes in PAR2 (Hughes et al., 2012). In the mouse PAR, which shares very little homology with either human PAR, there are five known protein coding genes (Mueller et al., 2013; Bellott et al., 2014).

1.4 Dosage compensation

Both Muller (1964) and Ohno (1967) predicted that the evolution of a heterogametic sex would require a system of dosage compensation to avoid the "...great peril..." of hemizygous gene expression: effectively a form of natural aneuploidy, the negative impact of disrupted chromosome balance has long been noted (see 1.5). The appearance across multiple species of efficient and stable mechanisms to relieve this situation attests to its significance (reviewed by Disteche, 2012). Two distinct aims of dosage compensation have been identified: i) to balance sex chromosome gene expression with that of the autosomes; and ii) to balance sex linked gene expression between the homogametic and heterogametic sexes. Ohno hypothesised that this could be achieved by two fold transcriptional upregulation of the X chromosome in males, X chromosome upregulation (XUR). However, this would leave females expressing X linked genes at twice the level of autosomal genes. Therefore a further step is the inactivation of one X chromosome in the homogametic sex - XCI (Figure 1.2).

1.4.1 X upregulation(XUR)

Initial evidence for XUR in mouse was limited to one gene, *Clcn4-2* (Adler et al., 1997), before a the appearance of more data produced by microarray in the mid 2000s (Nguyen and Disteche, 2006; Gupta et al., 2006). Assays across several tissues in multiple species supported increased expression of X linked genes relative to autosomal genes, thus resulting in an X:autosome expression ratio of 0.8-1.0. RNA sequencing (RNA-seq) analyses then appeared to contradict the previous data, with X:autosome expression ratios of 0.5 (Xiong et al., 2010), and subsequent work has seen the balance of evidence constantly shift. What has become clear is that the parameters surrounding the analysis, particularly normalisation, play a significant part in the outcome. Even expression levels between different autosomes can vary substantially (Castagné et al., 2011). A number of ways around this problem have been suggested. X:autosome expression ratios were shown to increase following

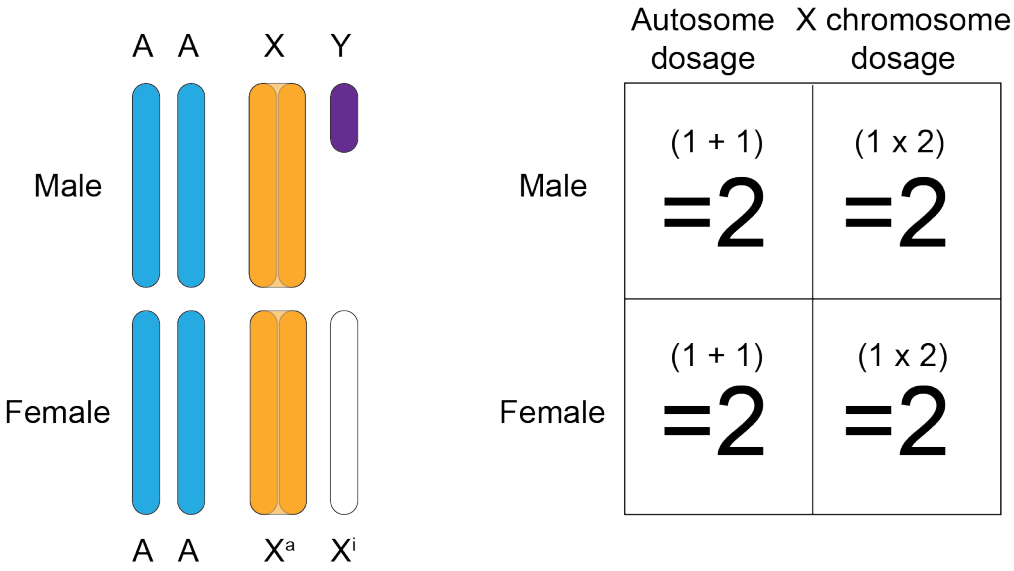

Figure 1.2: The theory of dosage compensation in eutherian mammals. (i) To balance gene dosage between the autosomes (A) and sex chromosomes, eutherian mammals upregulate gene expression from one X chromosome (X in males and X^a in females). This is depicted in the figure as increased size of the X chromosome relative to the autosomes. X upregulation in females leads to excess X chromosome gene expression relative to males. To balance X chromosome gene expression between males and females, one X chromosome is transcriptionally silenced in females by X chromosome inactivation (X^i). The inactivated chromosome is depicted as a white chromosome. (ii) Dosage compensation in numbers. The gene expression from a single autosome is arbitrarily represented as 1.

the exclusion of low/non expressed testis specific genes (Deng et al., 2011). Furthermore, when certain idiosyncracies of the X chromosome are accounted for - such as treating multi copy gene families differently to single copy genes - evidence for XUR in multiple tissues mounts (Sangrithi et al., 2017; Jue et al., 2013). Alternative approaches have also been trialled. Two recent studies compared expression of conserved ancestral genes on the mammalian X chromosome to the expression of autosomal orthologues in species where the sex chromosomes diverged before the origin of the X, i.e. chicken (Julien et al., 2012; Lin et al., 2012a). Although inter species comparisons are complicated by different levels of reference sequence annotation, neither of these studies found evidence for chromosome wide XUR. However, Lin and colleagues did find evidence to support a refinement to Ohno's hypothesis (Lin et al., 2012a). Along with a second study (Pessia et al., 2012), each provides transcriptomic and proteomic data showing upregulation of X linked

genes encoding the members of multi protein complexes. Additionally, comparing X linked genes to autosomal orthologues in divergent species has revealed a downregulation of autosomal genes whose protein products interact with those from X linked genes (Julien et al., 2012). Taken together, these data suggest that XUR, and possibly autosomal downregulation, are important for specific dosage sensitive genes where the stoichiometry of protein products involved in macromolecular complexes affects function, as reviewed by Veitia (Veitia and Birchler, 2010). Whether or not this equalising of X:autosome gene products was sufficient to drive the evolution of equalisation between XX females and XY males through XCI remains to be shown.

1.4.2 X chromosome inactivation (XCI)

XCI balances sex chromosome dosage between XX females and XY males in mammals via transcriptional inactivation of one X chromosome in the homogametic sex. The first cytological evidence was presented by Barr and Bertram (1949), whereby they observed nucleolar satellites in female but not male cat motor neurons. Ohno & Hauschka suggested that these satellites were heteropyknotic X chromosomes (Ohno and Hauschka, 1960), and Lyon was able to show that such a heteropyknotic X chromosome could be inherited from either parent, and was transcriptionally silent (Lyon, 1961). She went on to posit that the random inactivation of one of two different X linked coat colour alleles in each cell would result in the tortoishell coat of the cat, and thus began a field of research that has matured to become a fundamental paradigm in epigenetics.

XCI is mediated by the long non-coding RNA (lncRNA) *Xist* in eutherian mammals (Brown et al., 1991; Borsani et al., 1991; Brockdorff et al., 1991), and *Rsx* in metatherians (Grant et al., 2012). Following transcriptional upregulation of *Xist* from the future inactive X chromosome, a series of events takes place to ensure that the subsequent transcriptional silencing is locked in and stably transmitted to future cell progeny. *Xist* RNA coats the chromosome in *cis*, leading to the creation of an

inactive domain containing silenced genes, and excluding RNA polymerase II and transcription factors (Okamoto et al., 2005). Following the removal of active histone marks, PRC 1 and 2 are recruited (Silva et al., 2003; Schoeftner et al., 2006; Tavares et al., 2012), possibly via the repA domain in *Xist* (Wutz et al., 2002; Zhao et al., 2008), to add repressive marks such as H3K27me3 to histone tails (Plath et al., 2003; Okamoto et al., 2004). Finally, replication timing of the entire chromosome during mitosis changes relative to the rest of the nucleus (Takagi et al., 1982; Sugawara et al., 1983), and methylation of CpG islands situated at the 5' end of genes on the inactive X chromosome functions to stably maintain the inactive state (Norris et al., 1991; Pfeifer et al., 1990a,b).

In the mouse, *Xist* is first expressed from the paternally inherited X chromosome (X^P) at approximately the four cell stage (Okamoto et al., 2004, 2005). This imprinted XCI (iXCI) is maintained across the whole embryo until the first lineage specifications take place. It continues in the trophectoderm (Takagi and Sasaki, 1975; Mak et al., 2004), which goes on to contribute to the placenta, and in the primitive endoderm (PE) (Takagi and Sasaki, 1975; West et al., 1977). In the epiblast of the inner cell mass (ICM), *Xist* is downregulated. This downregulation results in a transient two active X state, followed by *Xist* mediated inactivation of either X^M or X^P (Takagi et al., 1982; Rastan, 1982): random XCI (rXCI). Both of these are now described in more detail and summarised in Figure 1.3.

1.4.2.1 Imprinted XCI

Imprinted inactivation, i.e. inactivation in a parent of origin dependent manner, of the X^p is found in all tissues of metatherian mammals (Sharman, 1971; Cooper et al., 1971; Richardson et al., 1971), and the extraembryonic tissue of some eutherians, i.e. mice (Takagi and Sasaki, 1975).

iXCI is necessary for embryonic survival in mouse. X^MX^P*Xist*- female embryos show transcriptional activity from both X chromosomes in the early embryo (Borensztein et al., 2017) and in trophoblast, become severely growth retarded from E6.5,

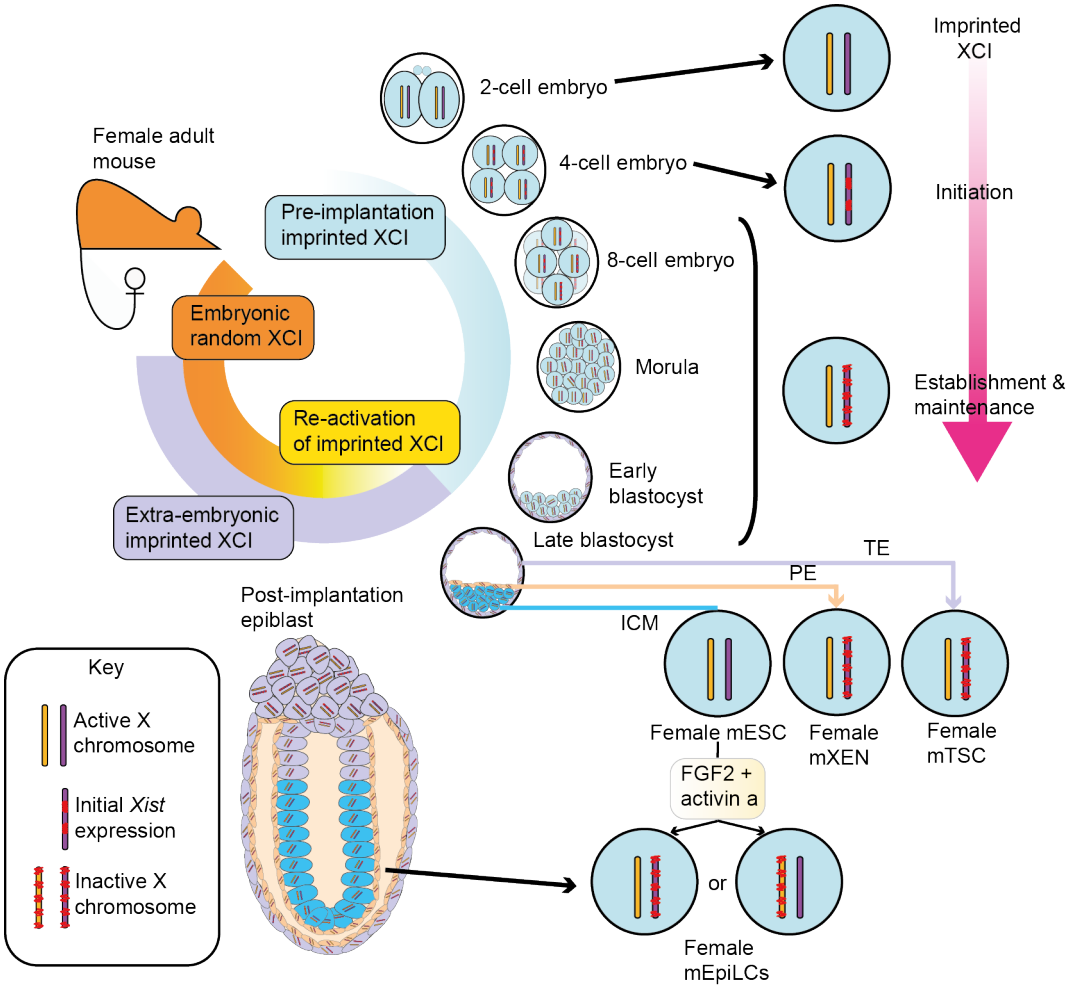

Figure 1.3: X chromosome inactivation in the mouse. From top, XCI is initiated in the XX female embryo at the 4 cell stage by expression of *Xist* (in red) from the paternally inherited X chromosome (X^p, purple). *Xist* RNA spreads to coat the X^p by the 8-16 cell stage which, with subsequent modifications, establishes XCI. The X^p remains inactivated until lineage specification takes place, concurrent with blastocyst formation. In the part of the inner cell mass (ICM) that goes on to form the embryo proper, the epiblast, *Xist* is downregulated, and this is followed by the process of random XCI, which is passed through to the adult mouse. In the primitive endoderm (PE) and the trophectoderm (TE), which contribute largely to the extraembryonic tissue, XCI is maintained on the X^p. Each of these lineages gives rise to a population of stem cells that can be used as *in vitro* models with different XCI states: mouse embryonic stem cells (mESCs) represent the preimplantation ICM, and have two active X chromosomes; and mouse trophoblast stem cells (mTSCs) and extraembryonic endoderm stem cells (mXENs) are derived from the TE and and PE respectively, and both show imprinted XCI of the X^p. mESCs can be used to derive cells representative of the post implantation epiblast, epiblast like cells (mEpiLCs), which have randomly inactivated one X chromosome. This process of differentiation can be used to model rXCI *in vitro*

.

and die before E12.5 (Marahrens et al., 1997). This phenotype is similar to that shown by PRC protein EED deficient embryos (Wang et al., 2001a), implicating a role for histone modifications in iXCI in the extraembryonic tissue. Extraembryonic tissue is known to show reduced methylation (Manes and Menzel, 1981; Rossant et al., 1986). This has been correlated with incomplete silencing of the inactive X *in vivo*, as assayed via either endogenous (Patrat et al., 2009) or transgene expression (Hadjantonakis et al., 2001). Such a state has also been observed *in vitro* in trophoblast stem cells (Dubois et al., 2014), in addition to a transient two active X chromosome state (Prudhomme et al., 2015). These instances of plasticity could result from the co existence of both heterochromatic and euchromatic marks, as observed in trophoblast giant cells (Corbel et al., 2013); and may serve to compensate for occurrences of pertubation of X linked monoallelic gene expression (Prudhomme et al., 2015). Other work has shown the presence of low level methylation of CpG islands at promoter regions in trophoblast tissues when compared to epiblast (Senner et al., 2012). When an enzyme responsible for the maintenance of this mark is removed (*Dnmt1*), reactivation of a reporter transgene is detected in the embryo but not in the extraembryonic tissue (Sado et al., 2000). Interpreted with evidence showing that neither *Dnmt1*, *Dnmt3a*, or *Dnmt3b* are required for survival and proliferation of mTSCs (Sakaue et al., 2010), it can be concluded that DNA methylation is not the primary epigenetic mark "locking in" the inactive state in extraembryonic iXCI. Much work remains still to be done on the role of histone modifications in this context.

Mechanism of iXCI

Although it has previously been thought that the X^P may be pre-inactivated in the preimplantation embryo as a result of MSCI (Huynh and Lee, 2003), subsequent work has shown active X^P transcription at the two cell stage (Okamoto et al., 2005). Multiple alternative mechanisms have been proposed to explain the data, a number of which are now reviewed.

A priori, an imprint could protect the X^M from silencing, or target the X^P to be inactivated. Early evidence from experiments utilising parthenogenetic embryos (X^MX^M) strongly supports the former hypothesis, as development is stalled in the early postimplantation stages following the failed growth of extraembryonic tissue (Shao and Takagi, 1990; Goto and Takagi, 1998, 2000). Furthermore, it seems that such an imprint is imposed during oogenesis, as combining maternal genomes from non-growing (ng) and fully-grown (fg) oocytes always resulted in inactivation of the ng derived genome in extraembryonic tissue. This observation is consistent with a mark imposed on the fg oocyte during maturation (Tada et al., 2000), though unlike classical genomic imprinting, this is independent of DNA methylation (McDonald et al., 1998; Liu et al., 2010). Recent work has implicated the H3K9me3 histone mark in X^M-*Xist* silencing, showing that reduction of H3K9me3 levels via over-expression of its specific demethylase *Kdm4b*, in addition to a histone deacetylase inhibitor trichostatin, results in detectable X^M-*Xist* de-repression (Fukuda et al., 2014). However, no difference in H3K9me3 levels was found when comparing ng and fg oocytes at the X^M-*Xist* locus (Fukuda et al., 2015). Most recently, the same authors showed that both transient histone alterations and chromatin decondensation are able to partially rescue the embryonic lethality that results from X^MX^P*Xist*- (Fukuda et al., 2015, 2016).

Also utilising histone alterations, Federici and colleagues reported partial rescue of X^MX^P*Xist*- female embryonic lethality (Federici et al., 2016). Using round spermatid injection, they were able to achieve fertilisation without the protamine associated condensation and decondensation of the paternal genome. Taken together, these results implicate a role for H3K9me3 in iXCI, though it seems likely this is within a wider context of genome organisation in the regulation of gene expression.

Namekawa and colleagues suggest that iXCI in mouse can be separated into two steps, with silencing of repetitive sequences preceding that of genic sequences (Namekawa et al., 2010). Using FISH and immunofluorescence (IF), they identified

a Cot1-, Pol-II-, Pol-III- silent compartment within which the repeat sequences of the X^P are localised at the two cell stage. The formation of this silent compartment is *Xist*-independent. In contrast, the inactivation of genic regions takes place a number of cell divisions later (reasonably consistent with other data: Okamoto et al., 2004, 2005, 2011), and this requires *Xist* expression. They favour a model whereby repeats arrive in the embryo pre-inactivated following MSCI. These repeats could comprise an imprint on the X^P predisposing to inactivation, independent of any X^M imprint laid down in the oocyte.

Experiments utilising *Xist* transgenes suggest a role for hemizygosity in iXCI. A 200-kb *Xist* locus transgene present in a multicopy array on an autosome is sufficient for ectopic *Xist* expression and chromatin silencing in the hemizygous state, but not the homozygous state (Sun et al., 2015). It is possible that chromatin modifications (like in MSCI) resulting from the unpaired state of the *Xist* transgenes are directly responsible for *Xist* imprinting in next generation (Sun et al., 2015). However, this is in contrast to previous work (Okamoto et al., 2005). Using a single copy 460-kb transgene, no difference was observed between homozygous and hemizygous males in terms of ectopic *Xist* expression. Moreover, there was also no evidence of the *Xist* transgene associating with the sex body, as would be expected if passage through the XY body is required for iXCI (Okamoto et al., 2005). Payer suggests that the differences observed may be due to the multicopy nature of the transgene in the former study, which might more completely reflect the endogenous situation (Payer, 2016). This has previously been reported when using *Xist* transgenes to recapitulate rXCI, whereby multicopy transgenes suceed whilst single copies failed (Heard et al., 1996, 1999b; Lee et al., 1999).

1.4.2.2 Random XCI

Early biochemical and cytogenetic evidence provided the first link between cellular differentiation and XCI *in vivo* (Rastan, 1982; Monk and Harper, 1979). It showed that both X chromosomes are active in the peri implanation mouse embryo until

rXCI takes place in the epiblast around E4.5. This event is re captured in the most well used model of XCI *in vitro*, mouse embryonic stem cells (mESCs). XX female mESCs have two active X chromosomes, and undergo XCI upon differentiation (Martin et al., 1978; Takagi and Martin, 1984), thereby facilitating investigation of the mechanisms underlying rXCI.

Regulation of *Xist* expression

XCI is controlled by the X inactivation centre (Xic), a region of around 1Mb shown to be both necessary and sufficient to trigger XCI when present in at least two copies (Heard et al., 1996; Lee et al., 1996; Heard et al., 1999a). Within the Xic locus are situated a number of genes - protein coding and non coding - that are involved in the process, many of which have been characterised using the mESC model.

Tsix is a negative regulator of *Xist*: it is a non-coding RNA that overlaps with and is transcribed antisense to *Xist* (Lee et al., 1999). Current evidence suggests that the act of *Tsix* transcription, as opposed to the RNA itself, represses *Xist* expression (Stavropoulos et al., 2001; Shibata and Lee, 2004; Sado et al., 2006). Heterozygous deletion of *Tsix* results in skewed XCI of the mutated chromosome in XX female cells, but deletion does not cause inactivation in XY male cells. This suggests that *Tsix* is involved in the choice of which chromosome to inactivate, but not the counting that ensures one X chromosome is left active (Lee and Lu, 1999; Lee, 2002; Stavropoulos et al., 2001). Mechanistically, it has been proposed that pairing observed between the *Tsix* and *Xpr* loci might mediate this choice process (Xu et al., 2006, 2007; Bacher et al., 2006). However, recent work using heterokaryons has provided evidence that pairing is not essential for XCI initiation, as XCI can take place in different nuclei within the same cytoplasm via *trans* acting factors (Barakat et al., 2014).

Tsix has also been implicated in iXCI. It is downregulated in the postimplantation embryo, but expression from the X^M persists in the extraembryonic tissue. Disruption of this allele results in ectopic *Xist* expression and early embryonic lethality

following *Xist* mediated inactivation of the single X in males and both Xs in females (Sado et al., 2001). Recent work has cast doubt on this interpretation, suggesting *Tsix* is not required for initiation of iXCI, but instead is involved in the differentiation of mouse trophoblast stem cells (mTSCs) towards a giant cell fate (Maclary et al., 2014). A further role for *Tsix* has been highlighted in mouse epiblast stem cells, where it is required to silence *Xist* on the active X chromosome (Xa) *in vivo* and *in vitro* as they differentiate (Gayen et al., 2015).

Loci upstream of *Xist* have also been proposed to play roles in the regulation of its expression, either in *cis* or in *trans*. *Jpx* was initially thought unlikely to regulate XCI (Chureau et al., 2002), however, later chromosome conformation capture (3C) analysis suggested a relationship between *Jpx* and *Xist* (Tian et al., 2008). The *Jpx* locus produces a long non coding RNA (lncRNA) that may act in *trans* to regulate *Xist* expression from the Xi (Tian et al., 2010) via dose dependent eviction of CTCF at the promoter (Sun et al., 2013a). Alternatively, the lncRNA could act in *cis* to coactivate *Xist* through promoter contacts (Barakat et al., 2014), though Sun and colleagues (2013) suggest that such contacts are not significant to XCI. Barakat et al. (2014) reached similar conclusions for the lncRNA *Ftx*. Whilst initial work in male mESCs suggested that *Ftx* deletion reduced expression of *Xist* and resulted in dysregulation of other loci across the Xic (Chureau et al., 2011), subsequent evidence from female mESCs and *in vivo* showed that *Ftx* deletion does not affect *Xist* expression or iXCI (Soma et al., 2014). Taken together, these data suggest that both *Jpx* and *Ftx* may act in *cis* to play a part in *Xist* regulation, lowering the threshold for activation by *trans* acting factors such as *Rnf12* (Barakat et al., 2014). It is, however, clear that neither acts alone, and whether the mechanism of regulation is driven by the act of transcription, the transcript itself, or at the DNA level, remains to be investigated. Finally, existence of two microRNAs within the Xic has recently been identified, though work is ongoing to explore their function (Kobayashi et al., 2013).

Pluripotency and XCI

The pluripotent state inhibits XCI (Minkovsky et al., 2012) via a number of pluripotency associated transcription factors that can be loosely grouped as either repressing *Xist* expression or promoting *Tsix*. *Xist* intron 1 can be bound by OCT4, SOX2, NANOG, and PRDM14 (Payer et al., 2013), and can also spatially associate with the *Xist* promoter (Tsai et al., 2008), repressing *Xist* transcription and therefore XCI (Navarro et al., 2008). However, whilst deletion of intron 1 in male and female mESC lines carrying a *Xist* transgene led to slightly increased *Xist* expression (Nesterova et al., 2011), recent work has removed endogenous intron 1 in both mESCs and mice without obvious effect on *Xist* expression or phenotype (Minkovsky et al., 2013). OCT4 has also been shown to bind to the promoter of *Tsix* and stimulate transcription, in addition to KLF4, c-MYC and REX1 (Navarro et al., 2008; Donohoe et al., 2009; Nesterova et al., 2011).

Rex1 likely sits in both groups as an *Xist* repressor and an activator of *Tsix* (Gontan et al., 2012). During differentiation, REX1 is targeted for degradation by the E3 ubiquitin ligase Rnf12(RLIM), which has been proposed to behave as a *trans* acting factor, working dosage dependently to trigger XCI (Gontan et al., 2012). Male mESCs usually have a single copy of *Rnf12* and therefore do not inactivate the single X chromosome; however, when extra copies are added, XCI is aberrently initiated (Jonkers et al., 2009). The picture in female mESCs is not so clear. Homozygous inheritance of an allele producing a 340 amino acid mutant protein (Jonkers et al., 2009) abolished XCI in differentiating cells; whereas production of a 83 amino acid mutant peptide (Shin et al., 2010) had no effect *in vitro*. The latter allele also had no effect on rXCI (Shin et al., 2014), but did perturb iXCI when inherited maternally (Shin et al., 2010).

Exit from the pluripotent state through differentiation is affected by X linked gene dosage. In female mESCs, when both X chromosomes are active, X linked genes show on average 2-fold higher expression than in male cells (Lin et al., 2007). This seems to stabilise the pluripotent state by inhibiting MAPK/Erk signaling and stim-

ulating Akt (Schulz et al., 2014). As differentiation requires MAPK signaling, the only way to exit pluripotency is for the cell to undergo XCI (Schulz et al., 2014). Utilising multiple mESC lines in serum and leukemia inhibitory factor (LIF) culture conditions, Schulz and colleagues showed that XX female cells are delayed in exiting the pluripotent state, following the induction of differentiation, when compared to XY and XO cells. They observed reduced activity of MAPK signaling, correlated with DNA hypomethylation, and suggest that these factors result in a population of cells shifted towards naive ground state pluripotency. Following induced expression of *Xist*, female cells were able to differentiate with similar kinetics to XY and XO cells. These observations support the hypothesis that two active X chromosomes inhibit downregulation of pluripotency factors, and only following feedback from XCI - indicative of X chromosome dosage compensation - is this inhibition released.

Further support for the link between exit from pluripotency and XCI can be identified from mouse development data, where it was first noted that XY male embryos show slightly accelerated growth relative to XX female embryos (Tsunoda et al., 1985). Paul Burgoyne utilised a plethora of different mutant mouse crosses to show the Y chromosome of most strains accelerates preimplantation development (Burgoyne, 1993); and furthermore that embryos with two X chromosomes show slightly delayed post implantation development (Thornhill and Burgoyne, 1993; Burgoyne et al., 1995). Intriguingly, this observation was true when comparing XX embryos to XY and $X^{M}O$ embryos (with a single X chromosome inherited maternally). However, $X^{P}O$ embryos (with a single X chromosome inherited paternally) showed delayed development relative to XX, XY and $X^{M}O$ embryos at E10.5 (Thornhill and Burgoyne, 1993). This phenotypic difference suggests that X^{M} and X^{P} are not equal in terms of their effects on embryonic development, and warrants further attention. The aneuploid XO model system isolates maternal and paternal X chromosomes efficiently in order to address this (see section 1.5).

1.4.3 Escape from X chromosome inactivation

A number of X-linked genes are not silenced during the process of XCI. In humans, it has been estimated that around 12% show consistent escape, and a further 8% escape variably in different individuals and different tissues (Schultz et al., 2015; Carrel and Willard, 1999); whereas in mouse, the numbers are 3% and 4% respectively (Berletch et al., 2015). These genes have been found to lack the *Xist* coating and repressive histone marks usually characteristic of the inactive X (Simon et al., 2014; Goto and Takagi, 2000; Yang et al., 2010; Marks et al., 2015), in addition to displaying unique methylation marks (reviewed in Balaton and Brown, 2016).

Whether these differences are the cause of escape or simply a result of escape has yet to be determined. Interestingly, large clones incorporating the locus of escapee gene *Kdm5c* can be integrated at different X linked locations and still show expression, suggesting that escape is a locus intrinsic property (Li and Carrel, 2008). Further work deleting a non-coding region within the cloned locus resulted in expression from genes outside the integrated clone, showing that the escape property can spread (Horvath et al., 2013).

It has previously been put forward that specific DNA sequences, such as long interspersed nuclear elements (LINEs) or CTCF binding domains, might be enriched around those genes subject to or escaping from XCI (Bailey et al., 2000; Chow et al., 2010; Dixon et al., 2012). Most recently, work on nuclear ultrastructure has described the existence of topologically associating domains (TADs), intra chromosomal compartments thought to represent functional domains of gene regulation (Dekker and Heard, 2015). Groups of human and mouse genes escaping XCI have been shown to exist within the same TADs (Marks et al., 2015), and in naturally occuring autosomal translocations onto the inactive X chromosome, the translocated gene(s) followed the general pattern of the TAD, i.e. subject to or escape from XCI (Cotton et al., 2014). The significant question of why these genes escape chromosome wide silencing remains unanswered.

1.5 Aneuploidy

Aneuploidy - a deviation from euploidy, i.e. not having a normal number of chromosomes - is a term that encompasses loss and gain of chromosomes, both of which are usually problematic to the organism. One of the first reports was in 1920, when it was shown that the flowering plant *Datura stramonium* exhibited fewer negative phenotypic effects from duplication of the whole genome than duplication of a single chromosome (Blakeslee et al., 1920). This result suggested that the balance between chromosomes is more important that the overall number of copies of the genome. Further examples can be found in human disease. The only monosomy compatible with perinatal life is monosomy X (TS), whereas three autosomal trisomies are compatible with perinatal life - trisomy 13 (Patau syndrome), 18 (Edwards syndrome), and 21 (Down's syndrome, Tybulewicz, 2006). Those afflicted with the latter present with severe phenotypes including developmental abnormalities, mental retardation and shortened life expectancy (weeks, months and around 50 years, respectively, Tybulewicz, 2006). Sex chromosome trisomies are signficantly less severe, possible due to the transcriptional inactivation of all but one X chromosomes (with the exception of XCI escapees: see section 1.4.3), and the relative paucity of widely expressed genes from the Y chromosome.

1.5.1 Sex chromosome aneuplodies

A brief description of the salient features of the most prevalent sex chromosome aneuploidies are summarised in Table 1.1

1.5.1.1 Klinefelter syndrome: XXY

First described in 1942 as male patients presenting primarily with small testes and gynaecomastia, Klinefelter syndrome has a prevalence of around 0.1-0.2% of males (Klinefelter et al., 1942; Lanfranco et al., 2004). It is the most common cause of genetic infertility (Lanfranco et al., 2004). There is some evidence to suggest that XXY embryos are selected against *in utero*, as one study showed that only 55%

Aneuploidy	Prevalence (birth)	Infertility	Intellectual disability	Congenital abnormalities	Growth phenotype	Karyotype
Klinefelter syndrome	0.1-0.2% of males	Yes	Mild	No	Tall	XXY
Triple X syndrome	0.1% of females	No	Mild	No	Tall	XXX
XYY syndrome	0.1-0.2% of males	Variable	Mild	No	Tall	XYY
Turner syndrome	0.04% of females	Yes	Mild-moderate	Heart, kidney	Short	XO

Table 1.1: Key features of human sex chromosome aneuploidies.

survive to term (Jacobs, 1990). Karyotypic analysis revealed the aetiology as an abnormal sex chromosome complement of XXY (Jacobs et al., 1959; Ford et al., 1959b) in around 80% of cases, with higher grade aneuploidies and structurally abnormal chromosomes making up the further 20% (Bonomi et al., 2017). Subsequent characterisation has added a number of other features to the syndrome, including osteoporosis, sexual dysfunction, and tall stature (Bonomi et al., 2017). It is likely that at least part of the spectrum of phenotypes attributed to Klinefelter syndrome result from abnormal dosage of genes escaping XCI, or those present in the PAR (see below, section 1.5.2).

1.5.1.2 Triple X syndrome

Originally described as a human "super female" (Jacobs et al., 1959), Triple X syndrome was reported only after the development of karyotyping techniques, as many cases, then and now, go undiagnosed due to the lack of clinical signs and symptoms (Otter et al., 2009). With a prevalence of around 0.1% of female births, Jacobs (1990) estimates that this represents around 70% of XXX fertilisation events; i.e. some negative *in utero* selection takes place. The relatively mild reported phenotype of slight developmental delay during childhood, possible correlation with increased psychiatric diagnoses in adulthood, and tall stature (Otter et al., 2009), suggest that this aneuploidy is at least partly compensated for by XCI.

1.5.1.3 Y chromosome aneuploidies

Whilst other Y chromosome aneuploidies exist as case reports, by far the most prevalent is XYY, which is detected at a rate of 0.1% of live male births (Geerts et al., 2003), with no detected selection *in utero* (Jacobs, 1990). Some individuals show delayed language acquisition and motor development, along with above average height, weight and head circumference from birth onwards. There is also an increased risk of child psychiatric disorders, including autism (Geerts et al., 2003), and variable rates of infertility (Kim et al., 2013).

1.5.2 Turner syndrome: XO

The clinical entity of Turner syndrome (TS) was first reported by Ullrich (Ullrich, 1930), before later being made eponymous by Henry Turner in his 1938 address to The Association for the Study of Internal Secretions (Turner, 1938). TS encompasses a core phenotype of short stature, streak ovaries, webbing of the neck, and congenital cardiovascular and renal defects (Ranke and Saenger, 2001). Notably, the severity of each of these shows significant inter individual variation (Ranke and Saenger, 2001). In 1959, Ford and colleagues linked karyotype with phenotype and thus formally identified TS as monosomy X (Ford et al., 1959a). TS is the most commonly diagnosed sex chromosome abnormality in humans, occurring in 1-2% of clinically recognised pregnancies (Hassold et al., 1992); though survival to term only occurs in about 1% of XO foetuses (Hook and Warburton, 1983). Such high *in utero* lethality supports the case for the importance of X linked genes in embryonic development. There are a number of mechanistic hypothesis that account for this, and the subsequent variable postnatal phenotype in survivors, including genomic imprinting and haploinsufficiency. These are now explored in further detail.

1.5.2.1 Genomic imprinting

In therian mammals, embryos derived solely from paternal genomes (androgenotes) or from maternal genomes (gynogenotes) do not survive *in utero* development. Androgenotes are characterised by poor progression in the embryo proper, but significant development of the extraembryonic tissue (Barton et al., 1984). Gynogenetic embryos progress further with some growth defects, though show pronounced abnormalities in the extraembryonic derivatives (Kaufman et al., 1977; Surani and Barton, 1983; Surani et al., 1984; McGrath and Solter, 1984). This requirement for one copy each of the paternal and maternal genome to initiate successful embryonic development is explained by genomic imprinting, the process whereby a group of genes is epigenetically regulated to show monoallelic expression in a parent of origin specific manner (Cleaton et al., 2014). In mouse, around 100 autosomal genes

are regulated in this way: they are usually found in small groups clustered around an imprinting control region (ICR) that is differentially methylated in either the male or female germline during development (Cleaton et al., 2014). Autosomal genomic imprinting is also found in humans - attested to by a number of severe disease phenotypes related to erroneous imprinting (see Soejima and Higashimoto, 2013) - and across the wider mammalian class, with the exception of monotremes. This observation has led to the hypothesis that the process evolved alongside evolution of the placenta (Smith et al., 2011). Interestingly, of the small number of X linked imprinted genes reported in mouse, most are expressed in placenta (Li and Behringer, 1998; Rodriguez et al., 2004; Shi et al., 2004), with brain being the other tissue (Davies et al., 2005). No related X linked ICR has been reported.

Genomic imprinting in TS

The parental origin of the X chromosome in XO spontaneous abortuses, late foetal deaths, and liveborn females is relatively constant, with approximately 70% maternal and 30% paternal (Hassold et al., 1985, 1988; Cockwell et al., 1991; Sanger et al., 1977; Jacobs et al., 1990). Hook and Warburton (2014) hypothesise that this deviation from 50:50 can be partly explained by a post conception mitotic sex chromosome loss. An XX embryo can lose either X^M or X^P, whereas an XY embryo must lose the Y and retain the X^M because YO embryos are not viable (Morris, 1968a; Burgoyne and Biggers, 1976). Jacobs further suggests that the paternal X chromosome from XX embryos may also be lost before pronuclear fusion, and that the Y chromosome may be lost due to its small size (Jacobs et al., 1997).

As the available data show a bias towards a maternally inherited X chromosome in individuals living with TS, does this manifest as a difference in phenotype? Evidence has been presented that skills mediating social interactions are better developed in X^PO females, and it was hypothesised this could be explained by the existence of an X linked imprinted locus (Skuse et al., 1997; Bishop et al., 2000). However, no specific loci were found. Further suggestion of X linked imprinting in humans was provided by studying the transmission of X linked maternal alleles in

families free of detectable genetic disease (Naumova et al., 1998). A significant deviation from the Mendelian ratio resulted in distorted inheritance at a specific locus among male offspring, though no follow up has since been published.

1.5.2.2 Haploinsufficiency

Ferguson-Smith (Ferguson-Smith, 1965) suggested that the phenotype observed in patients with an XO karyotype could be explained by the presence of homologous genes on the X and Y chromosomes that escape XCI, and thus are haploinsufficient in patients lacking a second sex chromosome. Following their identification, the PARs became an obvious location for such genes (Canki et al., 1988). In human, the short stature homeobox containing gene (*SHOX*) certainly influences the growth deficit observed in TS patients (see next section); however, it does not seem to be involved in any of the other phenotypic abnormalities (Ellison et al., 1997). More recently, Urbach and Benevisty used XX and XO human embryonic stem cells (hESCs) differentiated towards various lineages to propose that *CSF2RA*, located in PAR1, is haploinsufficient when present in only one copy in the placenta; and is therefore responsible for the embryonic lethality (Urbach and Benvenisty, 2009). This is in keeping with the concept of the existence of a karyotypically normal rescue line in all liveborn XO individuals. In 1983, Hook and Warburton suggested that the difference between viable and non viable XO conceptuses could be the existence of undetected mosaicism for a karyotypically viable cell line, e.g. XX, suggesting haploinsufficiency at key sex linked loci as the underlying reason for death *in utero* (Hook and Warburton, 1983, 2014). This position was supported by extensive abortion datasets from New York and New Jersey, highlighting the ratio of apparent non mosaic XO to XO/XX mosaics was higher in embryonic and foetal deaths than in living individuals, 13.5:1 and 3.6:1, respectively (Hook and Warburton, 1983). Subsequent work has specifically searched for such hidden mosaicism in living patients with a diagnosis of TS, with varying success. Jacobs initially counted 100 cells from peripheral blood (greater than the usual 30 used for clinical diagnosis), and found 2/84 mosaics (Jacobs et al., 1997). Cells from buccal smears

were then counted, and no further mosaicism was found. More recent work used FISH on buccal smears (subsequent to the initial diagnostic 30 cells from peripheral blood) and reported a detection rate of 30% (Freriks et al., 2013). These data are largely consistent with the cryptic mosaicism hypothesis: if the patients with "complete monosomy" (Hook and Warburton, 2014) have a more severe phenotype than those with rescue lines, they would be more likely to present with symptoms and signs for medical investigation, and thus the rate of undetected mosaicism is relatively low. Furthermore, screening for mosaicism in these patients using peripheral blood and buccal swabs will not detect placental mosaicism, and it is the latter that could explain their survival (Hook and Warburton, 2014).

Turner syndrome as an experimental paradigm

In order to more fully understand the role of X linked genes in development and, more specifically, differences between X^M and X^P, a measurable characteristic is required: the most quantifiable aspect of the TS phenotype is the growth deficit.

Short stature has long been recognised as an ever present feature of TS (Brook et al., 1974), starting with intrauterine growth retardation, as identified by sonographic studies. Using data resulting from prenatal screening, it has been shown that alongside the TS diagnostic anomalies of cystic hygroma and fetal hydrops, foetuses are generally small for gestational age (Wladimiroff et al., 1995). This continues postnatally, as evidenced by a retrospective study of an Italian cohort of patients with reduced birth weight (Larizza et al., 2002; Wisniewski et al., 2007). Children show a decline in growth velocity that is not rescued by a pubertal growth spurt, and adults are typically ~2.5-3.5 standard deviations below normal female height (Brook et al., 1974; Robles Valdés et al., 2003).

A number of other sex chromosome abnormalities have been associated with short stature, primarily including deletions of the short arms of the X or Y chromosome (Curry et al., 1984; Zuffardi et al., 1982). Further work localised the locus responsible to the PAR1 (Ballabio et al., 1989), and the gene was subsequently identified

as *SHOX*. Deficiency in this gene could explain the short stature observed in individuals with TS (Rao et al., 1997; Ellison et al., 1997). These individuals carry only one copy of *SHOX*, whereas individuals with a normal XX or XY karyotype carry two copies. Furthermore, some patients with idiopathic short stature (Rao et al., 1997; Fukami et al., 2016) and others with limb bone abnormalities (Belin et al., 1998; Chen et al., 2009; Benito-Sanz et al., 2005; Barca-Tierno et al., 2011) have mutations in the *SHOX* gene, independent of specific sex chromosome abnormalities. SHOX expression has since been observed in the developing limb, mainly in perichondrial layer, and in the pharyngeal arches (Clement-Jones et al., 2000; Rao et al., 2001). *In vitro* work suggests SHOX is an activator of the aggrecan enhancer in chondrogenesis and skeletal development (Aza-Carmona et al., 2011), thus supporting significant involvement in the TS phenotype. There is, however, some evidence to suggest that individuals with TS are generally shorter than those with *SHOX* mutations, and that other loci may be involved in the short stature phenotype (Ross et al., 2001; Fukami et al., 2016; Zinn and Ross, 1998).

1.5.3 XO aneuploid mice

The deduction that the female mouse can also harbour an XO sex chromosome complement came contemporaneously with the first reported human karyotype in 1959 (Welshons and Russell, 1959). A line was subsequently developed by Cattanach and colleagues in Edinburgh, UK (Cattanach, 1962). Animals of this karyotype showed no gross difference in growth from XX littermates, and were used for breeding, with apparently fewer XO daughters from XO mothers than expected. This observation was explained by the hypothesis that many oocytes segregated the chromosome set lacking an X chromosome to the polar body (Cattanach, 1962). Further work has gone on to show that XO female mice have reduced fertility when compared to XX females, both in terms of litter size and reproductive lifespan (Morris, 1968b; Burgoyne and Biggers, 1976; Burgoyne and Baker, 1981). This reduction is largely due to the presence of an unpaired X chromosome during meiosis (Burgoyne and Baker, 1985).

Originally reported as phenotypically normal (Welshons and Russell, 1959; Cattanach, 1962), XO female mice were subsequently found to recapitulate at least one aspect of the TS phenotype, with growth deficits occurring during embryonic and postnatal development. X^PO embryos have a developmental lag relative to XX littermates at preimplantation (Banzai et al., 1995a) and egg cylinder (E7.25) stages (Burgoyne et al., 1983b; Ishikawa et al., 1999). This lag could be explained, at least in part, by the reduced volume of the ectoplacental cone (Jamieson et al., 1998), part of the early placenta (Gardner et al., 1973). In contrast, the X^PO placenta during late development is increased in volume (Burgoyne et al., 1983b). Interestingly, placentas from X^MO and XY conceptuses also showed this hyperplastic phenotype (Ishikawa et al., 2003; Zechner et al., 1996, 2002). These apparently contradictory data can be reconciled by two separate explanations. The reduced ectoplacental cone volume in X^PO embryos was suggested to be a result of genomic imprinting, and late development placenta hyperplasticity was attributed to X chromosome dosage (Ishikawa et al., 2003).

Imprinting in XO mice

Further, more detailed work has identified additional evidence for a potential X chromosome imprinting effect, showing that the embryonic developmental lag is present only in X^PO embryos at E10.5. X^MO embryos and XY embryos are significantly larger than XX littermates at the same stage, and all are significantly larger than X^PO embryos (Thornhill and Burgoyne, 1993). Alternatively, this could be explained by inappropriate expression of *Xist* in the preimplantation embryo. *Xist* expression is imprinted in the early mouse embryo, such that it is always expressed from the X^P at 4-8 cell stage (Okamoto et al., 2005). Notably, *Xist* expression also occurs in X^PO embryos, which only have a single X chromosome (Matsui et al., 2001). *Xist* is then downregulated in the epiblast of all embryos at the blastocyst stage prior to random XCI, whereas imprinted XCI continues in the trophectoderm. Downregulation of *Xist* was found to take place in all cell types of X^PO embryos at the blastocyst stage. It is therefore conceivable that inappropriate *Xist* expres-

sion results in X^PO embryos functionally nullizygous for embryo derived X linked gene products for a number of cell cycles during this key developmental time window. This functional nullizygosity for an entire chromosome would likely have a significant impact on embryonic development.

Haploinsufficiency in XO mice

Whilst there is no growth deficit observed in XO mice during late embryonic development, and reports contrast about birth weight data (Burgoyne et al., 1983b; Deckers and Van der Kroon, 1981; Burgoyne et al., 1983a, 2002), it is clear that a postnatal growth deficit exists (Burgoyne et al., 1983a, 2002). In the earlier study, Burgoyne and colleagues compared X^PO female mice to XX littermates, and showed that the rate of growth differed significantly during the first three weeks of postnatal life. This difference disappeared during subsequent phases of growth (Burgoyne et al., 1983a). The follow up study sought to determine whether this effect could be attributable to imprinting, i.e. is it present in the X^MO, or X linked gene dosage deficiency (Burgoyne et al., 2002). By comparing the weights of X^PO and X^MO female mice with their XX littermates during the first five weeks of postnatal life, it was shown that a small but significant growth deficit exists regardless of the parental origin of the X chromosome. Reasoning that this could be due to haploinsuffiency of PAR localised genes, they utilised sex chromosome variant mice to show that two copies of the PAR did not rescue the growth deficit. Interestingly, a growth deficit was not observed in female mice carrying a Y chromosome deficient in *Sry* (an XY^{Tdy} female, Lovell-Badge and Robertson, 1990; Gubbay et al., 1992). The authors concluded that the postnatal growth deficit observed in XO female mice is not the result of genomic imprinting on the X chromosome, or of haploinsufficiency for genes localised to the PAR. The growth deficit was likely caused by haploinsufficiency of X linked genes that escape XCI, and that have homologues on the Y chromosome (Burgoyne et al., 2002). The identification of these genes - *Ddx3x/y*, *Kdm5c/d*, *Kdm6a/Uty*, and *Eif2s3x/y* - as likely candidates for a haploinsuffiency hypothesis is consistent with the conclusions made from the recent Y chromosome

sequencing data (Bellott et al., 2014). At least three of the four are highly conserved regulators of global gene activity, likely required for male viability, and responsible for male:female sexual dimorphism in health and disease (Bellott et al., 2014). A cartoon depicting the relative positions of these genes on their respective chromosomes is provided for reference (Figure 1.4).

1.6 X-Y gene pairs with candidate roles in postnatal growth

1.6.1 *Kdm5c*

KDM5C (lysine demethylase 5C) was the first gene described to escape XCI, initially in human, and very shortly after in mouse, showing ubiquitous expression in both organisms (Wu et al., 1994; Agulnik et al., 1994b; Sheardown et al., 1996; Carrel et al., 1996). Also known as *Smcx* and *Jarid1c*, the protein has a number of significant domains suggestive of histone lysine demethylase function: JmjC, a histone lysine demethylase domain (Chen et al., 2006; Klose et al., 2006), supported by a JumjN domain (Chen et al., 2006); an AT rich domain interacting domain (ARID) associates with DNA in both sequence specific and sequence independent manners (Kortschak et al., 2000; Wilsker et al., 2002); and C5HC2 and PHD zinc finger domains provide histone methyl lysine binding motifs (Shi et al., 2006; Wysocka et al., 2006; Horton et al., 2009).

Confirmation of histone lysine demethylase function was provided by a number of reports, showing activity at both H3K4 me3 and me2, and highlighting a key role in repression of transcription (Iwase et al., 2007; Christensen et al., 2007; Tahiliani et al., 2007). Work in *Drosophila* on the orthologue *Little imaginal discs* (*LID*, Eissenberg et al., 2007; Lee et al., 2007a) and in *C. elegans* on *rbr-2* has indicated that this function is highly conserved across species (Christensen et al., 2007). It is at least partly mediated by association with the transcriptional repressor REST in multi

protein complexes (Tahiliani et al., 2007). KDM5C and REST were shown to co occupy neuron restrictive silencing elements, and RNA-interference (RNAi) mediated knockdown of *Kdm5c* de-repressed several downstream targets (Tahiliani et al., 2007). Independently, a role for *Kdm5c* in neural development was shown utilising zebrafish morpholinos, and isolated primary granule neurons from rat pups manifest impaired dendritic growth following *Kdm5c* RNAi (Iwase et al., 2007).

The link between reduced KDM5C activity and impaired neuronal function in humans was first noted in a subset of patients with X linked intellectual disability (XLID) syndrome carrying mutations in *KDM5C* (Jensen et al., 2005; Tzschach et al., 2006; Santos et al., 2006; Abidi et al., 2008; Rujirabanjerd et al., 2010; Õunap et al., 2012; Peng et al., 2015; Fieremans et al., 2015). In XLID syndrome, affected individuals have an IQ<70 (Roeleveld et al., 1997). Some patients with mutations in *KDM5C* also have diagnoses of autism spectrum disorders, and many are of short stature (Adegbola et al., 2008). Patients reported in these papers are almost always male, and females carrying one copy of the mutation are usually described as phenotypically normal. There are, however, some reports of *KDM5C* mutant females with mild intellectual disability and XCI skewed to silence the mutation harbouring X chromosome. Where parental origin has been reported, the mutant allele is always maternally inherited (Abidi et al., 2008; Santos-Reboucas et al., 2011; Õunap et al., 2012). This case based evidence supports the hypothesis that dosage of *KDM5C* is important. Although the gene escapes XCI, expression from the inactive X allele has been estimated at between 20%-70% of that on the active X (Sheardown et al., 1996). Moreover, expression analysis in mouse brain indicates that *Kdm5c* is expressed more highly in adult females than adult males, and expression of the Y linked homologue *Kdm5d* does not fully compensate (Xu et al., 2002). This is consistent with the significantly higher incidence of XLID in males than females, suggesting that either the Y linked homologue does not provide complete functional compensation for loss of *KDM5C*, or it is not expressed at equivalent levels in correct subset of cells required for normal development.

Interestingly, and supporting a fundamental housekeeping role for *KDM5C* across multiple cell types, mutations are associated with a wide spectrum of cancers. In renal cell carcinoma (RCC), *KDM5C* could act as a tumour suppressor (Dalgliesh et al., 2010; Niu et al., 2012). *KDM5C* it is abundantly expressed in hepatocellular carcinoma (HCC) cell lines, and depletion reduced migration and epithelial mesenchymal transition (Ji et al., 2015). *KDM5C* is significantly upregulated in breast cancer, and levels positively correlate with metastasis (Wang et al., 2015). Finally, DNA methylation is significantly reduced in the leukocytes of these individuals carrying these mutations (Grafodatskaya et al., 2013).

1.6.2 *Kdm5d*

First described as an H Y antigen responsible for the rejection of male skin grafts by female mice of the same strain (Koo et al., 1977; Simpson, 1986; Simpson et al., 1987), *KDM5D* was then named *SMCY* following mapping in mouse and human, where it was shown to be expressed widely (Agulnik et al., 1994a; Scott et al., 1995). Work utilising both *Drosophila* and human cells lines has shown that in addition to functional conservation with *KDM5C* with regards to H3K4 demethylase activity, *KDM5D* associates with Ring6a/MBLR, which enhances demethylation activity (Lee et al., 2007a). Furthermore, *KDM5D* is implicated in the regulation of *Engrailed 2*. Depletion by RNAi led to increased H3K4 di- and tri-methylation levels at *Engrailed 2* promoter, increased transcription of this gene, and enhanced recruitment of the chromatin remodelling complex NURF (Lee et al., 2007a). This evidence suggests a more general role for *KDM5D* in transcriptional regulation. A similar role has also been implicated in mouse, where KDM5D co localises with MSH5, a meiosis regulator, during spermatogenesis (Akimoto et al., 2008). Finally, mutations in *KDM5D* have been found in a significant proportion of prostate cancer cases; and knockdown in prostate cancer cell lines resulted in an increased rate of growth alongside reduced apoptosis (Perinchery et al., 2000).

1.6.3 *Kdm6a*

Kdm6a (lysine demethylase 6a), also referred to by its former name *Ubiquitously transcribed Tetratricopeptide repeat on chromosome X* (*Utx*), was first described in 1998 in both mouse and human tissue as showing ubiquitous expression and escaping from XCI (Greenfield et al., 1998). A decade later, histone lysine demethylase function was attributed to this previously under annotated protein, and subsequent work has shown it essential for normal development.

Both UTX and the closely related Jumonji D3 (JMJD3) have been shown to catalyse the removal of di- and trimethyl moieties on histone H3 lysine 27, thus providing a counter balance for the activity of *Polycomb Repressor Complex 2* (PRC2), a H3K27 methyltransferase (Agger et al., 2007; Lan et al., 2007; Lee et al., 2007b). Whether the Y linked homologue *Uty* also has *in vivo* demethylase remains an open question (see section 1.6.4). The H3K27 methylation mark is a highly significant mediator of transcriptional repression, involved in a plethora of biological processes including genomic imprinting (Greenberg et al., 2017), XCI (Plath et al., 2003), and cancer (Conway et al., 2015). UTX demethylase activity is effected by a JmjC catalytic domain (Lan et al., 2007), and specificity towards H3K27me3 over the highly similar H3K9me3 results from the presence of a zinc binding domain (Sengoku and Yokoyama, 2011). Protein protein interactions are thought to be mediated by the tetratricopeptide repeat domains (TPRs), though these are not present in JMJD3, suggesting a slight functional divergence (Lan et al., 2007). Despite subtle changes between family members, the H3K27 demethylases are generally well conserved across multiple model organisms, including mouse (*Utx, Uty, Jmjd3*), *Drosophila* (*dUTX*), and *C. elegans* (*UTX1* - closest to mouse *Utx*, and *UTX2, 3* and *4* - closest to *Jmjd3*, Greenfield et al., 1998; Herz et al., 2010; Jin et al., 2011).

KDM6A has been shown to contribute to multiple protein complexes involved in the remodelling of chromatin via histone modifications. Complexes involving mixed lineage leukaemia protein 2 (MLL2) and KDM6A exhibit H3K4 methyltransferase activity, thus promoting transcription in humans (Issaeva et al., 2007;

Cho et al., 2007), *Drosophila* (Mohan et al., 2012), and *C. elegans* (Vandamme et al., 2012). This suggests a dynamic relationship between transcriptional de repression via H3K27 demethylation and transcriptional activation via H3K4 methylation. KDM6A, along with JMJD3, also interacts with the ATP dependent chromatin remodelling complex SWI/SNF (Miller et al., 2010). The authors showed that either KDM6A or JMJD3 demethylase is necessary for regulating inducible T-box factor mediated transcription independent of the demethylase activity. Finally, an interaction has also been demonstrated between dUTX and the histone acetylase Creb binding protein (CBP) (Tie et al., 2012). As histone acetylation functions to promote active chromatin, the co precipitation of dUTX, CBP and the ATPase Brm at Polycomb target genes enriched for H3K27ac might be interpreted as collective antagonism of PRC activity.

In *C. elegans* UTX-1 is required for progression to adulthood, as mutants lacking the protein die in late embryogenesis or early larval stages (Vandamme et al., 2012). Similarly, in *Drosophila*, *dUTX* is essential for survival: <5% of homozygous mutants pass the pupal stage but then die immediately after eclosion (Herz et al., 2010). *dUTX* homozygous mutant males have fewer teeth within the sex combs than wildtype males, along with rough eyes and wing defects (Herz et al., 2010). Such phenotypic features are reminiscent of Trithorax mutants, suggesting that *dUTX* is a Trithorax group gene, counteracting repression by Polycomb genes in the regulation of *Hox* genes. Unsurprisingly, H3K27me3 levels are increased in *dUTX* mutants and, consistent with previous work *in vitro* (Mohan et al., 2012), H3K4me1 levels are also affected, in a JmjC independent manner. Mutant tissue was shown to have an H3K27me3 dependent growth advantage when compared to wildtype in the developing eye. This increased proliferation was caused by increased Notch activity, and inactivation of the *Drosophila* orthologue of tumour supressor *Retinoblastoma*, *Rbf*, contributes to this phenotype (Herz et al., 2010).

In order to address the function of *Kdm6a* in mammalian development, a number of models have been created, first in mESCs and hESCs, and then subsequently in

mice. *KDM6A* is not required for ESC maintenance (Lee et al., 2012; Jiang et al., 2013), though there is evidence for a role in the differentiation of all germ cell layers. For example, *KDM6A* knockdown results in impaired endoderm differentiation via WNT signaling (Jiang et al., 2013). In the mesoderm, *Kdm6a* deficient cells show defects in cardiac differentiation (Wang et al., 2012; Welstead et al., 2012; Morales Torres et al., 2013), independent of demethylase activity (Lee et al., 2012). Moreover, *Kdm6a* is involved in the specification of ectoderm, which is also independent of demethylase activity (Morales Torres et al., 2013). Recent work has implicated *Kdm6a* in maintenance of DNA integrity, as use of a KDM6A inhibitor, along with knockdown of the gene, activated the DNA damage response in differentiating but not undifferentiated mESCs (Hofstetter et al., 2016). Interestingly, two independent groups have reported that in mESCs, but not in embryos, KDM6A regulates expression of *Uty* (Lee et al., 2012; Wang et al., 2012).

Several different *Kdm6a* knockout mouse lines have been created, all exhibiting relatively consistent phenotypes. Most prominently, female homozygous mutant embryos have severe cardiac malformations, neural tube closure defects, and reduced somite counts. A reduction in number of somites is indicative of retarded development (Tam, 1981). These embryos also show anaemia, myelodysplasia, and aberrant splenic haematopoiesis (Thieme et al., 2013), and invariably die between E9.5 and E13.5 (Lee et al., 2012; Wang et al., 2012; Shpargel et al., 2012; Welstead et al., 2012; Mansour et al., 2012; Thieme et al., 2013). Finally, there is some suggestion of disrupted primordial germ cell (PGC) development in *Kdm6a* knockout female embryos at E12.5, leading to reduced transmission of *Kdm6a* deficient germ cells in chimeras produced from targeted mESCs (Mansour et al., 2012).

Mutations in *KDM6A* have generally been detected in the context of either XLID or cancer. Many patients with Kabuki syndrome (KS) have complete deletion or loss of function mutations in *KDM6A*, or the H3K4 methyltransferase MLL2 (Miyake et al., 2012; Lederer et al., 2012; Priolo et al., 2012; Banka et al., 2013). KS is a developmental disorder, signs of which include craniofacial abnormalities, skele-

tal and visceral defects, mental retardation and short stature (Adam and Hudgins, 2005). Males with KS and a mutation in *KDM6A* show a more severe phenotype than females, suggesting *UTY* has functionally diverged from KDM6A (Miyake et al., 2012). Whilst the pathogenesis of KS is still not understood, a number of case reports have described predisposition to multiple different malignancies; and a number patients with malignancy have a *KDM6A* mutation but do not have KS. This was first shown in a study involving multiple tumour types (van Haaften et al., 2009), and later work has provided more detail on specific cancers including clear cell renal cell carcinoma (ccRCC, Dalgliesh et al., 2010), chronic myeloid leukaemia (CML, Jankowska et al., 2011), acute lymphoblastic leukaemia (ALL, Van der Meulen et al., 2015), and medulloblastoma (Jones et al., 2012; Robinson et al., 2012; Dubuc et al., 2012; Bunt et al., 2012). Initial mechanistic work suggests that *KDM6A* is putatively a tumour suppressor gene (Arcipowski et al., 2016), and the broad range of cell types affected by mutations here attest to the importance of regulated chromatin remodelling in health (Plass et al., 2013).

1.6.4 *Uty*

Uty (*Ubiquitously transcribed tetratricopeptide repeat gene on the Y chromosome*) is the Y linked homologue of *Kdm6a*, with expression reported across multiple tissues and developmental stages in male mice (Greenfield et al., 1996) and humans (Lahn and Page, 1997). Although there is a high degree of sequence conservation between the two genes, conflicting *in vitro* evidence exists regarding whether or not *Uty* has histone demethylase activity. Walport and colleagues support common functionality, whereas separate reports by Lan and Hong do not (Walport et al., 2014; Lan et al., 2007; Hong et al., 2007).

UTY is required for normal spermatogenesis in human (Foresta et al., 2000), and the protein also has a role in self recognition as part of the innate immune reponse. An epitope of UTY forms an MHC peptide (Warren et al., 2000) that contributes to graft rejection after HLA identical sex mismatched stem cell transplantation (Vogt

et al., 2000). Furthermore, in a male donor/female recipient situation, UTY specific peptides show gender specific antitumour effect *in vitro* (Ivanov et al., 2005; Riddell et al., 2002; Warren et al., 2000).

In the mouse mutant, UTY partially compensates for the absence of UTX in male embryos, suggesting some degree of functional conservation between the homologues. Whether this is demethylase dependent remains an open question (Shpargel et al., 2012; Walport et al., 2014). *Utx* mutant embryos are born at a sub Mendelian ratio and show life long growth retardation, though have normal fertility (Shpargel et al., 2012). The *Utx*/*Uty* compound mutant phenocopies the homozygous mutant female and is embryonic lethal (Shpargel et al., 2012).

1.6.5 *Eif2s3x*

Eukaryotic initiation factor 2 (eIF-2) is made up of three subunits, α, β, and γ. In the presence of guanosine triphosphate (GTP), the three subunits form a ternary complex with Met-tRNA and recruit it to the 40S ribosomal complex for translation initiation (Merrick, 1992). Subunit 2γ was initially described by Gaspar and colleagues (Gaspar et al., 1994), and subsequent work recognised that whilst this is a single X linked gene in human, there are two highly homologous genes on the X and Y chromosomes in mouse, *Eif2s3x* and *Eif2s3y*, respectively (Ehrmann et al., 1998).

Both mouse and human X linked orthologues are expressed ubiquitously and escape XCI (Ehrmann et al., 1998). Interestingly, higher concentrations of *Eif2s3x* transcript were found in XX females in both developing (Armoskus et al., 2014) and adult brain, and adult liver, when compared to XY males (Xu et al., 2006). However, this did not translate into differences at the protein level in adult brain or kidney (Xu et al., 2006). It is certainly possible that the low number of tissues and timepoints assayed in the latter experiment could have failed to detect relevant biological differences.

Similar to a number of other ubiquitously expressed X linked genes, EIF2S3X functions in multi protein complexes, and mutations are implicated in causation of XLID (Borck et al., 2012). Three male patients of Moroccan Jewish ancestry showed microcephaly, facial dysmorphism, and short stature, along with more specific neurological signs (Borck et al., 2012). Using human cells overexpressing one of these patient derived γ mutations, and yeast with an equivalent mutation, a defect in binding between the β and γ subunits was uncovered (Borck et al., 2012). In the yeast model, this defect impaired translation start codon selection and eIF2 function; and was rescued by overexpression of the β subunit. Although there is no Y linked homologue in human, an autosomally transposed copy of the gene exists (Ehrmann et al., 1998; Hughes et al., 2015), and it would be interesting to sequence this gene in the context of these patients to assess the degree of functional conservation. *Eif2s3x* is able to compensate for the loss of *Eif2s3y* in mouse spermatogenesis when present as a transgene in high copy number (Yamauchi et al., 2016), supporting the hypothesis that dosage of the X-Y gene pairs is critical in certain stages in certain tissues.

1.6.6 *Eif2s3y*

Eif2s3y was mapped to the mouse Y chromosome concurrent with the identification of *Eif2s3x* (Ehrmann et al., 1998). It is the only Y linked gene required to complete the first meiotic division in male mouse gametogenesis (Mazeyrat and Mitchell, 1998; Mazeyrat et al., 2001). Like *Eif2s3x*, *Eif2s3y* also shows ubiquitous expression (Xu et al., 2002). In mouse brain, three isoforms of the gene have been detected, compared to one isoform of the X linked homologue; with the former showing a higher ratio of embryonic:adult expression than the latter (Xue et al., 2002). There is no human orthologue of *Eif2s3y*. It is hypothesised that the loss is partly compensated for by retrotransposition to an autosome, which has occurred on three independent occasions in primates (Hughes et al., 2015); and that *DDX3Y* has an equivalent role in human spermatogenesis (Ditton et al., 2004).

1.6.7 *Ddx3x*

The first *Ddx3x* sequence was identified in mouse erythroid cells as mDEAD3 during a screen for RNA helicase genes (Gee and Conboy, 1994). This family had been previously been characterised as ATP dependent remodellers of nucleic acid secondary structure, all having in common the amino acid sequence D-E-A-D within the ATP binding domain (Linder et al., 1989), and showing high degrees of DNA sequence conservation from yeast to mammals (Gee and Conboy, 1994; Linder, 2006; Chu et al., 2006). The human orthologue, originally known as *DBX*, was mapped to the X chromosome (Park et al., 1998), shortly after its Y homologue was identified in a somatic cell hybrid search (Lahn, 1997). Both human and mouse genes have been shown to escape XCI, and are expressed ubiquitously (Lahn, 1997; Disteche et al., 2002).

As a member of the DEAD box protein family of RNA helicases, DDX3X has nine conserved structural motifs that facilitate its involvement in a wide variety of cellular processes (Cordin et al., 2006), including: pre mRNA splicing (Deckert et al., 2006), nuclear export and transport of RNA (Yedavalli et al., 2004; Kanai et al., 2004), translation initiation and regulation (Beckham et al., 2008; Shih et al., 2008), cell cycle regulation (Chang et al., 2005; Chao et al., 2006; Huang et al., 2004; Sekiguchi et al., 2007), and apoptosis (Sun et al., 2008). Likely resulting from this key role in RNA homeostasis, DDX3X is a host factor required for the replication of human immunodeficiency virus (HIV, Yedavalli et al., 2004; Sharma and Bhattacharya, 2010; Liu et al., 2011; Garbelli et al., 2011) and hepatitis C virus (HCV, Owsianka and Patel, 1999; Mamiya and Worman, 1999; Ariumi et al., 2007; Li et al., 2009b; Sun et al., 2010), in addition to its interaction with tank binding kinase 1 (TBK1) that results in the production of antiviral type I interferons (Soulat et al., 2008).

The ubiquitous expression and wide ranging involvement of DDX3X in multiple intracellular processes raises the question of what happens when a mutation arises, both experimentally and in the context of human health. The first reported work

in mouse embryos suggested an essential role for *Ddx3x* in early development (Li et al., 2014). Using short interfering RNA (siRNA) microinjection into mouse zygotes, a reduction in cell numbers was observed, which correlated with an increase in apoptosis and decreased progression to blastocyst when compared to scramble controls. The authors also noted that this phenotype was associated with p53 accumulation (Li et al., 2014), confirmed by later work (Chen et al., 2016a). Chen and colleagues created a conditional allele by inserting loxP sites 5' to exon 3 and 3' to exon 17 of *Ddx3x*, and initially showed that F1 animals inheriting the floxed allele on the X^p had a normal phenotype. When this same floxed allele was inherited maternally, females showed growth retardation from E12.5, then perished between E14.5 and E16.5, concurrent with evidence of oedema and peripheral haemorrhage. On further analysis of the placenta in these mutants, the labyrinth was vascularised abnormally, the spongiotrophoblast was thinner, and all placentas were smaller than wildtype littermates. A *Sox2*-Cre was then used to target the deletion specifically to the embryo and not the extraembryonic tissue, and these embryos were grossly normal with no significant deviation from Mendelian ratio at birth. Male conceptuses carrying the deleted allele died around E9.5, and those with the *Sox2*-Cre floxed allele in just the embryo were found to have abnormalities in neural tube closure, cardiac development, and chorio allantoic fusion, along with increased apoptosis in the embryo proper. Taken together, these results suggest that *Ddx3x* either shows tissue and developmental time specific variable escape from XCI; or that although the paternal allele escapes, expression is not sufficient to compensate for the lack of the maternal allele. Moreover, at least one copy of *Ddx3x* is required for normal embryonic development in the mouse, and the presence of *Ddx3y* alone is not sufficient.

Mutations in *DDX3X* have been associated with a variety of cancers, including HCC (Chang et al., 2005), head and neck squamous cell carcinoma (Stransky et al., 2011), oral squamous cell carcinoma (Koshio et al., 2013), lung cancer (Bol et al., 2015a), chronic lympocytic leukaemia (CLL, Wang et al., 2012), colorectal cancer (Su et al., 2015), and medulloblastoma (Jones et al., 2012; Pugh et al., 2012; Robinson et al.,

2012). Whilst there seems to be no consensus over the exact role of *DDX3X* in cancer pathogenesis, a number of small molecule inhibitors are being developed (Samal et al., 2015; Bol et al., 2015a,b).

Finally, *DDX3X* mutations have also been correlated with incidence of XLID and autism spectrum disorders, as part of a syndromic disorder with significant neurological involvement (Blok et al., 2015). The authors suggest functional mosaicism results in haploinsufficiency and a dose dependent phenotype (Blok et al., 2015).

1.6.8 *Ddx3y*

DDX3Y, also known as *DBY*, is ubiquitously transcribed in both human and mouse (Lahn and Page, 1997; Ditton et al., 2004; Foresta et al., 2000). Similar to *UTY*, *DDX3Y* was first recognised as a Y linked antigen, responsible for the rejection of human leucocyte antigen (HLA) matched allografts (Chen et al., 2004b). *In vitro* data suggest that it is able to functionally compensate for the loss of its X linked homologue *DDX3X* (Sekiguchi et al., 2004), thus implicating the protein in RNA folding and metabolism (for full description see section 1.6.7). DDX3Y is almost exclusively detected in the cytoplasm of spermatogonia, and individuals carrying mutations have severe germ cell loss (Ditton et al., 2004). In order to model this phenotype *in vitro*, human induced pluripotent stem cells (iPSCs) can be directed to differentiate into germ cell like cells. This ability is compromised in cells carrying *DDX3Y* mutant allele, but can be rescued by the addition of DDX3Y (Ramathal et al., 2015). Furthermore, during a neuronal differentiation programme, siRNA knockdown of *DDX3Y* reduced cell growth, proliferation and viability, and increased apoptosis (Vakilian et al., 2015), though humans with reduced levels of/mutations in DDX3Y show no apparent somatic phenotype (Ditton et al., 2004): this discrepancy remains to be explained.

1.6.9 X-Y gene pairs: summary

As these X-Y gene pairs have persisted across evolutionary space and through time, it can be deduced that they might have adopted a common survival strategy, implying a collective functional significance. A number of lines of evidence support this conclusion (summarised in Table 1.2). Following a gene expression analysis in eight mammalian species across multiple tissues and through developmental time, it was shown that X-Y pair genes are more broadly expressed than other ancestral survivors on the Y chromosome (Bellott et al., 2014). The authors reasoned that wide expression could constrain selection to prevent both loss of the Y linked gene and the appearance of a dosage compensated X linked replacement. Most X linked genes of the X-Y pairs escape X chromosome inactivation (see section 1.4.2) in human, mouse and opossum, thus preserving biallelic expression (Carrel and Willard, 2005; Yang et al., 2010; Wang et al., 2014). These genes are subject to stronger purifying selection than genes subject to XCI (Bellott et al., 2014; Park et al., 2010; Slavney et al., 2016). When added to the observation that all have functions pertaining to transcription, translation, splicing, chromatin modification, and ubiquitination (see above, and Bellott et al., 2014; Cortez et al., 2014), it becomes clear that the common factor is preservation of dosage.

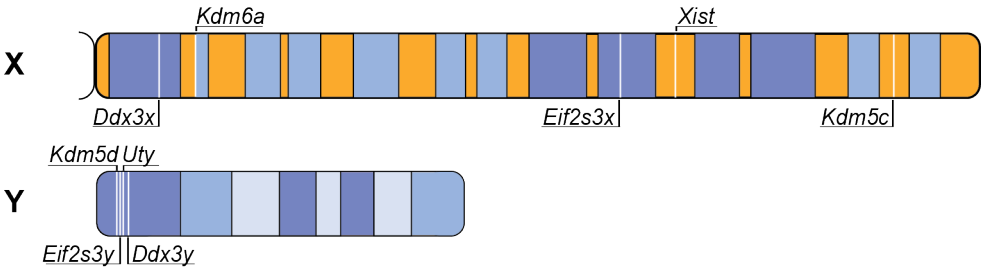

Figure 1.4: Cartoon depicting relative positions of X-Y gene pairs on mouse X and Y chromosomes. Banding is representative and not to scale.

Mouse gene (alternative names)	XCI status	Y homologue (alternative names)	%AA homology	Expression pattern	Mutant phenotype		
					Heterozygous female	**Homozygous female**	**Hemizygous male**
Ddx3x (*Dbx*)	Escapes	*Ddx3y* (*Dby*)	88	Ubiquitous	No phenotype when inherited paternally; growth retardation and embryonic lethality when inherited paternally; specifically required for ExE development	Not generated: likely lethal	Early embryonic lethality
Eif2s3x	Escapes	*Eif2s3y*	98	Ubiquitous	None reported	None reported	None reported
Kdm5c (*Jarid1c*, *Smcx*)	Escapes	*Kdm5d* (*HY*, *Jarid1d*, *Smcy*)	80	Ubiquitous	None reported	None reported	None reported
Kdm6a (*Utx*)	Escapes	*Uty*	76	Ubiquitous	No phenotype	Cardiac malformation, neural tube closure defects, embryonic lethality	Reduced perinatal viability, life long growth deficit

Human gene (alternative names)	XCI status	Y homologue (alternative names)	%AA homology	Expression pattern	Mutant phenotype	
					Female	**Male**
DDX3X (*DBX*)	Escapes	*DDX3Y* (*DBY*)	92	Ubiquitous	XLID	XLID
EIF2S3X	Escapes	n/a	n/a	Ubiquitous	Mutations reported, no obvious phenotype	XLID, short stature
KDM5C (*JARID1C*, *SMCX*)	Escapes	*KDM5D* (*HY*, *JARID1D*, *SMCY*)	85	Ubiquitous	Mild XLID, skewed XCI to inactivate mutation harbouring X	XLID
KDM6A (*UTX*)	Escapes	*UTY*	83	Ubiquitous	XLID, short stature, Kabuki syndrome	As female, more severe

Table 1.2: Extant X-Y gene pairs in mouse and human.

1.7 Aims

In conclusion, there is abundant evidence that sex chromosome genes control growth at two stages of mammalian development. *In utero*, the growth deficit observed in X^PO embryos is likely explained either by genomic imprinting or inappropriate imprinted *Xist* expression. Postnatally, haploinsufficiency underlies the growth deficit seen in all XO mice relative to XX littermates. However, the genetic bases of these effects is not known.

The overall aim of my thesis is to identify possible mechanisms for both phenotypes, which could subsequently open new avenues of exploration to further understand the phenotypic effects of Turner syndrome for the three million women with the condition worldwide.

- In Chapter 3, I will test whether inappropriate *Xist* expression is responsible for the embryonic growth deficit in X^PO embryos.

- In Chapter 4, I will describe experiments carried out to identify X linked imprinted genes expressed in mouse trophoblast stem cells as a model for mouse placenta.

- In Chapter 5, I will test whether haploinsufficiency for *Ddx3x*, *Kdm5c*, *Kdm6a*, or *Eif2s3x* are responsible for the postnatal growth deficit in XO female mice.

- Chapter 6 describes initial experiments to address the functional divergence of X encoded genes *Ddx3x*, *Kdm5c*, *Kdm6a*, and *Eif2s3x* from their Y homologues *Ddx3y*, *Kdm5d*, *Uty*, and *Eif2s3y*.

Chapter 2

Materials and Methods

2.1 Mouse work

2.1.1 Mouse strains

All mice used were generated and maintained on an outbred albino MF1 background (originating from MRC National Institute for Medical Research and Harlan (Blackthorn, UK)), unless otherwise stated. Specific crosses are detailed within the relevant chapters, and a summary of the origin of their constituent mutants is provided below.

2.1.1.1 In(X)1H: a large inversion in the X chromosome

The In(X)1H mutation was first reported in the offspring of a male that had received a fractionated dose of X rays to the spermatogonia (Russell, 1961; Evans and Phillips, 1975). It was noted that In(X)1H heterozygous females produced greater than expected numbers of $X^{P}O$ progeny (Evans and Phillips, 1975). Furthermore, the presence of an In(X)1H allele suppressed crossing over between previously reported X-linked mutants, including *Bpa*, *Ta*, and *Blo* (Phillips and Kaufman, 1974), suggesting a structural mutation of the X chromosome (Evans and Phillips, 1975). Cytogenetic and genetic evidence showed that the inversion spans almost the entire

length of the chromosome, and further work revealed that the formation of a dicentric chromatid during meiosis leads to the production of nulli-X oocytes (Koehler et al., 2002). Around 15% of offspring from a XY x In(X)/X cross are $X^{P}O$ (Burgoyne et al., 2002).

In this thesis, the In(X)1H line was used to generate $X^{P}O$ embryos for experiments described in Chapters 3 and 4, and $X^{P}O$ females for experiments described in Chapter 5.

2.1.1.2 Y*: a rearrangement in the Y chromosome

The Y* chromosome is a Y chromosome with a non-Y centromere that is attached to an inverted region of the Y PAR (Eicher et al., 1991). During male meiosis, recombination between the Y* and X chromosomes results in the generation of a large X^{Y*} chromosome and a small $X*^{Y}$ chromosome, and additionally a number of gametes lacking a sex chromosome (Burgoyne and Evans, 2000). The large chromosome consists of almost the entire X chromosome, in addition to the Y* chromosome without the Y* centromere. The small $X*^{Y}$ is essentially the centromeric portion of the Y* chromosome in addition to a PAR (Burgoyne and Evans, 2000).

Offspring inheriting the X^{Y*} chromosome develop as males but are sterile, likely due to the presence of two X chromosomes (Cattanach, 1961). In the absence of a second X chromosome, i.e. $X^{Y*}O$, a proportion of males carrying the X^{Y*} chromosome are fertile (Trent et al., 2012). Offspring inheriting the $X*^{Y}$ chromosome are female and fertile. Offspring inheriting gametes lacking a sex chromosome will contribute to forming $X^{M}O$ embryos.

In this thesis, the Y* line was used to generate $X^{M}O$ and $XY*^{X}$ females for experiments described in Chapter 5. It was also used to generate $X^{Y*}O$ males for Chapter 4.

2.1.1.3 Y^{Tdym1}TgN(Sry-129)2Ei: a deletion in *Sry*

The Y^{Tdym1}TgN(Sry-129)2Ei mutation consists of a 14kb deletion in *Sry*, and was generated in mESCs before injection into blastocysts to produce chimeric founders (Lovell-Badge and Robertson, 1990; Gubbay et al., 1992). It can be used to generate XY female offspring and, when complemented by an autosomally located *Sry* transgene, XX male offspring (Mahadevaiah et al., 1998).

In this thesis, the Y^{Tdym1}TgN(Sry-129)2Ei line was used to generate XY females (denoted XY^{-}) in Chapter 4. It was complemented by an *Sry* transgene and used to generate XX males (denoted XX*Sry*) in Chapter 6.

2.1.2 Timed matings

All animal work was carried out under UK Home Office license. Mice were kept on a 12:12 light:dark cycle, with food and water available *ad libitum*. Female and male mice were housed separately, with stud males alone and females in groups according to the cage size. Matings were set up as follows: at around 17:00 female mice would be placed into the male mouse cage, removed early the next morning and checked for the presence of a vaginal plug, which usually indicates a mating has taken place. Mating was assumed to take place during the hours of 00:00-02:00.

2.1.3 Blastocyst isolation

For the derivation of cell lines, blastocysts were retrieved at embryonic day (E) 3.5, as follows. Previously plugged females were culled via cervical dislocation, and death confirmed by severing the carotid artery. The uterine horns were removed into follicle holding medium (FHM, Appendix A), and flushed with a further 0.5-1ml of FHM utilising a 27G steel needle. Blastocysts were visualised on a Leica MC80 dissecting microscope (Leica: Wetzlar, Germany), collected using a Stripper® pipette (Origio: Malov, Denmark), and washed through a series of drops

of FHM, before a final wash and plating in the required derivation media (see below: 2.5.1, 2.5.2).

2.1.4 Isolation of post implantation embryos

Pregnant dams were culled as above at the appropriate time *post coitum*, and the uterine horns removed and placed in ice cold phosphate buffered saline (PBS, Thermo Scientific: Waltham, USA). Individual embryo sacs were dissected free of maternal tissue, and the embryo was freed from the membranes. After weighing and somite counting (when applicable: see section 2.1.6), representative images were taken with the Leica IC80 camera attached to Leica MC80 dissecting microscope, and acquired using LeicaAcquire software version 3.1 (all Leica: Wetzlar, Germany). Embryos were then frozen in liquid nitrogen before storage at 80°C awaiting genotyping.

2.1.5 Weighing of post implantation embryos

Each embryo was placed on a 30mm Petri dish and fluid removed with the corner of a lint free tissue, before weighing on a Sartorius Cubis analytical balance MSE225P (Sartorius: Gottingen, Germany).

2.1.6 Somite counting of post implantation embryos

Following imaging, phase contrast was used to obtain the best lighting, and somites were counted manually.

2.1.7 Generation of CRISPR targeted lines

2.1.7.1 Guide design and synthesis

Guide sequences were designed using MIT CRISPR Designer (Cong et al., 2013); *BbsI* restriction sequences were added to the 5' end; and oligonucleotides were

ordered (Appendix B, Eurofins: Ebersberg, Germany). Oligonucleotides were then cloned into plasmid PX330 (Cong et al., 2013), and this was transformed into chemically competent *E. coli*. Clones were screened for positive ligation by Sanger sequencing. A T7 promoter was then added to the guide sequence via PCR amplification, and sgRNA was produced by *in vitro* transcription using HiScribe T7 High Yield RNA Synthesis Kit (NEB: Ipswich, USA), and purified by MEGAclear Transcription Clean-Up (Thermo Scientific: Waltham, USA). *Cas9* mRNA was synthesised using the same method with alternative primers.

2.1.7.2 Microinjection of pronuclear mouse embryos

Cas9 mRNA and sgRNA were mixed at 100ng/ul and 50ng/ul respectively, centrifuged at 13,000rpm for 15 minutes at 4°C, and the supernatant moved to a new tube to remove any contamination from cleaning column fibres. Microinjection was performed by Genetic Manipulation Service Science Technology Platform (STP) into pronuclear stage mouse embryos following on from a standard superovulation protocol and *in vitro* fertilisation. Injected embryos were cultured overnight before transfer to pseudopregnant females.

2.1.7.3 Analysis of founder animals

Pups were ear biopsied at three weeks of age and, following DNA extraction, PCR (see 2.2.4) was carried out to amplify the locus surrounding the CRISPR target site. During early stages of the project PCR products were TA cloned (see 2.2.6) and Sanger sequenced; subsequently this was replaced by the Illumina MiSeq platform (see 2.6.1).

2.1.8 Weighing postnatal animals

Following successful mating, pregnant dams were housed alone and, on the day of birth, pups were weighed following tattooing/toe clipping (see below), and weekly until 35 days old, using a Scout Pro balance (Ohaus: New Jersey, USA). Pups were

housed with the dam until weaning at three weeks of age, and subsequently male and female pups were housed separately.

2.1.9 Identification of individuals

In initial experiments, new born pups were marked using a subcutaneous injection of black pigment (VWR: Lutterworth, UK) as follows: pups were incubated in a 10cm plastic dish on ice water for three minutes to provide light anaesthesia/analgesia; skin was cleaned with 70% EtOH and sterile gauze, and a 33G needle and glass syringe (Hamilton Company: Nevada, USA) were used to inject 2ul pigment subcutaneously into the paw pad; pups were kept on a heat pad until righting reflex was re gained.

In subsequent experiments, toe clipping was performed in order to identify individual animals: this method was faster and provided tissue for genotyping where required, removing the requirement for a subsequent ear biopsy procedure later. Local anaesthesia was applied to the paw. After an appropriate time, the distal phalanx was removed from one digit per animal, and any bleeding cauterised chemically with silver nitrate. Pups were again kept on a heat pad until return to the dam.

2.2 Molecular biology

For PCR, primer sequences were either obtained from previously published work or designed using Primer3 (Untergasser et al., 2007). All PCR primer sequences are provided in Appendix B; where commercial sources have been used, this is indicated.

2.2.1 Genomic DNA (gDNA) extraction

Generally, gDNA was extracted from mouse tissue samples lysed in KT buffer (Appendix A), by overnight incubation at 55°C, followed by 15 minutes at 95°C and five minutes centrifugation at 13,000rpm, room temperature (RT). For qRT-PCR (sec-

tion 2.2.5.2), gDNA was extracted using PureLink (Thermo Scientific, Waltham, USA), as per the manufacturer's protocol.

2.2.2 RNA extraction

Total RNA was extracted from frozen tissue samples and cell cultures using TRIzol (Thermo Fisher: Waltham, USA) or TRI reagent (Sigma-Aldrich: St Louis, USA) as per the manufacturers' protocols. When amount of available tissue was limited (i.e. E10.5 embryo) and both RNA and DNA were required, DNA was extracted from the lower phase, also per manufacturer's instructions. Extracted RNA was dissolved in ddH2O and quantified using a Nanodrop spectrophotometer (Thermo Fisher: Waltham, USA).

2.2.3 cDNA synthesis

Synthesis of cDNA for qRT-PCR was described in section 2.2.5.2. For general cDNA synthesis, total RNA was added to oligo(dT) (Thermo Fisher: Waltham, USA) and 10mM dNTPs and incubated at 65°C for five minutes. First strand buffer, DTT and RNAse Out (all Thermo Fisher) were then added and, following a further two minute incubation at 42°C, Superscript II (Thermo Fisher: Waltham, USA) was added, and the mixture incubated at 42°C for another 60 minutes. The enzyme was heat inactivated at 70°C for 15 minutes.

2.2.4 Polymerase Chain Reaction (PCR)

For standard genotyping, 0.5ul of tissue lysis supernatant was added to 2X MyTaq Redmix (Bioline: London, UK). Primers (Eurofins MWG: Ebersberg, Germany) were used at a final concentration of 0.2nM. For PCR to be followed by sequencing, the high fidelity q5 Taq polymerase was used, as per the manufacturer's protocol (NEB: Ipswich, USA). Product was loaded onto an agarose (Sigma-Aldrich: St Louis, USA) gel with 1kb ladder (Thermo Scientific: Waltham, USA) and run at

around 85V for an appropriate time. Images were then acquired using AlphaImager 2200 (ProteinSimple: California, USA) with AlphaImager software.

2.2.5 Quantitative real time PCR

2.2.5.1 qRT-PCR on gDNA

To assess X chromosome copy number, gDNA was quantified using qRT-PCR, as previously described (Yamauchi et al., 2015), but with minor variation. gDNA extracted using PureLink was amplified with primers targeting *Amelx* and *Prdx4* on the X chromosome, and *Myogenin* as an autosomal control. Both X linked gene products were normalised to the autosomal control (to generate ΔCt values), before comparison with a known XX sample (to generate ΔΔCt values, as per Livak method (Livak and Schmittgen, 2001)). The reaction was performed using SensiMix LoRox polymerase (Bioline: London, UK), on a ABI 7500 thermal cycler (Thermo Scientific: Waltham, USA).

2.2.5.2 qRT-PCR on cDNA

RNA was extracted as described (section 2.2.2). For relative quantification of gene expression, RNA was converted to cDNA using the Maxima First Strand cDNA Synthesis Kit following the manufacturer's protocol (Thermo Scientific: Waltham, USA). Briefly, between 500ng and 5ug total RNA was first treated with double stranded DNase, before conversion to cDNA using reverse transcriptase with a mix of random hexamer and oligo(dT) 18 primers. Minus reverse transcription controls were utilised to detect the presence of contaminating genomic DNA. Primers were first tested for specificity and efficiency via melt curve analysis and standard curve methods, respectively: the pairs that showed a single peak during the melt curve analysis and an efficiency of 2 +/- 0.1 were deemed suitable for use. On occasion, multiple primer pairs designed to amplify a given locus failed testing, so a commer-

cial alternative was sought and used following manufacturer's protocol (Taqman, Thermo Scientific: Waltham, USA).

384 plates were prepared with Lightcycler 480 Sybr Green I mastermix (Roche: Basel, Switzerland) as per the manufacturer's protocol; reactions were performed in triplicate and run on the Lightcycler 480 II thermal cycler (Roche: Basel, Switzerland). Data were exported from the proprietary software to Excel (Microsoft: Washington, USA) for statistical testing based on the Livak method (previous section).

2.2.6 TA cloning

PCR products were TA cloned (TOPO, Thermo Fisher: Waltham, USA). Cultures were grown from colonies in Luria Broth (LB), DNA was extracted by mini prep according to the manufacturer's instructions (Qiagen: Manchester, UK), and clones were Sanger sequenced by Beckman-Coulter genomics (Takley: Essex, UK) using M13 primers.

2.2.7 RFLP digest

SNPs were selected using the Mouse Genomes Project online browser (Wellcome Trust Sanger Institute), DNA sequences were acquired from UCSC Genome Browser (build GRCm38/mm10). Restriction enzymes were selected using NEBcutter (NEB: Ipswich, USA). Total RNA was extracted from mouse brain and liver and transcribed into cDNA as described (see 2.2.2, 2.2.5.2). Following PCR, products were run on a 2% agarose gel, isolated using a scalpel blade and UV light box, and purified using NucleoSpin ® PCR Gel and PCR Clean-up (Machery Nagel: Duren, Germany) according to the manufacturer's instructions. Products were then digested with restriction enzymes (all NEB: Ipswich, USA) as per manufacturer's guidelines, run on a 2% agarose gel, and visualised as described (2.2.4).

2.3 Cytology

2.3.1 Metaphase chromosome spreads for karyotyping

Mice were culled as described above. Using a 1ml syringe filled with HEPES buffered RPMI medium (Thermo Fisher: Waltham, USA) supplemented with colcemid (0.1ug/ul; Sigma-Aldrich: St Louis, USA), a 27G needle was inserted into the distal end of the femur, and bone marrow was flushed into a 15ml round bottomed polypropylene tube (Greiner Bio-One: Stonehouse, UK) with 0.5ml solution per femur. The tube was incubated horizontally for 10 minutes at 31°C, vortexed briefly and centrifuged at 180 x *g* for five minutes in a swinging rotor centrifuge at RT. The supernatant was drained, the pellet re suspended in 1-2ml 0.56% w/v potassium chloride (Sigma-Aldrich: St Louis, USA) dissolved in ddH2O, and the tube incubated at RT for at least 20 minutes. Following a further brief vortex and spin as previously, the supernatant was carefully drained, methanol:glacial acetic acid (3:1; MA) was added down the side of the tube, drop wise, until the pellet was coated, and the tube rotated to ensure even coverage. 1ml of MA was then added, and the tube vortexed briefly to re suspend the pellet, quickly followed by further centrifugation as before. The supernatant was drained carefully, 1-2ml of MA was added, and the tube incubated for 15 minutes at RT. Two further consecutive washes were carried out: first, the tubes were centrifuged as previously, followed by draining of the supernatant, fresh 1ml MA added, and the solution vortexed. After the second drainage step, a suitable amount of MA was added to result in a good final density of cells on the slides (judged based on experience, around 1ml); the tube was vortexed, left to settle for 30 seconds, and then three drops were spread onto a cleaned (98% EtOH/2% acetic acid) glass slide (VWR: Lutterworth, UK), from a height of about 30cm. After air drying, the slides were stained in 4% Giemsa buffered in PBS (pH 6.8, Sigma-Aldrich: St Louis, USA) for eight minutes, then viewed under an Olympus BH2 microscope (Olympus: Tokyo, Japan), and imaged using a Leica camera (Leica: Wetzlar, Germany). When used for DNA FISH, one

drop of the final MA fixed cell suspension was spread onto multi well glass slides (Thermo Scientific: Waltham, USA) and left to air dry.

2.3.2 DNA FISH

2.3.2.1 BAC extraction

BAC clones (Appendix C) were selected using Ensembl genome browser (Mouse, GRCm38) and obtained as stabs from CHORI BACPAC (California, USA). Cultures were set up using 20ml LB inoculated with chloramphenicol (25ug/ml, dissolved in 100% EtOH) and incubated at 37°C, 200rpm overnight. Glycerol stock was made using 500ul culture and 500ul 100% glycerol (autoclaved; Sigma-Aldrich: St Louis, USA), and stored in a 1ml Nunc tube (Thermo Fisher: Waltham, USA) at -80°C. The cultures were then centrifuged at 4500rpm, 4°C for 15 minutes. After discarding the supernatant, the pellet was resuspended in P1 (Appendix A) by vortexing; P2 (Appendix A) was then added, and the solution was inverted 20 times to mix, followed by an incubation of five minutes at RT. P3 (Appendix A) was added, and once again the solution was inverted 20 times to mix and incubated on ice for five minutes. The solution was then centrifuged at RT for 10 minutes at 13,000rpm, the supernatant transferred to fresh tubes, and 0.6 volumes of RT isopropanol was added, with inversion to mix; followed by immediate centrifugation at RT for 15 minutes, 13,000rpm. The supernatant was discarded, the pellet washed with 75% EtOH, and subsequently centrifuged down at 12,000rpm for 5 minutes at RT. The EtOH was then discarded and the pellet air dried, followed by resuspension in ddH2O. DNA was incubated overnight at 37°C with RNAse A (Sigma Aldrich: St Louis, USA). The next day, RNAse A was removed using subsequent washes of equal volume phenol, phenol:chloroform, and chloroform:isoamyl alcohol (all Sigma-Aldrich: St Louis, USA). 1:10 3M NaAc at pH5.2 and 2.5X 100% EtOH were added to the final supernatant, which was centrifuged at 13,000rpm for 15 minutes at 4°C. The supernatant was discarded, and the pellet washed with 75% EtOH; finally, the DNA was dissolved in ddH2O.

2.3.2.2 Probe labelling

Approximately 1ug BAC DNA was incubated with Abbott nick translation enzyme and either Spectrum Green dUTP, Spectrum Red dUTP (all Abbott Molecular: Illinois, USA), or Cy5 dUTP (Jena Bioscience: Jena, Germany) at 15°C for 12 hours. 1/10 of this reaction was run on a 2% agarose gel at 85V for 45 minutes to check for probe size of around 200bp. If the probe was found to be greater than 300-400bp, the reaction was incubated for varying times (minutes) at 37°C and the electrophoresis step repeated.

In order to prepare one probe for one slide, 1/10 of this reaction was added to 3ul mouse Cot1 DNA and 1.5ul salmon sperm (both Thermo Fisher: Waltham, USA); the mix was then precipitated using 2.5X 100% EtOH, mixed, and then centrifuged at 4°C for 15 minutes, 13,000rpm. The supernatant was removed, the pellet washed with 70% EtOH, and after centrifugation for five minutes at 13,000rpm, left to air dry. The probe was then dissolved in deionised formamide (Sigma-Aldrich: St Louis, USA) and either used immediately or stored at -20°C.

2.3.2.3 Hybridisation

Slides were washed in 2X saturated sodium citrate (SSC, Appendix A), and denatured in 70% formamide/30% 2XSSC at 75°C, before dehydration through a series of EtOH. Concurrently, the probe was denatured at 75°C and pre hybridised in hybridisation buffer (Appendix A). Probes were added to slides, followed by coverslips, and hybridisation took place in a formamide humid chamber overnight at 37°C. The following day, slides were washed four times in 2XSSC, then 0.1XSSC, before transfer to 4XSSC/0.1% Tween (Sigma-Aldrich: St Louis, USA). 4',6-diamidino-2-phenylindole (DAPI, Sigma-Aldrich: St Louis, USA) was then used to stain the slides for 10 minutes, before a final brief wash in 4XSSC/0.1% Tween, followed by mounting in Vectashield (Vector Laboratories: Burlingame, USA). Slides were visualised using an Olympus IX70 inverted microscope (Olympus: Tokyo,

Japan) with a 100 W mercury arc lamp and a 1003/1.35 UPLAN APO oil immersion objective; images were analysed using FIJI (ImageJ version 2.0.0).

2.4 Protein extraction and western blotting

2.4.1 Tissue harvest and protein extraction

Tissue was collected by dissection, snap frozen in liquid nitrogen, and stored at -80°C until required. Upon thawing, tissue was placed into a 2.0ml reinforced plastic tube (Bertin Instruments: Montigny-le-Bretonneux, France) containing RIPA buffer (Appendix A) and two-three metal beads (Bertin Instruments: Montigny-le-Bretonneux, France), and stored on ice for 15 minutes. Subsequently the samples were run on the Precellys 24 (Bertin Instruments: Montigny-le-Bretonneux, France) and for 45 seconds to break up the tissues. Following centrifugation at 13,000rpm, 4°C for 30 minutes, the supernatant was removed to a new tube and stored on ice.

2.4.2 Protein quantification

Protein extract supernatant was diluted 1:100 and subjected to a bicinchoninic acid assay (BCA, Thermo Scientific: Waltham, USA) as per the manufacturer's protocol. A standard curve was prepared using bovine serum albumin (BSA, Sigma-Aldrich: St Louis, USA). Colour change was quantified with Infinite M1000 Pro (Tecan: Mannedorf, Switzerland), and analysed using proprietary Tecan software. Following quantification, protein extract was stored at -80°C until required.

2.4.3 Western blotting

20-30mg protein was prepared for sodium dodecyl sulphate polyacrylamide gel electrophoresis (SDS-PAGE) by dilution with Laemmli loading buffer (Appendix A). Samples were run on a polyacrylamide gel (generally 4-15%, Bio-Rad: Her-

cules, USA) in running buffer (Appendix A); initially at 85V for 15 minutes and then 200V until an appropriate separation was achieved. This was judged by the running of a protein ladder: either Dual Color Standard (Bio-Rad: Hercules, USA), or PageRuler Prestained (Thermo Scientific: Waltham, USA). Proteins were transferred from gel to nitrocellulose membrane (GE Healthcare Life Sciences: Amersham, UK) in transfer buffer (Appendix A) at 100V, 4°C for 60 minutes. Following blocking in Tris buffered saline Tween (TBS-T: Appendix A) with either 5% milk or BSA (both Sigma-Aldrich: St Louis, USA), membranes were incubated with primary antibody (see Appendix C for list) by rolling overnight at 4°C. The next day, washes were performed in TST-T, followed by incubation in secondary antibody (Appendix C) at room temperature for 60 minutes. TBS-T washes were again performed, and signal was generated using enhanced chemiluminescence (ECL) substrate, as per the manufacturer's protocol (Bio-Rad: Hercules, USA). Detection was performed in a dark room with Hyperfilm ECL (GE Healthcare Life Sciences: Amersham, UK), and film was developed for visualisation.

2.5 Cell culture

Unless otherwise stated, all cell culture plasticware was obtained from Nunc (Thermo Fisher: Waltham, USA), and media components from Invitrogen (Thermo Fisher: Waltham, USA).

2.5.1 Mouse trophoblast stem cells (mTSCs)

mTSCs were derived and cultured as described previously (Himeno et al., 2008), and summarised below.

2.5.1.1 Derivation and maintenance

Gamma irradiated MEFs (section 2.5.3.1) were plated in 4 well plates at 4 x 10^4 cells per well, using mTSC medium (Appendix A). The next day, human recom-

binant FGF4 (25ug/ml; Peprotech: London, UK) and heparin (1mg/ml; Sigma-Aldrich: St Louis, USA) were freshly added to mTSC medium (mTSCM), and this was applied to the MEFs. Blastocysts were harvested at E3.5 as described above (section 2.1.3), and one embryo was added per well of MEFs. When embryos were observed to attach to the MEFs, medium was changed, and then subsequently every second day. Outgrowths appeared over the next three-five days, and upon reaching a size of 1mm, were dissociated in 0.1% trypsin/1mM EDTA back into the same well. Cultures were subsequently fed with a mix of MEF conditioned medium (CM, section 2.5.3.1) and fresh mTSC medium at a ratio of 70:30, in addition to 1.5X F4H. Tight epithelial mTSC like colonies were observed to appear over the next two weeks, and often differentiation was also noted. In the case of the latter, colonies were picked, dissociated, and re plated to obtain morphologically consistent mTSC lines. Upon reaching 50% confluence, colonies were expanded and passed onto new MEF feeders, and fed mTSCM + 1.5X F4H every second day. This process continued, with 1:20 passages approximately once per week, until reaching passage 10. At this point, lines became more stable, and could be passed without feeders using 70CM + 1X F4H medium. Cells could then be genotyped and characterised via gDNA and RNA extraction and DNA FISH.

2.5.1.2 Differentiation

To induce differentiation of mTSCs, cells were plated feeder free in mTSCM without F4H. RNA was isolated on days two, four, and six using TRI reagent as described (section 2.2.2).

2.5.1.3 Freezing

Prior to freezing, supernatant was removed from confluent cultures for *Mycoplasma* testing in-house (Cell Services Science Technology Platform, Francis Crick Institute). mTSCs were frozen in mTSCM with 10% dimethyl sulfoxide (DMSO, Sigma-Aldrich: St Louis, USA): approximately three x 1ml cryovials were ob-

tained from one confluent well of a 6 well plate. Vials were placed in a cell freezing container at -80°C overnight, before transfer to permanent storage in liquid nitrogen.

2.5.2 Mouse embryonic stem cells (mESCs)

mESCs were derived and maintained as described previously (Ying et al., 2008), and briefly outlined below.

2.5.2.1 Derivation

Blastocysts were harvested at E3.5 as described above (section 2.1.3), and one embryo was added per well of a 24 well plate containing 2i+LIF (Appendix A). After approximately seven-ten days, spherical outgrowths were observed, picked, and dissociated using TrypLE reagent. This was re plated into one well of a 4 well plate previously coated with poly-L-ornithine and laminin (as described previously Hayashi and Saitou, 2013), whilst a small quantity of the dissociated outgrowth was reserved for PCR genotyping. Upon reaching confluence, cells were expanded and frozen. X chromosome copy number was assessed via gDNA qRT-PCR and/or DNA FISH.

2.5.2.2 Freezing

One well of a 6 well plate was frozen in a single vial using 2i+LIF + 20% DMSO. Supernatant was reserved for *Mycoplasma* testing as described above.

2.5.2.3 Maintenance

mESCs were passed every two-three days at approximately 1:5. Passage number was kept low in order to reduce the occurrence of karyotypic abnormalities, as previously reported (Eggan et al., 2002; Robertson et al., 1983).

2.5.2.4 Electroporation

Electroporation was used to deliver a vector containing *Cas9* and guide sequences, along with a drug selection cassette (pPGKpuro, Tucker et al., 1996). mESCs in the early stage of growth were disaggregated into solution and counted using Scepter 2.0 (Merck Millipore: Billerica, USA). 2 x 10^6 cells were then electroporated using Mouse ES Cell Nucleofector Kit (Lonza: Basel, Switzerland), as per the manufacturer's protocol. Drug selection was carried out using 1.5ug/ml puromycin (Sigma-Aldrich: St Louis, USA) to identify clones that had taken up plasmid and, following a period of growth, colonies were picked, and genotyped by PCR followed by restriction digest.

2.5.2.5 Mouse epiblast like cell (mEpiLC) differentiation

mESCs were differentiated towards an epiblast-like cell fate according to a previously published protocol (Hayashi et al., 2011a; Hayashi and Saitou, 2013). In brief, mESCs were grown to confluence, disaggregated with TrypLE, and plated at 1 x 10^5 cells per well of a 12 well plate coated with human plasma fibronectin (Merck Millipore: Billerica, USA). N2B27 medium (Takara Bio: Tokyo, Japan) was supplemented with activin A at 20ng/ml (Peprotech: London, UK), FGF2 at 12ng/ml (Peprotech: London, UK), and 1% knockout serum replacement (KSR, Thermo Fisher: Waltham, USA); and cells were cultured for 48 hours prior to RNA extraction.

2.5.3 Derivation of MEFs

Gamma irradiated MEFs were used as feeder cells for mTSCs: originating primary cells were generated according to a published protocol (Xu, 2005). Briefly: 14 days following timed mating, pregnant dams were culled, and uterine were horns dissected out using sterile instruments followed by a thorough wash in sterile PBS (Thermo Fisher: Waltham, USA). In a laminar flow hood, the embryos were cleanly dissected away from the uterus and the viscera and brain were removed. Individual

embryos were then teased apart using fine forceps in ice cold trypsin EDTA, and incubated overnight at 4°C. The following morning, most of the trypsin EDTA was removed without disturbing the settled tissue, and the remainder was incubated at 37°C. Tissues were then dissociated into cells, plated in MEF medium (Appendix A) as one embryo per plate, and allowed to grow to confluence before freezing in vials with MEF medium/20% DMSO. Vials were placed in a cell freezing container at -80°C overnight, before transfer to permanent storage in liquid nitrogen.

2.5.3.1 Gamma irradiation of MEFs and production of conditioned medium

One vial of primary MEFs was thawed and expanded for two passages, generating between 5 and 10 x 10^7 cells. Following dissociation, cells were exposed to a radiation dose of approximately 35 Gy via a caesium source, counted, and frozen as described above. For the production of MEF conditioned medium (CM), irradiated cells were plated at a density of 6 x 10^6 per 150mm plate. mTSCM was added for five x three day periods: subsequent to collection of the final batch, all batches were pooled, centrifuged and filtered to remove cell debris, and stored at -20°C until use.

2.6 Next generation sequencing

2.6.1 Generation of data to screen CRISPR targeted loci

Illumina MiSeq platform was used to generate sequencing data for genotyping of CRISPR targeted cells and animals. Primer sequences were designed around the region of interest using Primer3 (Untergasser et al., 2007), with a maximum amplicon size of 500bp and synthesised by Eurofins MWG (Eurofins MWG (Ebersberg, Germany). Adapter sequence was added to the 5' and 3' ends of the forward and reverse primers, respectively, in order to enable further amplification with Illumina TruSeq indexing primers (Illumina: San Diego, USA). PCR was performed us-

ing q5 high fidelity polymerase (NEB: Ipswich, USA), according to manufacturer's protocol. Unused polymerase and enzyme was removed from the reaction using solid phase reverse immobilisation (SPRI) beads, to the specification of AMPure XP (Beckman-Coulter: Brea, USA), but made in house. Indexing was performed as per the Illumina protocol, and a further clean up step utilised SPRI beads. Sample quantification utilised the dsDNA dye Quanti-fluor (Promega: Fitchburg, USA); signal was recorded with Infinite M1000 Pro (Tecan: Mannedorf, Switzerland), and analysed using proprietary Tecan software. Samples were then normalised and pooled before submission to the Advanced Sequencing Facility (ASF) at the Francis Crick institute. Following quality control - library quantitation via Eco Real-Time PCR (Illumina: San Diego, USA) and sizing via 2100 Bioanalyzer (Agilent: Santa Clara, USA) - the library was loaded onto the MiSeq at 2nM, using MiSeq Reagent Kit v2 (Illumina: San Diego, USA) for 2 x 250bp sequencing.

2.6.2 Data analysis

Fastq files were collapsed using FastX Toolkit (v0.0.13) and aligned to the reference genome (mm10) using blastn.

2.6.3 RNA-seq

2.6.3.1 Library preparation

Total RNA was extracted as described above (section 2.2.2). 500ng was submitted to ASF and assessed for RNA integrity (RIN) using Caliper LabChip GX (Perkin Elmer: Waltham, USA). Samples that passed quality control were prepared for sequencing by ASF using TruSeq Stranded mRNA Library Prep Kit as per manufacturer's protocol (Illumina: San Diego, USA). Libraries were sequenced across two runs on Illumina HiSeq 4500.

2.6.3.2 Data quality control

Quality control was performed on FASTQ output files using the FastQC package (Andrews, 2010). Paired end reads from each library were each trimmed of 13 base pairs from the 5'-end and 3 base pairs from the 3' end using Trim-Galore (Krueger, 2012), based on output from the Per Base Sequence Quality metric.

2.6.3.3 Mapping and differential expression analysis

Trimmed reads were then aligned to the mm10 genome using HISAT2 (v2.0.6: Kim et al., 2015). Uniquely mapped reads, (ie. fragments that mapped once only to the reference genome) and with a MAPQ score > 40 were retained for further analysis. These were then reverted to FASTQ format using PicardTools SamToFastq prior to input for further steps.

Transcript abundances were then determined using Salmon (v.0.7.2, Patro et al., 2017). Mouse Gencode (VM12) transcriptome annotation was used to create a quasi Salmon index.

Differential gene expression analysis was performed in R (v.3.2.2, R Core Team, 2013) utilising two independent methods. Firstly output from Salmon were passed to Voom, limma package (Ritchie et al., 2015) using tximport (Soneson et al., 2015), and gene level differential expression (DE) testing was performed. Secondly, outputs from Salmon were also passed onto Sleuth (Pimentel et al., 2017) via kallisto (Bray et al., 2016), and again gene level DE testing was carried out. A comparison of XY and XX mESCs was included as a positive control for detection of DE genes, which guided the setting of filtering thresholds for the exclusion of lowly expressed genes.

2.6.3.4 Over representation analysis (ORA)

Over representation analyses were carried out as using the Web based gene set analysis toolkit (WebGestalt, Zhang et al., 2005; Wang et al., 2017) with standard settings.

2.7 Statistical analysis

2.7.1 Weight data analysis

There are major litter effects on growth during pregnancy and early postnatal life independent of genotype; therefore comparisons between genotypes were made within litters (Burgoyne et al., 1983). Mean weighted differences (MWD) were used in order to compare weight data, thus taking into account varying litter sizes and numbers of animals per genotype within each litter. The difference between the required two genotypes was weighted according to the number (n) of animals of those genotypes (i.e. w = n1 x n2/n1+n2). The MWD was then calculated by dividing the sum of the weighted differences over the sum of the weights (w), and standard error calculated from estimates of the variances in each genotype in each litter. MWD over standard error is distributed as Student's t (Burgoyne et al., 2002).

At E10.5, embryos are growing exponentially, therefore a log transformation was performed before the MWD calculation to bring the data into a normal distribution. Additionally, it has previously been noted that some XO embryos are more runted than expected, and can thus seriously affect XY-XO comparisons (Burgoyne et al., 1983b). To test for this effect, the differences between XY and XO, and XY and $X^{Xist-}O$ embryos were collated across litters and the distribution checked for outliers (Grubbs' test): none were found.

Postnatal growth rates were calculated by plotting each individual animal's weight data and fitting a regression line; the gradients from 0-3 weeks and 3-5 weeks were then compared using MWD as described in (Burgoyne et al., 2002). Data were

analysed using Excel (Microsoft: Washington, USA) and Prism (Graphpad: La Jolla, USA).

2.7.2 Postnatal survival analysis

The statistical significance of the differences between expected and observed numbers of each genotype was calculated using Fisher's Exact Test of Independence, using the package rcompanion in R (R Core Team, 2013) I corrected for multiple comparisons, where applicable, using the Holm-Bonferroni method (Holm, 1979). Mosaic plots were created using the package ggplot2 in R.

Chapter 3

Examining the role of *Xist* in the post-implantation growth deficit observed in $X^{P}O$ embryos

3.1 Introduction

TS is invariably associated with low birth weight, reduced growth during childhood, and adult short stature. These effects likely manifest from intrauterine growth retardation (IUGR) during embryogenesis. XO mouse embryos are similarly growth retarded during development. There is limited evidence to suggest that this manifests at the pre-implantation stage, though it is certainly present as a weight deficit by the egg cylinder stage, at around E7.25 (Banzai et al., 1995b; Burgoyne et al., 1983b). The weight deficit persists until around E12.25, with a further lag period between E14.5 and E16.5 (Burgoyne et al., 1983b). Interestingly, subsequent work focusing on the parent of origin of the single X chromosome in XO mice showed that this effect is only observed in $X^{P}O$ embryos (Thornhill and Burgoyne, 1993). In contrast, at E10.5 $X^{M}O$ embryos were shown to be heavier than XX littermates, and of equivalent weight to normal $X^{M}Y$ males (Thornhill and Burgoyne, 1993). Bringing these data together, it was hypothesised that the X^{P} carries an imprint that reduces

X linked gene expression across the whole chromosome, thus delaying growth; and that the X^M is more efficient at supporting early development. This could be explained by imprinted *Xist* expression from the X^P, thus silencing X linked genes in early X^PO embryos.

These observations were confirmed, and the reduced X linked gene expression hypothesis tested, using a *lacZ* transgene to assay gene activity from the single X chromosome in X^PO embryos (Jamieson et al., 1998). In XY males and homozygous carrier females, X-gal staining was positive in the embryo proper and in cells of both extraembryonic ectoderm (ExE) and ectoplacental cone (EPC). Heterozygous female embryos carrying the transgene on the X^M showed a similar pattern, whereas those carrying the transgene on the X^P displayed no expression in the ExE or EPC, in line with imprinted XCI of the X^P in these tissues. If the single X chromosome in the X^PO showed significantly reduced or absent staining, this would support a case for chromosome wide downregulated gene expression as a cause of the growth deficit in these embryos. Intriguingly, X^PO embryos stained positively for X-gal in all tissues, suggesting that the single X^P can behave as per the X^M in the absence of a second sex chromosome. The authors also observed that the EPC of X^PO embryos is significantly smaller than XX littermates, likely due to a reduction in the number of cells, as the packing density was normal (Jamieson et al., 1998). Taken together, whilst these data show that the X^P is transcriptionally active in the X^PO context at E7.5, it is still possible that global transcription across the chromosome is reduced, or indeed absent, at an earlier stage, possibly as a result of paternal *Xist* expression. Alternatively, specific genes may be required from the X^M that are not expressed from the X^P due to epigenetic differences independent of iXCI, and their absence compromises development.

XCI controls transcription across the X chromosome. In the pre-implantation embryo this process is mediated by *Xist* in an imprinted manner, such that X^P is always inactivated. *Xist* expression was assayed by RNA FISH in 8 cell and blastocyst stage mouse embryos (Matsui et al., 2001). Whereas in XY male embryos no expression

was observed at either stage - as would be expected in the presence of a single X^M- a distinct signal was present in every cell of the 8 cell X^PO embryos, with a decreased frequency of 20% of cells in fully expanded blastocysts (Matsui et al., 2001). Based on these data, it can be hypothesised that inappropriate *Xist* expression in the pre-implantation X^PO embryo results in temporary chromosome wide silencing, and an embryo nullizygous for X linked gene products. Functional nullisomy for X linked gene products has previously been shown to be extremely harmful to early embryonic development (Morris, 1968a; Burgoyne and Biggers, 1976), therefore it is possible that this causes the growth retardation phenotype observed from E7.25 onwards. I sought to test this hypothesis by asking whether deletion of *Xist* rescues the developmental retardation of X^PO embryos.

3.2 Results

I set out first to reproduce previously published data confirming that X^PO embryos show significant growth retardation when compared with XX littermates at E10.5. X^PO embryos resulted from cross 1 (Figure3.1 A(i)). Here, I utilised female mice heterozygous for a large pericentric inversion on the X chromosome, In(X), as a source of 'O' gametes (Evans and Phillips, 1975). When mated to an XY male, there are six possible offspring (Figure3.1 A(i)), five of which survive to E10.5. Four of these genotypes can be identified by PCR on genomic DNA (Figure 3.1B), whereas RT-PCR to detect *Xist* was used to distinguish between XX and XO embryos (see section 2.2.3).

Preliminary analyses showed no significant difference in weight or somite counts between XX and InX/X female embryos or between XY and InX/Y male embryos. These were therefore pooled as "XX" and "XY" for all future analyses. X^PO embryos were significantly smaller than XX littermates: this was clear from morphology (Figure 3.1D), weight data (Figure 3.1E), and somite counts (Table 3.1). I then compared X^PO embryos with XY littermates to confirm whether a single X^M is able to support development more effectively than a single X^P, as shown previ-

ously (Thornhill and Burgoyne, 1993). X^PO embryos are also significantly smaller than XY littermates (Figure 3.1D, E), and have fewer somites (Table 3.1). Taken together, these data confirm previous results showing X^PO growth retardation at E10.5, relative to XX littermates. Furthermore, I observed that a single X^M is more capable of supporting normal development than a single X^P. This result does not, however, enable us to determine whether inappropriate *Xist* expression or X linked gene imprinting is responsible for the reported embryonic growth deficit.

In order to test the *Xist* hypothesis, I utilised a male carrying the *Xist*^{tm1Jae} allele (Marahrens et al., 1997) to produce X^PO mice lacking *Xist* (hereafter denoted $X^{Xist\text{-}}O$). This allele is lethal to all XX females when inherited paternally because imprinted XCI is ablated, resulting in embryonic death and degradation by E10.5 (Marahrens et al., 1997). Accordingly, there are no XX females available as controls, and only three offspring genotypes are produced in this cross at E10.5 (Figure 3.1A(ii)). As an alternative, I used XY^{RIII} male embryos as controls. Whilst most Y chromosomes accelerate pre-implantation development, the RIII strain Y chromosome has previously been shown to lack this effect (Burgoyne, 1993). In order to confirm there is no acceleration of development in XY^{RIII} embryos, I compared to XX littermates in cross 1. No significant difference was observed in either weight (Figure 3.1E(i)) or somite data (Table 3.1). I therefore utilised XY^{RIII} male embryos as controls throughout this experiment.

I then assessed the contribution of inappropriate *Xist* expression to the growth deficit observed in X^PO embryos at E10.5. If the cause of the growth deficit was *Xist* expression, no difference in weight or somite count would be expected between XY^{RIII} and $X^{Xist}O$ embryos (Figure 3.1C(ii)). Most $X^{Xist\text{-}}O$ embryos showed growth retardation when compared to XY^{RIII} littermates, which was clear both from embryo morphology (Figure 3.1D, right hand side), weights (Figure 3.1E(ii)), and somite counts (Table 3.1). Based on these data, I conclude that inappropriate expression of *Xist* is not responsible for the growth retardation phenotype observed in X^PO embryos at E10.5.

Embryonic growth controls the kinetics of somitogenesis, both in wildtype and growth impaired embryos (Tam, 1981; Power and Tam, 1993). When embryo size is halved prior to the eight cell stage, morphogenesis and pattern formation are appropriate for tissue volume as opposed to chronological age (Power and Tam, 1993). I was interested to see if a similar relationship holds for $X^{P}O$ embryos, thereby gaining further insight into the nature of the growth deficit. I used log weight and somite count metrics to validate this relationship in the current model (Figure 3.1E(iii)): all four genotypes showed highly significant correlations (Figure 3.1E(iii)). Utilising the same data, I then created a linear regression model of developmental progression (Figure 3.1E(iv)). The gradients of the regression lines were not significantly different between any of the genotypes ($p = 0.3310$; Figure 3.1E(iv)). I conclude that the growth retardation and reduced somite counts represent a global developmental delay in $X^{P}O$ embryos at E10.5, i.e. the somite count is appropriate for the log weight. This was also true for $X^{Xist-}O$ embryos, further supporting my conclusion that *Xist* does not play a role in the retardation phenotype.

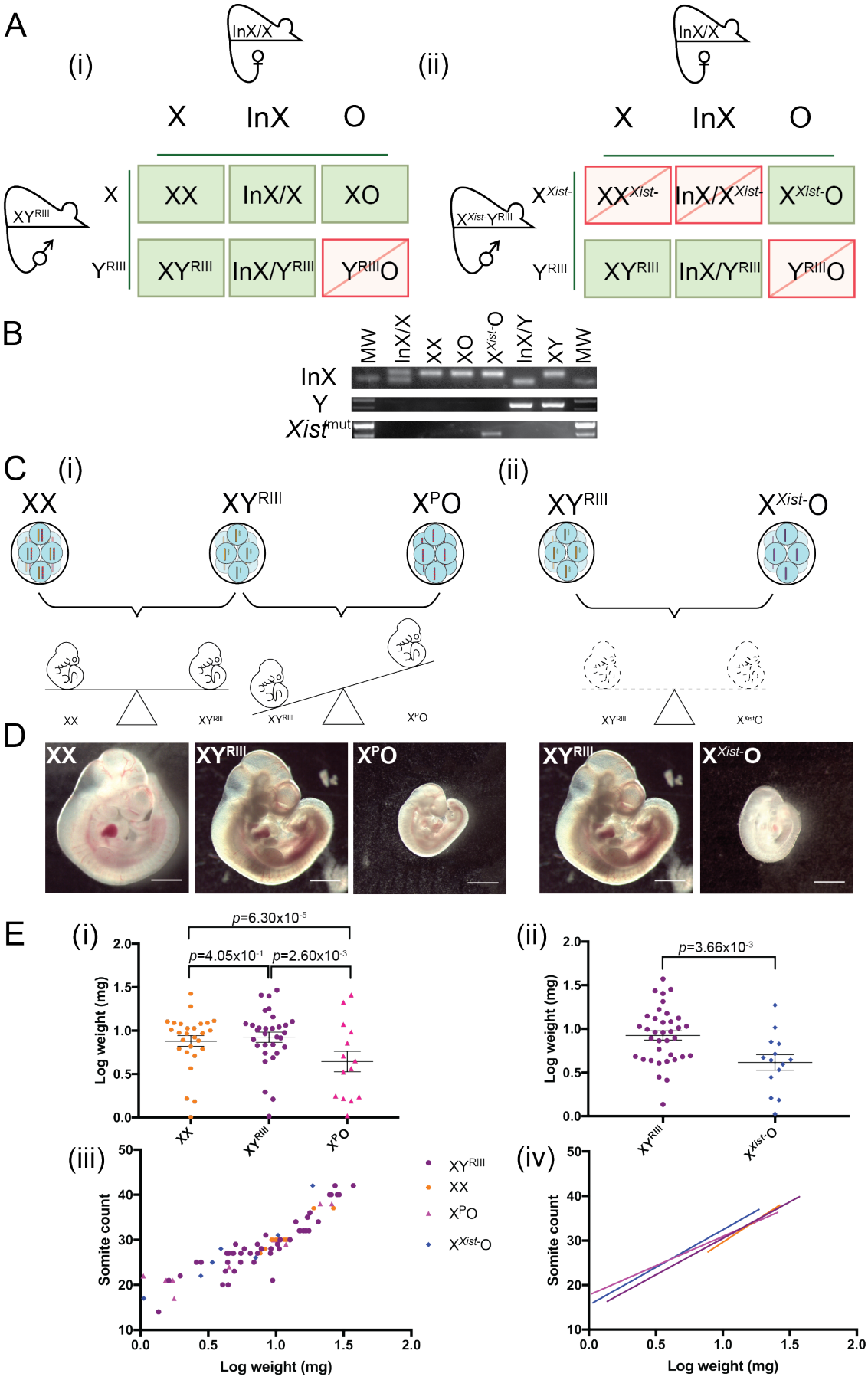
A
(i)
InX/X
X InX O
XY^RIII
X XX InX/X XO
Y^RIII XY^RIII InX/Y^RIII Y^RIIIO
(ii)
InX/X
X InX O
X^Xist- XX^Xist- InX/X^Xist- X^Xist-O
X^Xist-Y^RIII
Y^RIII XY^RIII InX/Y^RIII Y^RIIIO
B
MW InX/X XX XO X^Xist-O InX/Y XY MW
InX
Y
Xist^mut
C (i)
XX XY^RIII X^PO
(ii)
XY^RIII X^Xist-O
D
XX XY^RIII X^PO XY^RIII X^Xist-O
E (i)
p=6.30x10^-5
p=4.05x10^-1 p=2.60x10^-3
Log weight (mg)
XX XY^RIII X^PO
(ii)
p=3.66x10^-3
Log weight (mg)
XY^RIII X^Xist-O
(iii)
Somite count
Log weight (mg)
XY^RIII
XX
X^PO
X^Xist-O
(iv)
Somite count
Log weight (mg)

Figure 3.1: *Xist* KO does not rescue the developmental deficit observed in X^PO embryos at E10.5. (**A**)(i) Cross 1 utilised a XY^{RIII} male and a In(X)1HY female, with five possible offspring: $Y^{RIII}O$ embryos are not viable. (ii) Cross 2 utilised a $X^{Xist-}Y^{RIII}$ male and a In(X)1HY female, with three possible offspring: females with two X chromosomes are not viable due to a lack of imprinted XCI. (**B**) Representative genomic DNA PCR results for the inversion X chromosome (top row); the Y chromosome (middle row); and the mutated *Xist* allele (bottom row). (**C**) (i) and (ii) illustrate experimental hypotheses. (**D**) Representative images of all genotypes at E10.5 (scale bar = 100uM). (**E**) (i) The log weights of XX and X^PO, XX and XY^{RIII}, XY^{RIII} and X^PO embryos, and (ii) XY^{RIII} and $X^{Xist-}O$ embryos were compared at E10.5, with *P* values given by Student's *t*; bars represent mean±SEM; (iii) Somite count was significantly correlated with log weight for all genotypes (r^2 for XY^{RIII}=0.8173, XX=0.9245, X^PO=0.8814, $X^{Xist-}O$=0.8248); (iv) linear regression analysis included somite count and log weight as factors, with no significant difference between the gradients for different genotypes (p=3.31x10^{-1}).

3.3 Discussion

Whilst it has been known for a number of years that X^PO embryos are significantly smaller than XX littermates at E10.5 (Burgoyne et al., 1983b; Thornhill and Burgoyne, 1993; Jamieson et al., 1998), here I show that this is not as a result of inappropriate *Xist* expression. The *Xist* mutant allele has been shown to abolish *Xist* expression from the X^P (Marahrens et al., 1997). Nevertheless, X^PO mice carrying *Xist*- still exhibit a significant growth deficit at E10.5.

There are a number of possible explanations that could underlie this result, from both technical and biological perspectives. Firstly, loss of *Xist* expression should be confirmed by transcriptional analysis of X^{Xist-} embryos. Secondly, significant variation exists between mouse litters, largely resulting from the uterine environment (Hughes, 1979; Holson & Pearce 1992; Lazic and Essioux, 2013). I reduced this effect by keeping the maternal genotype constant across experiments, and utilising the MWD statistical technique to compare embryos within litters. However, it was not possible to generate normal X^PO females and X^PO females lacking *Xist* within the same litter. I cannot therefore fully exclude the effect of inter litter differences. In the XY^{RIII} male I believe I opted for the best proxy comparison; however, due to the genetically outbred nature of the MF1 strain, it is formally possible that this is an

Cross	Genotypes compared	Number of foetuses	Mean±SEM log weight (weight in mg)	Mean±SEM weighted difference	Significance of difference (*p*)	Mean somites± SEM (n)	Regression line gradient±SE
In(X)/X x XY^{RIII}	XX	26	0.880±0.062 (7.08)	0.243±0.066	$6.30x10^{-5}$	31±1.190 (9)	19.60±2.117
	vs.						
	$X^{P}O$	14	0.644±0.118 (4.30)			26.1±2.331 (10)	13.17±1.708
	XY^{RIII}	31	0.920±0.058 (8.31)	0.287±0.070	$3.00x10^{-3}$	29.24±0.894 8 (30)	16.38±1.130
	vs.						
	$X^{P}O$	14	0.644±0.118 (4.30)			26.1±2.331 (10)	13.17±1.708
	XY^{RIII}	31	0.920±0.058 (8.31)	0.070±0.049	$4.05x10^{-1}$	29.24±0.8948 (30)	16.38±1.130
	vs.						
	XX	26	0.880±0.062 (7.08)			31±1.190 (9)	19.60±2.117
In(X)/X x $X^{Xist}Y^{RIII}$	XY^{RIII}	36	0.925±0.053 (8.41)	0.215±0.072	$4.00x10^{-3}$	29.37±1.421 (19)	16.38±1.130
	vs						
	$X^{Xist}O$	14	0.678±0.0898			26.20±2.154 (10)	16.89±2.753

Table 3.1: Weight and somite comparison of E10.5 embryos

uncontrolled source of variation. A further source of variation lies within developmental timing between litters (Figure 3.1E); i.e. some litters were likely conceived many hours earlier than others, despite maintaining constant timing by embryonic day. Again, the mean weighted difference technique helped to ameliorate this effect in the data by making only relative comparisons within litters. Furthermore, the logistic regression analysis utilised both somite number and log weight, thus controlling for developmental timing.

3.3.1 *Xist* coating may not directly result in imprinted XCI

Previous work has shown by RNA FISH almost complete *Xist* coating of the paternally derived X chromosome(s) in X^PO and X^PX^P embryos at the 8-16 cell stage of pre-implantation development (Matsui et al., 2001; Okamoto et al., 2000). This expression was subsequently reduced at the blastocyst stage such that only around 20% of cells showed inappropriate numbers of *Xist* foci. Neither of these experiments, however, assayed whether this *Xist* expression causes X linked gene silencing.

Utilising a similar model system, but assaying instead by qRT-PCR, Latham and Rambhatla screened five X linked genes, including *Xist*, for differential expression between androgenetic and gynogenetic embryos at both 8 cell and late morula stages (Latham and Rambhatla, 1995). Androgenetic embryos showed reduced expression in all genes except *Xist*, which was more highly expressed. These results should, however, be explicated in the context of the experiment, which utilised pooled embryos and early qRT-PCR techniques. For example, a population of androgenetic embryos may include those with two X chromosomes, two Y chromosomes, or one of each, thus making interpretation of differential expression challenging. Later work from the same group rectified this ambiguity by using single embryos for experiments, though focusing on mid to late blastocyst stage embryos (Latham et al., 2000). There was a significant difference in *Xist* expression between XX and XY blastocysts in the control group. The same observation was made comparing X^PX^P

with X^PY embryos, though the difference was not statistically significant. Finally, they reported no significant difference in *Xist* expression between XX control and X^PX^P androgenetic blastocysts, despite the latter carrying two paternally derived X chromosomes (Latham et al., 2000). This is consistent with the RNA FISH data from androgenetic blastocysts (Okamoto et al., 2000). The embryo becomes competent to count at this stage, which effects a reduction in the expression of *Xist* appropriately in both androgenetic and control blastocysts (Latham et al., 2000; Okamoto et al., 2000).

Taken together, these data leave open two possibilities. Firstly, imprinted XCI may take place in X^PO embryos and reduce transcription from the X^P. This would be in keeping with the fact that X linked nullizygosity, as seen in the YO embryo, is detrimental to pre-implantation embryonic development (Morris, 1968a; Burgoyne and Biggers, 1976). Alternatively, *Xist* is expressed, but the downstream pathway that results in transcriptional inactivation is not complete. This implies that whilst imprinted expression of *Xist* from the X^P is absolute, i.e. it is blind to the number of X chromosomes present, a downstream counting or regulatory mechanism must exist to ensure continued X linked gene expression. Hypothetically, such a mechanism could act on X^M, so that *Xist* expression is only converted to transcriptional inactivation in the presence of at least one X^P and one X^M. A candidate for the effector of this mechanism is *Rnf12* (also known as *Rlim*). A maternally expressed copy of *Rnf12* is absolutely required for imprinted XCI in XX female embryos, as shown by the early post implantation female lethality of an *Rnf12* mutant allele (Shin et al., 2010). These *Rnf12* mutant embryos do, however, also display defective *Xist* expression at the blastocyst stage, and this defect has not been observed in X^PO embryos (Shin et al., 2010).

In order to distinguish between these two hypotheses, an analysis of X linked transcription in the early embryo is required. RNA FISH would enable a number of genes to be screened, but RNA-seq would provide a more comprehensive answer. Recently, single cell RNA-seq has facilitated the study of gene transcription in the

early embryo in even greater depth, thus providing a transcriptome wide view of iXCI. Transcription from X^P in wildtype XX embryos has been shown equivalent to that from X^M at the 4 cell stage, with a paternal to maternal ratio of 1.0. (Petropoulos et al., 2016). The ratio then progressively decreased to 0.4 at the early blastocyst stage (Petropoulos et al., 2016). *Xist* expression peaked at the 16 cell stage and was maintained until E4.5 (Deng et al., 2014; Wang et al., 2016). Borensztein and colleagues further classified the genes undergoing inactivation into early, intermediate and late silenced, at 16, 32 and blastocyst stages, respectively (Borensztein et al., 2017). As these data are entirely consistent with previously reported RNA FISH datasets, a complementary approach of RNA-seq validated by RNA FISH is ideally suited to begin to address the role of *Xist* in imprinted XCI in X^PO pre-implantation embryos.

3.3.2 The X chromosome may harbour imprinted genes that are primarily expressed in the extraembryonic tissue

Inappropriate *Xist* expression is not the cause of the growth retardation observed in X^PO embryos at E10.5, therefore I hypothesise the existence of imprinted genes on the X chromosome that are differentially expressed during embryonic development. This could also serve to explain the observation that X^MO female embryos show accelerated growth relative to XX littermates at E10.5 (Thornhill and Burgoyne, 1993). Such imprinted genes could function either as a normally silent growth suppressor(s) on the single X^P, or as a growth enhancer(s) from the X^M. There are a number of reported examples of X linked genes proposed to to be silenced on X^P due to imprinting, e.g. *Esx1* (Li and Behringer, 1998) and *Plac1* (Jackman et al., 2012). However, whether the silencing observed in these reports results from true imprinting or imprinted XCI remains to be shown. In order to separate the conceptually similar occurrences of imprinted XCI and genomic imprinting, the presently described XO model is required. Imprinted XCI does not occur in this model, thus any differences observed between X^P and X^M can be attributed to genomic imprint-

ing. This approach led to the discovery of the *Xlr* locus, a group of imprinted genes expressed in the developing mouse brain (Davies et al., 2005; Raefski and O'Neill, 2005).

Whilst imprinting could affect genes expressed in the embryonic or in the extraembryonic tissue, a number of lines of evidence make the latter more likely. Firstly, embryos that do not show growth retardation, i.e. X^MX^P, X^MY, and X^MO have an active X^M in extraembryonic tissue, whereas X^PO has an active X^P. Secondly, one of the recurring themes in the genomic imprinting literature is the correlation between the evolution of imprinting and the evolution of an invasive, gestation spanning placenta (Cleaton et al., 2014; Renfree et al., 2013). A significant number of the 100 or so currently recognised imprinted genes affect pre natal development through placental expression (Coan et al., 2005; Keverne, 2015). Thirdly, as previously described here, the placentas of XO embryos show morphological abnormalities during development. X^PO embryos show reduced EPC volume when compared to XX littermates, while X^MO embryos do not (Jamieson et al., 1998). Earlier work utilising the XO mouse model showed that X^PO placentas are larger than placentas from XX littermates, and further work described this hyperplasia in both X^PO and X^MO placentas at E17.5, with the latter larger than the former (Burgoyne et al., 1983a; Ishikawa et al., 2003). The authors reconcile this apparent contradiction by suggesting that the growth trajectories are simply maintained from EPC onwards, and that placentas with one X chromosome are generally larger than those with two X chromosomes (Ishikawa et al., 2003). Finally, XO mESCs have been shown to exit the pluripotent state and differentiate faster than XX mESCs, which must trigger XCI before exit from pluripotency (Schulz et al., 2014). If this also applies to the situation *in vivo*, it might be expected that the XO embryo proper is actually at an advantage relative to the XX embryo proper, at least initially.

In order to determine whether an embryonic or extraembryonic defect underlies the growth deficit in X^PO embryos, the definitive experiment would require an analysis of embryos in which sex chromosome complement differs between these two

lineages. By introducing an X^PO embryo into an XX/XY extraembryonic environment, and *vice versa*, the effects on development could be assessed. This can be achieved by either mechanical or chemical means. The cells of a two cell stage embryo can be electrically fused, thus making the cell tetraploid (4n). These cells can then be complemented at the four cell stage with donor mESCs, resulting in the creation of high grade chimeras. The recipient 4n cells form the extraembryonic compartment, and the mESCs differentiate into the embryo proper (Nagy et al., 1990, 1993). Alternatively, recipient embryos can be pre-treated with FGF4 and heparin in order to promote formation of PE and inhibit the development of the epiblast (Yamanaka et al., 2010). Very recently it has been shown that donor mESCs can be injected into FGF/heparin pre-treated embryos at the blastocyst stage, and that these cells make a significant contribution to the formation of the embryo proper (Dupont et al., 2017). There are compromises with both techniques. Firstly, tetraploid complementation has been correlated with a growth deficit in all wild-type embryos (Tam, 2003). More importantly, the karyotype of the extraembryonic tissue would be 4n, thus making it no longer possible to assess the contribution of a single X chromosome. FGF treatment does not currently achieve equivalent rates of chimerism to the tetraploid method. However, with appropriate controls, it should still be possible to detect relative changes to embryonic development. These experiments are in progress.

3.3.3 Mouse trophoblast stem cells can be utilised to identify imprinted genes *in vitro*

A tractable model is required to facilitate the search for any X linked imprinted genes expressed in the extraembryonic compartment. Undoubtedly the gold standard would be to show differential gene expression (DGE) between X^P and X^M chromosomes *in vivo*, followed by functional experiments to link cause and effect. However, the placenta is a dynamic tissue that changes significantly during development, therefore identifying the correct time and location for DGE may be chal-

lenging without an initial screen. This could be carried out in mouse trophoblast stem cells (mTSCs): an *ex vivo* derived population of multipotent cells originating from the extraembryonic compartment, amenable to propagation *in vitro*, manipulations such as overexpression or genome editing, and shown to maintain imprints originally observed in the embryo (Tanaka et al., 1998; Calabrese et al., 2015). The derivation and use of mTSCs to identify X linked imprinted genes will be the focus of the next chapter.

Chapter 4

Using *in vitro* models to identify candidates for X linked imprinted genes in mouse extraembryonic tissue

4.1 Introduction

4.1.1 Genomic imprinting

Parent of origin biased gene expression - genomic imprinting - has been observed across fauna and flora, though among vertebrates it is most well characterised in eutherian mammals. Early studies utilising androgenetic and gynogenetic mouse embryos established that one copy of the genome from each parent was required for successful embryonic development (Barton et al., 1984; Kaufman et al., 1977; Surani and Barton, 1983; Surani et al., 1984). Subsequent work showed that this uniparental embryonic lethality phenotype resulted from a necessity for expression of a small subset of genes from a specific parental allele, denoted *paternally expressed genes, Pegs* and *maternally expressed genes, Megs*, respectively (Cleaton

et al., 2014). These subsets are most often found in groups known as imprinted domains, which themselves are coordinately regulated by a germline differentially methylated region (gDMR) or imprinting control region (ICR). gDMRs are CpG rich, and the two parental alleles are differentially methylated during gametogenesis (Iurlaro et al., 2017). The majority of gDMRs are maternally methylated, though a small number are paternally methylated, including the *Igf2-H19* cluster. Whilst it is clear that such differential methylation drives the imprinting status of the cluster, there are also a number of other mechanisms by which allele specific gene expression can be achieved, including lncRNA mediated recruitment of epigenetic modifiers (Nagano et al., 2008).

The biological purpose of imprinting is unknown; though the timing of its appearance in both eutherian mammals and, to a limited extent, metatherians has been correlated with the evolution of viviparity through placentation (Smith et al., 2011). It has previously been suggested that imprinting regulates the balance between the demands of the maternal and paternal genomes via the *in utero* foetus; the kinship, or parental conflict hypothesis (Haig and Westoby, 1989). This posits that paternally derived genes generally enhance foetal growth because they look to increase resource grabbing from the mother, thus maximising the probability of further genetic propagation. Maternally derived genes, in contrast, often suppress foetal growth in order to balance resources between current and future litters (Haig and Westoby, 1989).

Alternatively, imprinting may serve to regulate the balance of resources *in utero* between mother and foetus, with maternal interests represented by the placenta (Reik et al., 2003). By this hypothesis, nutrient supply is genetically controlled by expression of imprinted genes in the placenta, and demand is controlled by expression of imprinted genes in the foetus. Such a hypothesis also accounts for the evolution of clusters, suggesting that the existence of supply and demand genes in close proximity (e.g. the region around *Igf2*) facilitates the fine balance required in expression during development (Reik et al., 2003).

A third theory suggests that imprinting evolved because it increases the genetic integration of co adapted maternal and offspring traits, thereby enhancing the fitness of offspring (Wolf and Hager, 2006). No single theory fully explains the existence of all imprinted genes; though it is clear that all theories take into account the evolution of the placenta and the significant number of imprinted genes expressed by the shortest lived of all organs.

4.1.2 The placenta

The placenta is the physiological interface between mother and foetus (Smith et al., 2011). It mediates the exchange of nutrients and waste products between foetal and maternal blood, as well as acting as a centre for the production of hormones and growth factors during pregnancy (Rossant and Cross, 2001). Whilst the placenta is most commonly associated with eutherian mammals, it is also present in metatherians, and has been found in diverse vertebrate classes including amniotes such as Amphibia, Reptilia, and the anamniotic Chondrichthyes (sharks, Blackburn and Flemming, 2011; Hamlett, 1989). In mammals, and amniotes more generally, placental development includes the fusion of pairs of the four foetal membranes, the amnion, the yolk sac, the allantois, and the chorion (Smith et al., 2011). The amnion directly surrounds the foetus and serves to protect it from shock. The yolk sac encapsulates the egg yolk in egg bearing species, and carries out many duties of the placenta before the allantoic placenta is established, including blood synthesis and blood vessel formation and nutrient and gas exchange. The allantois is continuous with the embryonic bladder; and the chorion is formed by the extraembryonic mesoderm and a layer of outer trophoblast - it joins with the yolk sac to form the chorio vitelline placenta or the allantois to form the chorio allantoic placenta (Smith et al., 2011).

The mature mouse placenta is a chorio allantoic placenta, composed of multiple cell types across three layers: i) the decidua, formed of maternal tissue; ii) the junctional zone, and; iii) the labyrinth (John and Hemberger, 2012). Within the

labyrinth, exchange of nutrients, waste, and gases takes place between maternal and foetal circulations. The exchange interface is made up of two layers of multinucleated syncytiotrophoblast cells, in addition to sinusoidal trophoblast giant cells (TGCs, Simmons et al., 2008). TGCs also exist within the decidua, in the form of spiral artery associated TGCs and canal associated TGCs, and between the layers as parietal TGCs. They produce a number of endocrine molecules, including prolactin, that serve to mediate the continuation of pregnancy, maternal vascular remodelling, and possibly parturition (Hu and Cross, 2010). Placental prolactins are also produced by spongiotrophoblast cells from within the junctional zone, in addition to other pregnancy specific glycoproteins thought to have a role in the immune privileged status of the foetus (Wu et al., 2008). The function of the spongiotrophoblast within the junctional zone was previously thought to be primarily structural (Rossant and Cross, 2001), however, in addition to the production of hormones and glycoproteins, it also produces molecules that affect the maternal brain to mediate maternal instinct (Glynn and Sandman, 2011). Glycogen cells are also found within the junctional zone and, by migration, also within the maternal decidua, though the function of these aptly named glycogen heavy cells remains to be found (Prudhomme and Morey, 2015). A summary of mouse placenta development is provided in Figure 4.1.

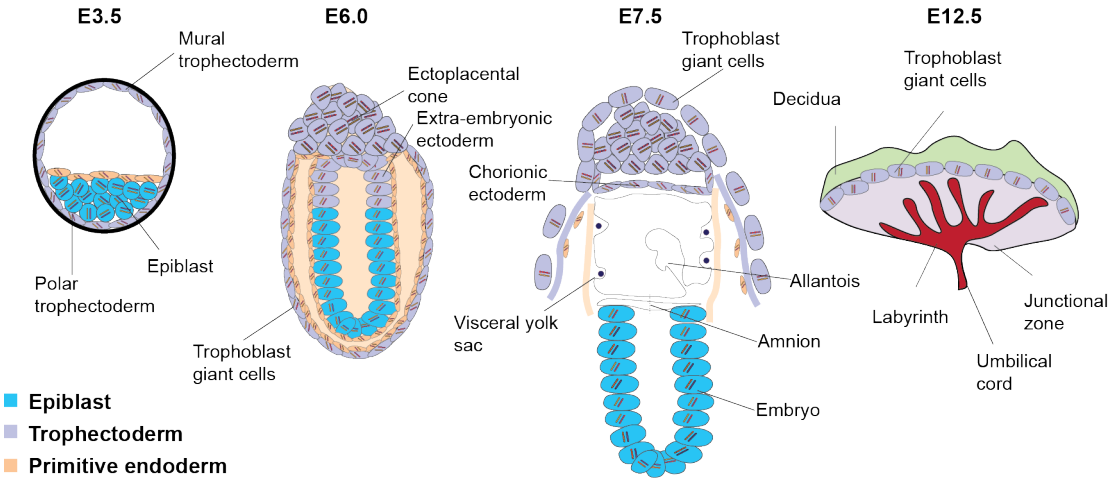

Figure 4.1: Mouse placenta development. Around the time of implantation (E3.5), the trophoectodermal cells overlying the ICM, the polar TE, proliferate and give rise to diploid extraembryonic ectoderm and the ectoplacental cone (EPC). The trophectodermal cells in contact with the blastocoele cavity, the mural TE, endoreduplicate their DNA to become polyploid primary trophoblast giant cells (TGCs). Secondary TGCs are formed from the EPC, which migrate to surround the conceptus. Between E6.0 and E7.5, the extraembryonic ectoderm expands and joins with extraembryonic mesoderm to form the chorion, which itself then makes contact with the mesoderm derived allantois. This attachment is followed by folding of the chorion, thus marking the sites of foeto placental blood vessel growth from the allantois. By E12.5, the foetal blood vessels become a densely packed labyrinth with extensive villous branching, and chorionic trophoblast cells differentiate to become syncytiotrophoblast cells. These multinucleated cells form two distinct layers which, in addition to sinusoidal TGCs, form the interface between the maternal and foetal blood within the placental labyrinth. In order to make contact with the foetal blood supply via the trophoblast villi, the maternal blood passes through the junctional zone, comprised mainly of spongiotrophoblast cells. This is formed by differentiation from the EPC. After Rossant and Cross, 2001.

Many imprinted genes are expressed in the placenta (Cleaton et al., 2014; Tunster et al., 2013). A number of these imprinted genes have been functionally characterised by targeted deletion, often resulting in growth phenotypes affecting either the placenta and/or the foetus. Placental growth restriction has been reported following individual deletion of the paternally expressed genes *Igf2*, *Peg1*, and *Plag1*; in contrast to deletion of the maternally expressed *Igf2r*, *Cdkn1c*, *Phlda2* and *Grb10*, which resulted in enhanced placenta growth (Cleaton et al., 2014). Foetal overgrowth was observed following targeting of the maternally expressed *Igf2r* or *H19* (Wang et al., 1994; Leighton et al., 1995). An embryonic growth retardation phenotype was reported after deletion of *Igf2*, *Peg1/Mest*, and *Peg3*, all normally ex-

pressed from the paternal allele (DeChiara et al., 1991; Lefebvre et al., 1998; Li et al., 1999).

X^PO female embryos are smaller than XX littermates at E10.5 (Thornhill and Burgoyne, 1993). In this thesis, I previously showed that this growth deficit is not caused by *Xist* expression (Chapter 3). Furthermore, X^PO embryos also have a smaller ectoplacental cone (EPC) than XX littermates at E7.5 (Jamieson et al., 1998). Neither of these defects are present in X^MO embryos, which are heavier than XX littermates at E10.5 (Thornhill and Burgoyne, 1993; Jamieson et al., 1998). This X^PO growth deficit is likely to result from genomic imprinting affecting the X chromosome.

XCI always silences the X^P in mouse extraembryonic tissue, whereas in the embryo, XCI randomly affects either X^M or X^P (Okamoto et al., 2004). Genes from the X^P are therefore expressed in 50% of cells in the normal XX embryo proper, but are never expressed in the XX, XY, or X^MO placenta. I hypothesise that the absence of the X^M in X^PO placentas could result in loss of expression of a growth promoting gene(s) expressed only from X^M in placenta. Alternatively, there may be a gene(s) present on X^P that is usually silenced by XCI in the XX placenta, and whose expression in the X^PO is disadvantageous to embryonic growth. It is also formally possible, though less likely, that the phenotype could be explained by genes expressed in the embryo proper. In order to search for candidate genes to support these hypotheses, I performed RNA sequencing (RNA-seq) on X^PO and X^MO mouse stem cell lines to model the different embryonic compartments: pluripotent - mouse embryonic stem cells (mESCs); epiblast - mouse epiblast like cells (mEpiLCs); and the trophectoderm - mouse trophoblast stem cells (mTSCs).

4.2 Results

4.2.1 Derivation of stem cell lines

First I set out to derive mTSC lines from blastocyst stage embryos, as described previously (Tanaka et al., 1998; Himeno et al., 2008) and summarised in Figure 4.2A. In order to generate $X^{P}O$ embryos, I used the cross described in Chapter 3 between an In(X)/X female and a XY^{RIII} male (Figure 4.2B(i)), here designated Cross I. $X^{M}O$ embryos were generated by crossing an $X^{Y*}O$ male (Burgoyne et al., 1998) with a wildtype XX female (Figure 4.2B(ii)), hereafter Cross II. After ten passages supported by mouse embryonic fibroblast (MEF) feeders, mTSC lines stabilised. Feeders were removed, cell lines were maintained in MEF conditioned media, and genotyping was carried out. PCR revealed the presence of only female mTSC lines from Cross I. No XY or InX/Y lines were derived (Figure 4.2C(i)). Three of these female mTSC lines were determined to be $X^{P}O$, with the presence of a single X chromosome shown by DNA FISH (Figure 4.2D) and qRT-PCR. Four mTSC lines were derived from Cross II outgrowths (Figure 4.2C(ii)), and two of these lines were determined to be $X^{M}O$, based on PCR and DNA FISH (Figure 4.2D).

Transcription factors including *Cdx2*, *Eomes*, *Esrrb*, *Elf5*, and *Tfap2c*, and the growth factor *Bmp4*, have previously been shown to be highly expressed in mTSCs (Tanaka et al., 1998; Kubaczka et al., 2014). In order to confirm mTSC identity, expression levels of these key genes were assayed by qRT-PCR, and compared with expression levels from the EGFP mTSC line, originally derived in the Rossant laboratory and here designated Rossant (Tanaka et al., 1998). All newly derived cell lines showed equivalent expression to the Rossant line (Figure 4.2E), as measured by log2 fold change, with the exception of lines $X^{M}O$ 2 and $X^{P}O$ 1. These two XO lines had increased expression for most of the genes assayed. I conclude that I had successfully derived $X^{P}O$ and $X^{M}O$ mTSC lines, in addition to female control lines.

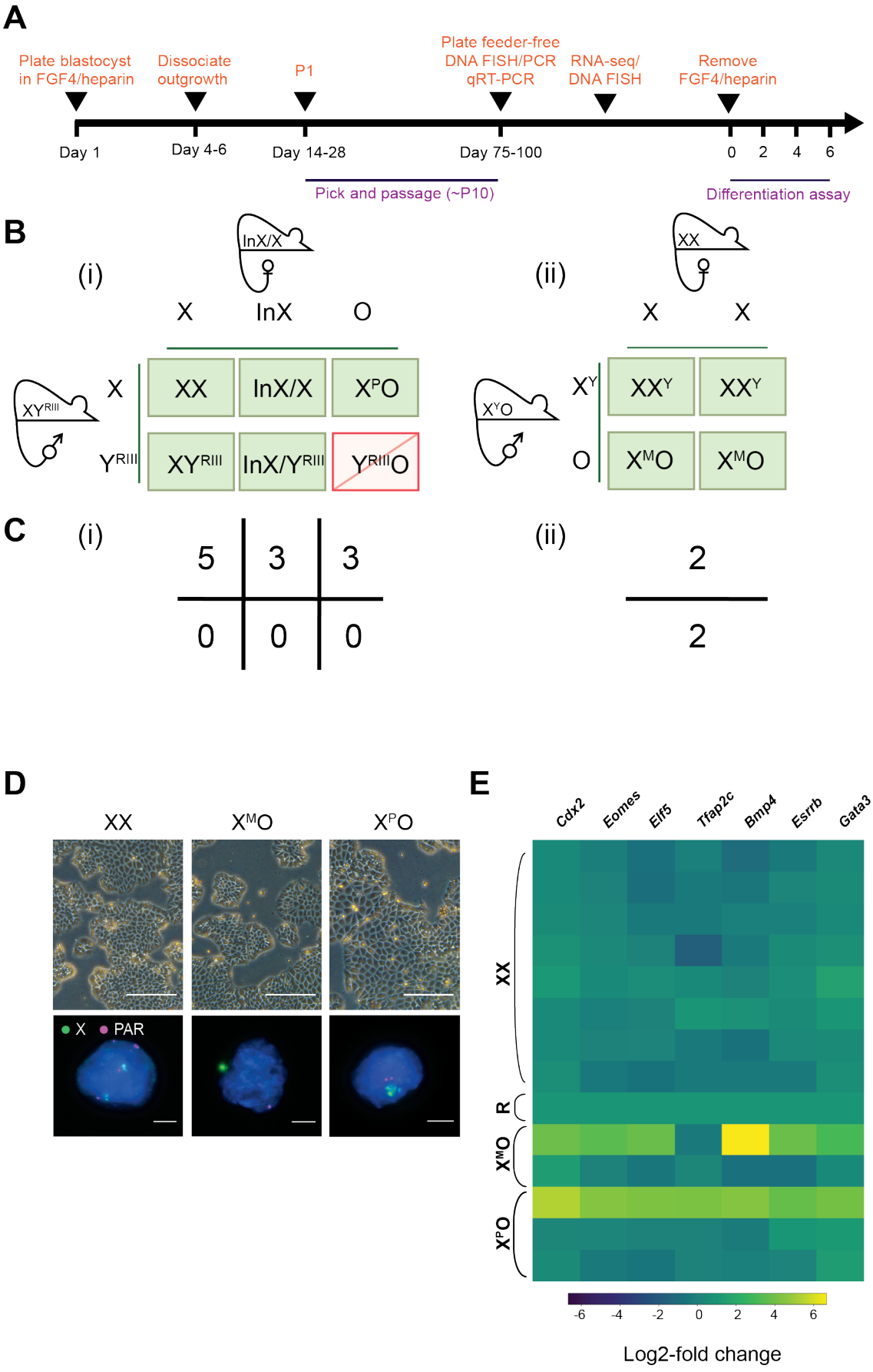
A
Plate blastocyst in FGF4/heparin
Dissociate outgrowth
P1
Plate feeder-free DNA FISH/PCR qRT-PCR
RNA-seq/ DNA FISH
Remove FGF4/heparin
Day 1
Day 4-6
Day 14-28
Day 75-100
0 2 4 6
Pick and passage (~P10)
Differentiation assay
B
(i)
InX/X
X InX O
XY^RIII
X
Y^RIII
XX
InX/X
X^PO
XY^RIII
InX/Y^RIII
Y^RIIIO
(ii)
XX
X X
X^YO
X^Y
O
XX^Y
XX^Y
X^MO
X^MO
C
(i)
5 3 3
0 0 0
(ii)
2
2
D
XX
X^MO
X^PO
X PAR
E
Cdx2
Eomes
Elf5
Tfap2c
Bmp4
Esrrb
Gata3
XX
R
X^MO
X^PO
-6 -4 -2 0 2 4 6
Log2-fold change

Figure 4.2: Derivation of mouse trophoblast stem cells (mTSCs). (**A**) Schematic depicting derivation process. (**B**) (i) Mouse cross used to generate XX and X^PO blastocysts, and (ii) X^MO blastocysts. (**C**) (i) Number of cell lines derived, corresponding to genotypes in (**B**) (i), and (ii) corresponding to (**B**) (ii). (**D**) (i) Brightfield microscopy showing feeder free mTSCs of different sex chromosome genotypes (scale bar = 100uM); (ii) Representative images of DNA FISH probing for sex chromosomes (scale bar = 10uM). 50 cells were counted per cell line, with 80% agreement required to denote a sex chromosome genotype. (**E**) Heatmap summarising qRT-PCR results following screening of all cell lines for mTSC marker genes. Results were first normalised to *Gapdh* and *Srp72*, before log-fold change was determined based on a reference cell line (Rossant).

4.2.2 X^PO, X^MO, and XX mTSCs show equivalent differentiation potential *in vitro*

The EPC originates from the polar trophectoderm, and later gives rise to the spongiotrophoblast in the mature placenta (Cross et al., 1994). Previous work has shown that the EPC in X^PO conceptuses is deficient in size at E7.5 relative to XX littermates (Jamieson et al., 1998). In contrast, X^MO EPC was morphologically normal (Jamieson et al., 1998). As the EPC represents a relatively early, transient progenitor population of cells in the placenta, I was interested to see if the *in vivo* phenotype manifests as a differentiation bias in X^PO mTSCs *in vitro*. I hypothesised that, in an undirected differentiation protocol, X^PO mTSCs might be less likely to form the differentiation products of EPC, i.e. spongiotrophoblast cells, when compared with X^MO and XX mTSCs.

In order to test this hypothesis, three X^PO, two X^MO, three XX, and the Rossant EGFP mTSC lines were differentiated by removal of FGF4 and heparin. I first noted that there were no obvious morphological differences between mTSC genotypes during the differentiation (Figure 4.3). To assay for the presence of cells from different placental lineages within the differentiated cultures, I performed qRT-PCR. If X^PO differentiated mTSC cultures are deficient in EPC cells and other cell types downstream, I would expect to detect reduced expression of markers for these cell types, relative to XX differentiated mTSC cultures or the Rossant EGFP control. I might also observe increased expression of markers for other placenta lineages, as

when *Ascl2* function is ablated *in vivo*, trophoblast giant cells predominate (Guillemot et al., 1994, 1995).

I first looked to confirm the effectiveness of the differentiation protocol by assaying expression of the key mouse trophoblast marker gene *Cdx2* (Tanaka et al., 1998; Niwa et al., 2005). All mTSC genotypes (X^PO, X^MO, and XX) showed downregulation of *Cdx2* expression at day two of differentiation when compared to the Rossant XX EGFP line at day 0 (Figure 4.4) and this was maintained throughout the six day time course. For each individual timepoint, there were no significant differences in *Cdx2* expression between mTSC genotypes. I conclude that mTSC genotype does not affect the ability of the cell to exit the multipotent state, as tested by *Cdx2* expression.

Next I tested the ability of the three mTSC genotypes to differentiate into spongiotrophoblast via EPC, compared with the Rossant XX EGFP line. EPC is characterised by expression of the basic helix loop helix (bHLH) transcription factor *Ascl2/Mash2* (Guillemot et al., 1994, 1995), and one of the key markers of the spongiotrophoblast is *Tpbpa/4311* (Carney et al., 1993). Notably, I observed increased expression of *Ascl2* across all mTSC genotypes at day two (Figure 4.4), consistent with the downregulation of *Cdx2* and exit from the stem cell state. There was, however, no significant difference in *Ascl2* between genotypes. I also observed upregulation of the spongiotrophoblast marker *Tpbpa*, which continued throughout the differentiation timecourse, though again there was no significant difference between genotypes. Finally, I found downregulation of the glycogen trophoblast marker *Pcdh12* across all cell lines at day two, and this level of expression was maintained through to day six. There was no significant difference between the mTSC genotypes. From these data I conclude that X^PO or X^MO mTSCs do not show a differentiation bias away from EPC, or its derivative spongiotrophoblast, when compared to Rossant XX EGFP mTSCs.

Although there was no difference in differentiation potential between X^PO and XX mTSCs towards the spongiotrophoblast lineage, I continued to investigate differential potential towards other placenta lineages.

In order to assay trophoblast giant cell (TGC) differentiation potential, I first measured *Hand1* expression. *Hand1* is a bHLH transcription factor co expressed with *Ascl2* in the EPC (Scott et al., 2000), though these two genes have mutually antagonistic functions in differentiation. As described above, *Ascl2* maintains spongiotrophoblast, whereas *Hand1* is required for giant cell differentiation. Unsurprisingly, in mTSCs *Hand1* showed a similar expression pattern to *Ascl2*, with upregulation at day two, which then reduced almost back to baseline at day six (Figure 4.4). There was no significant difference in *Hand1* expression between X^PO, X^MO and XX mTSCs, though all three genotypes showed lower expression than the Rossant XX EGFP line at all time points.

I next looked for the presence of markers for the terminally differentiated TGC cell types, including sinusoidal TGCs (s-TGCs) found lining the maternal sinusoids (Simmons et al., 2007). *Pl1*, *Prl2c2*, and *Prl3d3* are expressed in TGCs (Simmons et al., 2007), and were upregulated from day four of differentiation in all cell lines (Figure 4.4). These three markers were generally less expressed in XX mTSCs than both X^PO and X^MO mTSCs, though the differences were not statistically significant. *Ctsq*, a marker of s-TGCs, showed slight upregulation at day two, and became highly upregulated on days four and six. There was no significant difference in *Ctsq* expression between mTSC genotypes. I conclude that, whilst the data suggest lower expression of TGC markers in XX mTSCs when compared to XO mTSCs and Rossant XX EGFP mTSCs, these differences were not significant. Therefore I found no difference in the expression of giant cell lineage markers between XX, X^PO, X^MO, and Rossant XX EGFP mTSCs. Notably, both X^PO and X^MO mTSC lines generally showed larger confidence intervals than those for XX mTSCs.

Finally I assayed for syncytiotrophoblast (Syn) differentiation. As a marker for Syn progenitors, I used *Rhox4b*/*Ehox* (Watson et al., 2011). Expression relative

to Rossant XX EGFP was reduced in all cell lines at day zero, and this difference persisted throughout differentiation (Figure 4.4). *Rhox4b* was downregulated in all mTSC lines and, notwithstanding the difference when compared to Rossant XX EGFP, there was no difference in expression between XX, $X^{P}O$ and $X^{M}O$ lines.

Coincident with the reduction in Syn progenitors, expression of markers for terminally differentiated syncytiotrophoblast-I (SynT-I) increased at day two, and this increase persisted through the differentiation timecourse (Figure 4.4). *Syna* (Simmons et al., 2008) showed marked upregulation at day two, which was maintained, whereas *Snai1* (Watson et al., 2011) showed a small upregulation at day two, which continued to day six. Expression of *Snai1* in Rossant XX EGFP mTSCs was slighly higher than XX, $X^{P}O$ and $X^{M}O$ mTSCs, though there was no difference between the latter three genotypes. Expression of *Synb*, a marker for syncytiotrophoblast-II (SynT-II, Simmons et al., 2008), was decreased in all cell lines relative to Rossant XX EGFP at day 0. *Synb* transcript levels then increased incrementally in all cell lines to day six. Interestingly, expression of a second marker of SynT-II, *Gcm1*, decreased in all mTSC lines on day two, and continued to decrease in XX and Rossant XX EGFP mTSC lines through to day six. Expression of *Gcm1* in $X^{P}O$ and $X^{M}O$ cell lines troughed at day two this level was maintained relative to Rossant XX EGFP day 0. From these data I was able to conclude that there was no difference between $X^{P}O$, $X^{M}O$, and XX mTSCs in their ability to differentiate to all placenta cell lineages.

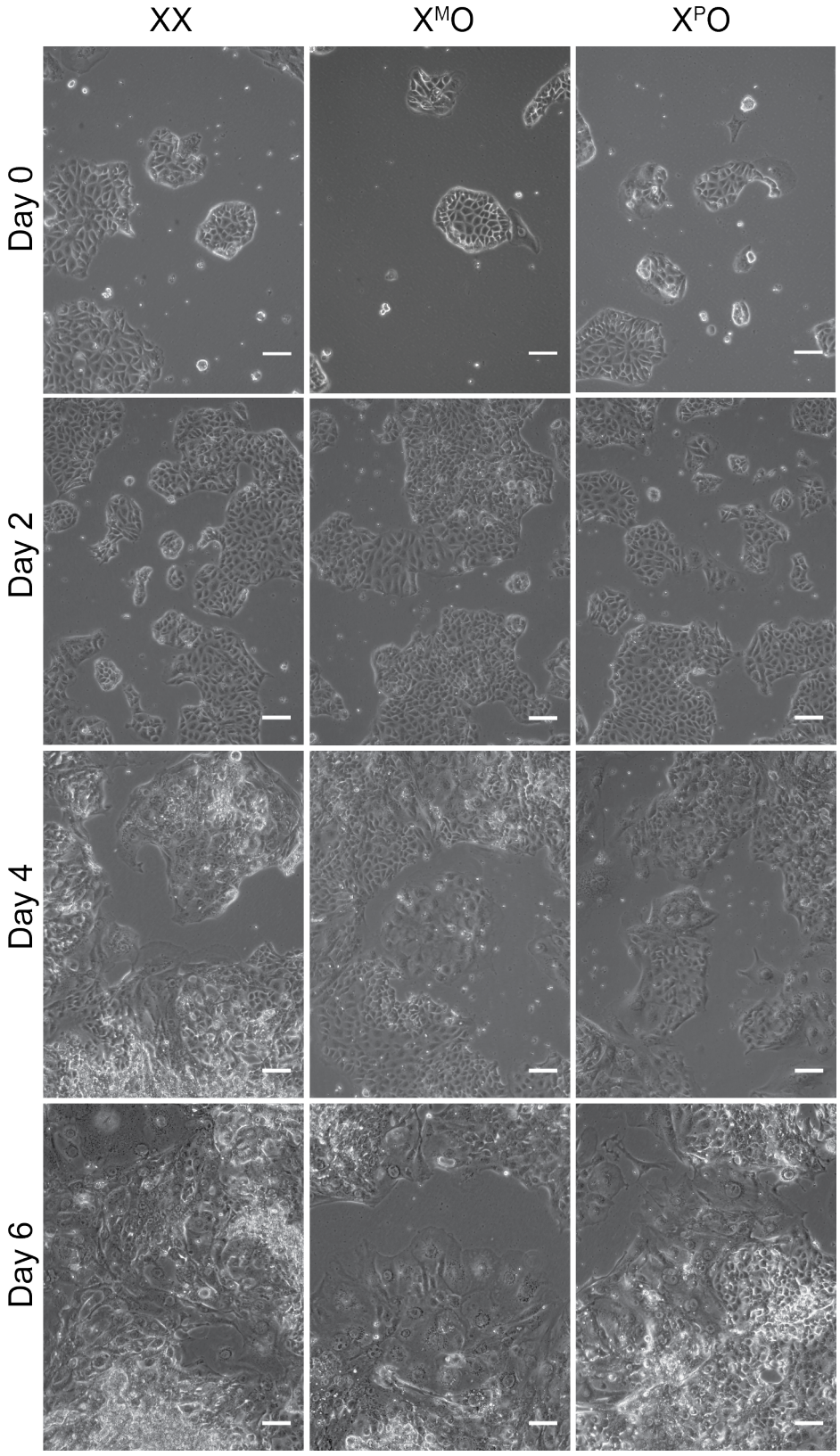
XX
X^MO
X^PO
Day 0
Day 2
Day 4
Day 6

Figure 4.3: Differentiation of mTSCs. Representative brightfield images of mTSC lines with different sex chromosome genotypes following a six day differentiation timecourse (scale bars = 100uM).

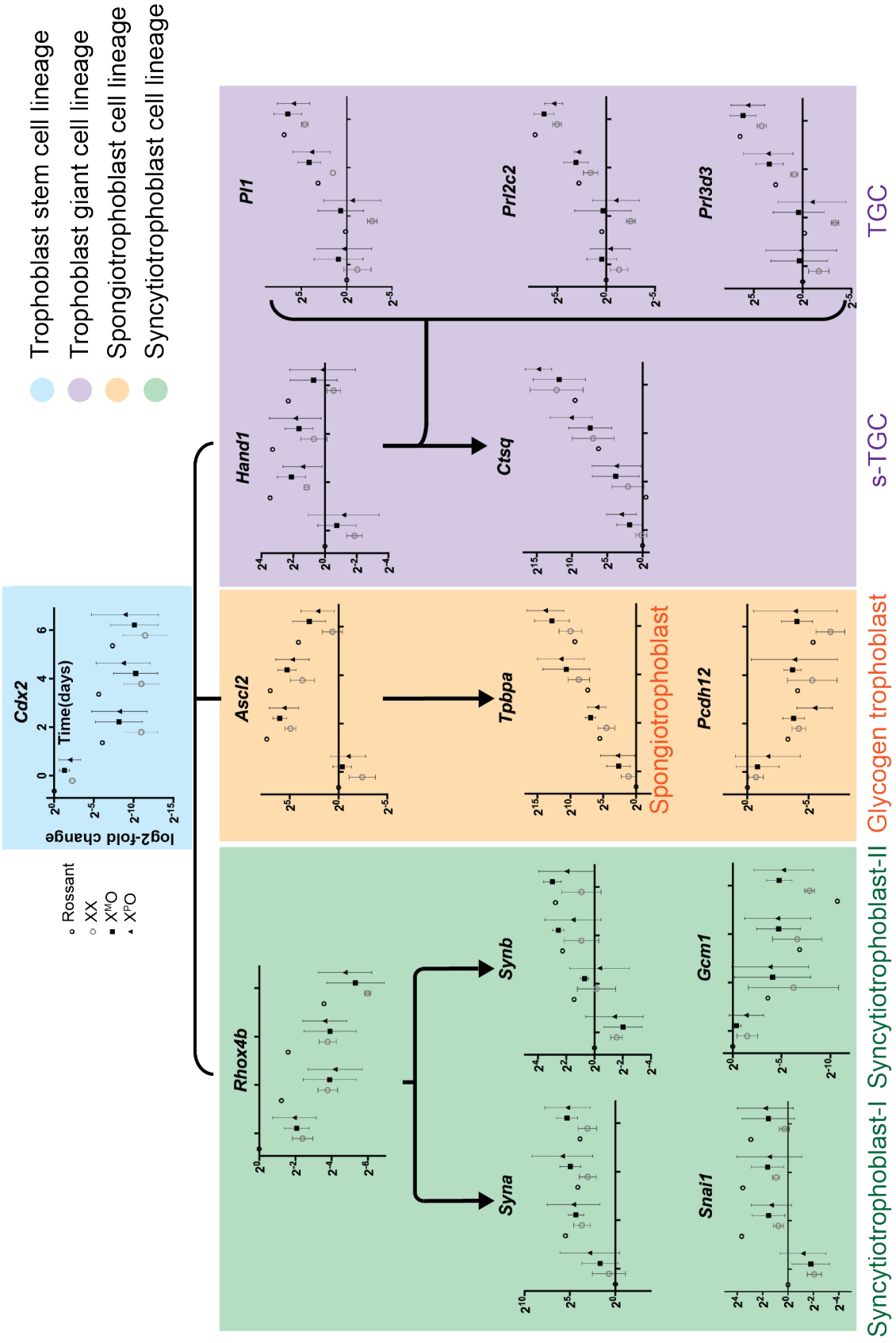
Trophoblast stem cell lineage
Trophoblast giant cell lineage
Spongiotrophoblast cell lineage
Syncytiotrophoblast cell lineage
Cdx2
log2-fold change
Time(days)
Rossant
XX
XMO
XPO
Hand1
Ctsq
Pl1
Prl2c2
Prl3d3
Ascl2
Tpbpa
Pcdh12
Rhox4b
Syna
Synb
Gcm1
Snai1
s-TGC
TGC
Spongiotrophoblast
Syncytiotrophoblast-I
Syncytiotrophoblast-II
Glycogen trophoblast

Figure 4.4: qRT-PCR analysis of gene expression during mTSC differentiation. Data are presented in the form of a differentiation tree, whereby *Cdx2*, a marker for the stem cell lineage, is at the base; with the three main lineages of the mouse placenta branching out. Each graph shows the mean logFC and 95% CI at days 0, 2, 4 and 6 for each sex chromosome genotype per gene, relative to day 0 Rossant EGFP. Data represent values obtained from three independent XX mTSC lines, three independent $X^{P}O$ mTSC lines, and two independent $X^{M}O$ mTSC lines.

4.2.3 Derivation of mESC and mEpiLC lines and qRT-PCR verification of identity

I considered it most likely that X linked imprinting candidates would be expressed in the extraembryonic tissue (as described in 4.1), making mTSC lines the most relevant for my screening experiment. However, I also wanted to model the embryo proper as an alternative hypothesis. To this end, I derived mESC lines to capture the pluripotent compartment, and differentiated these lines into mEpiLCs to model the epiblast. $X^{P}O$ and $X^{M}O$ mESC lines were derived from blastocysts from cross 1 and cross 2, respectively. Each embryo was plated individually in 2i+LIF, as previously described (Ying et al., 2008). Outgrowths were picked after 10-14 days and, concurrent with genotyping, cell lines were expanded to passage five (Figure 4.5A). DNA FISH was used to confirm sex chromosome genotype, and three mESC lines were maintained for each genotype, including XX and XY control lines (Figure 4.5B). A corresponding, isogenic mEpiLC line was differentiated from each mESC line using bFGF and Activin A (Figure 4.5A), as described (Hayashi et al., 2011b; Hayashi and Saitou, 2013). EpiLCs have been shown to represent the epiblast of the mouse blastocyst stage embryo, thus downregulating pluripotency markers including *Sox2* and *Nanog*, and upregulating genes associated with exit from pluripotency, including *Dnmt3b* and *Fgf5* (Hayashi et al., 2011b). I compared expression of these genes in mEpiLCs with the mESCs from which they were derived by qRT-PCR, and noted downregulation of pluripotency associated genes and upregulation of epiblast associated genes (Figure 4.5C). These results were entirely consistent with the literature, and were taken to confirm the lineage identity of the derived cell lines.

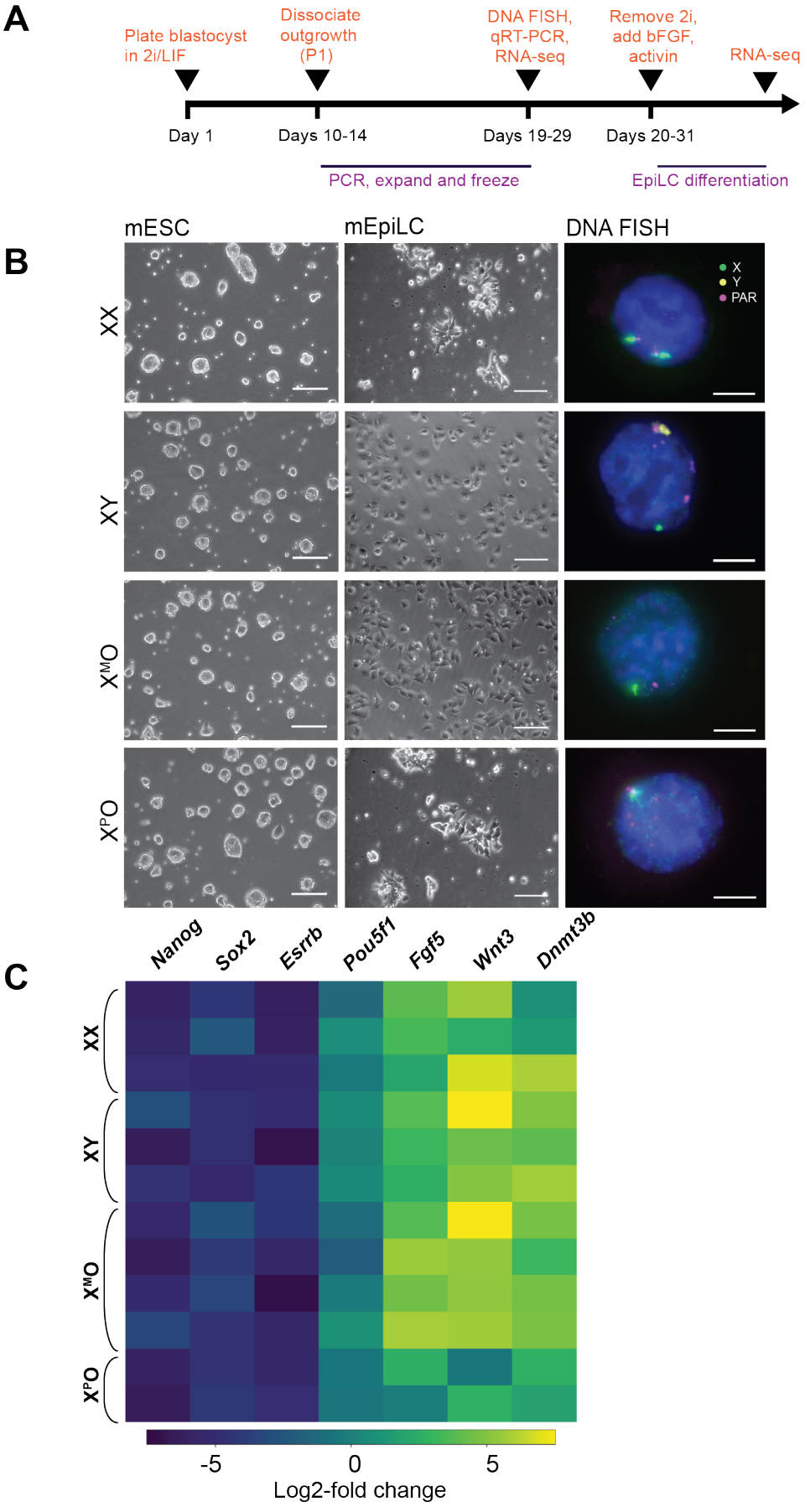
A
Plate blastocyst in 2i/LIF
Dissociate outgrowth (P1)
DNA FISH, qRT-PCR, RNA-seq
Remove 2i, add bFGF, activin
RNA-seq
Day 1
Days 10-14
Days 19-29
Days 20-31
PCR, expand and freeze
EpiLC differentiation
B
mESC
mEpiLC
DNA FISH
X
Y
PAR
XX
XY
XMO
XPO
C
Nanog
Sox2
Esrrb
Pou5f1
Fgf5
Wnt3
Dnmt3b
XX
XY
XMO
XPO
-5
0
5
Log2-fold change

Figure 4.5: Derivation of mouse embryonic stem cells (mESCs) and mouse epiblast like stem cells (mEpiLCs). (**A**) Schematic depicting derivation process. (**B**) Representative brightfield images of mESCs and the resultant mEpiLCs following differentiation (scale bars = 50uM), alongside DNA FISH used for genotyping. 50 cells were counted per cell line, with 80% agreement required to denote a sex chromosome genotype. (**C**) Heatmap summarising qRT-PCR data comparing mEpiLC lines with their originating mESC line for mEpiLC and mESC marker gene expression. Results were first normalised to *Gapdh* and *Srp72*, before log fold change was determined based on the originating mESC line for each mEpiLC line.

4.2.4 RNA-seq analysis of gene expression in mTSC, mESC and mEpiLC lines

In order to look for genes differentially expressed between X^PO and X^MO cell lines, and thus identify candidates that may be imprinted, RNA-seq was performed on RNA isolated from all mTSC, mESCs and mEpiLCs. Sequencing was performed by the Advanced Sequencing Facility STP at Francis Crick Institute, and returned between 39-54x10^6 paired end, strand specific reads per sample (Table 4.1). Data were analysed and plotted by a Turner lab post doc, Mahesh Sangrithi, as per the pipeline detailed in Figure 4.6A.

To gain an initial, graphical overview of how the samples related to one another, and specifically look at the relationship between biological replicates, multi dimensional scaling (MDS: Figure 4.6B) and t-stochastic neighbour embedding (t-SNE: Figure 4.6C) analyses were performed. Both techniques showed tight clustering of samples by cell type and, pleasingly, within cell type clustering by genotype. Further analysis of the mTSC data by unsupervised hierarchical clustering (UHC) showed with greater resolution that XX mTSCs clustered with the XX Rossant reference line, and separately from all XO mTSC lines (Figure 4.6D). Within XO mTSCs, all X^PO lines were shown to be more closely related to one another than to the X^MO mTSCs lines.

Cell type	Sample	Raw reads	Percentage mapped
mESC	XX 2	41552922	87.23
	XX 1	43290415	88.83
	XX 0	48235209	88.81
	XY 2	33649772	91.26
	XY 1	39843527	86.18
	XY 0	52491568	85.55
	$X^{M}O$ 2	50469556	89.3
	$X^{M}O$ 1	40778312	78.15
	$X^{M}O$ 0	46829273	87.38
	$X^{P}O$ 1	46481635	87.34
	$X^{P}O$ 0	40710940	93.3
mEpiLC	XX 2	55837430	90.82
	XX 1	45576928	92.35
	XX 0	50715628	90.91
	XY 2	51420726	91.85
	XY 0	50108108	91.91
	$X^{M}O$ 3	33436541	90.62
	$X^{M}O$ 2	46689812	91.04
	$X^{M}O$ 1	53982073	91.63
	$X^{M}O$ 0	48211831	91.39
	$X^{P}O$ 2	47362417	91.36
	$X^{P}O$ 0	60231527	90.94
mTSC	XX 7	41863904	91.89
	XX 6	44532910	92.42
	XX 5	39112596	93.35
	XX 4	41064513	91.62
	XX 3	31578074	94.77
	XX 2	37020197	92.7
	XX 1	41419287	92.11
	XX 0	39396116	93.07
	Rossant	42482645	93.08
	$X^{M}O$ 2	52206246	91.37
	$X^{M}O$ 0	54152268	90.27
	$X^{P}O$ 3	63225432	91.23
	$X^{P}O$ 1	54999428	91.46
	$X^{P}O$ 0	43603825	90.46

Table 4.1: RNA-seq mapping percentages

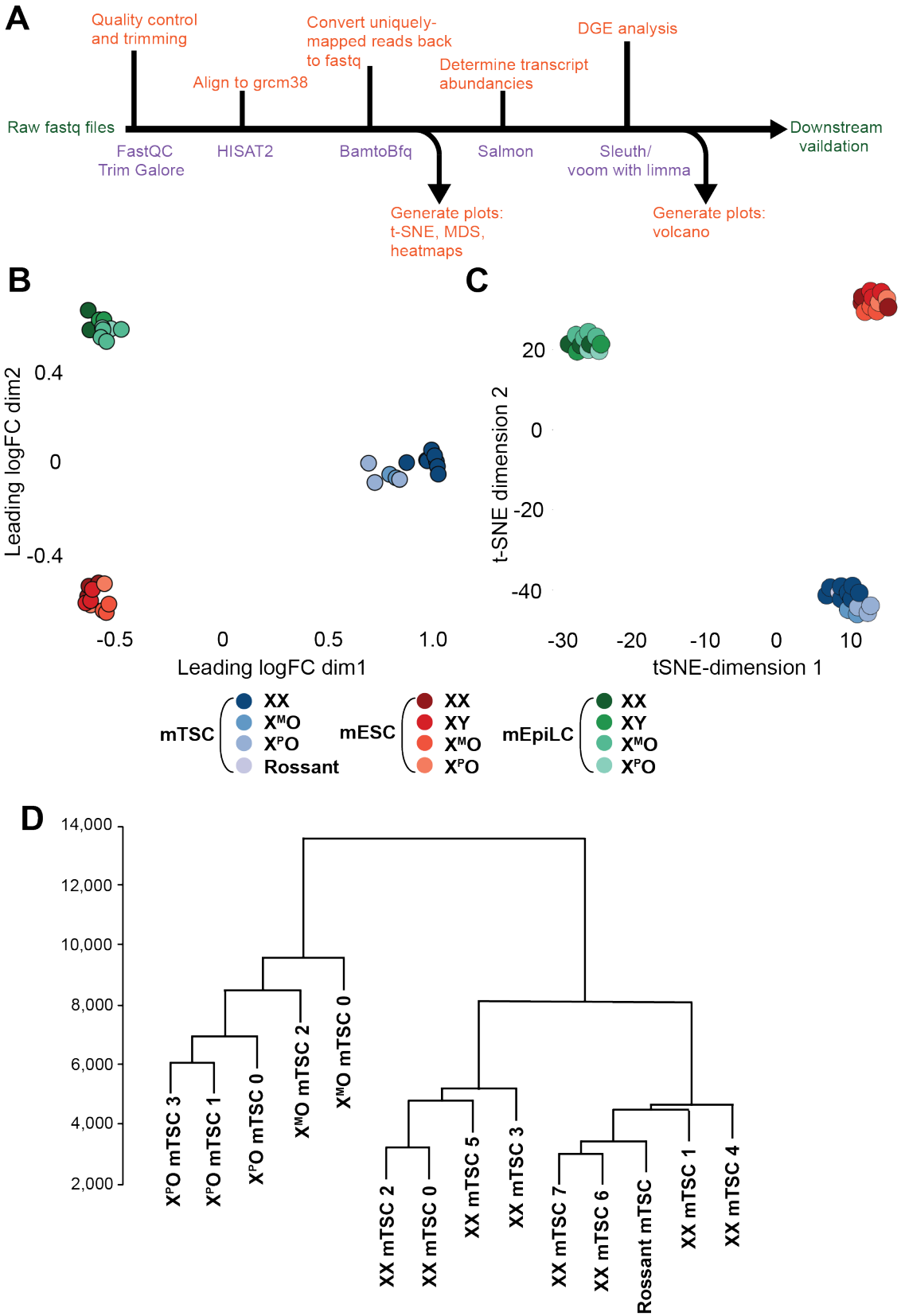
A
Quality control and trimming
Align to grcm38
Convert uniquely-mapped reads back to fastq
Determine transcript abundancies
DGE analysis
Raw fastq files
FastQC
Trim Galore
HISAT2
BamtoBfq
Salmon
Sleuth/ voom with limma
Downstream vaildation
Generate plots: t-SNE, MDS, heatmaps
Generate plots: volcano
B
Leading logFC dim2
0.4
0
-0.4
-0.5
0
0.5
1.0
Leading logFC dim1
C
t-SNE dimension 2
20
0
-20
-40
-30
-20
-10
0
10
tSNE-dimension 1
mTSC
XX
XMO
XPO
Rossant
mESC
XX
XY
XMO
XPO
mEpiLC
XX
XY
XMO
XPO
D
14,000
12,000
10,000
8,000
6,000
4,000
2,000
XPO mTSC 3
XPO mTSC 1
XPO mTSC 0
XMO mTSC 2
XMO mTSC 0
XX mTSC 2
XX mTSC 0
XX mTSC 5
XX mTSC 3
XX mTSC 7
XX mTSC 6
Rossant mTSC
XX mTSC 1
XX mTSC 4

Figure 4.6: Initial analyses of RNA-seq on mTSC, mESC and mEpiLC. (**A**) Schematic of bioinformatic analysis pipeline: tasks are shown in orange and software utilised is shown in purple. (**B**) Multi-dimensional scaling plot of all RNA-seq datasets. (**C**) T-distributed stochastic neighbour embedding plot of RNA-seq datasets. (**D**) Unsupervised hierarchical clustering plot of mTSC RNA-seq data.

Expression of specific marker genes was analysed next. Y linked gene expression was first used to confirm the XY cell line genotyping data (Figure 4.7A). XY cell lines showed relatively higher expression of Y linked genes when compared with either XX or XO cell lines. Notably, *Kdm5d* appears to be expressed equally in cell lines of all sex chromosome genotypes, in particular mESCs and mEpiLCs (Figure 4.7A). This artifact is likely the result of mismapping of *Kdm5c* reads to *Kdm5d*, an effect documented for highly expressed genes, such as *Kdm5c* in mESCs (Conesa et al., 2016).

As there were no XY mTSC lines available, expression of *Xist*, the lncRNA that mediates XCI, was analysed. XCI takes place in XX mTSCs, such that *Xist* expression was expected from the X^P (Mak et al., 2002). As XO mTSCs carry only a single X chromosome, XCI is not required, and *Xist* expression was not expected. These predictions were met (Figure 4.7A). XCI is imprinted in extraembryonic tissue, such that *Xist* is always expressed from the X^P in XX mTSCs (Kunath et al., 2005). Notably, this imprinted expression was not maintained in X^PO mTSCs, consistent with the requirement for X linked gene expression in extraembryonic tissue. Furthermore, I observed relatively low level *Xist* expression in mESCs, likely because they have not undergone XCI. This process has been initiated in mEpiLCs, hence the slight upregulation of *Xist* when compared to mESCs.

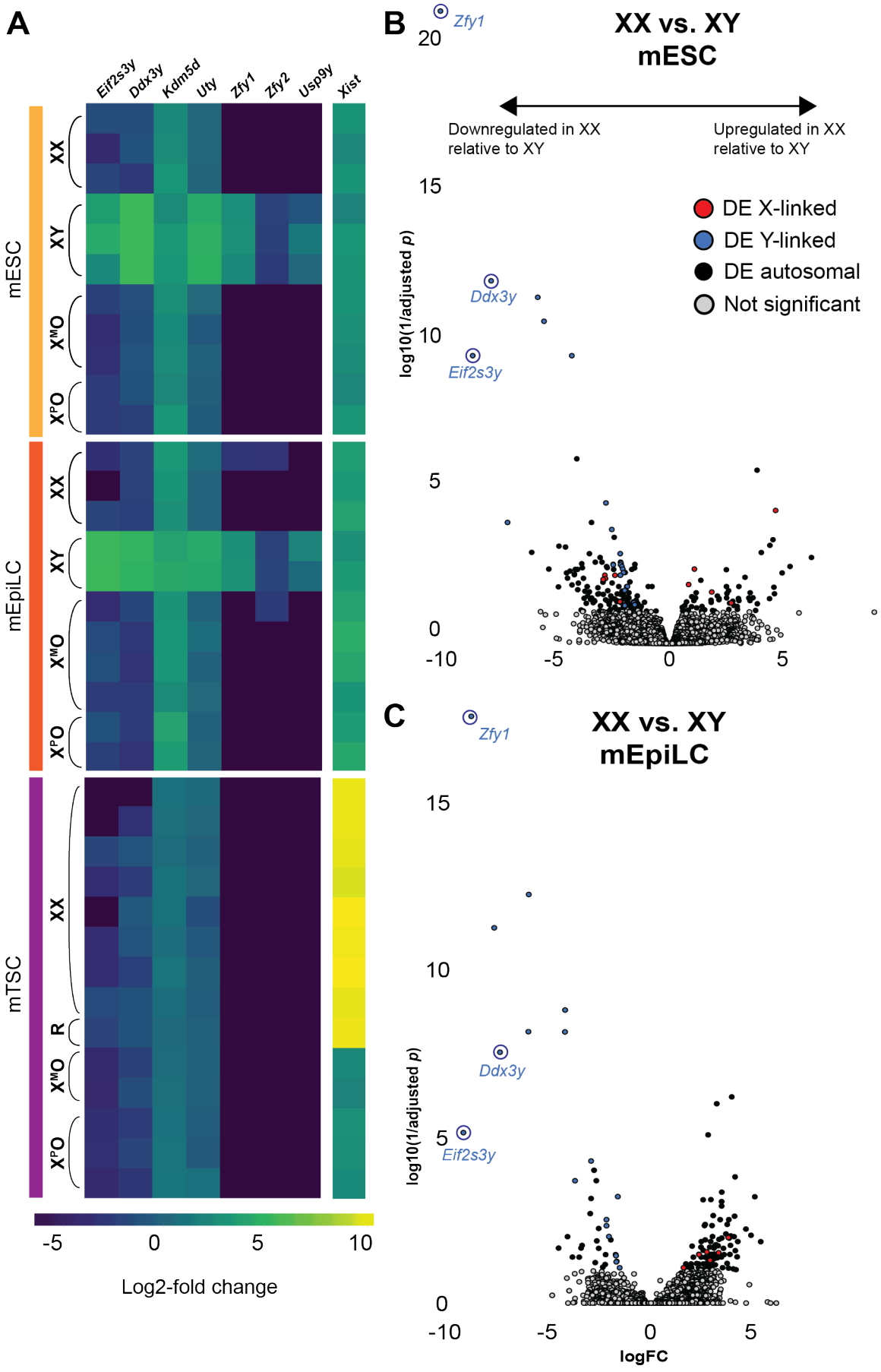
A
Eif2s3y
Ddx3y
Kdm5d
Uty
Zfy1
Zfy2
Usp9y
Xist
mESC
mEpiLC
mTSC
XX
XY
XMO
XPO
R
-5
0
5
10
Log2-fold change
B
Zfy1
XX vs. XY
mESC
Downregulated in XX relative to XY
Upregulated in XX relative to XY
DE X-linked
DE Y-linked
DE autosomal
Not significant
log10(1/adjusted p)
Ddx3y
Eif2s3y
C
XX vs. XY
mEpiLC
logFC

Figure 4.7: Genotyping confirmation from RNA-seq data in all cell types. (**A**) Heatmap showing relative expression of Y linked genes and *Xist* in all RNA-seq datasets. (**B**) Volcano plot representing genes differentially expressed in XX mESCs compared to XY mESCs. (**C**) Volcano plot representing genes differentially expressed in XX mEpiLCs compared to XY mEpiLCs.

4.2.5 Identification of candidate imprinted genes by differential gene expression analysis (DGE)

Before comparing gene expression between X^PO and X^MO cell lines to identify potential candidates for the imprinting hypothesis, the differential gene expression (DGE) analysis pipeline was validated. Expression of genes from the Y chromosome sets apart the transcriptomes of XY from XX and XO cell lines. XX and XY mESC and XX and XY mEpiLC datasets were analysed for differentially expressed genes (Figure 4.7B,C). These two plots compare XX mESC and mEpiLC lines to XY mESC and mEpiLC baselines, respectively, therefore relative downregulation of Y linked genes was predicted. As expected, most highly significantly downregulated genes were Y linked (Figure 4.7B,C, circled). This provided confirmation that the bioinformatic pipeline was able to detect biologically relevant differential expression.

In order to identify all differentially expressed genes within cell type, pairwise comparisons were made between all sex chromosome genotypes (Figure 4.9A(i)). Focusing on the comparison between X^PO and X^MO lines, I used volcano plots to visualise the degree of differential expression for each gene and the significance of the hit (Figure 4.8).

For mESC, the total number of genes differentially expressed between X^MO and X^PO was 123, which were split evenly between upregulation and downregulation (Figure 4.8A). Interestingly, of these 123, 8 were X linked, again distributed evenly between upregulation and downregulation.

For mEpiLCs, 244 genes were differentially expressed in $X^{M}O$ relative to $X^{P}O$, and more of these were upregulated (Figure 4.8B). Of the 244 total differentially expressed genes, 10 were X linked genes, mostly upregulated in $X^{M}O$ relative to $X^{P}O$ EpiLCs.

For mTSCs, 201 genes were differentially expressed in $X^{M}O$ relative to $X^{P}O$, and significant number of these were downregulated (Figure 4.8C). Of 201 total differentially expressed genes, 24 were X linked, and these X linked genes were mostly downregulated in $X^{M}O$ relative to $X^{P}O$ mTSCs.

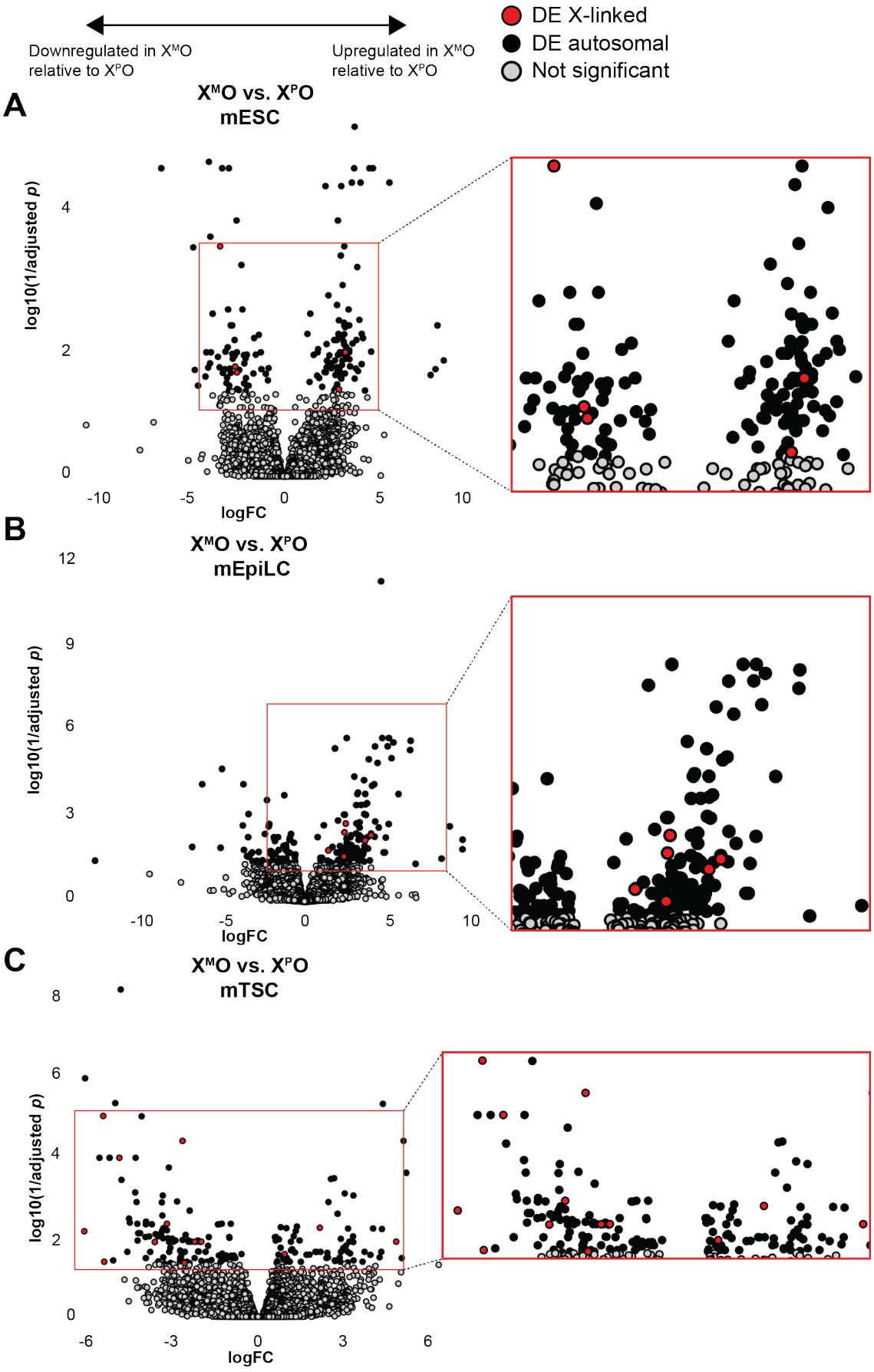
Downregulated in XMO relative to XPO
Upregulated in XMO relative to XPO
DE X-linked
DE autosomal
Not significant
A
XMO vs. XPO mESC
log10(1/adjusted p)
logFC
B
XMO vs. XPO mEpiLC
log10(1/adjusted p)
logFC
C
XMO vs. XPO mTSC
log10(1/adjusted p)
logFC

Figure 4.8: Differential gene expression analyses. (**A**) Volcano plot showing DGE between X^MO relative to X^PO mESCs, magnified on the right hand side. (**B**) Volcano plot showing DGE between X^MO relative to X^PO mEpiLCs. (**C**) Volcano plot showing DGE between X^MO relative to X^PO mTSCs.

I next compared the lists of differentially expressed genes between cells types to look for commonality. As mEpiLCs are differentiated from mESCs, and both contribute to the embryo proper, I expected to observe a degree of conservation between the differentially expressed genes. This proved to be correct, as 20 genes were significantly differentially expressed between X^PO and X^MO mESC and mEpiLC lines (Figure 4.9A(ii)). In contrast, only two genes were differentially expressed between X^PO and X^MO mTSCs and mESCs. Two other genes were differentially expressed between X^PO and X^MO in mTSCs and mEpiLCs. There were no genes differentially expressed between X^PO and X^MO cells common to all three cell types (Figure 4.9A(ii)).

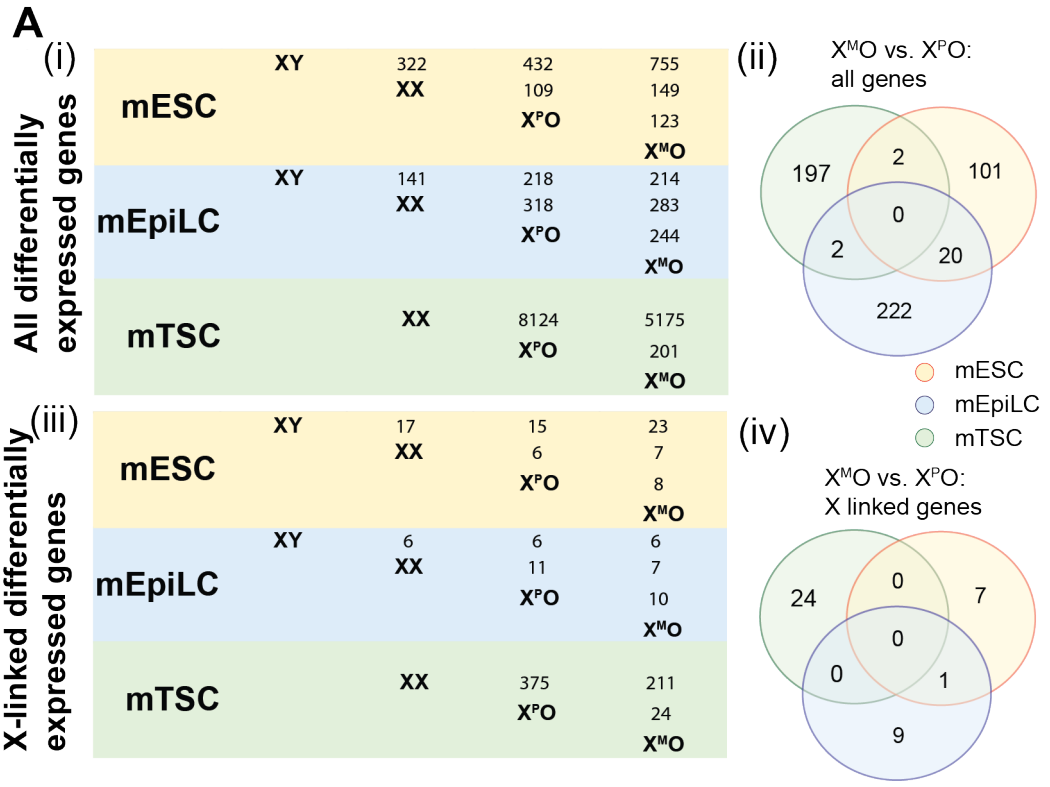

Figure 4.9: Differential gene expression analyses. (**A**) (i) Summary data of all genes differentially expressed between sex chromosome genotypes, within cell type; (ii) Venn diagram showing cross over between genes differentially expressed in X^MO relative to X^PO cell lines; (iii) Summary data of all X linked genes differentially expressed between sex chromosome genotypes, within cell type; (iv) Venn diagram showing cross over between X linked genes differentially expressed in X^MO relative to X^PO cell lines.

The fundamental difference between X^PO and X^MO cell lines is the parental origin of the X chromosome, therefore one would expect any candidate genes for the imprinting hypothesis to be localised to the X chromosome. Autosomal genes may also be differentially expressed, though these genes would theoretically be downstream of any X linked candidates. I therefore chose to focus on the X chromosome, and looked to see how many of the genes identified in the DGE analysis localised to the X (Figure 4.9A(iii)). Once again focusing on the X^PO and X^MO comparison, I compared the relatively short lists to look for any conservation. Unsurprisingly, there was only one gene differentially expressed between X^PO and X^MO in more than one cell type. *Mageb10-ps* appeared in both mESC and mEpiLC lists (Table 4.3, 4.4), otherwise all candidates were unique to the cell type.

Gene	Upreg. in X^MO relative to X^PO (logFC)	Downreg. in X^MO relative to X^PO (logFC)	Comments	References
Hs6st2$^{\$}$	4.48		Heparan sulphate 6-*O*-sulphotransferase, placenta phenotype in homologue *Hs6st1*	Habuchi et al., 2000, 2007
Srpk3	3.29		Muscle specific protein kinase, myopathy	Nakagawa et al., 2005
Etd$^{\$}$	1.90		Testis, gonad differentiation	Menke and Page, 2002; Bouma et al., 2010; Correa et al., 2012; Zhao et al., 2015
Rbmx	1.09		RNA binding protein, spermatogenesis	Mazeyrat et al., 1999; Elliott, 2004
Acot9$^{\$}$	1.01		Mitochondrial acyl-CoA thioesterase	Poupon et al., 1999
Prr32		-1.25	Interacts with miRNAs	Diez-Roux et al., 2011
Gm14668		-1.40	None	n/a
Gm14988		-1.43	None	n/a
Rhox3a2		-1.52		
Rhox3c		-1.53		MacLean et al., 2005;
Rhox3e		-1.53	Testis, placenta, DNA-binding domain	Maclean et al., 2006,
Rhox3f		-1.76		2011
Rhox3b-ps		-1.80		
Gm15367*		-2.64	No annotation	n/a
Gm8908*		-2.92	No annotation	n/a
Gm4911*		-3.22	No annotation	n/a
Pbsn*		-3.32	Androgen-related, prostate	Johnson et al., 2000
Dmrtc1c2*		-3.38	Male-biased expression, lacks DNA methyl transferase activity	Veith et al., 2006
Gm15023		-3.38	Homology to *Pramel3*, a cancer testis antigen	Zhou et al., 2013, 2014
AV320801*		-3.69	None associated	Zhou et al., 2014
Mageb18		-4.72	Melanoma antigen, sperm, apoptosis	Lin et al., 2012b
Chrdl1*		-4.73	Chondrogenesis	Nakayama et al., 2001
Tlr7*		-4.74	Innate immunity, sex linked neurodegeneration	Hemmi et al., 2002; Traub et al., 2012; Du et al., 2014
Heph*		-5.00	Iron metabolism, sex linked anaemia	Vulpe et al., 1999; Chen et al., 2004a; Jiang et al., 2015

Table 4.2: X linked genes significantly differentially expressed in X^MO vs X^PO mTSCs. * indicates genes also significantly differentially expressed in X^PO relative to XX mTSC analysis. $ indicates genes also significantly differentially expressed in X^MO relative to XX mTSC analysis.

Most of the candidate genes across all three cell types were annotated as either predicted genes or pseudogenes, and were therefore not analysed further at this point. Focusing on the mTSCs, some of the annotated candidates with ascribed function have potential based on what is already known. For example, *Hs6st2* was upregulated in X^MO mTSCs (Table 4.2). It is a heparan sulphate 6-*O*-sulphotransferase enzyme involved in the metabolism of the extracellular matrix (Habuchi et al., 2000). Its autosomal homologue *Hs6st1* is homozygous lethal during development, and conceptuses showed vascular abnormalities in the labyrinth of the placenta (Habuchi et al., 2007). Multiple genes from the reproductive homeobox (*Rhox*) cluster were highlighted as downregulated in X^MO mTSCs. The *Rhox* genes all have a conserved homeodomain, and are expressed in placenta, testis, and ovary (Maclean et al., 2006; Kobayashi et al., 2006). Interestingly, it has been suggested that a number of genes within this cluster are imprinted, though *Rhox3* is not among these (Maclean et al., 2011).

Gene	Upreg. in X^MO relative to X^PO (logFC)	Downreg. in X^MO relative to X^PO (logFC)	Comments	References
Mageb18-ps	3.62		Melanoma-associated antigen, testis	De Plaen et al., 1999; Chomez et al., 2001
Gm14985	1.93		None	n/a
Samt2	1.21		None	n/a
Gm15142	1.18		None	n/a
Fthl17e		-2.50	Testis, iron metabolism, ?imprinted	Wang et al., 2001b; Kobayashi et al., 2010
Gm44		-3.02	None	n/a
Magea2		-3.25	Melanoma-associated antigen, testis	De Plaen et al., 1999; Chomez et al., 2001
Gm14921		-3.46	None	n/a

Table 4.3: X linked genes significantly differentially expressed in X^MO vs X^PO mESCs

Gene	Upreg. in X^MO relative to X^PO (logFC)	Downreg. in X^MO relative to X^PO (logFC)	Comments	References
P2ry10	3.61		Identified by screen	n/a
Mageb18-ps	2.95		Melanoma-associated antigen, testis	De Plaen et al., 1999; Chomez et al., 2001
Zcchc5	2.51		Retrotranposon derived	Brandt et al., 2005a,b
Cdr1	2.36		Cortical thymic epithelial cell	Nowell et al., 2011
Gm14736	1.53		None	n/a
Gm14448	1.44		None	n/a
Gm14581	1.21		None	n/a
Gm14957		-1.19	None	n/a
Rpl7l1-ps1		-2.03	None	n/a
Gm14766		-2.43	None	n/a

Table 4.4: X linked genes significantly differentially expressed in X^MO vs X^PO mEpiLCs

The X^PO embryonic growth deficit phenotype has been quantified relative to either XX or XY littermates (Chapter 3). Any candidate genes that might have an affect on this X^PO phenotype might therefore be expected to also be differentially expressed in X^PO mTSCs relative to XX mTSCs. It would also be interesting to compare XO to XY mTSCs, however, XY mTSCs were not recovered during the derivation process. I therefore looked in more detail at the comparisons between X^PO and XX mTSCs, and then X^MO and XX mTSCs.

First considering genes downregulated in X^MO relative to X^PO mTSCs; this result could either be interpreted as genes downregulated in X^MO relative to other genotypes, or upregulated in X^PO relative to other genotypes. Ten genes were found in common between those downregulated in X^MO relative to X^PO mTSCs and those upregulated in X^PO relative to XX mTSCs (*, Table 4.2). I conclude that these ten genes are upregulated in X^PO mTSCs. These genes could potentially contribute to the X^PO embryonic growth deficit phenotype, and their expression would merit further investigation by qRT-PCR.

I then considered genes upregulated in X^MO relative to X^PO mTSCs. This result could be interpreted as either genes downregulated in X^PO relative to other genotypes, or upregulated in X^MO relative to other genotypes. Three genes were found in common to the lists of differentially expressed genes comparing X^MO relative to X^PO mTSCs, and X^MO relative to XX mTSCs (\$, Table 4.2). I conclude that these three genes are upregulated in X^MO mTSCs. As no difference in expression was observed for these genes between X^PO and XX mTSCs, I considered it unlikely that they would contribute to the X^PO embryonic growth deficit phenotype.

4.2.6 A significant number of genes were differentially expressed between XO and XX mTSCs

The comparisons utilised in the previous section also highlighted the significant number of genes differentially expressed between X^PO and XX mTSCs, and X^MO mTSCs and XX mTSCs: 8124 and 5175, respectively (Figure 4.10A). Following this unexpected result, I analysed the overlap between the two lists. Given that the X^P is always inactivated in XX mTSCs, XX mTSCs are theoretically more similar to X^MO mTSCs than X^PO mTSCs. I therefore expected to observe a greater number of genes differentially expressed in X^PO relative to XX mTSCs than X^MO relative to XX mTSCs, taking into account commonality between the two lists. I first excluded the 3817 genes commonly differentially expressed between both X^PO and X^MO relative to XX mTSCs (Figure 4.9B). There were significantly more genes specifically differentially expressed in X^PO relative to XX mTSCs, than in X^MO relative to XX mTSCs.

The numbers of genes differentially expressed between XO and XX mTSCs represent a difference of more than an order of magnitude when making the same comparisons for the mESCs and mEpiLCs (Figure 4.9A(i)). As there is no obvious biological explanation for the observation, I looked for order or pattern within the differentially expressed genes by performing over representation enrichment analysis (ORA) using WebGestalt (Zhang et al., 2005). As the observation related to all

XO mTSCs, I first considered those genes significantly differentially expressed in both X^PO relative to XX and X^MO relative to XX.

Analysis type	over representation category	Expected genes	Observed genes	*p* value	FDR
GO(biological process)	morphogenesis of an epithelium	82.27	115	$7.04x10^{-5}$	$4.50x10^{-2}$
	tube morphogenesis	63.20	91	$1.31x10^{-4}$	$4.50x10^{-2}$
	cell junction organization	31.35	51	$1.91x10^{-4}$	$4.50x10^{-2}$
	gland development	75.64	104	$2.95x10^{-4}$	$4.50x10^{-2}$
	cell-substrate adhesion	44.78	67	$3.15x10^{-4}$	$4.50x10^{-2}$
GO(cellular process)	cell-substrate junction	65.08	108	$1.59x10^{-8}$	$2.31x10^{-6}$
	cell leading edge	55.93	79	$5.96x10^{-4}$	$4.32x10^{-2}$
GO(molecular function)	rRNA binding	9.08	208	$3.13x10^{-4}$	$7.51x10^{-2}$
Pathway (KEGG)	Metabolic pathways	189.32	248	$5.95x10^{-7}$	$1.78x10^{-4}$
	Lysosome	17.93	36	$1.92x10^{-5}$	$2.86x10^{-3}$
	Influenza A	24.59	42	$2.50x10^{-4}$	$2.49x10^{-2}$

Table 4.5: Gene groups over represented in both DGE analyses comparing X^PO with XX mTSCs and X^MO with XX mTSCs. FDR cut off = 0.05.

Chromosome band	Expected genes	Observed genes	*p* value	FDR
11E2	29.54	80	0	0
11B1.3	24.52	45	$2.75x10^{-5}$	$5.27x10^{-3}$
4D2.2	20.64	39	$4.60x10^{-5}$	$5.89x10^{-3}$
11C	16.49	32	$1.23x10^{-4}$	$1.18x10^{-2}$
11D	43.02	65	$3.61x10^{-4}$	$2.59x10^{-2}$
12C3	10.47	22	$4.05x10^{-4}$	$2.59x10^{-2}$
11B2	7.46	17	$6.40x10^{-4}$	$3.02x10^{-2}$
14D2	5.59	14	$6.61x10^{-4}$	$3.02x10^{-2}$
4D2.3	6.88	16	$7.21x10^{-4}$	$3.02x10^{-2}$
14B	15.20	28	$7.87x10^{-4}$	$3.02x10^{-2}$

Table 4.6: Chromosomal locations over represented in DGE analyses comparing X^PO with XX mTSCs and X^MO with XX mTSCs. FDR cut off = 0.05.

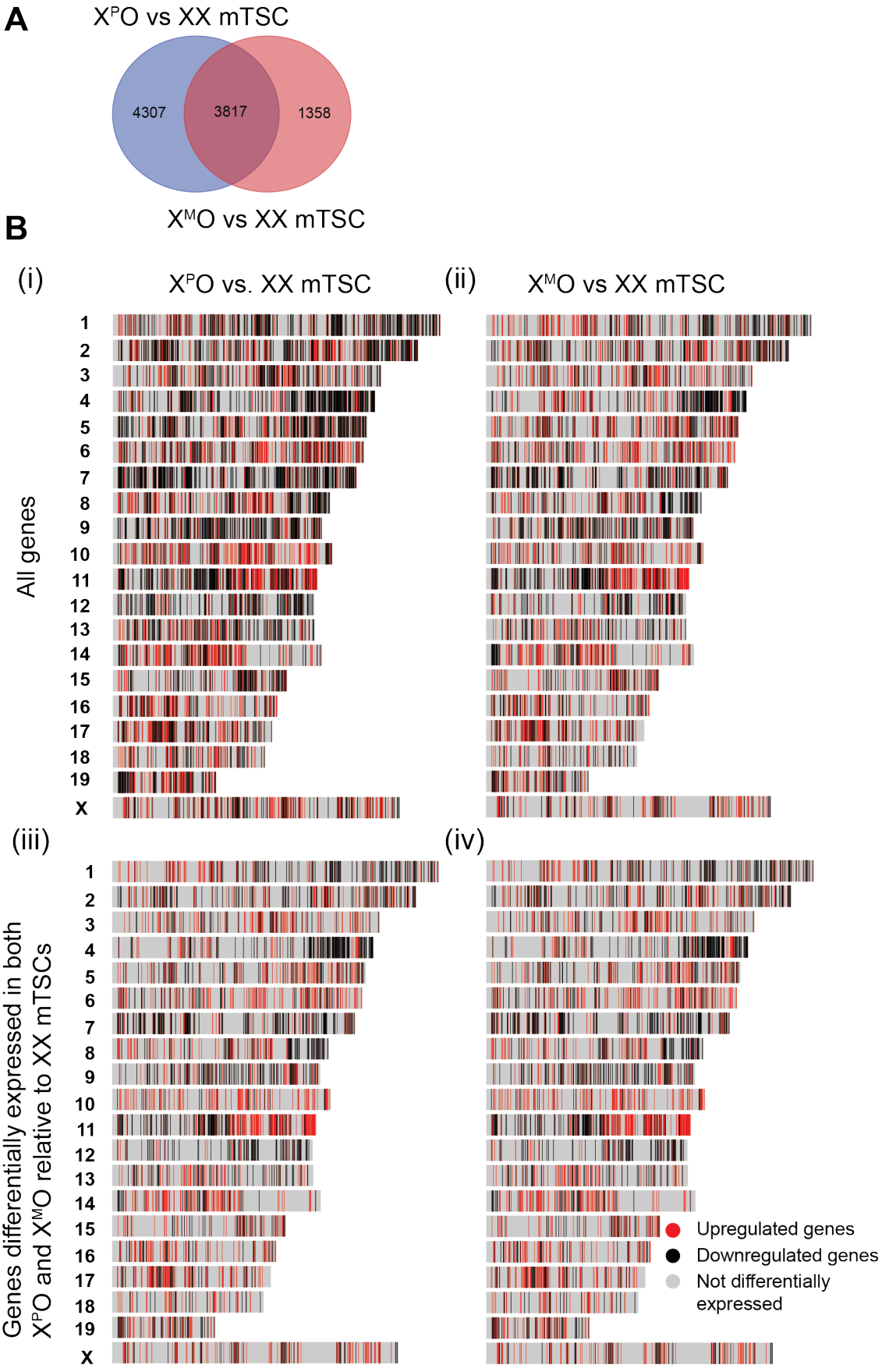
A
X^PO vs XX mTSC
4307
3817
1358
X^MO vs XX mTSC
B
(i)
X^PO vs. XX mTSC
(ii)
X^MO vs XX mTSC
All genes
(iii)
(iv)
Genes differentially expressed in both X^PO and X^MO relative to XX mTSCs
1
2
3
4
5
6
7
8
9
10
11
12
13
14
15
16
17
18
19
X
Upregulated genes
Downregulated genes
Not differentially expressed

Figure 4.10: Genes differentially expressed between XO and XX mTSCs. (**A**) Venn diagram showing overlap between genes differentially expressed in X^PO relative to XX mTSCs and genes differentially expressed in X^MO relative to XX mTSCs. (**B**) (i) Ideogram of the mouse genome showing upregulation or downregulation based on relative log fold change of genes differentially expressed in X^PO relative to XX mTSCs. All genes are depicted as a single coloured bar in their relative chromosomal location; (ii) Ideogram of the mouse genome showing upregulation or downregulation based on relative log fold change of genes differentially expressed in X^MO relative to XX mTSCs. All genes are depicted as a single coloured bar in their relative chromosomal location; (iii, iv) Ideograms of the mouse genome showing upregulation and downregulation of genes differentially expressed in both X^PO and X^MO relative to XX mTSCs. (iii) represents logFC in X^PO mTSCs relative to XX mTSCs; and (iv) represents logFC in X^MO relative to XX mTSCs. All genes are depicted as a single coloured bar in their relative chromosomal location. (B) plotted by Jasmin Zohren.

A limited number of over representation categories were identified per analysis type, using a relatively conservative false discovery rate of 0.05 (Zhang et al., 2005), as detailed in Tables 4.5 & 4.6. Most notably, the analysis with the highest number of significant hits was Chromosomal location (Table 4.6). The results suggest significant over representation of genes from chromosome 11, in addition to some bands within chromosomes 4, 12 and 14. In order to determine whether there was a prevailing general trend of upregulation or downregulation, idiograms were plotted based on logFC (Jasmin Zohren: Figure 4.10). First, direction of change, i.e. upregulation or downregulation, was plotted for all genes differentially expressed in X^PO relative to XX mTSCs (Figure 4.10B(i)); and for all genes differentially expressed in X^MO relative to XX mTSCs (Figure 4.10B(ii)). For both comparisons, there was a mix of upregulation and downregulation. The upregulation and downregulation of genes common to both comparisons (overlap in Venn, Figure 4.10A) was then plotted for X^PO relative to XX mTSCs (Figure 4.10B(iii)), and for X^MO relative to XX mTSCs (Figure 4.10B(iv)). This revealed that the 3817 genes in common to both comparisons were differentially expressed in the same direction, i.e. upregulated or downregulated, for all XO mTSCs. Graphical representation of the common genes also aided visualisation of the regions highlighted in the ORA. For example, 11E2, the most significant chromosomal location identified in the ORA can be seen as upregulated in both X^PO and X^MO relative to XX mTSCs. In contrast, 4D2.2 and 4D2.3 were downregulated in both X^PO and X^MO relative to XX mTSCs. I

conclude that, based on these results, further work is required in order to further elucidate the mechanisms underlying this significant differential gene expression between XO and XX mTSCs.

4.3 Discussion

In mouse extraembryonic tissue, X linked genes are expressed from the X^M, and the X^P is always inactivated (Takagi and Sasaki, 1975; Okamoto et al., 2004). This is true for XX, XY and X^MO conceptuses. Embryos with an X^PO sex chromosome genotype, in contrast, only have a single X^P and no X^M, therefore the X^P is active in the extraembryonic tissue. When combined with the observations that X^PO embryos are growth retarded relative to XX (Thornhill and Burgoyne, 1993) and XY^{RIII} (Chapter 3) littermates at E10.5; and that X^PO embryos have smaller EPCs at E7.5 (Jamieson et al., 1996), a causative link is plausible. In this Chapter I set out to identify genes differentially expressed between X^P and X^M chromosomes, thus serving as candidates to potentially explain the X^PO embryonic growth deficit phenotype. I utilised *in vitro* models for the extraembryonic, pluripotent and epiblast compartments of the mouse embryo and, following RNA-seq analysis, highlighted a number of interesting differentially expressed genes that now require further testing. Prior to addressing the next steps for this experiment, a number of notable observations will be discussed.

4.3.1 No XY mTSC lines were recovered during the derivation process

In order to generate X^PO mTSCs, I crossed an XY^{RIII} male with an InX/X female. I expected to recover roughly equal numbers of female (XX;InX/X;X^PO) and male (XY^{RIII}; InX/Y^{RIII}) blastocysts, and therefore derive cell lines in approximately equal proportions. It was therefore surprising to find no male mTSC lines following genotyping. This could be explained by a number of factors. Firstly, it is possible that there we no male blastocysts on day 1 of the derivation. However, as the same

cross was utilised to derive mESCs, and male lines were recovered, this reasoning is unlikely to be true. Secondly, the Y chromosome may have a previously uncharacterised deleterious effect on the survival of mTSCs. This explanation is also unlikely, as I successfully derived XX^{Y} mTSC lines as an unused product of the cross to generate $X^{M}O$ mTSCs (Figure 4.2B(ii)). In these XX^{Y} cells, the Y chromosome is physically linked to one of the X chromosomes, with no overt adverse phenotypic effects reported (Burgoyne et al., 1998; Trent et al., 2012). Moreover, XY mTSC lines have previously been reported in the literature (Tanaka et al., 1998; Motomura et al., 2016), though most papers continue to fail to report the sex chromosome karyotype of cell lines used.

A third theoretical explanation for the failure to derive XY mTSCs could be X chromosome number. However, the successful derivation to XO mTSCs effectively rules out any single X effect, and derivation specifically of $X^{M}O$ and $X^{P}O$ lines eliminates the possibility of an X chromosome imprinting effect on XY mTSC survival. The final explanation is experimental artifact, which asserts that if the experiment were repeated, male mTSCs would be obtained. This could be addressed by a repeat derivation utilising the same mouse cross, but instead of using feeders of mixed sex chromosome karyotype, use XX MEFs. Genotyping by PCR could then be performed around day 28.

4.3.2 Significantly more genes are differentially expressed between XX and XO cell lines in mTSCs than mESCs or mEpiLCs

Differential expression analyses comparing $X^{M}O$ with $X^{P}O$ RNA-seq datasets for mTSCs, mESCs and mEpiLCs identified of a small number of genes for each cell type. In contrast, the analyses of $X^{P}O$ relative to XX mTSCs, and $X^{M}O$ relative to XX mTSCs, revealed surprisingly high numbers, at 8124 and 5175, respectively. 3817 genes were common to both lists, and over representation analysis revealed relative enrichment for genes located on chromosome 11, among others. Several

possible explanations exist for these observations, including aneuploidy independent of the sex chromosomes, and a previously unrecognised effect of sex chromosome genotype on mTSC gene expression.

There are very little published data on mTSC karyotypes. A number of studies found euploid and aneuploid mTSC lines following routine karyotyping, but none characterised the nature of the aneuploidies (Tanaka et al., 1998; Kubaczka et al., 2015; Benchetrit et al., 2015). A contributory factor to this apparent oversight may stem from studies of tetraploidy. Whilst tetraploid embryos do not survive gestation (Kaufman and Webb, 1990; Henery et al., 1992), diploid embryos with tetraploid extraembryonic tissue do (Nagy et al., 1990). This could be taken to imply that the extraembryonic tissue is more tolerant than the epiblast to aneuploidy. However, duplication of the whole genome has significantly fewer transcriptional, and phenotypic, consequences in comparison to loss or gain of single chromosomes (Birchler, 2014).

In contrast, it is well documented that mESC lines have a tendency to develop karyotypic abnormalities following prolonged culture. Trisomies 8 and 11 are both common in mESCs and, when present together, result in a recognisable growth advantage (Sugawara et al., 2006; Rebuzzini et al., 2008; Gaztelumendi and Nogués, 2014; Rebuzzini et al., 2016). The X chromosome is also often affected in XX mESC lines, with loss resulting in the creation of a pseudo XO line (Robertson et al., 1983).

Based on the data presented here, if autosomal aneuploidy is present, it is possible that either all eight independently derived XX mTSC lines carry similar chromosomal abnormalities, or all five independently derived XO mTSC lines carry similar chromosomal abnormalities. Importantly, I confirmed that the sex chromosome complements were as reported for all cell lines, by DNA FISH. Autosomal aneuploidy could be investigated first by karyotyping of each cell line, thus revealing whether the overall ploidy is normal. If there is any doubt, spectral karyotyping, multiple (M) FISH, or comparative genomic hybridisation would provide more de-

tailed information on specific chromosomal rearrangements (Liyanage et al., 1996; Anderson and Brown, 2005; Saldarriaga et al., 2015).

Alternatively, chromosome territories in mTSCs may be disturbed by the sex chromosome aneuploid state. In the nucleus, chromosomes are positioned within defined areas, with gene rich chromosomes located towards the interior and gene poor chromosomes closer to the periphery (Cremer et al., 2006). This organisation is altered in disease states such as cancer (Meaburn and Misteli, 2008; Barutcu et al., 2015), which frequently involves structural chromosomal rearrangements and aneuploidy. Such chromosome territory alterations can have a significant impact on gene expression profiles (Meaburn and Misteli, 2008; Barutcu et al., 2015). Little is known about the nuclear organisation in mTSCs, as the only study to date focused on escape from XCI and, as such, only utilised female cell lines. It would therefore be highly informative to investigate the nuclear organisation of XX, XY, $X^{P}O$ and $X^{M}O$ mTSCs using techniques such as 3-D FISH and chromosome conformation capture (Fudenberg and Imakaev, 2017).

A third explanation for the high numbers of differentially expressed genes in XO mTSCs relative to XX mTSCs is non genetic phenotypic heterogeneity.

4.3.3 Non genetic phenotypic heterogeneity in aneuploid cells

Recent work has highlighted that aneuploidy may cause phenotypic variability independent of genetic variation. Working primarily in yeast, Beach and colleagues created karyotypically homogeneous populations of aneuploid cells that showed significant phenotypic changes within the population when compared with euploid cells (Beach et al., 2017). They showed that cells with chronic aneuploidies - defined as a chromosomal gain/loss propagated for more than two cell divisions - exhibited heterogeneity in cell cycle timing, variability in gene expression in response to cellular stress, and altered protein expression levels relative to wildtype. Data

are also provided to show phenotypic variability in inbred mice carrying identical Robertsonian translocations (Beach et al., 2017).

The heterogeneity in gene expression reported in Beach et al. study is likely to apply equally to sex chromosome aneuploidy as it applies to autosomal aneuploidy. For example, this phenomenon could underlie the increased variation in gene expression observed for XO but not XX mTSC lines during the differentiation analysis (section 4.2.2). It is, therefore, conceivable that such heterogeneity could also impact on differential gene expression analysis. In the present study I have relied upon reproducibility between biological replicates to identify genes as differentially expressed. However, if the findings of Beach and colleagues apply to these cell lines, there would theoretically be very few conserved differentially expressed genes found across all $X^{P}O$ biological replicates or across all $X^{M}O$ biological replicates. Importantly, the number of differentially expressed genes identified here in euploid cell line comparisons, i.e. XX and XY mESCs (322 genes), is within the same order of magnitude as the number identified in aneuploid cell line comparisons, i.e. $X^{P}O$ and XX (109 genes). It therefore seems likely that, despite the reported phenotypic variability in aneuploid conditions, a core set of genes underlies conserved aspects of the phenotype. Undoubtedly further work is required to determine the effects of non genetic phenotypic variability in human aneuplodies, though this could potentially provide an explanation for the highly variable phenotype observed in women with Turner syndrome (Hook and Warburton, 2014).

4.3.4 Confounding factors in analysis of RNA-seq data from aneuploid samples

It has previously been assumed that a change in chromosomal complement inside a cell will only impact on gene expression from the chromosome(s) directly affected, and thus gene expression from the unaffected chromosomes can be used for normalisation. This approach was taken in the analysis of early work on X chromosome upregulation (XUR), as previously described (section 1.4.1). However, based on

the Beach et al. (2017) study, in addition to previous work detailing the genomic instability of aneuploid cells (Nicholson et al., 2015; Blank et al., 2015; Passerini et al., 2016), and the literature on XUR, this assumption is not supported by the recent data. It is becomingly increasingly clear that there are global transcriptional changes in aneuploidy, and these must be taken into account during the data analysis to enable accurate differential expression analyses (Birchler, 2014).

In the preparation of libraries for sequencing, the total RNA input was equalised across all samples, and the concentrations of all libraries were equal on the flow cell. These normalisations assume that total RNA per cell is approximately equal. Samples were then normalised for sequencing depth by calculating transcripts per million (tpm). Tpm is defined as the number of trancripts of one specific type (e.g. *GAPDH*-001) that would be detected if one sequenced one million full length transcripts, given the abundance of the other transcripts in the sample (Li et al., 2009a). It is therefore important that relative transcript abundances for the whole transcriptome are comparable between samples. In the case of aneuploid cell lines, the potential global changes in gene expression mean that this criterion may not be met and, as such, downstream differential gene expression analyses may not be optimal.

In order to mitigate these difficulties, a number of approaches could be utilised; the first two as an extension to current work, and the second two in future work. Using existing data, a ratio of read counts for each transcript in the X^PO versus XX could be calculated, and subsequently plotted in a distribution. This would serve to highlight if there are any abnormal patterns of potential interest (Sun et al., 2013a, 2010, 2013b). Although relatively low throughput, quantitative RNA FISH allows direct visualisation of the nascent transcript, facilitating comparison of per cell expression in two different sex chromosome genotypes (Pal Bhadra, 2005). The addition of a pre determined concentration of exogenous spike in RNA to every sample prior to cDNA preparation would provide an absolute reference for across sample RNA abundance comparisons (Jiang et al., 2011; Lovén et al., 2012). Alternatively, the

mRNA to genomic DNA relationship could be preserved during sample preparation such that genomic DNA acts as a control for the calculation of transcriptome size. This has been developed primarily for polyploid cells, but could effectively be used in the study of aneuploidies, too (Coate and Doyle, 2010).

4.3.5 Validation of cell lines for the study of imprinted genes

The primary aim of the derivation and transcriptome analysis of X^PO and X^MO stem cell lines was to identify X linked differentially expressed genes. A subset of these candidate genes could be imprinted, and therefore underlie the X^PO embryonic growth deficit phenotype. It has been shown that culture conditions can influence the maintenance of genomic imprinting in mESCs (Habibi et al., 2013), and the potential impact of such an effect should have been assessed in my cell lines. Previously reported imprinted loci, such as *Peg3* and *Kcnq1ot* in both mESCs and mTSCs (Leitch et al., 2013; Calabrese et al., 2015), could have been used as positive controls for parent of origin expression. However, in order to determine the parental origin of a given allele, single nucleotide polymorphisms (SNPs) are required. I used MF1 strain sex chromosome variant mice to generate both X^PO and X^MO blastocysts for cell line derivation. Whilst the MF1 strain is outbred, it does not have enough SNPs to perform accurate and effective variant calling. As a consequence, it was not possible to confirm that autosomal imprinting is reliably maintained within the model. The ability to assess potential X chromosome imprinting was not affected, as two X chromosome monosomic states were used whereby parent of origin was known *a priori*.

A number of studies in mESCs have suggested that culture conditions impact the DNA methylation status of imprinting control regions, creating a potential risk of culture artifacts (Ficz et al., 2013; Habibi et al., 2013; Blaschke et al., 2013). Cells derived and maintained in 2iLIF conditions were reported to show faithful maintenance of parental imprints, as per the ICM of the blastocyst stage embryos, at three

loci examined (Leitch et al., 2013). However, two other reports found sexually dimorphic ICR methylation maintenance at the *Peg3* and *Peg10* loci in both serum and LIF and 2iLIF conditions (Ooi et al., 2010; Zvetkova et al., 2005). Recently it has been shown that histone modifications, such as H3K27me3, also play a role in the regulation of imprinted gene expression in the early mouse embryo independently of DNA methylation (Inoue et al., 2017). It will therefore be important to determine whether culture conditions impact on the genes regulated by this mechanism, too.

There are no reports of culture induced changes in DNA methylation or imprinting in mTSCs, however, there are also only a small number of reports showing imprinting in mTSCs. The most comprehensive study to date utilised eight F1 mTSC lines produced by reciprocal cross between C57BL/6J and *Mus musculus castaneus* mouse strains (Calabrese et al., 2015). The authors found evidence for imprinted expression of 31 previously described imprinted genes and 17 new candidates, based on RNA-seq and pyrosequencing data. They also noted that several of the known imprinted genes showed variability in parent of origin expression across their lines, and suggest this could either be an example of developmental plasticity at imprinted loci (Radford et al., 2011), or alternatively an artifact of culture.

It would be useful to further understand the mechanisms of imprint maintenance in mTSCs, as this was not addressed in the Calabrese et al. study. Recently it was shown that DNA methylation marks originating in the oocyte are important for trophoblast development, and play a role in trophoblast cell adhesion both *in vivo* and *in vitro* (Branco et al., 2016). Furthermore, loci specifically imprinted in extraembryonic tissue are enriched for repressive histone modifications such as H3K27me3 and H3K9me2 (Lewis et al., 2004; Umlauf et al., 2004), and the active histone mark H3K4me2 (Lewis et al., 2006). However, some placentally imprinted genes appear to be biallelically expressed in mTSCs and blastocysts, and as such show no enrichment for histone modifications at these loci (Lewis et al., 2006). More-

over, following *in vitro* differentiation, there was no change in allelic expression or histone modifications.

In summary, the cell lines I have derived as a model for X chromosome imprinting in the X^PO embryo require validation to confirm the expression of known imprinted genes. It would therefore be useful to perform whole genome bisulphite sequencing on F1 mESC, mEpiLC, and mTSC lines. This would enable confirmation of the methylation status of known ICRs based on allele calling data and, furthermore, in conjunction with RNA-seq data, would facilitate the identification of any imprinted genes on the X chromosome in mESCs, mEpiLCs, and mTSCs. ChIP-seq analysis in all cell types for histone modifications such as H3K27me3 would also be important (Inoue et al., 2017; Lewis et al., 2006), with the caveat that mTSCs have been shown to recapitulate genes imprinted at the blastocyst stage but no later. If imprinting candidates are not found at this early stage, alternative models will be required.

4.3.6 Alternative models for investigating the X^PO embryonic growth deficit

Whilst stem cells *in vitro* undoubtedly contribute a significant amount to our understanding of biological systems and, importantly, facilitate a reduction in the use of live animals in research, it is sometimes challenging to accurately recapitulate the *in vivo* phenotype in a plate or dish. In order to investigate the X^PO embryonic growth deficit question further, a number of *in vivo* options could complement the current cell focused approach.

As it has previously been shown that the EPC of X^PO conceptuses is significantly smaller than the EPC of XX littermates (Jamieson et al., 1998), it would be useful to reinvestigate this model with modern techniques. A reporter for *Ascl2*, expressed only in the EPC of the extraembryonic tissue at E7.5 (Guillemot et al., 1994), could be generated by CRISPR-Cas genome editing (Yang et al., 2013) and, following

dissection of the conceptus, used to FACS sort the EPC cells for RNA-seq or proteomic analysis.

A secondary alternative to access the same population would be to fix or freeze the conceptuses and utilise laser capture microdissection (DeCarlo et al., 2011). This technique would enable the isolation of the morphologically identifiable EPC cells in the E7.5 conceptus for use in downstream RNA-seq or proteomic analysis.

A third model could be utilised for a direct comparison with *in vitro* derived mTSCs. Using laser assisted microdissection on the blastocyst stage embryo, it is possible to separate the mural TE from the polar TE and ICM. These two different cell populations could then be dissociated into single cells for RNA-seq analysis. Using lineage specific marker genes such as *Cdx2* and *Eomes* for the TE and *Pou5f1* and *Nanog* for the ICM, it would be possible to bioinformatically separate the polar TE/ICM population into trophectoderm and ICM (Blakeley et al., 2015); and possibly further separate the ICM into epiblast and primitive endoderm. Finally, differential gene expression analyses could be performed, both between genotypes, as described for mTSCs during this study, and within embryos between cell types. It has previously been shown that transcriptional differences exist between polar and mural TE at E3.5 (Nakamura et al., 2015), and it would be interesting to observe if these differences change with sex chromosome genotype.

4.3.7 Potential use of proteogenomics to further investigate the X^PO growth deficit phenotype

The identification and relative measurement of mRNA species by RNA-seq enables the study of transcriptional activity within a given cell or tissue sample. By comparing transcriptomes between samples from different experimental conditions, we are able to determine the impact of the condition on gene expression. RNA species are not generally, however, the final effectors of cellular output; this task falls to protein. Conservative estimates suggest that the correlation between cellular pro-

tein concentration and abundance of their corresponding mRNA is around 40% (de Sousa Abreu et al., 2009; Maier et al., 2009). The 60% variance is attributed to post transcriptional, translational, and degradation regulation (Vogel and Marcotte, 2012). Recent work characterised human colon and rectal tumours by proteogenomic analysis (Zhang et al., 2014). They noted that whilst copy number alterations showed *cis* and *trans* effects on mRNA abundance, mRNA transcript abundance did not generally predict protein abundance differences between tumours. The combined study of mRNA and protein profiles helped the authors to prioritise candidate driver genes, and provided functional context to genetic abnormalities, such as duplication of chromosome 20q (Zhang et al., 2014). Such a combined mRNA/protein approach might enabled more effective identification of candidate genes when looking to understand a complex phenotype, such as the growth deficit observed in $X^{P}O$ embryos at E10.5.

Chapter 5

Assessing the contribution of X-linked dosage sensitive genes to the postnatal growth deficit in XO female mice

5.1 Introduction

Short stature is one of the most recognisable features associated with Turner syndrome, and is a major cause of disability during childhood and adolescence (Kappelgaard and Laursen, 2011; Lee and Conway, 2014). Haploinsufficiency of *SHOX*, a gene located within PAR1, is likely a major contributor to the phenotype (Rao et al., 1997; Ellison et al., 1997). *SHOX* is a transcription factor highly expressed in chondrocytes and bone marrow fibroblasts (Rao et al., 1997; Ellison et al., 1997; Rao et al., 2001; Aza-Carmona et al., 2011). Mutations in the gene are one of the primary genetic causes of Leri-Weill syndrome, which itself encompasses a short stature phenotype (Belin et al., 1998), and have also been associated with many other cases of short stature (Marstrand-Joergensen et al., 2016; Fukami et al., 2016). However, women with Turner syndrome are generally shorter than patients

with mutations in *SHOX*, suggesting that other factors may contribute (Ross et al., 2001; Fukami et al., 2016; Zinn and Ross, 1998).

Similar to Turner syndrome in humans, female mice with an XO karyotype are smaller than those with a normal XX karyotype during early postnatal life (Burgoyne et al., 1983a). Although originally suggested to result from genomic imprinting, this phenotype has been shown to be independent of the parental origin of the X chromosome (Burgoyne et al., 2002). Furthermore, mice have no *SHOX* orthologue, and their PAR is significantly reduced in size and gene content compared to humans. Burgoyne and colleagues (2002) showed that female mice with one normal X chromosome and an additional PAR-only chromosome are small compared to XX littermates. Interestingly, the addition of a second sex chromosome, in the form of a Y chromosome lacking the sex determining gene *Sry* (XY^-), fully rescued the phenotype. The authors therefore concluded that haploinsufficiency for an X linked gene that is located outside the PAR, and has a widely-expressed Y-linked homologue, is the most likely cause of the growth deficit. This gene would also be expected to escape XCI.

In this Chapter I set out to confirm the results from the Burgoyne et al. dataset, and to identify the genes involved in the growth retardation phenotype. A small number of candidates were highlighted following a Y-linked gene expression analysis and RFLP assay to test for escape from XCI. I then sought to address each candidate's role in the XO postnatal growth deficit by creating mutant lines by CRISPR/Cas9 genome engineering.

5.2 Results

5.2.1 Recapitulation of previous results

I first sought to reproduce the results of Burgoyne et al. (2002) that, relative to XX littermates, X^PO and X^MO female mice grow at a reduced rate during the first

five weeks of postnatal life. In the Burgoyne et al. study, XO female mice with an additional PAR, denoted XY^{*X}, also grew at a reduced rate across the same period, whereas XY^{-} females grew at the same rate as XX littermates.

In order to generate $X^{P}O$ females alongside XX littermates, I crossed In(X)/X female mice with XY^{RIII} males (Figure 5.1A(i)). In addition to $X^{P}O$ females, XX and In(X)/X females were present in the offspring. It has previously been reported that there is no difference in postnatal weight gain between XX and In(X)/X females, so results were pooled (Burgoyne et al., 2002). $X^{M}O$ females were produced by crossing XX female mice with $X^{Paf}Y^{*}$ males (Figure 5.1B(i)). XO female mice with an additional PAR (XY^{*X}) were generated by crossing XX females with XY^{*} males (Figure 5.1C(i)). Finally, we generated XY^{-} females by utilising a male with this variant Y chromosome, in addition to an autosomal *Sry* transgene, crossed with a wildtype female (Figure 5.1D(i)).

I first compared weights at birth. $X^{P}O$ females showed no significant birth weight difference when compared with XX littermates (Table 5.1, $p=3.86\text{x}10^{-1}$). Interestingly, $X^{M}O$ females were significantly lighter than XX littermates at birth (Table 5.1, $p=2.20\text{x}10^{-2}$), as were XY^{*X} females (Table 5.1, $p=6\text{x}10^{-3}$). XY^{-} females were significantly heavier than XX littermates at birth (Table 5.1, $p=2.80\text{x}10^{-3}$),

In order to estimate the rate of growth across the periods 0-3 weeks and 3-5 weeks, a regression line was fitted to the weight data for each animal. Relative to XX littermates, $X^{P}O$ females grew at a reduced rate during the 0-3 week period (Figure 5.1A(ii), Table 5.2, $p=2.00\text{x}10^{-2}$). $X^{M}O$ females (Figure 5.1B(ii), Table 5.2: $p=4.60\text{x}10^{-2}$) and XY^{*X} females (Figure 5.1C(ii), Table 5.2: $p=2.80\text{x}10^{-2}$) also grew at a significantly reduced rate when compared to XX littermates between 0 and 3 weeks. In contrast, and consistent with previous results, XY^{-} females showed no difference in rate of growth when compared to XX littermates across the 0-3 week period (Figure 5.1D(i), Table 5.2: $p=1.39\text{x}10^{-1}$).

Across the 3-5 week period, $X^{P}O$ females grew at at a rate not significantly different from XX littermates (p=7.12x10^{-1}). Similarly, relative to XX littermates, $X^{M}O$ females (Table 5.2: p=3.16x10^{-1}) and XY^{*X} females (Table 5.2: p=2.64x10^{-1}) grew at an equivalent rate. Interestingly, XY^{-} females slowed a slight, but significant, reduction in weight gain during the 3-5 week period in comparison to XX littermates (Table 5.2: p=3.60x10^{-2}): this is in keeping with the trend shown previously (Burgoyne et al., 2002). Figure 5.1E utilises MWD from XX to bring results from all genotypes together. In summary, I confirmed that XO female mice grow at a reduced rate relative to XX littermates during the 0-3 week period, and that this is not a result of haploinsufficiency for PAR genes. I conclude that haploinsufficiency for genes present on both the X and Y chromosomes, and that map outside the PAR, is the most likely cause of a reduced rate of postnatal growth in XO mice.

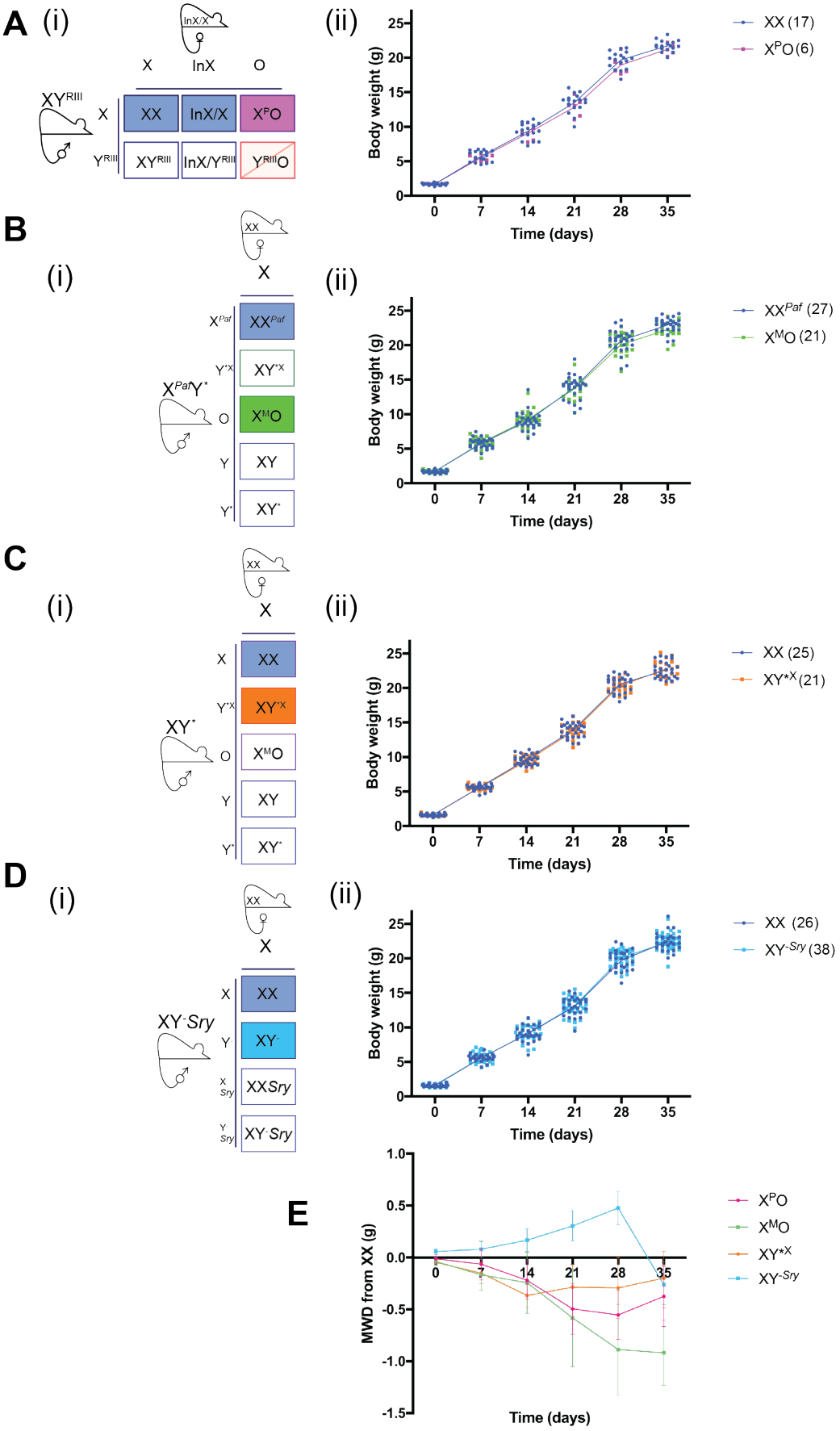
A
(i)
InX/X
X
InX
O
XY^RIII
X
XX
InX/X
X^PO
Y^RIII
XY^RIII
InX/Y^RIII
Y^RIIIO
(ii)
Body weight (g)
Time (days)
XX (17)
X^PO (6)
B
(i)
XX
X
X^Paf
XX^Paf
Y*X
XY*X
X^PafY*
O
X^MO
Y
XY
Y*
XY*
(ii)
Body weight (g)
Time (days)
XX^Paf (27)
X^MO (21)
C
(i)
XX
X
X
XX
Y*X
XY*X
XY*
O
X^MO
Y
XY
Y*
XY*
(ii)
Body weight (g)
Time (days)
XX (25)
XY*X (21)
D
(i)
XX
X
X
XX
XY-Sry
Y
XY-
X Sry
XXSry
Y Sry
XY-Sry
(ii)
Body weight (g)
Time (days)
XX (26)
XY-Sry (38)
E
MWD from XX (g)
Time (days)
X^PO
X^MO
XY*X
XY-Sry

Figure 5.1: Recapitulation of postnatal growth retardation phenotype in XO female mice. (**A**) (i) Mouse cross used to generate XX and $X^{P}O$ littermates, and (ii) body weight data of these animals, measured weekly for five weeks. Each data point represents an individual animal, and the line depicts the mean for each genotype. (**B**) (i) Mouse cross used to generate XX and $X^{M}O$ littermates, and (ii) body weight data. (**C**) (i) Mouse cross used to generate XX and XY^{*X} littermates, and (ii) body weight data. (**D**) (i) Mouse cross used to generate XX and XY^{-Sry} littermates, and (ii) body weight data. (**E**) Mean weighted difference between genotypes indicated and XX littermates. Bars represent 95% confidence intervals.

Comparison	Number		Birth weight (g)			
A v B	na	nb	A	B	MWD±SE (g)	Signif. of MWD (*p*)
XX v X^PO	17	6	1.719±0.040	1.699±0.376	0.020±0.045	$3.86x10^{-1}$
XX v X^MO	27	21	1.755±0.039	1.747±0.046	0.038±0.042	$2.20x10^{-2}$
XX v XY^{*X}	25	21	1.638±0.037	1.600±0.036	0.041±0.038	$6.00x10^{-3}$
XX v XY^-	26	38	1.610±0.035	1.675±0.032	-0.064±0.028	$2.80x10^{-2}$

Table 5.1: Birth weight data compared by mean weighted difference (MWD)

Comparison	Number		0-3 weeks: mean ±SE (g)				3-5 weeks: mean ±SE (g)			
A v B	na	nb	xA^a	xB^a	MWD±SE (g)	Signif. of MWD (*P*)	xA^a	xB^a	MWD±SE (g)	Signif. of MWD (*p*)
XX v X^PO	17	6	4.034±0.117	3.860±0.210	0.190±0.072	2.10x10-*2*	4.121±0.277	4.202±0.184	0.226±0.157	$7.12x10^{-1}$
XX v X^MO	27	21	4.140±0.093	3.920±0.095	0.219±0.105	$4.60x10^{-2}$	3.940±0.122	4.209±0.112	0.133±0.131	$3.16x10^{-1}$
XX v XY^{*X}	37	29	3.968±0.057	3.828±0.090	0.116±0.051	$2.80x10^{-2}$	4.356±0.071	4.517±0.116	0.110±0.097	$2.64x10^{-1}$
XX v XY^-	26	38	3.741±0.086	3.848±0.064	0.081±0.092	$1.39x10^{-1}$	4.762±0.131	4.508±0.109	0.270±0.101	$3.60x10^{-2}$

Table 5.2: Means and mean weighted differences (MWD) for phasic weight gain between genotype comparisons shown in Figure 5.1. "a" represents mean of means.

5.2.2 Verification of potential postnatal growth retardation candidates

Next I sought to narrow down potential candidate genes for the haploinsufficiency hypothesis. As elucidated previously (Burgoyne et al., 2002) and here, such genes will not be imprinted, will not be present in the PAR, and the Y linked homologues will likely exhibit widespread expression. I looked to confirm this pattern by using RT-PCR to assay for expression of all 14 Y linked protein coding genes across multiple tissues representing ectoderm, mesoderm and endoderm (Figure 5.2). Eight Y-linked genes showed expression exclusive to the testis (*Zfy1*, *Ube1y1*, *Usp9y*, *Zfy2*, *Sry*, *Ssty1*, *Ssty2*, and *Sly*). Two genes showed expression in the testis and limited expression outside the gonad (*H2al2y* and *Rbmy1a1*). The final four genes (*Kdm5d*, *Eif2s3y*, *Uty*, and *Ddx3y*) showed widespread expression across tissues derived from all three embryonic germ layers. These patterns were consistent with previously reported data (Bellott et al., 2014).

Each of the broadly expressed Y linked genes has a conserved X linked homologue in mouse (Disteche et al., 2002). This conservation not only applies to the mouse sex chromosomes, but also across the eutherian clade, which has been taken to suggest that levels of expression of these X-Y pairs might be important (Bellott et al., 2014; Cortez et al., 2014). In XX female mice, the expression of most X linked genes is controlled by XCI; though it is likely that dosage sensitive genes such as the X linked genes in these X-Y pairs, will escape the chromosome wide silencing. I looked to confirm that the X linked orthologue of each of the widely expressed Y linked genes escapes XCI, as has been previously reported (Disteche et al., 2002). I determined whether one or both alleles of *Ddx3x*, *Eif2s3x*, *Kdm5c*, and *Kdm6a* was being expressed in adult XX female mice by restriction fragment length polymorphism analysis (RFLP).

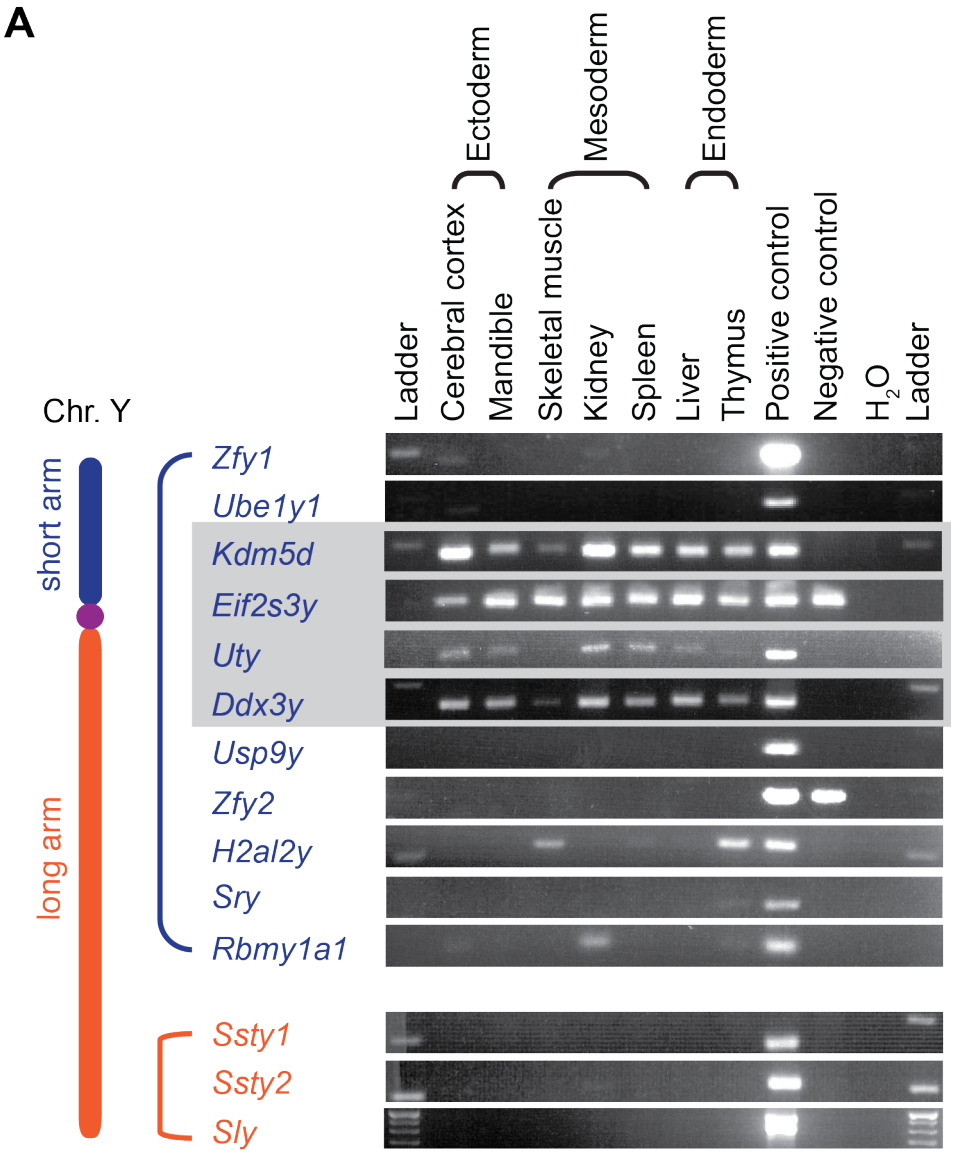

Figure 5.2: Expression analysis of genes on the mouse Y chromosome by RT-PCR. Relative positions of genes on the mouse Y chromosome are depicted by cartoon on the left hand side. The positive control was adult wildtype mouse testis; the negative control was testis from an adult male mouse lacking the Y chromosome but carrying *Eif2s3y* and *Zfy2* transgenes.

XCI is usually random in all adult somatic cells, such that either X^M or X^P could be inactivated. As a result, on a tissue level, both alleles from every expressed gene would be detected, regardless of whether genes are subject to or escape from XCI. In order to isolate expression from potential XCI escapees only, I again utilised the *Xist* mutant allele (Marahrens et al., 1997). The X chromosome carrying this allele cannot be inactivated, and any detected expression from the second X chromosome in XX females could be attributed to escape from XCI.

In order to differentiate between transcripts from the two different X chromosomes, I used an F1 cross between strains bearing known single nucleotide polymorphisms (SNPs) in the genes of interest. After amplifying the locus containing the SNP from cDNA by PCR, I then digested the product with a restriction enzyme specific to one of the variant nucleotides at the SNP. If the gene escaped XCI, I expected to see two products after digest, i.e. one from each allele. If the gene was subject to XCI, I expected to observe only a single product after digest, the product from the active X chromosome.

Foxo4, a gene known to be subject to XCI, was assayed first as a negative control. I amplified and digested PCR products from cDNA of the parental strains to test the RFLP assay, expecting to observe a single, digested product in one strain, and a single undigested product in the other strain. In both of the parental strains, following digest, distinct bands were observed on the agarose gel (Figure 5.3A). As a result the *Xist* mutation on the C57BL/6 X chromosome, the XX female F1 was expected to express *Foxo4* from the C57BL/6 X chromosome - the active X chromosome - only. This expectation was fulfilled.

I then assayed *Ddx3x*, *Eif2s3x*, *Kdm5c*, and *Kdm6a*. If a gene escapes XCI, I expected to observe expression from both X chromosomes in the XX female F1, in the form of two different allele specific bands. For each of *Ddx3x*, *Eif2s3x*, *Kdm5c*, and *Kdm6a*, this expectation was fulfilled, in both brain and liver tissue samples (Figure 5.3A,B). I therefore confirmed that *Ddx3x*, *Eif2s3x*, *Kdm5c*, and *Kdm6a* escape XCI across multiple tissues in the mouse. When compiled with the data showing

presence and widespread expression of Y linked orthologues, I conclude that one or more of these four candidates is most likely to be haploinsufficient in XO female mice, resulting in a reduced rate of growth in the early postnatal period.

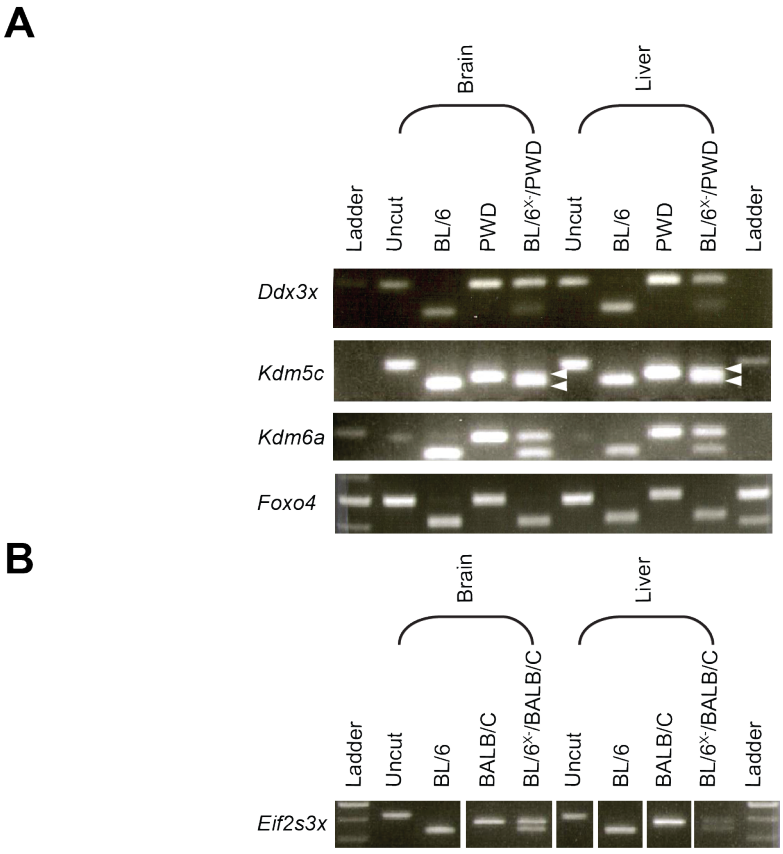

Figure 5.3: Restriction fragment length polymorphism analysis to confirm escape from XCI in mouse brain and liver. (**A**) Agarose gels showing restriction enzyme digests of cDNA from C57BL/6 (BL/6), PWD/PhK (PWD), and C57BL/6^{Xist-} x PWD/PhK animals. Arrowheads indicate two separate bands. (**B**) As (A), with cDNA from C57BL/6 (BL/6), BALB/C, and C57BL/6^{Xist-} x BALB/C animals (BL/6^{X-}/BALB/C) animals.

5.2.3 The generation of mutant alleles by CRISPR Cas9 genome engineering

I next looked to identify which of these genes mediates the postnatal growth retardation phenotype by utilising individual knockout alleles for *Kdm5c*, *Kdm6a*, *Ddx3x* and *Eif2s3x*. As all crosses described up to this point have utilised the MF1 mouse strain, I wanted to maintain consistency and reduce variation attributable to strain specific effects (Latham, 1994) by utilising the same strain for the knockouts. Whilst a number of mutant lines had already been published for *Kdm6a*, none used

the MF1 strain. Rather than adopting a lengthy backcrossing strategy, I opted to create new lines via CRISPR/Cas9 genome editing (Jinek et al., 2012; Cong et al., 2013). Guide RNAs were designed utilising the MIT CRISPR Design Tool (Ran et al., 2013), with the aims of removing the translation initiation site, whilst minimising off target mutations. Initially, each guide was shown to successfully cut the target locus by digest of a PCR product containing the guide target sequence (Figure 5.4).

To assess guide efficiency, XY mESCs were then electroporated with each guide validated individually, along with *Cas9* mRNA. All guides for *Ddx3x*, *Kdm5c*, and *Kdm6a* were able to create mutations *in vitro*, as assessed by either RFLP or Sanger sequencing (Table 5.3). Targeting efficiency, measured as the percentage of all picked clones carrying a mutation, ranged between 9.7% and 21.9% for *Kdm6a*, *Kdm5c*, and *Ddx3x* guides. *Eif2s3x* proved more problematic, with the first two guides yielding no mutant clones, and the third guide only one mutant from 40 clones screened. Guides that successfully cut PCR products and showed activity in mESCs were microinjected into pronuclear stage MF1 mouse embryos by Genetic Manipulation Services (Science Technology Platform at Francis Crick Institute), and transferred to pseudopregnant females in order to generate stable mouse lines. Lines generated for each gene will now be discussed in more detail.

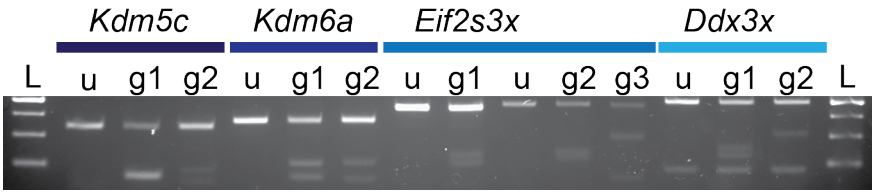

Figure 5.4: Demonstrating sgRNA cutting of target genomic DNA. Agarose gel showing Cas9 with sgRNA digest of PCR amplicons derived from target locus. Each PCR amplicon is shown first as uncut (U), followed by results of a incubation with Cas9 and each guide (sgRNA1,2 etc.) specific to the locus. Two different amplicons were utilised for *Eif2s3x*.

Gene	sgRNA name	Mutant clones/total clones	Percentage carrying a mutation	Screening method
Kdm6a	Kdm6a 1	5/32	15.6	RFLP
	Kdm6a 2	4/22	18.2	RFLP
Kdm5c	Kdm5c 1	5/30	16.7	RFLP
	Kdm5c 2	3/31	9.7	RFLP
Ddx3x	Ddx3x 1	7/32	21.9	Sanger seq.
	Ddx3x 2	5/28	17.9	Sanger seq.
Eif2s3x	Eif2s3x 1	0/40	n/a	Sanger seq.
	Eif2s3x 2	0/40	n/a	Sanger seq.
	Eif2s3x 3	1/40	2.5	RFLP

Table 5.3: Guide efficacy as tested in XY mESCs

5.2.4 *Kdm5c*

Two lines carrying mutations in *Kdm5c* were generated and propagated. One line carried a 189bp. deletion and the other a 166bp. deletion. Both mutant lines featured the removal of the translation initiation site (Figure 5.5A, red line) and, based on sequencing evidence, also resulted in frameshift mutations within exon 1. All four protein coding isoforms of *Kdm5c* were likely affected (Figure 5.5A, lower). This loss of protein was confirmed by western blot (Figure 5.5B), using an antibody raised to antigen from outside of the deleted region (Figure 5.5A, 'Ab'). I compared females heterozygous for the mutant allele with wildtype females (Figure 5.5B +/- and +/+ respectively), and expected to see a reduction in protein in the mutant: this proved to be correct. I then compared males carrying only a mutant allele with wildtype males (Figure 5.5B -/y, +/y, respectively), and expected to observe complete absence of protein in the mutant: this also proved to be correct. I wanted to compare homozygous mutant females with wildtype females, expecting to see complete absence of protein in the homozygotes. However, I was unable to generate homozygous mutant females. In summary, both mutations resulted in ablation of KDM5C protein expression.

Next I wanted to check for the presence of off target mutations. I decided to proceed with off target analysis for the 189bp. line only, as a single line was required for

the weighing experiment. I chose to screen loci located within exons, and having four or fewer mismatches between guide and target sequence. These were identified using the results from the MIT CRISPR Design Tool. The off target analysis was performed on three male F1s that were used to generate all mutant animals for future experiments. I also sequenced three unrelated wildtype males to capture any background non specific mutations. No mutations were observed at any of the off target loci screened, in either 189bp deletion males or wildtype males (Figure 5.5C), based on PCR and next generation sequencing data. I conclude that I had successfully generated a *Kdm5c* mutant line with no detectable off target effects.

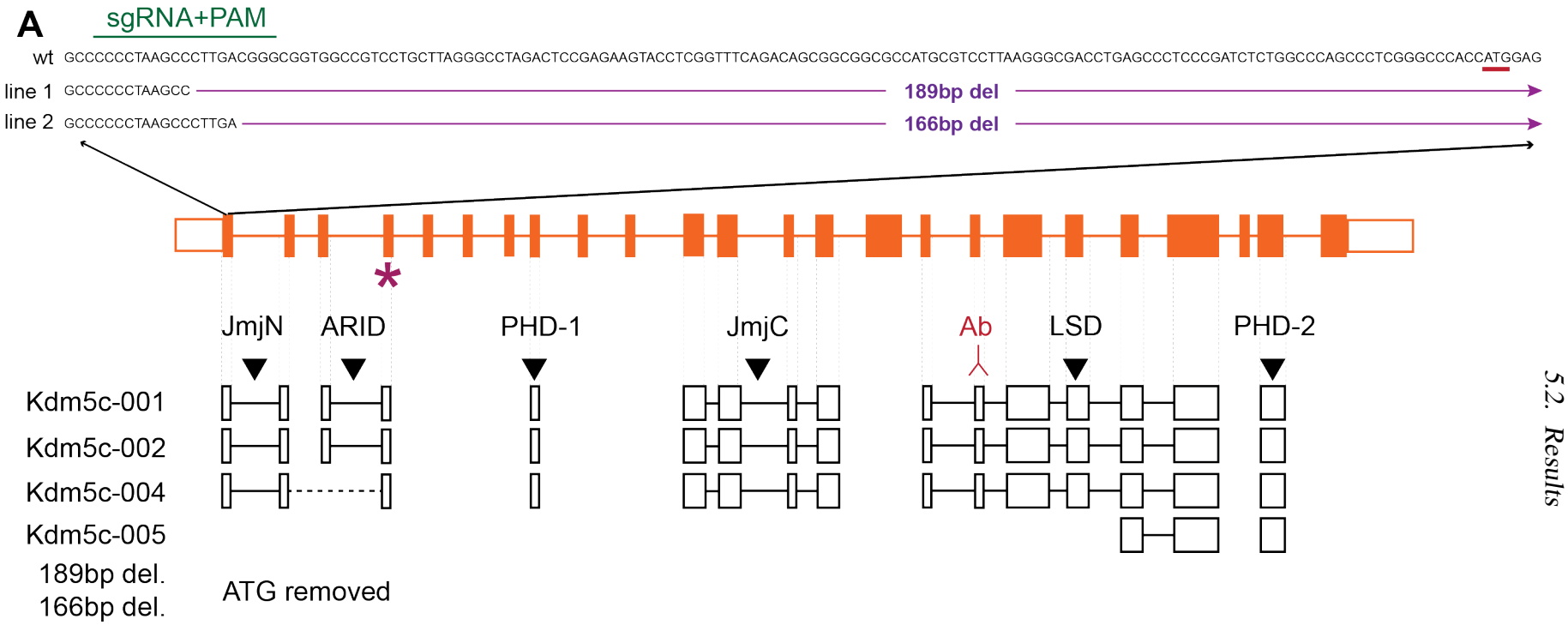
A
sgRNA+PAM
wt GCCCCCCTAAGCCCTTGACGGGCGGTGGCCGTCCTGCTTAGGGCCTAGACTCCGAGAAGTACCTCGGTTTCAGACAGCGGCGGCGCCATGCGTCCTTAAGGGCGACCTGAGCCCTCCCGATCTCTGGCCCAGCCCTCGGGCCCACCATGGAG
line 1 GCCCCCCTAAGCC
189bp del
line 2 GCCCCCCTAAGCCCTTGA
166bp del
JmjN
ARID
PHD-1
JmjC
Ab
LSD
PHD-2
Kdm5c-001
Kdm5c-002
Kdm5c-004
Kdm5c-005
189bp del.
166bp del.
ATG removed
B
189bp del.
166bp del.
+/+
-/+
-/-
+/y
-/y
-/-
KDM5C
GAPDH
C
(i)
(ii)
12bp seed
189bp del
wildtype
wildtype
variant
Locus CCCCCTAAGCCCTTGACGGGCGG
OT1 CCCCGTAAGCCCTAGATGGGGGG
OT2 CCGCCTACGCCCTTGAGGGACGG
OT3 TCCCTTAAGCCCTTCTCGGGAGG
OT4 CCCCATAAGCCTTTCAGGGGAGG
OT5 GCCCCTAAGCCCTTCCTGGGGGG
OT6 CCCCCTAAACCCTTTCCGGAAGG

Figure 5.5: Generation of mutant *Kdm5c* alleles by CRISPR. (**A**) Cartoon depiction of the target locus. Wildtype (wt) sequence enables visualisation of the guide and PAM, along with the annotated ATG (red line). Line 1 and line 2 show the origins of the mutations generated following injection of Cas9+sgRNA into pronuclear stage mouse embryos. This is contextualised below, with exons shown as orange boxes. Splice variants of the gene are used to indicate positions of important functional domains, along with the predicted result of the mutations on protein structure. (**B**) Western blot on protein extracted from brain of seven day old pups with genotypes as indicated. The location of the epitope used to raise the antibody is indicated by Ab in (A). GAPDH was used as a loading control. (**C**) Off target screening by MiSeq sequencing of amplicon PCRs. The wildtype guide sequence and PAM are shown on the top line, with predicted off target sequences, organised by increasing variation from the guide sequence (orange), shown below. On the right hand side, sequencing results are summarised as filled boxes. Relative abundance of reads per individual animal is depicted by fill level of the squares: for example, the each of the heterozygous females shows 50:50 blue:orange to represent 50% read variation from wildtype. Three mutant males from generation F1 and three unrelated wildtype males were sequenced. Amplicons were sequenced to depths of between 200X and 10000X.

5.2.5 *Kdm6a*

A *Kdm6a* mutant line was generated harbouring a 285bp deletion in exon 1, just downstream of the translation initiation site (Figure 5.6A). This deletion was predicted to result in a frameshift, leading to a premature stop codon 13 amino acids after translation initiation and no protein product. I sought to verify this by western blot, using an antibody raised to the C terminal end of KDM6A (Figure 5.6A, red line). I compared protein extracted from wildtype female brain with heterozygous mutant female brain, expecting to see a reduction in the intensity of the protein band in the mutant. Surprisingly, there was no difference between wildtype and heterozygous mutant females (Figure 5.6B). I also compared wildtype male with hemizygous mutant male, expecting to detect no protein in the mutant. Once again, there was no difference between wildtype and mutant. A number of alternative antibodies were tested, but all gave multiple non specific bands under various different conditions. The antibody presented in Figure 5.6B produced a single band of the appropriate size, however, further work is required to confirm the specificity of the blot.

Despite not finding a difference at the protein level, I decided to look for a phenotype in my *Kdm6a* mutant line. I noted that I was not able to generate homozygous mutant females, which was consistent with previous reports of mutations in *Kdm6a* (Shpargel et al., 2012; Welstead et al., 2012). Furthermore, hemizygous mutant males allele were smaller than XY littermates at birth (Figure 5.6C(i)). Although this difference did not reach significance, it was again consistent with previous reports. A subset of these animals were followed through to weaning at three weeks: 100% of the wildtype males survived, whereas only 22% of the hemizygous mutants survived (Table 5.4). These phenotypic results were in complete agreement with the literature, further questioning the specificity of the western blot, and showing that a non functioning *Kdm6a* allele had been generated.

Finally, I screened three F1 males for off target mutations using the same approach as that implemented for the *Kdm5c* line. No mutations were observed at any of the loci sequenced (Figure 5.6C), and I conclude that the targeting of *Kdm6a* was successful.

	XY		**X^{-}Y**	
	Observed	**Expected**	**Observed**	**Expected**
PN1	16 (0.53)	15 (0.5)	14 (0.47)	15 (0.5)
PN21	16 (0.53)	15 (0.5)	4 (0.13)	15 (0.5)

Table 5.4: Numbers of wildtype and *Kdm6a* hemizygous males recorded across five litters produced from a wildtype male and a heterozygous mutant female cross. Expected numbers and proportions based on male pups only, i.e. the null hypothesis of 50% XY and 50% X^{-}Y per litter.

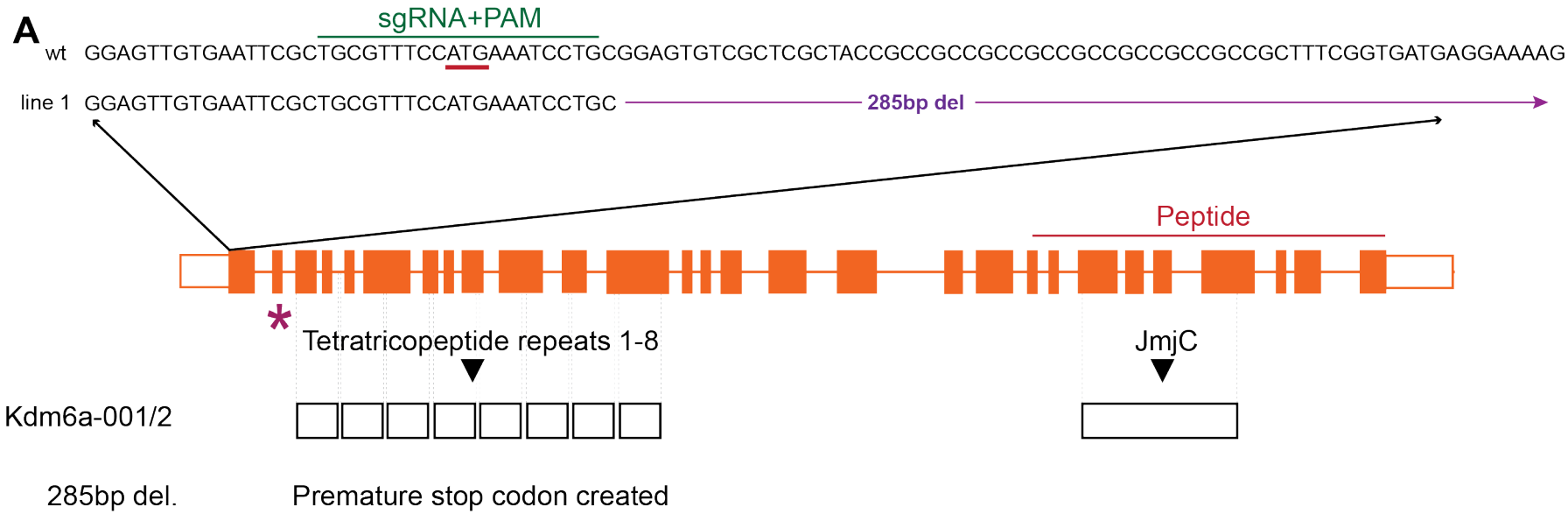
A
sgRNA+PAM
wt GGAGTTGTGAATTCGCTGCGTTTCCATGAAATCCTGCGGAGTGTCGCTCGCTACCGCCGCCGCCGCCGCCGCCGCCGCCGCTTTCGGTGATGAGGAAAAG
line 1 GGAGTTGTGAATTCGCTGCGTTTCCATGAAATCCTGC
285bp del
Peptide
Tetratricopeptide repeats 1-8
JmjC
Kdm6a-001/2
285bp del.
Premature stop codon created

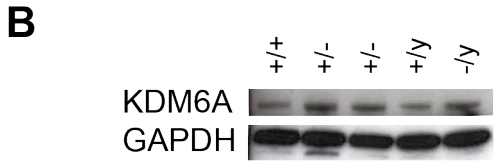
B
+/+
+/-
+/-
+/y
-/y
KDM6A
GAPDH

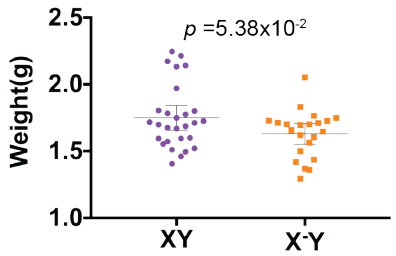
C
p =5.38x10-2
Weight(g)
2.5
2.0
1.5
1.0
XY
X-Y

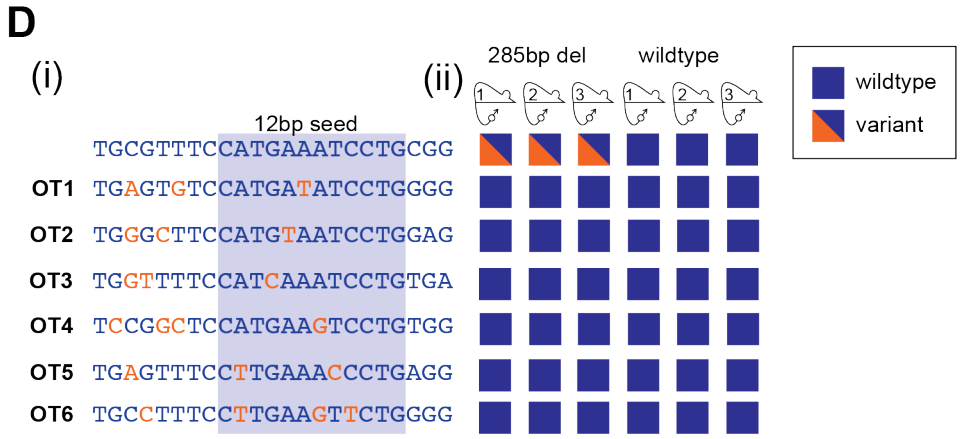
D
(i)
12bp seed
TGCGTTTCCATGAAATCCTGCGG
OT1 TGAGTGTCCATGATATCCTGGGG
OT2 TGGGCTTCCATGTAATCCTGGAG
OT3 TGGTTTTCCATCAAATCCTGTGA
OT4 TCCGGCTCCATGAAGTCCTGTGG
OT5 TGAGTTTCCTTGAAACCCTGAGG
OT6 TGCCTTTCCTTGAAGTTCTGGGG
(ii)
285bp del
wildtype
wildtype
variant

Figure 5.6: Generation of mutant *Kdm6a* allele by CRISPR. (**A**) Cartoon depiction of the target locus. Wildtype (wt) sequence enables visualisation of the guide and PAM, along with the annotated ATG (red line). Line 1 shows the origin of the mutation generated following injection of Cas9+sgRNA into pronuclear stage mouse embryos. This is contextualised below, with exons shown as orange boxes. Splice variants of the gene are used to indicate positions of important functional domains, along with the predicted result of the mutations on protein structure. (**B**) Western blot on protein extracted from brain of seven day old pups with genotypes as indicated. The location of the peptide sequence used to raise the antibody is indicated by peptide in (A). GAPDH was used as a loading control. (**C**) Graph showing birth weight of XY and X^{-}Y pups: each point represents an individual, with mean and 95% CI as bars. *P* value is calculated from Student's t. (**D**) Off target screening by MiSeq sequencing of amplicon PCRs. The wildtype guide sequence and PAM are shown on the top line, with predicted off target sequences, organised by increasing variation from the guide sequence (orange), shown below. On the right hand side, sequencing results are summarised as filled boxes. Relative abundance of reads per individual animal is depicted by fill level of the squares: for example, the each of the heterozygous females shows 50:50 blue:orange to represent 50% read variation from wildtype. Three mutant males from generation F1 and three unrelated wildtype males were sequenced. Amplicons were sequenced to depths of between 200X and 10000X.

5.2.6 *Ddx3x*

A 17bp deletion within exon 1 of *Ddx3x* was created, downstream of the translation initiation site (Figure 5.7A). This mutation was predicted to result in the generation of a premature stop codon after six amino acids. To verify that the protein was no longer present (Figure 5.7B), western blot was performed using an antibody raised to the whole protein. Wildtype female liver was compared with heterozygous mutant female liver, and a reduction in DDX3X in the mutant tissue was expected. A slight reduction in band intensity was observed. When wildtype XY male liver was compared with hemizygous mutant male liver, complete absence of DDX3X in the mutant was expected. Interestingly, only a slight reduction of DDX3X protein was observed in the mutant. In contrast to the *Kdm6a* and *Kdm5c* mutant lines, for *Ddx3x* I was able to generate homozygous mutant females (Figure 5.7B: -/-). Contrary to predictions, tissue from these animals showed a marked depletion, but not complete loss, of DDX3X protein band by western blot. Based on this result, I concluded that I had generated a DDX3X knockdown line. No off target mutations were observed in the three F1 females screened from this line (Figure 5.7C).

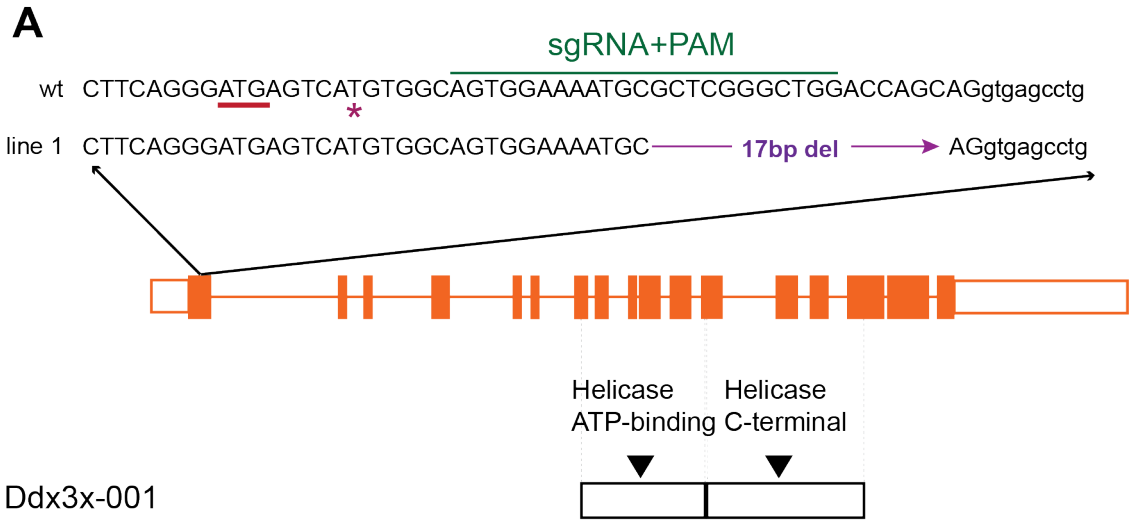

17bp del. Premature stop codon

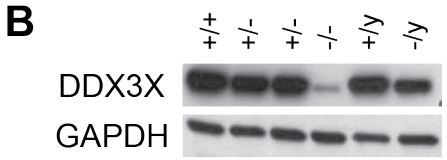

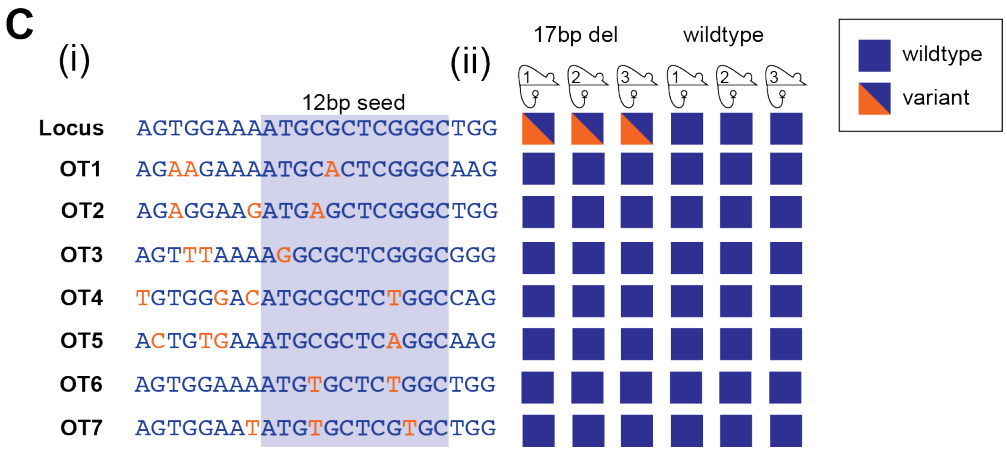

Figure 5.7: Generation of mutant *Ddx3x* allele by CRISPR. (**A**) Cartoon depiction of the target locus. Wildtype (wt) sequence enables visualisation of the guide and PAM, along with the annotated ATG (red line), and alternative ATG (*). Line 1 shows the origin of the mutation generated following injection of Cas9+sgRNA into pronuclear stage mouse embryos. This is contextualised below, with exons shown as orange boxes. Splice variants of the gene are used to indicate positions of important functional domains, along with the predicted result of the mutations on protein structure. (**B**) Western blot on protein extracted from brain of seven day old pups with genotypes as indicated. The location of the peptide sequence used to raise the antibody is indicated by peptide in (A). GAPDH was used as a loading control. (**C**) Off target screening by MiSeq sequencing of amplicon PCRs. The wildtype guide sequence and PAM are shown on the top line, with predicted off target sequences, organised by increasing variation from the guide sequence (orange), shown below. On the right hand side, sequencing results are summarised as filled boxes. Relative abundance of reads per individual animal is depicted by fill level of the squares: for example, the each of the heterozygous females shows 50:50 blue:orange to represent 50% read variation from wildtype. Three mutant females from generation F1 and three unrelated wildtype females were sequenced. Amplicons were sequenced to depths of between 200X and 10000X.

5.2.7 *Eif2s3x*

Due to the very high degree of similarity between the sequence around the translation initiation site of *Eif2s3x* and its Y linked homologue *Eif2s3y*, I instead chose to target exon 7 of *Eif2s3x* (Figure 5.8A). Fewer live offspring were recovered when injecting guides targeting *Eif2s3x*, compared to *Kdm5c*, *Kdm6a*, and *Ddx3x*. Only two pups born from *Eif2s3x* injections carried frameshifted alleles. These were found at very low frequency (Figure 5.8B, box), and were not transmitted in the germ line. I considered two possibilities to explain these observations. Firstly, the guide may not have been efficient at cutting in the context of the mouse embryo: indeed, efficiency appeared very low in mESCs (Table 5.3). Secondly, *Eif2s3x* could be critical for early embryo development, and those embryos with a high percentage of frameshift mutations did not survive. This loss of embryos could impact on the development of embryos carrying wildtype or in frame alleles in the same uterus, resulting in a failed pregnancy and explaining the relatively low number of pups born.

To differentiate between the two hypotheses, 39 pronuclear stage embryos were injected with guides targeting *Eif2s3x* and cultured *in vitro* for three days to E3.5. 15 embryos arrested before reaching the expected morphology of a blastocyst at

E3.5, and seven of these failed to give analysable sequencing data. Of the 32 embryos genotyped, all carried mutated alleles, with a very low proportion of wildtype reads (Figure 5.8B). This demonstrated that the guide was highly mutagenic. I also observed that the seven genotyped embryos that failed to develop to blastocyst generally showed a higher proportion of frameshift alleles compared to those successfully reaching this stage (51.4% vs. 30.8%). One embryo arrested at the morula stage (E2.5) and contained only frameshift alleles, and one blastocyst stage embryo had >99% of reads with frameshift mutations. I conclude that mutations in *Eif2s3x* did not preclude the completion of pre implantation development, as assessed by embryo morphology.

Finally, I attempted to elucidate the timing of embryonic lethality in *Eif2s3x* mutants by utilising pronuclear injection, followed by embryo transfer, and harvest at E6.5, E9.5 and E12.5. For each of the timepoints at least 50 injected embryos were transferred (Table 5.5). Approximately 50% of recipient females were pregnant and contained implantation sites in the uterus. 50% of these sites contained viable embryos at E6.5, 29% at E9.5, and 50% at E12.5 (Table 5.5). The remaining sites had supported implantation, but there was no embryonic tissue found at the time of dissection due to conceptus reabsorption.

The vast majority of the morphologically normal embryos were entirely wildtype (Figure 5.8B), based on genotyping by next generation sequencing. Two embryos at E6.5 harboured frameshift alleles, but as a low proportion of the overall reads. No frameshift alleles were detected at either E9.5 or E12.5, though in frame mutations were picked up in three embryos at E9.5 and one embryo at E12.5. Taken together, these data suggest that *Eif2s3x* plays a critical role in mouse embryonic development. As I was unable to identify any mutants with significant contribution from frameshift alleles later than E3.5, I concluded that these conceptuses fail peri implantation.

Time	Embryos transferred	Transferred females		Harvested embryos	
		Pregnant	Not pregnant	Normal morphology (as % of transferred)	Reabsorbed (as % of transferred)
E6.5	70	3	3	12 (17.1)	12 (17.1)
E9.5	51	2	1	5 (9.8)	12 (23.5)
E12.5	52	1	2	4 (7.7)	4 (7.7)

Table 5.5: Targeting *Eif2s3x* in mouse embryos. Microinjection and surgical transfers were carried out by Sophie Wood and Katharine Mankelow in Genetic Manipulation Services.

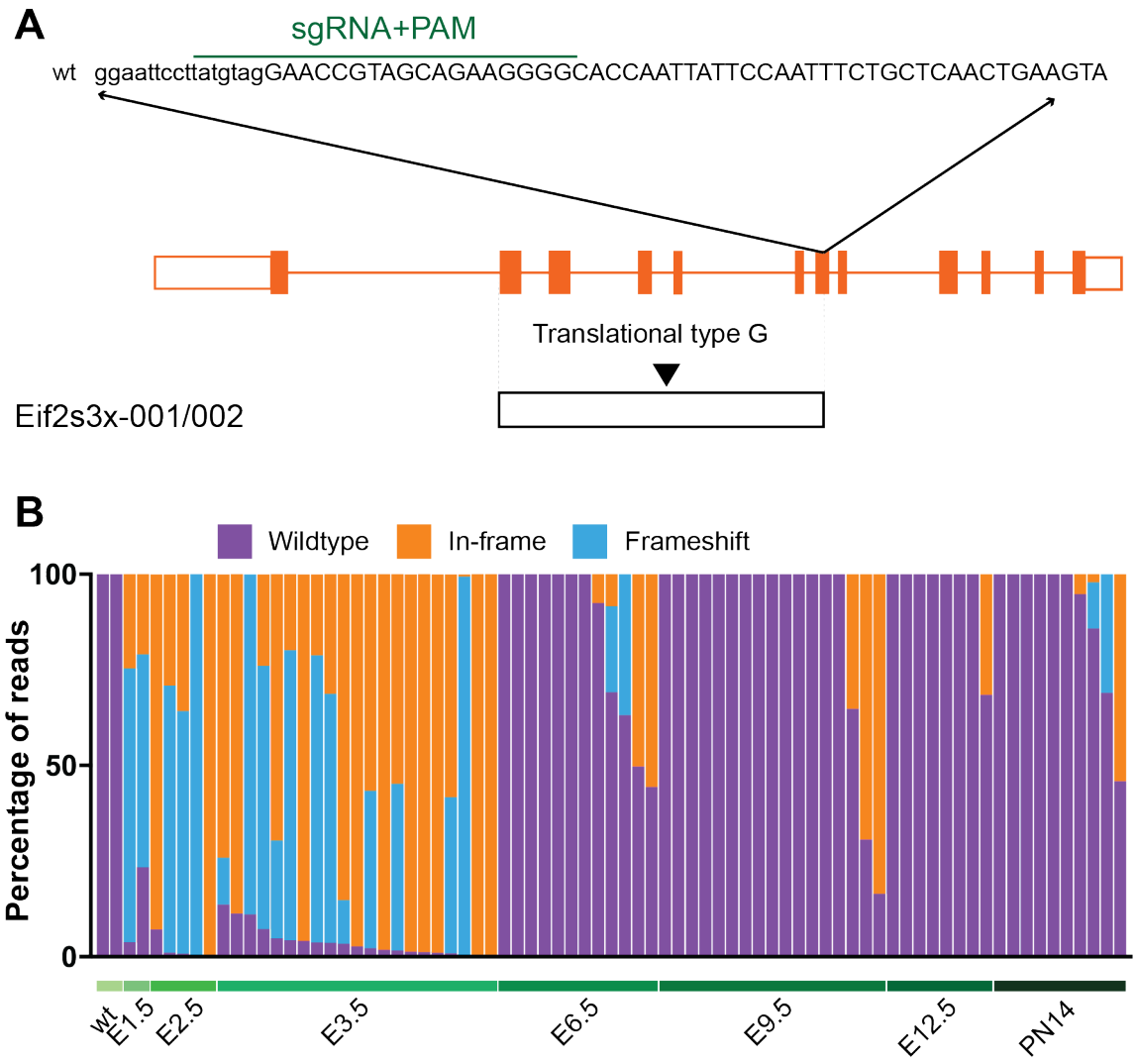

Figure 5.8: Generation of mutant *Eif2s3x* alleles by CRISPR. (**A**) Cartoon depiction of the target locus. Wildtype (wt) sequence enables visualisation of the guide and PAM, which is contextualised below, with exons shown as orange boxes. Splice variants of the gene are used to indicate positions of important functional domains. (**B**) Graphical summary of sequencing results following microinjection of Cas9 and sgRNA into pronuclear stage mouse embryos, followed by harvest at times indicated. Each column represents a single embryo with >200X coverage of the target locus. Mutations were categorised as indicated by the colour scheme.

5.2.8 Haploinsufficiency for *Kdm5c*, *Kdm6a*, or *Ddx3x* does not fully recapitulate the postnatal XO growth deficit

I next sought to utilise these new mutant alleles to test whether haploinsufficiency for *Kdm5c*, *Kdm6a*, or *Ddx3x* would recapitulate the growth deficit phenotype ob-

served in XO female mice. *Eif2s3x* was excluded as I was not able to generate a mutant line, as described above.

In order to generate females heterozygous for a mutant allele alongside wildtype female littermates, I crossed heterozygous females with wildtype males (Figure 5.9A(i), B(i), C(i)). Compared to XX littermates, *Kdm5c* heterozygous mutant females were lighter at birth, though this difference did not reach significance (Table 5.6: p=6.90x10^{-2}). *Kdm6a* heterozygous mutant females were not significantly different in weight from XX littermates at birth (Table 5.6, p=4.46x10^{-1}). *Ddx3x* heterozygous mutant females were slightly, but not significantly, smaller than XX littermates at birth (Table 5.7: p=4.67x10^{-1}).

During the 0-3 week period, there was no significant difference in the rate of growth between wildtype XX females and *Kdm5c* heterozygous mutant females (Figure 5.9A(ii), Table 5.7: p=1.68x10^{-1}). There was also no significant difference in rate of growth between XX females and *Kdm6a* heterozygous mutant females across 0-3 weeks (Figure 5.9B(ii), Table 5.7: p=4.80x10^{-1}); and no significant difference was found between wildtype XX females and *Ddx3x* heterozygous mutant females across the same time period (Figure 5.9C(ii), Table 5.7: p=9.03x10^{-1}).

Finally, I compared the rates of growth for heterozygous mutant females to XX wildtype female littermates during the 3-5 week period. *Kdm5c* heterozygous mutant females gained weight at a slightly reduced rate relative to XX littermates, a difference that was borderline statistically significant (Table 5.7: p=5.30x10^{-2}). There was no difference in rate of growth between *Kdm6a* heterozygous mutant females and their XX wildtype female littermates during this period (Table 5.7: p=4.81x10^{-1}). Interestingly, and similar to *Kdm6a* females, *Ddx3x* heterozygous mutant females gained weight at a reduced rate compared to their XX wildtype female siblings (Table 5.7: p=3.00x10^{-2}). These general trends were reflected when analysing the mean weighted difference from wildtype XX female littermates for each genotype at each timepoint (Figure 5.9D).

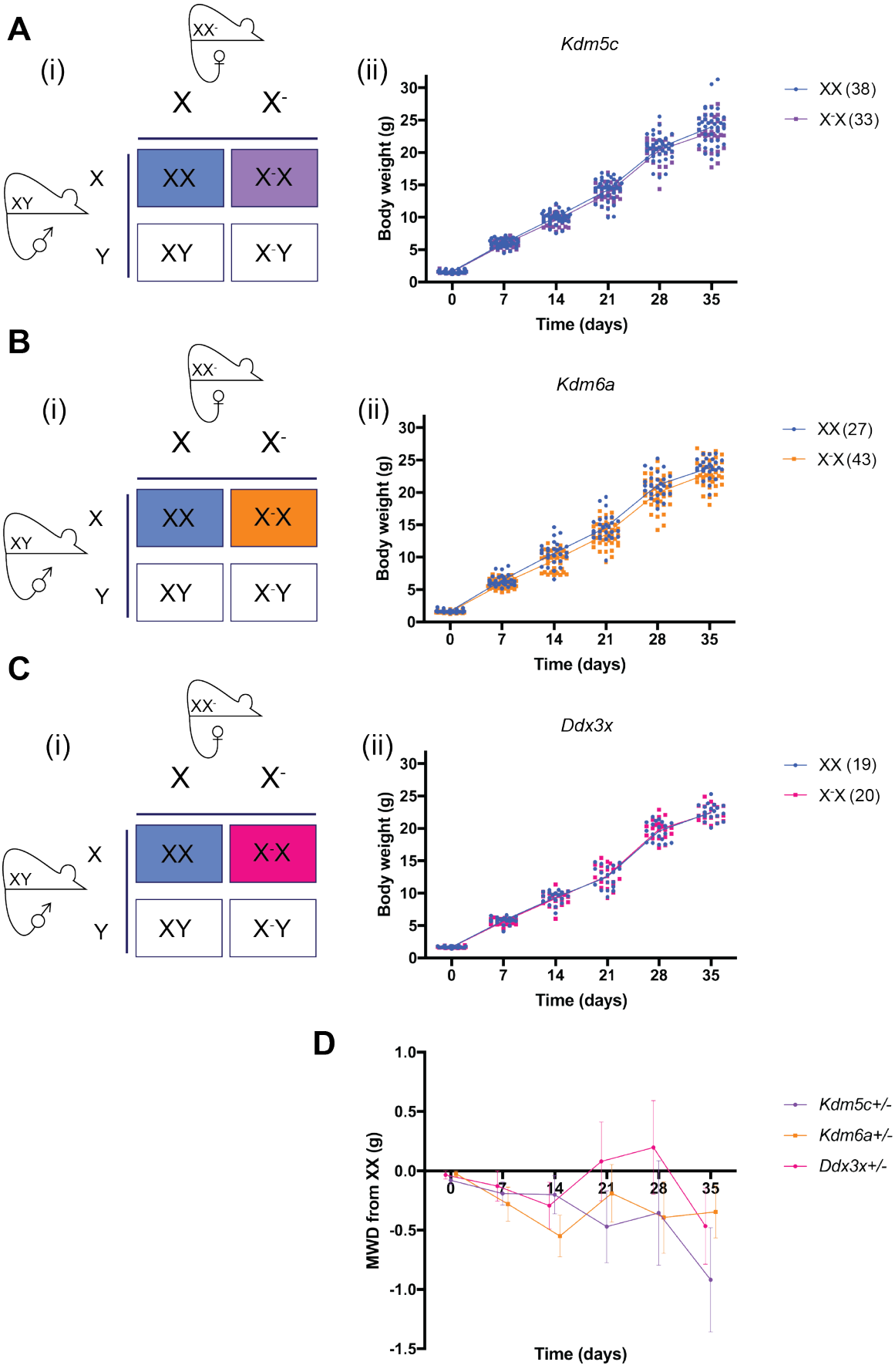
A
(i)
XX-
X
X-
XY
X
Y
XX
X-X
XY
X-Y
(ii)
Kdm5c
Body weight (g)
Time (days)
XX (38)
X-X (33)
B
(i)
XX-
X
X-
XY
X
Y
XX
X-X
XY
X-Y
(ii)
Kdm6a
Body weight (g)
Time (days)
XX (27)
X-X (43)
C
(i)
XX-
X
X-
XY
X
Y
XX
X-X
XY
X-Y
(ii)
Ddx3x
Body weight (g)
Time (days)
XX (19)
X-X (20)
D
MWD from XX (g)
Time (days)
Kdm5c+/-
Kdm6a+/-
Ddx3x+/-

Figure 5.9: Assessment of postnatal growth in heterozygous mutant females compared to wildtype littermates. (**A-C**) Mating schemes to produce heterozygous mutant females alongside wildtype littermates are depicted on the left hand side. Weight data are shown on the right hand side, with each data point representing an individual animal at a single time point. Coloured lines show the mean weight per timepoint for each genotype. (A) shows *Kdm5c*; (B) shows *Kdm6a*; (C) shows *Ddx3x*. (**E**) Mean weighted difference between genotypes indicated and XX littermates. Bars represent 95% confidence intervals.

Comparison	Number		Birth weight (g)			
A v B	na	nb	A	B	**MWD±SE (g)**	**Signif. of MWD (*p*)**
XX v XX^{Kdm5c-}	38	33	1.669±0.032	1.596±0.033	0.080±0.033	$6.90x10^{-2}$
XX v XX^{Kdm6a-}	27	43	1.650±0.044	1.612±0.026	0.023±0.025	$4.46x10^{-1}$
XX v XX^{Ddx3x-}	19	20	1.735±0.028	1.688±0.029	0.034±0.035	$4.67x10^{-1}$

Table 5.6: Birth weight compared by mean weighted difference (MWD) for XX vs. XX^{-}

Comparison	Number		0-3 weeks: mean ±SE (g)				3-5 weeks: mean ±SE (g)			
A v B	na	nb	xA^{a}	xB^{a}	**MWD±SE (g)**	**Signif. of MWD (*p*)**	xA^{a}	xB^{a}	**MWD±SE (g)**	**Signif. of MWD (*p*)**
XX v XX^{Kdm5c-}	38	33	4.140±0.088	4.074±0.073	0.093±0.067	$1.68x10^{-1}$	4.780±0.220	4.550±0.174	0.274±0.138	$5.30x10^{-2}$
XX v XX^{Kdm6a-}	27	43	4.212±0.173	4.095±0.154	0.060±0.085	$4.80x10^{-1}$	4.570±0.238	4.549±0.172	0.066±0.092	$4.81x10^{-1}$
XX v XX^{Ddx3x-}	19	20	3.615±0.200	3.638±0.195	0.013±0.114	$9.03x10^{-1}$	5.029±0.209	4.712±0.222	0.298±0.130	$3.00x10^{-2}$

Table 5.7: Means and mean weighted differences (MWD) for phasic weight gain between genotype comparisons shown in Figure 5.8. "a" represents mean of means.

5.3 Discussion

The results presented here show that XO female mice gain weight at a reduced rate relative to their XX littermates during the first three weeks of postnatal life. This effect is not attributable to imprinting, as it was observed in both $X^{P}O$ and $X^{M}O$ females. Furthermore, the growth deficit remains following the addition of a second PAR, and is only rescued by the presence of a second sex chromosome. These data are consistent with previous data (Burgoyne et al., 2002), and implicated haploinsufficiency for an X linked gene that escapes XCI and has a broadly expressed Y linked homologue. There were, however, a number of inconsistencies with other reports, primarily concerning birth weights.

5.3.1 Comparison of birth weight data

It has previously been reported that relative to XX females, $X^{P}O$ females are underweight at birth (Burgoyne et al., 1983a, 2002), though here I found no significant difference. These results likely reflect low sample size and reduced statistical power. If the number of animals were increased, it is highly likely that standard error would decrease and the magnitude of the difference between genotypes would be more apparent, becoming statistically significant.

$X^{M}O$ and XY^{*X} female embryos were significantly smaller than XX littermates at birth, where no difference was reported previously (Burgoyne et al., 2002). Here, it is unlikely that increasing sample size would have a significant effect on reducing the standard error, the value of which is relatively in line with the standard error in XX littermates for both genotypes. There are two further datasets with some relevance to the current discrepancy. Thornhill & Burgoyne (1993) reported that at E10.5, $X^{M}O$ embryos were significantly larger than XX littermates; and the same observation was made at E17.5 (Ishikawa et al., 2003). Additionally, Ishikawa et al. noted no difference between XX and XY^{*X} embryo weights at E17.5, but $X^{P}O$ embryos were significantly smaller than XX littermates. Taken together, these results suggest that the birth weight deficit noted in $X^{M}O$ and XY^{*X} females is unlikely to be due to carryover of an *in utero* phenotype, though this cannot formally be

excluded without collecting further data from E18.5. The discrepancy is also unlikely to be the result of genetic differences between the animal cohorts, because mice used in the present study were direct descendants of those used in the previous study, maintained on the same strain, and generated from the same crosses. It is difficult to formally exclude whether unknown genetic differences were present then, and/or are now present in these mice, and could impact on the results. I could test this hypothesis, and therefore confirm an $X^{M}O$ and XY^{*X} birth weight deficit, by repeating the experiment in a different mouse strain.

5.3.2 XY^{-} females at birth and post weaning

Two non significant trends in the Burgoyne et al. dataset became significant differences in the present dataset. Burgoyne et al. reported that XY^{-} females were slightly heavier than XX littermates at birth, and here I utilised an increased sample size to show that this difference was statistically significant. Moreover, our larger sample also showed that XY^{-} females then lag behind XX littermates in rate of growth during the 3-5 week period. These results could be due to a Y linked acceleration effect during embryonic and perinatal growth, which then drops off postnatally to the extent that a growth rate deficit ensues. Most Y chromosomes have a mechanistically undefined accelerating effect on mouse embryonic development, first identified at the pre implantation stages (Burgoyne, 1993; Tsunoda et al., 1985). Increased growth relative to XX female littermates is carried over into the postimplantation period, and has been shown present up to E17.5 (Ishikawa et al., 1999). Analysis of birth weight data collected from XY males during the present study extends this trend further, showing that XY males are also significantly larger than XX females at birth (Table 5.8). Moreover, of most relevance here, XY^{-} females are heavier than XX littermates at E10.5 (Burgoyne et al., 1995). In order to test whether the increased birth weight results from a Y linked accelerating effect in XY^{-} females, a Y chromosome variant that lacks the preimplantation acceleration could be modified by removal of *Sry*, using CRISPR Cas9 genome engineering, to generate $XY^{RIII/-}$ females. As described in Chapter 3, the RIII variant Y

chromosome (Tease and Cattanach, 1989) has no effect on preimplantation growth (Burgoyne, 1993), or indeed postimplantation growth up to E10.5 (Burgoyne et al., 1995). $XY^{RIII/-}$ females would be of an equivalent weight at birth to XX littermates, and there would be no lag in growth rate behind XX littermates during the 3-5 week period.

Comparison	**Number**		**Birth weight (g)**			
A v B	na	nb	A	B	**MWD±SE (g)**	**Signif. of MWD (*p*)**
XX v XY	29	28	1.650±0.032	1.732±0.045	0.090±0.026	$<1.00 \times 10^{-5}$

Table 5.8: Birth weight compared by mean weighted difference (MWD) for XX vs. XY

5.3.3 Increasing the XO:XX weight difference

The magnitude of the difference in both absolute weights and rates of growth between XO females and XX littermates is very small, and this was acknowledged in the previous report (Burgoyne et al., 2002). A proportional, reproducible increase in this difference could increase the sensitivity of subsequent experiments to detect potentially incremental contributions from *Kdm5c*, *Kdm6a*, *Ddx3x*, or *Eif2s3x*. This might be achieved by more faithful modeling of the human phenotype, or through adding a stressor to the experimental system that may preferentially impact on XO embryos.

A significant proportion of the human Turner syndrome phenotype occurs as a result of haploinsufficiency of *SHOX*, a gene located within the PAR and involved in chondrogenesis (Ellison et al., 1997; Rao et al., 1997, 2001). Whilst there is no *SHOX* orthologue in the mouse, an orthologue for the closely related human gene *SHOX2* is present on chromosome 3 (Rovescalli et al., 1996) (Clement-Jones et al., 2000). Mouse SHOX2 is 99% homologous to human SHOX2 at the amino acid level, and shows very similar expression patterns (Blaschke et al., 1998; Semina et al., 1998). *Shox2* mutations in mouse have been shown to result in embryonic

lethality around E12.5, due to cardiac and vascular defects (Yu, 2005). Further work targeting the mutation to the limb using a specific Cre driver revealed that complete lack of the protein results in almost complete absence of humerus and femur (Cobb et al., 2006). Whilst heterozygous *Shox2* mutants had no obvious abnormal limb phenotype, no quantitative data were provided (Cobb et al., 2006), and it would be interesting to analyse these mice more thoroughly. Perhaps a *Shox2* mutant would synergise with the existing XO growth deficit, resulting in a more easily distinguishable phenotype. Such a model would further facilitate the detection of incremental contributions from the haploinsufficiency candidates *Kdm5c*, *Kdm6a*, *Ddx3x*, and *Eif2s3x*.

An alternative method to achieve a similar result would be caloric restriction of the pregnant dam for a defined period during pregnancy. A 50% reduction in caloric intake from E12.5 to E18.5 has been shown to cause reduced weight *in utero* at E16.5 and birth, followed by a catch up at around 3-4 weeks (Jimenez-Chillaron et al., 2005). Notably, there was also a significant reduction in litter size at birth, and other physiological effects result from *in utero* under nutrition, such as glucose intolerance (Jimenez-Chillaron et al., 2005). Taking these effects into consideration, it would nevertheless be interesting to compare XO with XX females in undernourished litters, as the physiological stress could have a more significant effect on those already compromised by XO genotype. A previously described example of this effect highlights the preferential loss of embryos carrying a single paternal X over XX littermate in the context of an XO uterine environments (Hunt, 1991).

5.3.4 The postnatal growth phenotype of heterozygous females mutant for *Kdm5c*, *Kdm6a*, or *Ddx3x*

One of the main aims of this chapter was to generate females heterozygous for each of the haploinsufficiency hypothesis candidate genes, and assess for recapitulation of the postnatal growth retardation phenotype. Whilst such females were generated for three out of four genes, these animals did not fully reproduce the phenotype

reported here and previously when comparing XO and XX littermates. Female mice heterozygous for a mutation in either *Kdm5c*, *Kdm6a*, or *Ddx3x* were born with a reduced weight relative to XX littermates, though the difference reached borderline significance only for *Kdm5c*. There was no significant difference in rate of growth between females heterozygous for either *Kdm5c*, *Kdm6a*, or *Ddx3x* and XX littermates across the 0-3 week period. During 3-5 weeks, *Ddx3x* heterozygous mutants gained weight at a significantly reduced rate relative to their XX siblings. The difference in rate of growth was borderline significant for *Kdm5c* heterozygous mutants relative to XX littermates and there was no difference in *Kdm6a* mutants. These observations could be explained by a number of factors, including the impact of random XCI on escapee expression, the need for mutants carrying mutations in all four genes concurrently, or an incorrect hypothesis.

XX female mice undergo XCI, inactivating one X chromosome in every somatic cell. Most X linked genes are subject to this process, though a small number escape and are expressed from both X chromosomes, often in specific tissues and/or at a set developmental time (Disteche et al., 2002). We showed here, as has also been shown previously, that *Kdm5c*, *Kdm6a*, *Ddx3x*, and *Eif2s3x*, all escape XCI in two different adult tissues. Extensive data in the literature extend this to multiple tissues throughout the embryo and adult, across developmental time (Li and Carrel, 2008; Berletch et al., 2015; Disteche, 2016; Balaton and Brown, 2016). Interestingly, a number of these escapees show significant female expression bias at the RNA and protein levels, implying that two active copies of the gene results in higher expression (Reinius et al., 2012; Xu et al., 2002, 2008a,b; Isensee et al., 2007). However, it seems that expression from the escapee alleles on the active X chromosome is not equivalent to alleles on the inactive X chromosome. For example, *Kdm5c* expression was lower from the inactive X chromosome at between E6.5 and E13.5, though this difference reduced to almost 50:50 in adult tissues, as assayed by single nucleotide primer extension assay (Lingenfelter et al., 1998). More recent work utilising RNA-seq has shown decreased relative *Kdm5c* expression from the inactive X chromosome in 4 cell through to early blastocyst stage pre implantation embryos

(Deng et al., 2014). Using the same technique, similar patterns were observed in adult tissues for *Kdm5c*, *Kdm6a*, *Ddx3x*, and *Eif2s3x* (Berletch et al., 2015), and this has also been noted in microarray data (Reinius et al., 2012). Taken together, these data show that escapee genes are expressed more highly in XX females when compared to XY males, and a significantly higher proportion of the total transcripts originate from the active allele.

This XX:XY comparison should theoretically be similar to the XX:XO comparison regarding escapee gene expression, as both have a single X chromosome. If expression of a given escapee from the active X chromosome is arbitrarily represented as 1.0, and from the inactive X chromosome as 0.5, total expression in XX female somatic cells is 1.5 (Figure 5.10). In XO female somatic cells, there is no XCI, therefore expression from the single active X chromosome is 1.0, and total expression is 1.0 (Figure 5.10). XX^- females have two genetically distinct X chromosomes (due to the mutation) and, as a result, each somatic cell will inactivate one of these two X chromosomes at random: the mouse is mosaic. 50% of cells will inactivate the mutant X chromosome, therefore expression from the active wildtype X chromosome is 1.0 (Figure 5.10). In the other 50% of somatic cells, the mutant X chromosome will remain active, with expression of 0, and inactivation of the wildtype X chromosome leads to expression equivalent of the inactive X chromosome in XX cells, i.e. 0.5 (Figure 5.10). When these two levels are averaged across the animal, expression in XX^- females is therefore expected to be lower than in XO females, an arbitrary 0.75.

Whilst this example is purely theoretical, and does not take into account X chromosome upregulation (Sangrithi et al., 2017), or genome wide dosage modulation in aneuploidies (Birchler, 2014), the difference could still partly explain the discrepancy between observations of growth rate in XO females and XX^- females. Were this hypothesis to be correct, the presently described XX^- females have lower expression of each given gene than XO females.

Loss of a single copy of a single gene does not, in itself, appear enough to reproduce the birth weight deficit or the 0-3 weeks rate of growth deficit, but may manifest as the novel post weaning phenotype. I could test the hypothesis, and eliminate random XCI as a variable, by making using of the *Xist*- allele (Marahrens et al., 1997). XCI would become biased towards a specific, known X chromosome, allowing the dissection of effects relating to expression of either a single wildtype allele, or a single mutant allele. Such a model with multiple, reproducible expression levels could also serve to facilitate greater understanding of the relationship between gene dosage and phenotype, as these genes are widely acknowledged to be sensitive to dosage modulation (Bellott et al., 2014; Cortez et al., 2014).

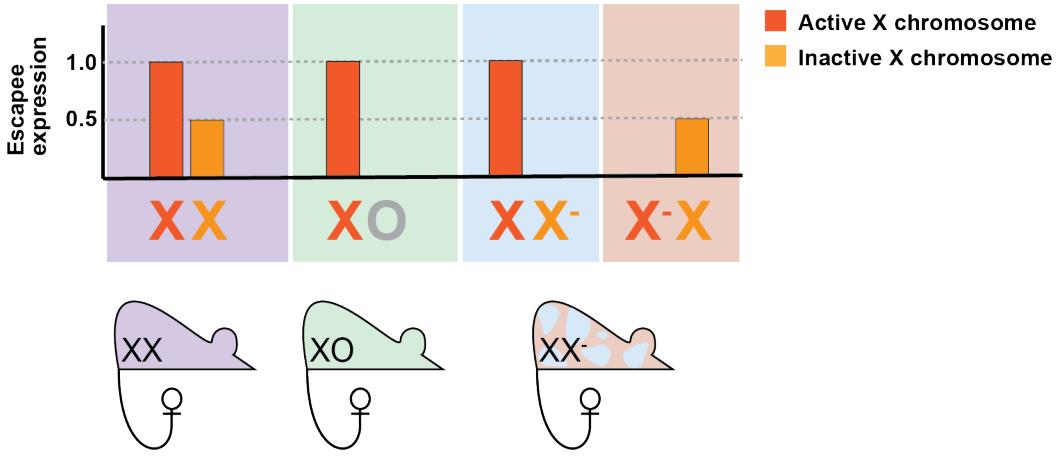

Figure 5.10: Model depicting XCI escapee expression in XX, XO, and XX$^-$ females. Top: cartoon bar graphs representing arbitrary escapee expression levels from each sex chromosome in XX, XO, and XX$^-$ female somatic cells. Bottom: Representation of the composition of mice from which the above cells are taken, i.e. block colour = 100%.

Each of the heterozygous mutants used in the present study carries one mutant allele for a single gene, although four genes have been identified and targeted as part of the haploinsufficiency hypothesis. It therefore seems logical, and likely, that a female carrying a mutation all four genes will recapitulate the XO phenotype to a greater extent. Whilst this strategy was initially considered, the likelihood of being able to generate enough female animals carrying four mutations on the same chromosome, alongside wildtype littermates, to make biologically relevant conclusions is very small. Instead, utilising the XY$^-$ female would be more straightforward (notwithstanding the experiments proposed in 5.3.2), as the Y chromosome does not un-

dergo recombination or XCI. Even taking into account the relatively poor breeding performance of XY^- females (A. Ojarikre, personal communication), these experiments would undoubtedly be more achievable than the compound X linked mutant. Generating mutations in Y linked homologues of the haploinsufficiency candidates would also increased understanding of the roles of X:Y pairs not only in the context of growth, but also more generally in terms of survival. I briefly touched on this topic during the present chapter by demonstrating that *Eif2s3x* is essential for postimplantation embryonic development (see 5.3.5).

5.3.5 Targeting and re targeting *Eif2s3x*

I was unable to generate a mutant line for the fourth candidate highlighted in the Y expression and XCI escapee screens, *Eif2s3x*. After a number of initial *in vivo* attempts, I failed to generate mutant pups, and doubted the veracity of the guide RNA. I used injected embryos cultured to blastocyst primarily to test guide effectiveness and confirm that mutations were being generated. Only secondarily was I interested to see if there was any correlation between developmental progression and the mutation suite observed following sequencing. Whilst I achieved the former, I did not utilise a sufficient number of control embryos to report the success rate of culture to the blastocyst stage of embryos injected with a scramble guide. It is clear that the suite of mutations observed in preimplantation blastocysts is no longer present in later stage embryos, and the embryos carrying such mutations must therefore be eliminated prior to collection. However, based on the present blastocyst culture data and paucity of control data, I cannot conclude whether this elimination occurs pre or postimplantation, and further work is required.

The inability to generate a *Eif2s3x* mutant line was not surprising, given the reported dosage sensitivity of the four haploinsufficiency candidates. However, it was notable because targeting of *Kdm5c*, *Kdm6a*, and *Ddx3x* was almost immediately successful *in vivo*. In hindsight, the apparently low success rate of the initial targeting of *Eif2s3x* in mESCs could be interpreted as highly efficient targeting of a gene necessary for mESC survival. The discrepancy between success and failure is likely

a result of different guide design strategies and efficiencies: a highly efficient guide may increase the proportion of frameshift mutations (Haeussler et al., 2016), and facilitate observation of the dominant phenotype, i.e. lethality, more often. In terms of design, for this guide I targeted an exon in the centre of the coding sequence instead of the initiator methionine (ATG), due to high homology between *Eif2s3x* and *Eif2s3x*. Such a strategy may also be more efficient at ablating protein function (Li et al., 2016).

I did not see any *Eif2s3x* mutant male animals born. It would be interesting to look at the sex of the embryos analysed at E3.5, E6.5, E9.5 and E12.5, as I would expect to see mutant males surviving over mutant females, given the presence of a 97% similar homologue on the Y chromosome. Indeed, it has previously been shown that *Eif2s3x* is able to partly compensate for the absence of its Y linked homologue in spermatogenesis (Yamauchi et al., 2016). Based on the data presented here, no *Eif2s3x* mutants with mutation suites reflecting those observed in the preimplantation embryo survived postimplanation development, let alone birth. I must therefore conclude that males and females are equally affected by the loss of *Eif2s3x*, and *Eif2s3y* is not able to provide functional compensation. The roles of *Kdm5c*, *Kdm6a*, and *Ddx3x*, and their Y linked homologues, in postnatal survival are the subject of the next chapter.

Finally, as only a single guide sequence was utilised, and an off target screen was not carried out, it is formally possible that the lethality phenotype observed could be explained by an off target mutation. As methods for the detection of off target mutations is a highly contentious area (Iyer et al., 2015; Haeussler et al., 2016; Schaefer et al., 2017), the use of a number of different guides to achieve the same phenotype would provide the most robust confirmation. The work to re target *Eif2s3x* by generating a conditional allele, followed by an off target screen, is ongoing.

Chapter 6

The contribution of X-Y homologous genes to postnatal survival in the mouse

6.1 Introduction

The mammalian sex chromosomes are thought to have originated from a pair of autosomes around 180-200 million years ago (Cortez et al., 2014). The proto Y chromosome evolved a dominant male determining locus, which resulted in the acquisition of sexually antagonistic alleles nearby, and this in turn led to the suppression of recombination with the proto X (Wright et al., 2016). Over time, mammalian Y chromosomes generally, and the mouse Y specifically, has lost, and gained, a significant amount of gene-encoding DNA (Soh et al., 2014); though a small number of genes have been conserved. These genes are the Y linked homologues of the X linked genes targeted in Chapter 5: *Ddx3y*, *Eif2s3y*, *Kdm5d*, and *Uty*. Both X-Y copies are broadly expressed, the X linked partner escapes XCI, and it is under more intense purifying selection than neighbours on the X chromosome (Bellott et al., 2014). Collectively, these characteristics suggest the longevity of X-Y pairs can be attributed to selection pressure resulting from dosage sensitivity: copies have been

maintained on both sex chromosomes because the organism cannot survive with only a single copy. This is likely true for humans, evidenced by the X chromosome monosomy Turner syndrome. Approximately 99% of XO female foetuses die *in utero*, and those that survive are often mosaic for at least part of a second sex chromosome (Cockwell et al., 1991; Hook and Warburton, 1983, 2014). In contrast, XO female mice survive, albeit with a slight growth deficit (Chapter 5) and reduced fertility (Burgoyne and Baker, 1981, 1985). The difference in survival between these two mammalian species may result from the relatively small number of mouse X linked genes that require two doses: there are only nine murine X-Y pairs, but 17 pairs in human (Bellott et al., 2014). The survival of XO female mice does, nevertheless, provide the opportunity to address X-Y pair functional divergence in mouse using this model.

Our current understanding of X-Y pair divergence in the mouse stems from a number of transgenic mouse models. Male mice lacking the whole Y chromosome are viable (Yamauchi et al., 2016). Yamauchi and colleagues showed that replacement of the Y chromosome with transgenic copies of *Eif2s3x* and *Sox9* could result in males capable of siring offspring. In contrast, results from experiments targeting X linked genes from X-Y pairs suggest functional divergence, as assessed by postnatal survival. Numerous *Kdm6a* mutants have been published, and in all cases homozygous mutant females die *in utero* (Lee et al., 2012; Wang et al., 2012; Shpargel et al., 2012; Welstead et al., 2012; Mansour et al., 2012; Thieme et al., 2013). Hemizygous mutant males showed reduced perinatal viability, and survivors exhibited a lifelong growth deficit. Similarly, females carrying homozygous mutations in *Ddx3x* die *in utero*, but in contrast to *Kdm6a*, hemizygous mutant males do not survive beyond E6.5 (Chen et al., 2016a). Taken together, these data show that the Y linked genes from X-Y pairs are no longer required for normal postnatal survival in mouse; however, at least one copy of the X linked genes *Ddx3x* and *Kdm6a* are necessary. In this Chapter, I looked to first confirm these results using the mutant lines generated in house. I then utilised these animals, along with sex chromosome

variant lines, to explore the functional redundancy of X-Y genes pairs in postnatal survival.

6.2 Results

6.2.1 *Kdm6a* and *Kdm5c* are required for postnatal survival in female mice

It has previously been shown that XX females homozygous for mutations in either *Kdm6a* or *Ddx3x* die *in utero* (Lee et al., 2012; Shpargel et al., 2012; Welstead et al., 2012; Chen et al., 2016a). I first sought to confirm this result, and test whether the same conclusion could be applied to *Kdm5c*. To exclude XCI as a confounding factor when comparing the postnatal survival of heterozygous mutant females with homozygous mutant females, I used XO female mice, that do not undergo XCI. I crossed a heterozygous mutant female with a $X^{Y}O$ male (Burgoyne et al., 1998; Odorisio et al., 1998), which could produce mutant $X^{-}O$ females along with wild-type XO females within the same litter (Figure 6.1A; Table 6.5, Comparison 1). I predicted that $X^{-}O$ females would not survive, consistent with previous data for *Kdm6a* and *Ddx3x*. Such a result would serve to emphasise the importance of at least one copy of each X linked gene from the X-Y gene pairs. I assayed survival by genotyping pups at PN7. There were no *Kdm6a* $X^{-}O$ mutant females present, in contrast to 27 XO wildtype females (Figure 6.1B, p=1.54x10^{-4}; Table 6.1, adjusted p=1.02x10^{-4}). I conclude that at least one copy of *Kdm6a* is essential for postnatal survival.

For *Ddx3x* I noted the survival of 12 *Ddx3x* $X^{-}O$ mutant females, compared with 3 XO wildtype females (Figure 6.1C, p=0.1207; Table 6.1, adjusted p=0.202). Although the ratio of $X^{-}O$ mutant to XO wildtype females was undoubtedly impacted by the low number of animals generated for the cross, the presence of any mutant $X^{-}O$ mutant females was unexpected, based on previously reported data (Chen et al., 2016b). This will be discussed further later.

For *Kdm5c*, I recovered a single $X^{-}O$ mutant female at PN7, alongside 26 XO wild-type females (Figure 6.1D, p=1.03x10^{-3}; Table 6.1, adjusted p=1.21x10^{-3}). In conclusion, in XO females, the loss of the single copy of *Kdm6a* and *Kdm5c*, but not *Ddx3x*, compromises postnatal survival.

	Number		
Gene	XO	$X^{-}O$	**adjusted *p***
Kdm6a	27	0	1.02x10^{-4}
Ddx3x	3	12	2.02x10^{-1}
Kdm5c	26	1	1.21x10^{-3}

Table 6.1: Postnatal survival for XO vs $X^{-}O$ females.

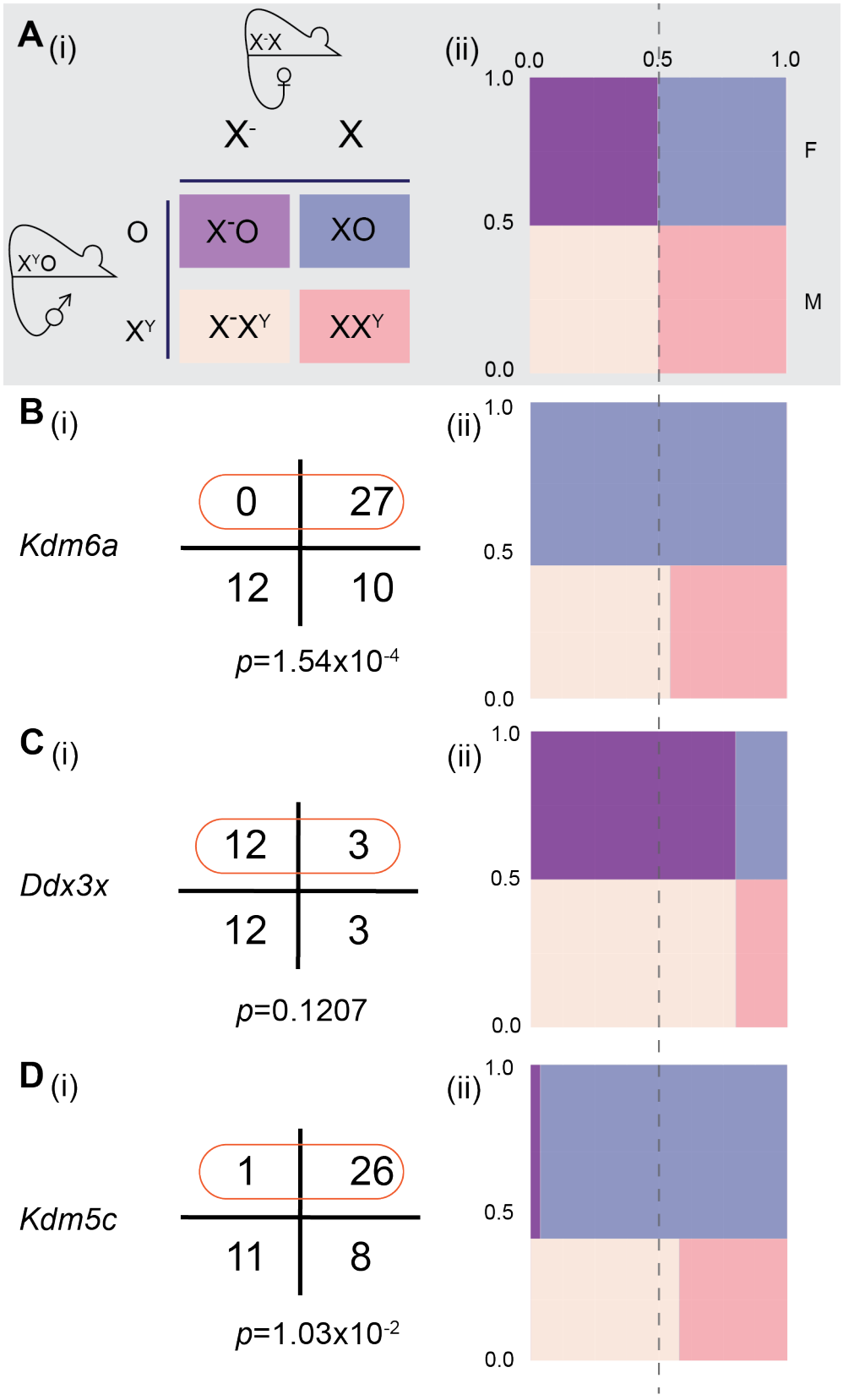
A (i)
X-X
X- X
O
XYO
XY
X-O
XO
X-XY
XXY
(ii)
0.0
0.5
1.0
F
M
B (i)
Kdm6a
0
27
12
10
p=1.54x10-4
(ii)
C (i)
Ddx3x
12
3
12
3
p=0.1207
(ii)
D (i)
Kdm5c
1
26
11
8
p=1.03x10-2
(ii)

Figure 6.1: Postnatal survival of XO female mice carrying a single mutated allele, relative to XO littermates. (**A**)(i) Mouse cross used to generate $X^{-}O$ and XO female mice, and (ii) mosaic plot showing proportion of each genotype expected under the null hypothesis. The Y axis represents the relative proportion of female:male as assessed by gonadal sex, and the X axis breaks down the proportional contribution of each genotype per gonadal sex. The hatched line shows 0.5 on the X axis. (**B**)(i) Number of animals per genotype alive at postnatal day 7 for *Kdm6a* mutant line; numbers relate to genotypes in equivalent location in A(i). The *p* value is derived from Fisher's exact test. Orange ring represents comparison of interest: see text. (**C**) As (B), for *Ddx3x* mutant line. (**D**) As (B), for *Kdm5c* mutant line.

6.2.2 Y linked genes partially compensate for loss of their X linked homologues

Next I looked to determine whether Y linked genes from X-Y pairs could compensate for loss of their X linked homologues. For this experiment, I wanted to compare survival of XX homozygous mutant females to survival of X^-Y hemizygous mutant males. Given the results of the previous section, whereby *Kdm6a* and *Kdm5c* XO mutant females did not survive, survival of any hemizygous mutant males would suggest a degree of functional compensation. To generate homozygous mutant females alongside hemizygous mutant males, heterozygous mutant females were crossed with hemizygous mutant males (Figure 6.2A(i)).

For *Kdm6a*, as predicted, I observed no homozygous mutant females, and 9 hemizygous mutant males (Figure 6.2B, p=2.92x10^{-2}; Table 6.2, adjusted p=4.50x10^{-2}). I conclude that the presence of the Y chromosome compensated for the loss of *Kdm6a*.

	Number		
Gene	X^-X^-	X^-Y	**adjusted *p***
Kdm6a	0	9	4.50x10^{-2}
Ddx3x	8	26	1.73x10^{-2}
Kdm5c	1	23	3.46x10^{-4}

Table 6.2: Postnatal survival for X^-X^- vs X^-Y animals

For *Ddx3x*, there were 8 homozygous mutant females, compared with 26 hemizygous mutant males (Figure 6.2C, p=9.95x10^{-4}; Table 6.2, adjusted p=1.73x10^{-2}). This showed that the presence of the Y chromosome compensated for the loss of *Ddx3x*.

For *Kdm5c*, one homozygous mutant female was observed, compared with 23 hemizygous mutant males (Figure 6.2D, p=1.07x10^{-4}; Table 6.2, adjusted p=3.46x10^{-4}). Taken together, these data suggested that the presence of a Y chromosome could compensate for the loss of X linked genes *Kdm6a*, *Ddx3x*, and *Kdm5c*.

In order to assess whether this compensation was complete or partial, I compared the survival of hemizygous mutant males with wildtype males (Table 6.5, Comparison 3). Complete compensation was predicted to result in no difference in postnatal survival between wildtype and hemizygous mutant males. I looked to crosses that would enable a direct comparison between X^-Y hemizygous mutant and XY wildtype males. As data were available from the X^-X x X^-Y cross detailed in Figure 6.2, and the X^-X x XY cross in Figure 6.3, a pool was created to increase statistical power (Table 6.3).

For *Kdm6a*, hemizygous mutant males survived in significantly reduced numbers compared to XY males (Table 6.3, p=1.00x10^{-2}) as described previously (Lee et al., 2012; Welstead et al., 2012; Shpargel et al., 2012) and in Chapter 5. I conclude that loss of *Kdm6a* was not fully compensated for by its Y linked homologue, *Uty*.

Hemizygous males mutant for either *Ddx3x* or *Kdm5c* survived in fewer numbers than XY wildtype males, though this difference did not reach significance (Table 6.3, p=2.89x10^{-1} and 3.31x10^{-1} respectively). Taken together, these data show that Y linked genes *Uty*, *Ddx3y* and *Kdm5d* are able to at least partially compensate for the loss of *Kdm6a*, *Ddx3x*, and *Kdm5c*, respectively. This compensation may be more complete for the *Kdm5c* and *Ddx3x*, as there was no evidence of a significant difference in postnatal survival between hemizygous mutant males and XY wildtype males for these comparisons.

	Number		
Gene	XY	X^-Y	***p***
Kdm6a	52	20	1.00x10^{-2}
Ddx3x	51	36	2.89x10^{-1}
Kdm5c	77	59	3.31x10^{-1}

Table 6.3: Postnatal survival for pooled XY vs X^-Y males

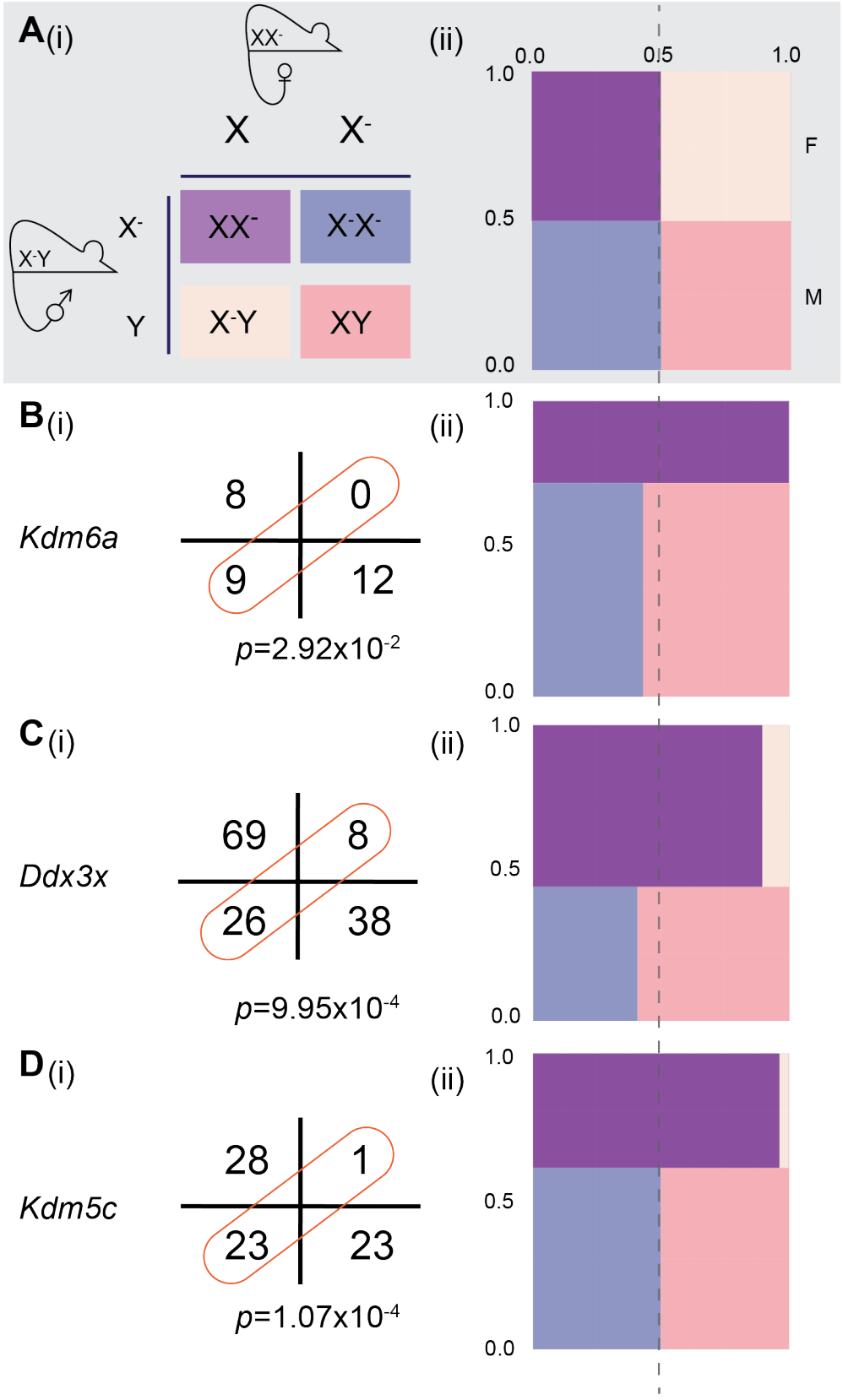
A (i)
XX-
X
X-
X-
X-Y
Y
XX-
X-X-
X-Y
XY
(ii)
0.0
0.5
1.0
1.0
0.5
0.0
F
M
B (i)
Kdm6a
8
0
9
12
p=2.92x10-2
(ii)
1.0
0.5
0.0
C (i)
Ddx3x
69
8
26
38
p=9.95x10-4
(ii)
1.0
0.5
0.0
D (i)
Kdm5c
28
1
23
23
p=1.07x10-4
(ii)
1.0
0.5
0.0

Figure 6.2: Postnatal survival of female mice carrying two mutated alleles, relative to males with one mutated allele and an intact Y chromosome. (**A**)(i) Mouse cross used to generate $X^{-}X^{-}$, XX^{-}, $X^{-}Y$, and XY wildtype littermates, and (ii) mosaic plot showing proportion of each genotype expected under the null hypothesis. The Y axis represents the relative proportion of female:male as assessed by gonadal sex, and the X axis breaks down the proportional contribution of each genotype per gonadal sex. The hatched line shows 0.5 on the X axis. (**B**) (i) Number of animals per genotype alive at postnatal day 7 for *Kdm6a* mutant line; numbers relate to genotypes in equivalent location in A(i). The *p* value is derived from Fisher's exact test. Orange ring represents comparison of interest: see text. (**C**) As (B), for *Ddx3x* mutant line. (**D**) As (B), for *Kdm5c* mutant line.

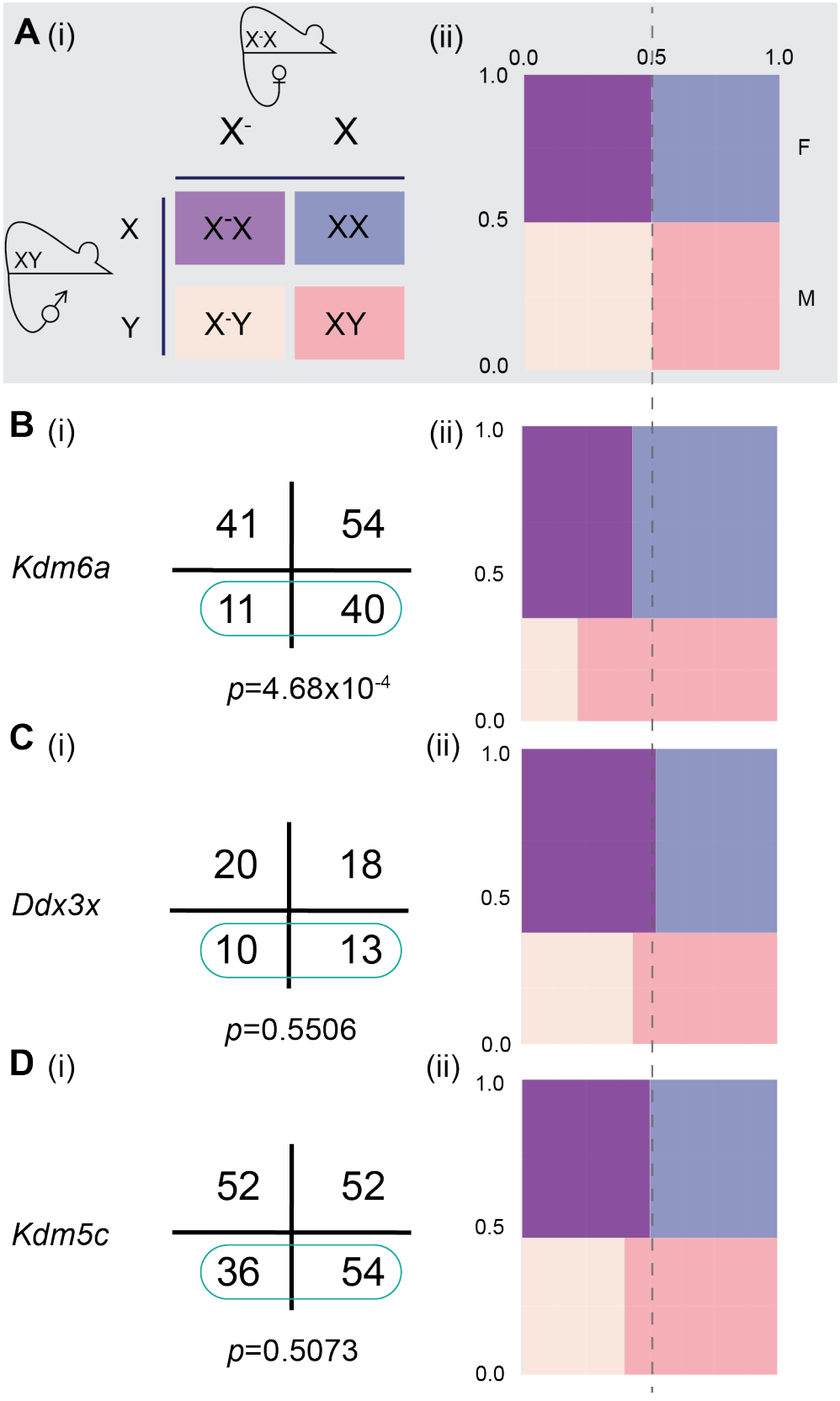
A (i)
X-X
X-
X
XY
X
Y
X-X
XX
X-Y
XY
(ii)
0.0
0.5
1.0
F
M
B (i)
Kdm6a
41
54
11
40
p=4.68x10-4
(ii)
C (i)
Ddx3x
20
18
10
13
p=0.5506
(ii)
D (i)
Kdm5c
52
52
36
54
p=0.5073
(ii)

Figure 6.3: Postnatal survival of male and female mice carrying a single mutated allele, relative to wildtype littermates. (**A**)(i) Mouse cross used to generate $X^{-}X$, $X^{-}Y$ and wildtype littermates, and (ii) mosaic plot showing proportion of each genotype expected under the null hypothesis. The Y axis represents the relative proportion of female:male as assessed by gonadal sex, and the X axis breaks down the proportional contribution of each genotype per gonadal sex. The hatched line shows 0.5 on the X axis. (**B**)(i) Number of animals per genotype alive at postnatal day 7 for *Kdm6a* mutant line; numbers relate to genotypes in equivalent location in A(i). The *p* value is derived from Fisher's exact test. Coloured ring represents comparison of interest: see text. (**C**) As (B), for *Ddx3x* mutant line. (**D**) As (B), for *Kdm5c* mutant line.

6.2.3 Some Y linked genes can compensate for loss of their X linked homologue independent of the hormonal milieu

Phenotypic sex differences between male and female mammals arise from the unequal effects of the sex chromosomes. Such effects can occur either directly, due to differential gene expression from the X and Y chromosomes in XX and XY non gonadal cells; or indirectly, via the gonads, resulting in hormonal differences throughout life (Burgoyne and Arnold, 2016). In the previous experiment, I compared postnatal survival between males and females without controlling for gonadal sex, and thus not taking into account potential confounding effects of sex hormones. I therefore looked to compare X-Y gene function within males and within females separately.

As shown in Table 6.3, I had already established that hemizygous mutant males survived in reduced numbers compared to wildtype males for all three mutant lines, though this difference was only statistically significant for *Kdm6a*. I then looked to test the female hormonal environment for the same X-Y pair effects. I assessed whether the Y linked gene could compensate for the loss of its X linked homologue within females.

For this experiment, I separated karyotypic sex from gonadal sex by using a male carrying a Y chromosome engineered to lack the sex determining gene *Sry*, carrying this gene instead as a transgene on an autosome (Gubbay et al., 1990). This XY^{Tdy}*Sry* male (denoted XY^{-} in Chapter 5) is thus able to produce four different genotypes of sperm. Two of these genotypes will, following fertilisation, produce female offspring, carrying either an X chromosome or a Y^{Tdy} chromosome. The two others will result in male offspring post fertilisation, and these sperm carry either an X chromosome and the *Sry* transgene, or the Y^{Tdy} chromosome and the *Sry* transgene. I crossed this male with a female heterozygous for one of the mutant alleles (Figure 6.4A(i,ii)). I compared postnatal survival in hemizygous mutant fe-

males ($X^{-}Y^{Tdy}$) with XY^{Tdy} females (Table 6.5, Comparison 4). If the Y linked gene could fully compensate, I would expect no significant difference in survival between the two genotypes.

For *Kdm6a*, only one $X^{-}Y^{Tdy}$ mutant female survived, whereas there were four XY^{Tdy} females (Figure 6.4B(i,ii)). This cross also produced one hemizygous mutant male and five wildtype males. I tentatively conclude that in both males and females, the loss of *Kdm6a* is not fully compensated for by the presence of the Y chromosome.

I did not recover any XY^{Tdy} control females from the *Ddx3x* cross, therefore no conclusions can yet be drawn.

For *Kdm5c*, there was no significant difference in survival of $X^{-}Y^{Tdy}$ mutant females survived compared to XY^{Tdy} females (Figure 6.4D(i,ii); Table 6.4, adjusted p=9.20x10^{-1}). Consistent with a previous cross (Figure 6.3D(i,ii)) there were fewer surviving ($X^{-}Y^{Tdy}$*Sry*) mutant males than XY^{Tdy}*Sry* males, though again this difference was not significant (Table 6.3). I conclude from these data that in both males and females, the loss of *Kdm5c* is fully compensated for by the presence of the Y chromosome.

Gene	**Number**		***p***
	XY^{Tdy}	$X^{-}Y^{Tdy}$	
Kdm6a	4	1	n/a
Ddx3x	0	2	n/a
Kdm5c	15	23	9.20x10^{-1}

Table 6.4: Postnatal survival for pooled XY^{Tdy} vs $X^{-}Y^{Tdy}$ females

The total number of animals used for each experiment described here was sub optimal, partly due to the complexity of the mouse cross and the resulting eight possible offspring genotypes. Taking into account this caveat, I conclude that in the female hormonal environment *Uty* partially compensates for loss of its X linked homologue

Kdm6a. *Kdm5d* appears to fully compensate for the loss of its X linked homologue *Kdm5c* in the female hormonal environment. Further work is required to make any conclusions regarding *Ddx3y* compensation for *Ddx3x*.

Comparison	Genotype	**Number of copies** X linked allele	Y linked allele	Sum X+Y	PAR	Male gonads
Wildtype	XX	2	0	2	2	0
	XY	1	1	2	2	1
1	XO	1	0	1	1	0
	$X^{-}O$	0	0	0	1	0
2	$X^{-}X^{-}$	0	0	0	2	0
	$X^{-}Y$	0	1	1	2	1
3	XY	1	1	2	2	1
	$X^{-}Y$	0	1	1	2	1
4	XY^{Tdy}	1	1	2	2	0
	$X^{-}Y^{Tdy}$	0	1	1	2	0

Table 6.5: X-Y pair copy number summary for all comparisons

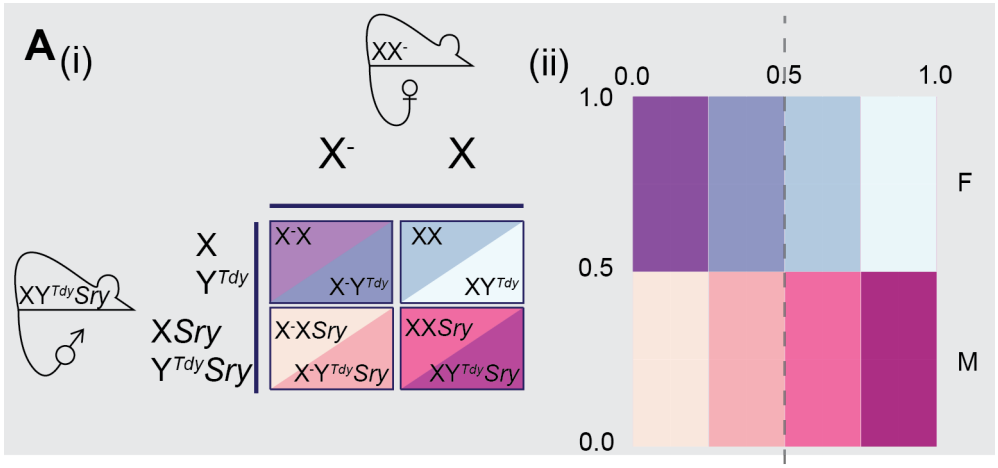

B (i)

2	1	8	4
5	1	3	5

Kdm6a

p=0.6019

(ii)

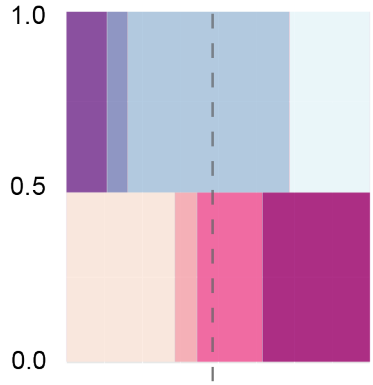

C (i)

2	2	0	0
4	1	4	1

Ddx3x

p=0.6768

(ii)

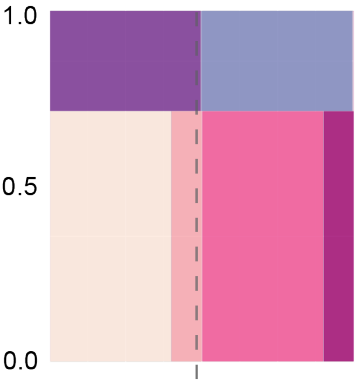

D (i)

17	23	15	15
13	12	20	23

Kdm5c

p=0.8215

(ii)

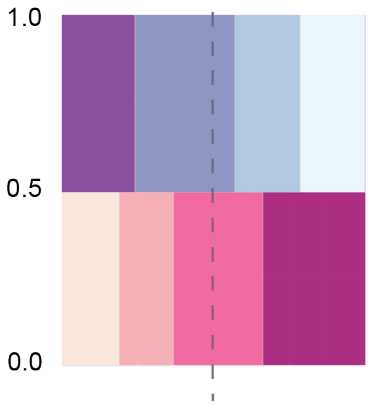

Figure 6.4: Postnatal survival of XX and XY male, and XX and XY female mice carrying a single mutated allele, relative to wildtype littermates. (**A**)(i) Mouse cross used to generate $X^{-}X$, $X^{-}Y$ and wildtype littermates, and (ii) mosaic plot showing proportion of each genotype expected under the null hypothesis. The Y axis represents the relative proportion of female:male as assessed by gonadal sex, and the X axis breaks down the proportional contribution of each genotype per gonadal sex. The hatched line shows 0.5 on the X axis. (**B**) (i) Number of animals per genotype alive at postnatal day 7 for *Kdm6a* mutant line; numbers relate to genotypes in equivalent location in A(i). The *p* value is derived from Fisher's exact test. Orange ring represents comparison of interest: see text. (**C**) As (B), for *Ddx3x* mutant line. (**D**) As (B), for *Kdm5c* mutant line.

6.3 Discussion

Around 180-200 million years ago, one chromosome from a pair of ancestral mammalian autosomes acquired a male determining locus, setting it on the path to becoming the present day Y chromosome via a process of degeneration and evolutionary divergence. A small number of genes remained constant, and changed very little, between the current X and Y chromosomes; and it has been suggested that these genes were retained to maintain dosage.

6.3.1 The *Ddx3x* mutant allele is a hypomorph, not a knockout

Here, I have utilised mutant alleles generated previously (Chapter 5) to interrogate the necessity of both members of these X-Y pairs in postnatal survival in mouse. I have shown that at least one copy of *Kdm6a* is essential for survival; and this is likely also true for *Kdm5c* and *Eif2s3x*. My data for *Ddx3x* are different to that published by Chen and colleagues (2016). Their mutant allele consisted of an excised block of 14 exons. In contrast, I removed 17bp within exon 1 of *Ddx3x*, which was predicted to result in a frameshift and premature stop codon. Based on western blot data from homozygous female tissue, I conclude that the mutation resulted in almost complete ablation of protein expression (Chapter 5, Fig. 5.7). Furthermore, homozygous mutant females showed significantly reduced survival compared to $X^{-}Y$ males. Together, these data suggest that the 17bp mutation impairs DDX3X protein function.

Interestingly, there are two alternative ATG sites downstream of the annotated ATG, both in different reading frames (* in Chapter 5, Fig. 5.7). Whilst translation initiation sites can be accurately predicted using classical methods (Kozak, 1984), mutations have been associated with alternative translation products (Greene et al., 2003). Moreover, recent work has suggested that mutations induced by CRISPR/Cas can cause exon skipping, whereby the exon containing the deletion is omitted from the final protein product (Kapahnke et al., 2016; Prykhozhij et al.,

2017; Mou et al., 2017). Taken together, these data would suggest that an alternative translation initiation site or splicing event could be giving rise to reduced levels of DDX3X expression in these mutant animals. This protein would function in a similar way to the wildtype DDX3X protein, such that only a mild phenotype is observed in females homozygous for the mutant allele. As this phenotype is inconsistent with the published phenotype, I will use the data reported by Chen et al. (2016) for further discussion of the roles of *Ddx3x* in postnatal survival.

6.3.2 Conservation of protein coding sequence does not equate to conservation of gene function

Based on the results presented here, there exists a spectrum of functional divergence between members of X-Y gene pairs in the mouse. Whilst *Kdm5c* undoubtedly contributes to postnatal survival, this function can be at least partially, if not fully, compensated for by the presence of the Y linked homologue *Kdm5d* in both males and females. If at least one copy of either gene is present, the animal will survive. This is in contrast to the evidence for *Kdm6a*, *Ddx3x*, and *Eif2s3x*. Regardless of gonadal sex, the Y linked gene *Uty* can only partly compensate for loss of its X linked homologue, *Kdm6a*. One copy of *Ddx3x* is essential for postnatal survival. In the absence of *Ddx3x*, *Ddx3y* supports development until E6.5 in XY males (Chen et al., 2016a). Further work is required to address the same question in hemizygous mutant females. Finally, utilising the preliminary embryo data from Chapter 5, *Eif2s3x* is also required in at least one copy for development to progress further than E6.5.

Previous work has reported that X-Y pair genes are under more intense purifying selection than other genes on the X chromosome, as evaluated by the ratio of non synonymous to synonymous substitutions between human and mouse (Bellott et al., 2014). Based on this result, it could be asserted that a high degree of protein coding sequence conservation between X-Y pair genes would support functional interchangeability. Interestingly, I have observed that there is a negative corre-

lation between phenotype in hemizygous mutant males and amino acid sequence homology in X-Y pairs (Table 6.6). *Kdm5c* and *Kdm6a* have moderate-high degrees of similarity to their Y linked homologues, and their loss of function gives rise to a mild phenotype when the Y homologue is present. *Ddx3x* and *Eif2s3x* are almost identical to their Y linked homologues at the amino acid level, and their loss of function gives rise to a severe embryonic lethality phenotype when the Y homologue is present. This suggests that, whilst homology in the protein coding sequence is important to facilitate functional conservation, other factors certainly contribute to the inability of these highly similar proteins to compensate for loss of their homologue.

6.3.3 Differences in gene regulation likely underlie the apparent functional differences in X-Y gene pairs

Recent work has begun to highlight the influence of *cis* and *trans* acting regulatory mechanisms on gene expression and, therefore, phenotype. The concept of gene regulation differences accounting for a significant proportion of phenotypic variation is not new (King and Wilson, 1975), however, the development of microarray and RNA-seq technology has allowed a greater depth of study than was previously possible. A well characterised example of this is alternative splicing, which can be species, sex, organ or tissue specific (Blekhman et al., 2010; Merkin et al., 2012). A mouse model of Down syndrome carrying a single human chromosome 21 was shown to exhibit human specific exon skipping frequencies on this chromosome (Barbosa-Morais et al., 2012). Such a result is likely explained by the activity of *cis* acting regulatory elements specific to the human chromosome.

Of more direct relevance to X-Y pair genes is the evolution of testis specific expression by regulatory decay (Cortez et al., 2014). Across therian mammals, many Y linked genes have undergone an almost complete reduction in expression in somatic tissues than in the testis, thus becoming testis specific. Interestingly, the genes that remained ubiquitously expressed, i.e. those from X-Y pairs, also have decreased

expression levels (Cortez et al., 2014). This regulatory decay based reduction in Y linked gene expression could potentially explain the observations that *Ddx3y*, *Eif2s3y* and, to a certain extent *Uty*, cannot compensate for loss of X linked homologues, despite a high degree of protein coding sequence similarity. Whilst all three genes show widespread expression, the levels may not be equivalent to the X linked copy. In support of this hypothesis, it was observed that in XO male mice, a single transgenic copy of *Eif2s3x* could replace *Eif2s3y* in the initiation of spermatogenesis; but at least four transgenic copies were required for progression through meiosis (Yamauchi et al., 2016). *Kdm5d* remains an anomaly; it is possible that this gene has specifically evolved increased expression for an alternative function. A qRT-PCR based approach assaying all four X-Y gene pairs across multiple tissues would test this hypothesis and potentially show correlation.

In order to then determine the possible impact of an X chromosome based regulatory environment versus a Y chromosome based environment, a further experiment would be to exchange the whole protein coding sequence of X and Y genes. Whilst transgenic approaches have been used previously, these have typically utilised randomly inserted BAC constructs, often in multiple copy arrays (Mazeyrat et al., 2001). By taking advantage of the increased efficiency shown by CRISPR assisted homologous recombination, it would be possible to replace, for example, the endogenous protein coding sequence for *Eif2s3x* with the protein coding sequence for *Eif2s3y* (Yoshimi et al., 2016). A conceptually similar experiment has previously been used to show that regulatory sequences immediately surrounding a gene can directly control its expression, independent of the chromosomal context. BAC based *Kdm5c* transgenes were inserted into multiple differences locations on the X chromosome in single copies, and were able to escape XCI similar to the endogenous gene (Li and Carrel, 2008). It would therefore be of significant interest to observe how the Y linked gene sequence behaves within the X linked regulatory context, and vice versa. Eventually, this would provide a focus for future work by concisely addressing whether the survival phenotypes observed result from slight

changes in protein coding sequence, or if we should increase efforts to understand the sex chromosome gene regulatory landscape.

Gene	X-Y male phenotype	XY pair amino acid similarity (%)
Kdm5c	Normal	76.6
Kdm6a	Reduced viability	67.7
Ddx3x	Embryonic lethal	90.2
Eif2s3x	Embryonic lethal	97.9

Table 6.6: Phenotype: amino acid similarity correlation for X linked mutants

Multiple studies in recent years have focused on protein coding sequence variation between species in order to infer the evolutionary path of the mammalian sex chromosomes (eg. Bellott et al., 2014; Cortez et al., 2014). We now know that *Kdm5d*, *Ddx3y* and *Uty* are conserved across all eutherian mammals; with *Eif2s3y* present in all non primate species, and possibly having been replaced by *Eif1ay* in primates (Cortez et al., 2014; Hughes et al., 2015). When combined with significantly increased annotation data on the X linked partners, ascribing functions such as nucleic acid binding, transcription, and translation, we can infer that these genes have been widely conserved, and maintain ubiquitous expression, because they regulate expression of target genes across the genome (Bellott et al., 2014). As I have shown during this Chapter, significant homology at the protein coding level does not, however, automatically lead to functional conservation. It is becoming increasingly clear that changes in the regulation of gene expression may be of equal or even greater importance than variation in protein coding sequence for understanding speciation, or even intra species phenotypic differences between sexes. With the ultimate goal of being able to predict how changes in sequences at regulatory elements effect changes in gene expression, tractable model systems are required. I believe that X-Y gene replacement model hypothesised here would provide the opportunity to address some of these questions both *in vitro* and *in vivo*.

Chapter 7

Summary

In this thesis I have reported experiments I performed to begin to address the role of the X chromosome in growth regulation in the mouse. This work was based around the XO mouse, a model that has previously been shown to exhibit two distinct periods of growth deficit relative to XX littermates (Thornhill and Burgoyne, 1993; Burgoyne et al., 2002).

In Chapter 3, I hypothesised that the growth deficit previously observed in $X^{P}O$ embryos could result from inappropriate expression of *Xist* from the single X chromosome. Using a previously published mutant *Xist* allele (Marahrens et al., 1997) I found that, in the genetic absence of *Xist*, $X^{P}O$ embryos were still growth retarded relative to XY^{RIII} littermates. I concluded that *Xist* is not the cause of the growth deficit, and put forward an alternative hypothesis that the phenotype could result from differential expression of imprinted genes affecting embryonic growth. As embryos with an active X^{M} in extraembryonic tissue do not show the growth deficit phenotype, and $X^{P}O$ embryos have only an active X^{P} in extraembryonic tissue, I suggested that an extraembryonic defect would be more likely than an embryonic defect.

In Chapter 4, I used *in vitro* stem cell models to facilitate the search for candidate imprinted genes differentially expressed between $X^{P}O$, $X^{M}O$, and XX geno-

types. Initially I derived cell lines from both extraembryonic and embryonic compartments, mTSCs and mESCs respectively, and the latter were differentiated towards mEpiLCs in order to model the epiblast. I differentiated the mTSCs to model terminally differentiated placental cells, and found no difference between the sex chromosome genotypes in propensity towards or away from a given lineage.

Using RNA-seq followed by differential gene expression analysis, I identified a small number of genes differentially expressed between genotypes within cell types for both mESCs and mEpiLCs. Most interestingly, I highlighted around 3800 genes differentially expressed between either $X^{P}O$ or $X^{M}O$ and XX mTSCs. These genes were physically distributed across the whole genome, suggesting global transcriptional dysregulation in the aneuploid state. There were potential confounding factors in the bioinformatic analysis that could change the current interpretation of the results, and further work is undoubtedly warranted.

In Chapter 5, I set out to investigate the genetic basis underlying the postnatal growth deficit of both $X^{P}O$ and $X^{M}O$ female mice. Firstly I recapitulated previous results: both $X^{P}O$ and $X^{M}O$ female mice had a period of reduced rate of growth in the 0-3 week period, as did female mice with a single X chromosome and a second copy of the PAR. I further confirmed that XY^{-} females do not show the reduced rate of growth. I then used RT-PCR and RFLP analyses to identify four candidate genes on the mouse Y chromosome that may underlie this apparent rescue: *Kdm5d*, *Uty*, *Ddx3y*, and *Eif2s3y*. I hypothesised that carrying only a single X linked copy of these genes, as per the XO female, may be detrimental to the growth of the animal. I used CRISPR-Cas genome editing to generate new mutant lines for the X linked genes, aiming to compare XX females, carrying two copies of a given target gene, with $X^{-}X$ females, carrying a single copy of the gene. The results for *Kdm5c*, *Kdm6a*, or *Ddx3x* did not recapitulate the postnatal growth deficit phenotype, likely due to a combination of factors, as discussed in the Chapter. I was not able to generate a mutant line for *Eif2s3x*, and I found that embryos carrying mutations in this gene do not survive beyond E6.5. This gene is therefore embryonic lethal,

and not functionally compensated for by the presence of its Y linked homologue *Eif2s3y*.

In Chapter 6, I sought to address functional conservation between X-Y gene pairs on the mouse sex chromosomes, utilising the mutant models reported in Chapter 5. It has previously been shown that at least one copy of both *Kdm6a* and *Ddx3x* are required for postnatal survival, suggesting that the Y linked homologues of these genes have functionally diverged from their former X linked pairing partners. (Shpargel et al., 2012; Chen et al., 2016a). I confirmed that *Kdm6a* is required for postnatal survival in females, and that *Uty* only partially compensates for the loss of *Kdm6a* in males. Furthermore, I showed that *Kdm5c* is also required for postnatal survival in females, whereas in males, *Kdm5d* fully compensates for loss of *Kdm5c*. The data for *Ddx3x* were not consistent with the previously published phenotype, and this led me to conclude that the mutant allele reported in this thesis is a hypomorph. Taken together with the results from Chapter 5 regarding *Eif2s3x* and Chen and colleagues study on *Ddx3x*, I concluded that *Kdm6a* and *Uty*, *Ddx3x* and *Ddx3y*, and *Eif2s3x* and *Eif2s3y* are functionally divergent in the mouse. In contrast, *Kdm5c* and *Kdm5d* appear to have conserved function, as assessed by postnatal survival. Given that both the X and Y linked genes in the X-Y gene pairs are highly similar at the amino acid level, it is likely that changes in gene regulation underlie the functional divergence reported here.

In summary, I have generated data supporting a role for the X chromosome in both embryonic and postnatal growth in the mouse, though further work is undoubtedly required to confirm the individual loci involved. I have also provided initial evidence regarding the significance of sex chromosome aneuploidy in the mouse placenta, and I am excited to continue investigations in this area. Finally, preliminary data addressing functional convergence between X-Y gene pairs suggest that three of the four Y linked genes have diverged, and are no longer able to functionally compensate for loss of the X linked homologues. These results are at odds with

recent hypotheses regarding mammalian sex chromosome evolution in the literature (eg. Bellott et al., 2014), and certainly merit further work.

Appendix A

Cell culture media and solutions

Component	Concentration(mM)	
	Follicle holding medium (FHM)	**Potassium-supplemented simplex optimised medium (KSOM)**
NaCl	95	95
KH_2PO_4	2.5	2.5
$MgSO_4$	0.2	0.2
Lactate	10	10
Pyruvate	0.2	0.2
Glucose	0.2	0.2
Glutamine	1	1
Bovine serum albumin	1mg/ml	1mg/ml
EDTA	0.01	0.01
$NaHCO_3$	4	25
HEPES	20	n/a
$CaCl_2$	1.71	1.71

Table A.1: Components of embryo culture media used in this thesis

Medium	Component	Source	Product code	Volume	Final conc.
2iLIF	Penicillin-streptomycin	Thermo Fisher Scientific (Waltham, USA)	150700A973163	5ml	50U/ml and 50ug/ml
	Glutamax	Thermo Fisher Scientific (Waltham, USA)	35050038	5ml	2mM
	Human recombinant serum albumin	Sigma-Aldrich (St Louis, USA)	A9731	500ul	50ug/ml
	PD 0325901	Axon Medchem (Groningen, Netherlands)	1408	167ul	1uM
	CHIR 99021	Axon Medchem (Groningen, Netherlands)	1386	167ul	3uM
	Human recombinant LIF	Merck-Millipore()	ESG1107	50ul	1000U/ml
	2-mercaptoethanol	Sigma-Aldrich (St Louis, USA)	M6250	3ul	0.1uM
	NDiff227	Cellartis/Takara-Clontech (Tokyo, Japan)	Y40002	(to 500ml)	n/a
Trophoblast stem cell	Foetal bovine serum	Thermo Fisher Scientific (Waltham, USA)	16000044	75ml	15% (v/v)
	Penicillin-streptomycin	Thermo Fisher Scientific (Waltham, USA)	150700A973163	5ml	50U/ml and 50ug/ml
	Sodium pyruvate	Thermo Fisher Scientific (Waltham, USA)	11360070	5ml	1mM
	Recombinant human FGF4	Peprotech (London, UK)	100-31	500ul	25ng/ml
	Heparin	Sigma-Aldrich (St Louis, USA)	H3149	50ul	1ug/ml
	2-mercaptoethanol	Sigma-Aldrich (St Louis, USA)	M6250	3ul	0.1uM
	RPMI1640 +Glutamax	Thermo Fisher Scientific (Waltham, USA)	61870010	(to 500ml)	n/a
Mouse embryonic fibroblast	Foetal bovine serum	Thermo Fisher Scientific (Waltham, USA)	16000044	50ml	10% (v/v)
	Penicillin-streptomycin	Thermo Fisher Scientific (Waltham, USA)	150700A973163	5ml	50U/ml and 50ug/ml
	2-mercaptoethanol	Sigma-Aldrich (St Louis, USA)	M6250	3ul	0.1uM
	DMEM +Glutamax	Thermo Fisher Scientific (Waltham, USA)	61965026	(to 500ml)	n/a

Table A.2: Components of cell culture media used in this thesis

Solution	Component	Concentration
P1	Tris (pH8)	15mM
	EDTA	10mM
	RNAse A	100ug/ml
P2	NaOH	200mM
	Sodium dodecyl sulphate	1%
P3	KOAc (pH5.5)	3M
2X saline sodium salt (SSC)	NaCl	300mM
	$Na_3C_6H_5O_7$	30mM
	HCl	to pH7.0
2X hybridisation buffer	SSC	4X
	Dextran sulphate	50%
	Bovine serum albumin	2mg/ml
	Vanadyl ribonucleoside	2mM
Radioimmunoprecipitation assay (RIPA) buffer	Tris-Cl (pH8.0)	10mM
	EDTA	1mM
	EGTA	0.5mM
	Triton-X100	1%
	Sodium deoxycholate	0.1%
	Sodium dodecyl sulphate	0.1%
	NaCl	140mM
	Phenylmethane sulphonyl fluoride (PMSF)	1mM
Laemmli buffer	Tris-Cl (pH6.8)	60mM
	Sodium dodecyl sulphate	2%
	Glycerol	10%
	2-mercaptoethanol	5%
	Bromophenol blue	0.01%
Western blot running buffer	Tris base	3g/L
	Glycine	14.4g/L
	Sodium dodecyl sulphate	1g/L
Western blot transfer buffer	Tris base	3g/L
	Glycine	14.4g/L
	Sodium dodecyl sulphate	50mg/L
Tris buffered saline/Tween (TBS/T)	Tris-Cl (pH7.5)	20mM
	NaCl	150mM
	Tween-20	0.2%
KT lysis buffer	Tris Cl (pH9.1)	67mM
	$(NH_4)_2SO_4$	16mM
	$MgCl_2$	3.5mM
	Bovine serum albumin	150ug/ml
	Proteinase K	800ug/ml
	Triton-X100	0.5%

Table A.3: Components of solutions used in this thesis

Appendix B

Oligonucleotide sequences

Chapter	Oligo	Sequence	Reference
3	InX_F	CTGCAATGCCTGCTGTTTTA	
	InX_R	CCGGAGTACAAAGGGAGTCA	
	Ymt2b_F	CTGGAGCTCTACAGTGATGA	Bishop and Hatat, 1987
	Ymt2b_R	CAGTTACCAATCAACACATCAC	
	Xist_mut_F	TCTTTTTCTTTTGCCCATCG	Marahrens et al., 1997
	Xist_mut_R	TACCGGTGGATGTGGAATGT	
	Xist_RT_F	CGACCTATTCCCTTTGACGA	
	Xist_RT_R	GTTGATCCTCGGGTCATTTA	
	GAPDH_RT_F	TGTCGTGGAGTCTACTGGTG	
	GAPDH_RT_R	TTCACACCCATCACAAACAT	

Continued on next page

Chapter	Oligo	Sequence	Reference
4	Cdx2_F	TCCTGCTGACTGCTTTCTGA	
	Cdx2_R	CCCTTCCTGATTTGTGGAGA	
	Eomes_F	GGAAGTGACAGAGGACGGTG	
	Eomes_R	GCCGTGTACATGGAATCGTAG	
	Elf5_F	GGACTCCGTAACCCATAGCA	
	Elf5_R	TACTGGTCGCAGCAGAATTG	
	Tfap2c_F	TGCACACAGGGTATTGAAAC	
	Tfap2c_R	CGTCACCCACACAAACTAAA	
	Bmp4_F	GAGTTTCCATCACGAAGAACA	
	Bmp4_R	GCTCACATCGAAAGTTTCCC	
	Esrrb_F	AACAGCCCCTACCTGAACCT	
	Esrrb_R	CTCATCTGGTCCCCAAGTGT	
	Gata3_F	GGGTTCGGATGTAAGTCGAG	
	Gata3_R	CCACAGTGGGGTAGAGGTTG	
	Rhox4b_F	AGGGAAGCACTCAGGACATG	
	Rhox4b_R	TTTGTCCCATTCCACTGCTG	
	Syna_F	TTGCAATCACACCTTTCAGC	
	Syna_R	TGGTGTCCACAGACAGGGTA	
	Synb_F	CTTTCCACCACCCATACGTT	
	Synb_R	TGACCTTGAAGTGGGTAGGG	
	Snai1_F	CACGCTGCCTTGTGTCTG	
	Snai1_R	AGACTCTTGGTGCTTGTGGA	
	Gcm1_F	CTGCCTCAGAACGTGAAAACG	
	Gcm1_R	TTGTGGTTGTTGGTGTTGCG	
	Ascl2_F	TAAGGGCTGAGCACCAGGAC	
	Ascl2_R	CGTACCAGTCAAGGTGTGCTT	

Continued on next page

Chapter	Oligo	Sequence	Reference
	Tpbpa_F	CCAGCACAGCTTTGGACATCA	
	Tpbpa_R	AGCATCCAACTGCGCTTCA	
	Pcdh12_F	GCTGCTTTTGCGGAACGGAA	
	Pcdh12_R	TTTGGGCTGGAATTGGCCCT	
	Hand1_F	CAAGATCAAGACTCTGCGCC	
	Hand1_R	TTAATCCTCTTCTCGCCGGG	
	Pl1_F	GGAGCCTACATTGTGGTGGA	
	Pl1_R	TCCCTATACACATCTGCGGC	
	Prl2c2_F	TGCTCCTGGATACTGCTCCT	
	Prl2c2_R	TGAGACAAACTGCCGGCTAA	
	Prl3d3_F	GGCTCCGGAATGCAATTGTT	
	Prl3d3_R	TCCCTATACACATCTGCGGC	
	Gapdh_qrt_F	TGTCGTGGAGTCTACTGGTG	
	Gapdh_qrt_R	TTCACACCCATCACAAACAT	
	Srp72_F	GGAGTGAGGTGAACCGTTATG	
	Srp72_R	AGGCAAACTACTTTACAGTGCAG	
	Ctsq_probe	TAQMAN MM01349948_M1	
	Gapdh_probe	TAQMAN MM99999915_G1	
	Srp72_probe	TAQMAN MM01211622_G1	
	Nanog_F	AGCAGATGCAAGAACTCTCCTC	
	Nanog_R	AAGTTGGGTTGGTCCAAGTCT	
	Pou5f1_F	CCCCAATGCCGTGAAGTTG	
	Pou5f1_R	TCAGCAGCTTGGCAAACTGTT	
	Fgf5_F	AAAGTCAATGGCTCCCACGAA	
	Fgf5_R	CTTCAGTCTGTACTTCACT	
	Wnt3_F	CAAGCACAACAATGAAGCAGGC	

Continued on next page

Chapter	Oligo	Sequence	Reference
	Wnt3_R	TCGGGACTCACGGTGTTTCTC	
	Dnmt3b_F	CTCGCAAGGTGTGGGCTTTTGTAAC	
	Dnmt3b_R	CTGGGCATCTGTCATCTTTGCACC	
	Sox2_probe	TAQMAN MM03053810_S1	
5	Zfy1_RT_F	CACGCAGTAGAGAGTGAGACC	
	Zfy1_RT_R	GGTACTGTTTGGATTCAGGTC	
	Ube1y1_RT_F	CTTACGAGCTCTGGAGCACTT	
	Ube1y1_RT_R	CTTCTCAAAGTCAATGGGGTA	
	Kdm5d_RT_F	GAGACCCGTGAGGCTCTAAC	
	Kdm5d_RT_R	TTGAATCTCATTCACATCAGCA	
	Eif2s3y_RT_F	GTACAGTAGCCGAAGGAGCTC	
	Eif2s3y_RT_R	ACCACCTGGAGCAGCATACT	
	Uty_RT_F	TTCTGGAAGGAGACAGAAAGC	
	Uty_RT_R	GAACACCCCAATAATCTTCAGG	
	Ddx3y_RT_F	GTTCGATGATCATGGTCGA	
	Ddx3y_RT_R	CTTCATAGCCTTCAAAGCCTC	
	Usp9y_RT_F	GGATGGTCAACTCTGGCTCTG	
	Usp9y_RT_R	CTGATTAGCTTGCAATTTGGG	
	Zfy2_RT_F	GGATGAGCCTAGCAAAACAG	
	Zfy2_RT_R	CATAAGCTGCTGTCCATGC	
	H2al2y_RT_F	CCGTGTAGATCGTTTCCTTG	Royo et al., 2010
	H2al2y_RT_R	AGAGTTGGTGGAGCTGTTCC	
	Sry_RT_F	GAGGGCCATGTCAAGCG	
	Sry_RT_R	AGGTGCCCAGTGGGGATAT	
	Rbmy1a1_RT_F	GCGTCTTCCAGAAGAGATGAGT	
	Rbmy1a1_RT_R	GAGTGGTAATTGCCATAGTCACAG	

Continued on next page

Chapter	Oligo	Sequence	Reference
	Ssty1_RT_F	GAGCCTGTCACCCAATGG	
	Ssty1_RT_R	CCTCAGAGCCATCTTTCCTCTC	
	Ssty2_RT_F	GCCATCATTCTAGGTCAACTG	
	Sly_RT_F	TAAACAACCCAGCAATTGGT	
	Sly_RT_R	GGTCCATGGACTTCTCATGC	
	Ddx3x_RFLP_F	AAAGCCGCAGTTCTCCCG	
	Ddx3x_RFLP_R	TGCTTGCTGTACTTCCTCCA	
	Kdm5c_RFLP_F	AGAAGGAGCTGGGGTTGTAC	
	Kdm5c_RFLP_R	AGCTGTAGAGGAGGCTGTTG	
	Kdm6a_RFLP_F	AGCTGAAGGGAAAGTGGAGT	
	Kdm6a_RFLP_R	AGCCCACTGAAATGCATTGT	
	Foxo4_RFLP_F	AGCTCGGCAGGATGGAAG	
	Foxo4_RFLP_R	GCCCATCCAGTAGCTCTAGA	
	Eif2s3x_RFLP_F	ATCCCGTGTGCACAGAAGTA	
	Eif2s3x_RFLP_R	GTTGGTGTGCTACTTTGGGG	
	Kdm5c_g1_F	CACCGCCCCCTAAGCCCTTGACGGG	
	Kdm5c_g1_R	AAACCCCGTCAAGGGCTTAGGGGGC	
	Kdm5c_g2_F	CACCGGCGGCGCCATGCGTCCTTAA	
	Kdm5c_g2_R	AAACTTAAGGACGCATGGCGCCGCC	
	Kdm5c_g1_T7	TTAATACGACTCACTATAGGCCCCCTAAGCCCTTGACGGG	
	Kdm5c_g2_T7	TTAATACGACTCACTATAGGGCGGCGCCATGCGTCCTTAA	
	Kdm5c_screen_F	TTTCGCGATGTAGCCAAGAG	
	Kdm5c_screen_R	AGGCTTCAGTAGTTGGGAGG	
	Kdm5c_geno_F	TGTGGTGAGGTACAGAGGTG	
	Kdm5c_geno_R	CGGCGATGGGTCTGATTTTC	
	Kdm5c_miseq_F	TCGTCGGCAGCGTCAGATGTGTATAAGAGACAGTGTGGTGAGGTACAGAGGTG	

Continued on next page

Chapter	Oligo	Sequence	Reference
	Kdm5c_miseq_R	GTCTCGTGGGCTCGGAGATGTGTATAAGAGACAGTTTCGCGATGTAGCCAAGAG	
	Kdm6a_g1_F	CACCGTGCGTTTCCATGAAATCCTG	
	Kdm6a_g1_R	AAACCAGGATTTCATGGAAACGCAC	
	Kdm6a_g2_F	CACCGGGTAGCGAGCGACACTCCGC	
	Kdm6a_g2_R	AAACGCGGAGTGTCGCTCGCTACCC	
	Kdm6a_g1_T7	TTAATACGACTCACTATAGGTGCGTTTCCATGAAATCCTG	
	Kdm6a_g2_T7	TTAATACGACTCACTATAGGGGTAGCGAGCGACACTCCGC	
	Kdm6a_screen_F	CCTTCACCTCTACCGCGTTA	
	Kdm6a_screen_R	GACCCGTCCGTGCCAAAG	
	Kdm6a_miseq_F	TCGTCGGCAGCGTCAGATGTGTATAAGAGACAGCCTCTGCCTTCACCTCTACC	
	Kdm6a_miseq_R	GTCTCGTGGGCTCGGAGATGTGTATAAGAGACAGCCGTACCTGTCCAGTCCG	
	Ddx3x_g1_F	CACCGAGTGGAAAATGCGCTCGGGC	
	Ddx3x_g1_R	AAACGCCCGAGCGCATTTTCCACTC	
	Ddx3x_g2_F	CACCGCGCGGCTCAGGCTCACCTGC	
	Ddx3x_g2_R	AAACGCAGGTGAGCCTGAGCCGCGC	
	Ddx3x_g1_T7	TTAATACGACTCACTATAGGAGTGGAAAATGCGCTCGGGC	
	Ddx3x_g2_T7	TTAATACGACTCACTATAGGCGCGGCTCAGGCTCACCTGC	
	Ddx3x_screen_F	GTAGCAGTCCTCCGAGTCG	
	Ddx3x_screen_R	CATCCAGTCCCTCCAGAGC	
	Ddx3x_miseq_F	TCGTCGGCAGCGTCAGATGTGTATAAGAGACAGGAGAGGAGGGCACACGTC	
	Ddx3x_miseq_R	GTCTCGTGGGCTCGGAGATGTGTATAAGAGACAGCTCGGGCCAGGGACAATAC	
	Eif2s3x_g1_F	CACCGCCGACAGGATCTCGCCACAT	
	Eif2s3x_g1_R	AAACATGTGGCGAGATCCTGTCGGC	
	Eif2s3x_g2_F	CACCGAAAGCCAGGGCCTACCAATG	
	Eif2s3x_g2_R	AAACCATTGGTAGGCCCTGGCTTTC	
	Eif2s3x_g3_F	CACCGTATGTAGGAACCGTAGCAGA	

Continued on next page

Chapter	Oligo	Sequence	Reference
	Eif2s3x_g3_R	AAACTCTGCTACGGTTCCTACATAC	
	Eif2s3x_g1_T7	TTAATACGACTCACTATAGGCCGACAGGATCTCGCCACAT	
	Eif2s3x_g2_T7	TTAATACGACTCACTATAGGAAAGCCAGGGCCTACCAATG	
	Eif2s3x_g3_T7	TTAATACGACTCACTATAGGTATGTAGGAACCGTAGCAGA	
	Eif2s3x_screen_F	TGAGTTTGAAATCTACAGGGGAC	
	Eif2s3x_screen_R	AGAATCTTGATCGAGGGGCT	
	Eif2s3x_miseq_F	TCGTCGGCAGCGTCAGATGTGTATAAGAGACAGACTAATAAGAAGCACGGAAGAGT	
	Eif2s3x_miseq_R	GTCTCGTGGGCTCGGAGATGTGTATAAGAGACAGCCTTTGTTAACTAGGCCCAGTG	
	Kdm5c_OT1_F	TCGTCGGCAGCGTCAGATGTGTATAAGAGACAGGTAAACAACCCTGGGCAGTG	
	Kdm5c_OT1_R	GTCTCGTGGGCTCGGAGATGTGTATAAGAGACAGTGTCTAGCCAGGAGTGACAC	
	Kdm5c_OT2_F	TCGTCGGCAGCGTCAGATGTGTATAAGAGACAGACTCTCTGCACCTGACTCAC	
	Kdm5c_OT2_R	GTCTCGTGGGCTCGGAGATGTGTATAAGAGACAGCTGAAGGTGCCACTTGAACC	
	Kdm5c_OT3_F	TCGTCGGCAGCGTCAGATGTGTATAAGAGACAGGCAGCTGGACACTAGCATTAC	
	Kdm5c_OT3_R	GTCTCGTGGGCTCGGAGATGTGTATAAGAGACAGCAGGGCTGGAATGATGTTTACA	
	Kdm5c_OT4_F	TCGTCGGCAGCGTCAGATGTGTATAAGAGACAGCAGGGCTGGTATCATCTCCA	
	Kdm5c_OT4_R	GTCTCGTGGGCTCGGAGATGTGTATAAGAGACAGATCATGAAGACCTGGGGCTT	
	Kdm5c_OT5_F	TCGTCGGCAGCGTCAGATGTGTATAAGAGACAGTTTAGGCTGTAAAGTTTCGGGA	
	Kdm5c_OT5_R	GTCTCGTGGGCTCGGAGATGTGTATAAGAGACAGGTCAACAGTGCGGTGAATCC	
	Kdm5c_OT6_F	TCGTCGGCAGCGTCAGATGTGTATAAGAGACAGCTGCCTTCTGTGTTATGCCC	
	Kdm5c_OT6_R	GTCTCGTGGGCTCGGAGATGTGTATAAGAGACAGATCCCAGACACTTCACCCAG	
	Kdm6a_OT1_F	TCGTCGGCAGCGTCAGATGTGTATAAGAGACAGCTCCTTCCCTTCCCCATCTC	
	Kdm6a_OT1_R	GTCTCGTGGGCTCGGAGATGTGTATAAGAGACAGCTTTCGTCTCCTCCTGCAGA	
	Kdm6a_OT2_F	TCGTCGGCAGCGTCAGATGTGTATAAGAGACAGTGGGGCCTTCATTGTTTGTG	
	Kdm6a_OT2_R	GTCTCGTGGGCTCGGAGATGTGTATAAGAGACAGCTTCCCAGGGCTCTCAAAGA	
	Kdm6a_OT3_F	TCGTCGGCAGCGTCAGATGTGTATAAGAGACAGTGTTGGAACGCAGAGGTTTC	
	Kdm6a_OT3_R	GTCTCGTGGGCTCGGAGATGTGTATAAGAGACAGCAGGAGTTTTCACACAGGCC	

Continued on next page

Chapter	Oligo	Sequence	Reference
	Kdm6a_OT4_F	TCGTCGGCAGCGTCAGATGTGTATAAGAGACAGGTGGGACTGAGACTTTAGGCT	
	Kdm6a_OT4_R	GTCTCGTGGGCTCGGAGATGTGTATAAGAGACAGATACTGCAGCATTGACTCGC	
	Kdm6a_OT5_F	TCGTCGGCAGCGTCAGATGTGTATAAGAGACAGAACCGAGTTCATGGTGGTGA	
	Kdm6a_OT5_R	GTCTCGTGGGCTCGGAGATGTGTATAAGAGACAGCCAGAGCACATCCACAAATGA	
	Kdm6a_OT6_F	TCGTCGGCAGCGTCAGATGTGTATAAGAGACAGAAACAAGTTTCAGGGCAGCC	
	Kdm6a_OT6_R	GTCTCGTGGGCTCGGAGATGTGTATAAGAGACAGAAGTGCTGTGAAGACGACCT	
	Ddx3x_OT1_F	TCGTCGGCAGCGTCAGATGTGTATAAGAGACAGAGTGAGTGGTGATGTCTGTGT	
	Ddx3x_OT1_R	GTCTCGTGGGCTCGGAGATGTGTATAAGAGACAGCCCGATGCTCTGAGTGAAAAC	
	Ddx3x_OT2_F	TCGTCGGCAGCGTCAGATGTGTATAAGAGACAGGGTTGACGTGGCCAGTAAAG	
	Ddx3x_OT2_R	GTCTCGTGGGCTCGGAGATGTGTATAAGAGACAGACAACTCCAGTACAGCCTCT	
	Ddx3x_OT3_F	TCGTCGGCAGCGTCAGATGTGTATAAGAGACAGAAAAGCCCCACTCCAAAGC	
	Ddx3x_OT3_R	GTCTCGTGGGCTCGGAGATGTGTATAAGAGACAGGGTCTTCCTTGCTGTGTGAG	
	Ddx3x_OT4_F	TCGTCGGCAGCGTCAGATGTGTATAAGAGACAGCGGTAGCCTCCTCGTCAG	
	Ddx3x_OT4_R	GTCTCGTGGGCTCGGAGATGTGTATAAGAGACAGGTCCACTGCCCCTCTCTG	
	Ddx3x_OT5_F	TCGTCGGCAGCGTCAGATGTGTATAAGAGACAGGTGCTTGCTTTCCTTCGTCA	
	Ddx3x_OT5_R	GTCTCGTGGGCTCGGAGATGTGTATAAGAGACAGATTTTGTGAGGTGCCCAACA	
	Ddx3x_OT6_F	TCGTCGGCAGCGTCAGATGTGTATAAGAGACAGGCCAAGTCAGACAGAAGCCA	
	Ddx3x_OT6_R	GTCTCGTGGGCTCGGAGATGTGTATAAGAGACAGGTGTGGTGGTGGGTAGGTC	
	Ddx3x_OT7_F	TCGTCGGCAGCGTCAGATGTGTATAAGAGACAGCAGCCCACACTTCAGAATGG	
	Ddx3x_OT7_R	GTCTCGTGGGCTCGGAGATGTGTATAAGAGACAGCCATTTGTGTCCCTGGCTTC	

Appendix C

Antibodies and BACs

Antibody	Species	Supplier	Product code	Dilution
KDM5C (JARID1C)	Rabbit mAb	Cell Signaling Technology (Boston, USA)	5361	1:1000
DDX3X	Rabbit pAb	Abcam (Cambridge, UK)	ab128206	1:1000
KDM6A (UTX)	Rabbit pAb	Proteintech (Manchester, UK)	23984	1:1000
GAPDH	Rabbit pAb	Abcam (Cambridge, UK)	ab9485	1:10000
Anti rabbit, HRP linked	Goat	Cell Signaling (Boston, USA)	7074S	1:4000
Anti mouse, HRP linked	Goat	Santa Cruz Biotechnology (Dallas, USA)	sc-20005	1:4000

Table C.1: Antibodies used in this thesis

Target	CHORI BAC clone
SLX (X chromosome)	RP23 470D15
SLY (Y chromosome)	RP24 502P05
PAR	RP24 255O24

Table C.2: BAC clones used in this thesis

Appendix D

Colophon

This document was set in the Times Roman typeface using LaTeX and BibTeX, composed with a text editor.

Bibliography

Abidi, F. E., L. Holloway, C. A. Moore, D. D. Weaver, R. J. Simensen, R. E. Stevenson, R. C. Rogers, and C. E. Schwartz

2008. Mutations in JARID1C are associated with X-linked mental retardation, short stature and hyperreflexia. *Journal of Medical Genetics*, 45(12):787–793.

Adam, M. P. and L. Hudgins

2005. Kabuki syndrome: a review. *Clinical Genetics*, 67(3):209–219.

Adegbola, A., H. Gao, S. Sommer, and M. Browning

2008. A novel mutation in JARID1C/SMCX in a patient with autism spectrum disorder (ASD). *American Journal of Medical Genetics. Part A*, 146A(4):505–511.

Adler, D. A., E. I. Rugarli, P. A. Lingenfelter, K. Tsuchiya, D. Poslinski, H. D. Liggitt, V. M. Chapman, R. W. Elliott, A. Ballabio, and C. M. Disteche

1997. Evidence of evolutionary up-regulation of the single active X chromosome in mammals based on Clc4 expression levels in Mus spretus and Mus musculus. *Proceedings of the National Academy of Sciences of the United States of America*, 94(17):9244–9248.

Agger, K., P. A. C. Cloos, J. Christensen, D. Pasini, S. Rose, J. Rappsilber, I. Issaeva, E. Canaani, A. E. Salcini, and K. Helin

2007. UTX and JMJD3 are histone H3K27 demethylases involved in HOX gene regulation and development. *Nature*, 449(7163):731–734.

Agulnik, A. I., M. J. Mitchell, J. L. Lerner, D. R. Woods, and C. E. Bishop

1994a. A mouse Y chromosome gene encoded by a region essential for spermatogenesis and expression of male-specific minor histocompatibility antigens. *Human Molecular Genetics*, 3(6):873–878.

Agulnik, A. I., M. J. Mitchell, M. G. Mattei, G. Borsani, P. A. Avner, J. L. Lerner, and C. E. Bishop

1994b. A novel X gene with a widely transcribed Y-linked homologue escapes X-inactivation in mouse and human. *Human Molecular Genetics*, 3(6):879–884.

Aitken, R. J. and J. Graves

2002. Human spermatozoa: the future of sex. *Nature*, 415(6875):963–963.

Akimoto, C., H. Kitagawa, T. Matsumoto, and S. Kato

2008. Spermatogenesis-specific association of SMCY and MSH5. *Genes to Cells*, 13(6):623–633.

Anderson, C. L. and C. J. Brown

2005. Epigenetic predisposition to expression of TIMP1 from the human inactive X chromosome. *BMC Genetics*, 6(1):48.

Arcipowski, K. M., C. A. Martinez, and P. Ntziachristos

2016. Histone demethylases in physiology and cancer: a tale of two enzymes, JMJD3 and UTX. *Current Opinion in Genetics & Development*, 36:59–67.

Ariumi, Y., M. Kuroki, K. Abe, H. Dansako, M. Ikeda, T. Wakita, and N. Kato

2007. DDX3 DEAD-Box RNA Helicase Is Required for Hepatitis C Virus RNA Replication. *Journal of Virology*, 81(24):13922–13926.

Armoskus, C., D. Moreira, K. Bollinger, O. Jimenez, S. Taniguchi, and H.-W. Tsai

2014. Identification of sexually dimorphic genes in the neonatal mouse cortex and hippocampus. *Brain Research*, 1562(C):23–38.

Aza-Carmona, M., D. J. Shears, P. Yuste-Checa, V. Barca-Tierno, A. Hisado-Oliva, A. Belinchon, S. Benito-Sanz, J. I. Rodriguez, J. Argente, A. Campos-Barros,

P. J. Scambler, and K. E. Heath

2011. SHOX interacts with the chondrogenic transcription factors SOX5 and SOX6 to activate the aggrecan enhancer. *Human Molecular Genetics*, 20(8):1547–1559.

Bacher, C. P., M. Guggiari, B. Brors, S. Augui, P. Clerc, P. Avner, R. Eils, and E. Heard

2006. Transient colocalization of X-inactivation centres accompanies the initiation of X inactivation. *Nature Cell Biology*, 8(3):293–299.

Bachtrog, D.

2014. Signs of Genomic Battlesin Mouse Sex Chromosomes. *Cell*, 159(4):716–718.

Bachtrog, D., J. E. Mank, C. L. Peichel, M. Kirkpatrick, S. P. Otto, T.-L. Ashman, M. W. Hahn, J. Kitano, I. Mayrose, R. Ming, N. Perrin, L. Ross, N. Valenzuela, J. C. Vamosi, and The Tree of Sex Consortium

2014. Sex Determination: Why So Many Ways of Doing It? *PLoS Biology*, 12(7):e1001899–13.

Bailey, J. A., L. Carrel, A. Chakravarti, and E. E. Eichler

2000. Molecular evidence for a relationship between LINE-1 elements and X chromosome inactivation: The Lyon repeat hypothesis. *Proceedings of the National Academy of Sciences of the United States of America*, 97(12):6634–6639.

Balaton, B. P. and C. J. Brown

2016. Escape Artists of the X Chromosome. *Trends in Genetics*, 32(6):348–359.

Ballabio, A., R. Carrozzo, A. Gil, B. Gillard, N. Affara, M. A. Ferguson-Smith, N. Fraser, I. Craig, M. Rocchi, and G. Romeo

1989. Molecular characterization of human X/Y translocations suggests their aetiology through aberrant exchange between homologous sequences on Xp and Yq. *Annals of Human Genetics*, 53(Pt 1):9–14.

Banka, S., E. Howard, S. Bunstone, K. E. Chandler, B. Kerr, K. Lachlan, S. McKee, S. G. Mehta, A. L. T. Tavares, J. Tolmie, and D. Donnai

2013. MLL2 mosaic mutations and intragenic deletion-duplications in patients with Kabuki syndrome. *Clinical Genetics*, 83(5):467–471.

Banzai, M., K. Omoe, H. Ishikawa, and A. Endo

1995a. Viability, development and incidence of chromosome anomalies of preimplantation embryos from XO mice. *Cytogenetics and Cell Genetics*, 70(3-4):273–277.

Banzai, M., K. Omoe, H. Ishikawa, and A. Endo

1995b. Viability, development and incidence of chromosome anomalies of preimplantation embryos from XO mice. *Cytogenetic and Genome Research*, 70(3-4):273–277.

Barakat, T. S., F. Loos, S. van Staveren, E. Myronova, M. Ghazvini, J. A. Grootegoed, and J. Gribnau

2014. The Trans-Activator RNF12 and Cis-Acting Elements Effectuate X Chromosome Inactivation Independent of X-Pairing. *Molecular Cell*, 53(6):965–978.

Barbosa-Morais, N. L., M. Irimia, Q. Pan, H. Y. Xiong, S. Gueroussov, L. J. Lee, V. Slobodeniuc, C. Kutter, S. Watt, R. Colak, T. Kim, C. M. Misquitta-Ali, M. D. Wilson, P. M. Kim, D. T. Odom, B. J. Frey, and B. J. Blencowe

2012. The evolutionary landscape of alternative splicing in vertebrate species. *Science*, 338(6114):1587–1593.

Barca-Tierno, V., M. Aza-Carmona, E. Barroso, D. Heine-Suner, D. Azmanov, J. Rosell, B. Ezquieta, L. S. Montané, T. Vendrell, J. Cruz, F. Santos, J. I. Rodríguez, J. Pozo, J. Argente, L. Kalaydjieva, R. Gracia, A. Campos-Barros, S. Benito-Sanz, and K. E. Heath

2011. Identification of a Gypsy SHOX mutation (p.A170P) in Léri-Weill dyschondrosteosis and Langer mesomelic dysplasia. *European Journal of Human Genetics*, 19(12):1218–1225.

Barton, S. C., M. A. Surani, and M. L. Norris

1984. Role of paternal and maternal genomes in mouse development. *Nature*, 311(5984):374–376.

Barutcu, A. R., B. R. Lajoie, R. P. McCord, C. E. Tye, D. Hong, T. L. Messier, G. Browne, A. J. van Wijnen, J. B. Lian, J. L. Stein, J. Dekker, A. N. Imbalzano, and G. S. Stein

2015. Chromatin interaction analysis reveals changes in small chromosome and telomere clustering between epithelial and breast cancer cells. *Genome Biology*, Pp. 1–14.

Beach, R. R., C. Ricci-Tam, C. M. Brennan, C. A. Moomau, P.-h. Hsu, B. Hua, R. E. Silberman, M. Springer, and A. Amon

2017. Aneuploidy Causes Non-genetic Individuality. *Cell*, 169(2):229–242.e21.

Beckham, C., A. Hilliker, A.-M. Cziko, A. Noueiry, M. Ramaswami, and R. Parker

2008. The DEAD-box RNA helicase Ded1p affects and accumulates in Saccharomyces cerevisiae P-bodies. *Molecular Biology of the Cell*, 19(3):984–993.

Belin, V., V. Cusin, G. Viot, D. Girlich, A. Toutain, A. Moncla, M. Vekemans, M. Le Merrer, A. Munnich, and V. Cormier-Daire

1998. SHOX mutations in dyschondrosteosis (Leri-Weill syndrome). *Nature Genetics*, 19(1):67–69.

Bellott, D. W., J. F. Hughes, H. Skaletsky, L. G. Brown, T. Pyntikova, T.-J. Cho, N. Koutseva, S. Zaghlul, T. Graves, S. Rock, C. Kremitzki, R. S. Fulton, S. Dugan, Y. Ding, D. Morton, Z. Khan, L. Lewis, C. Buhay, Q. Wang, J. Watt, M. Holder, S. Lee, L. Nazareth, S. Rozen, D. M. Muzny, W. C. Warren, R. A. Gibbs, R. K. Wilson, and D. C. Page

2014. Mammalian Y chromosomes retain widely expressed dosage-sensitive regulators. *Nature*, 508(7497):494–499.

Bellott, D. W. and D. C. Page

2009. Reconstructing the evolution of vertebrate sex chromosomes. *Cold Spring Harbor Symposia on Quantitative Biology*, 74(0):345–353.

Benchetrit, H., S. Herman, N. van Wietmarschen, T. Wu, K. Makedonski, N. Maoz, N. Y. Tov, D. Stave, R. Lasry, V. Zayat, A. Xiao, P. M. Lansdorp, S. Sebban, and Y. Buganim

2015. Extensive Nuclear Reprogramming Underlies Lineage Conversion into Functional Trophoblast Stem-like Cells. *Cell Stem Cell*, 17(5):1–40.

Benito-Sanz, S., N. S. Thomas, C. Huber, D. Gorbenko del Blanco, D. G. Del Blanco, M. Aza-Carmona, J. A. Crolla, V. Maloney, G. Rappold, J. Argente, A. Campos-Barros, V. Cormier-Daire, and K. E. Heath

2005. A novel class of Pseudoautosomal region 1 deletions downstream of SHOX is associated with Leri-Weill dyschondrosteosis. *American Journal of Human Genetics*, 77(4):533–544.

Berletch, J. B., W. Ma, F. Yang, J. Shendure, W. S. Noble, C. M. Disteche, and X. Deng

2015. Escape from X Inactivation Varies in Mouse Tissues. *PLoS Genetics*, 11(3):e1005079–26.

Birchler, J. A.

2014. Facts and artifacts in studies of gene expression in aneuploids and sex chromosomes. *Chromosoma*, 123(5):459–469.

Birtle, Z., L. Goodstadt, and C. Ponting

2005. Duplication and positive selection among hominin-specific PRAME genes. *BMC Genomics*, 6:120.

Bishop, C. E. and D. Hatat

1987. Molecular cloning and sequence analysis of a mouse Y chromosome RNA transcript expressed in the testis. *Nucleic Acids Research*, 15(7):2959–2969.

Bishop, D. V., E. Canning, K. Elgar, E. Morris, P. A. Jacobs, and D. H. Skuse
2000. Distinctive patterns of memory function in subgroups of females with Turner syndrome: evidence for imprinted loci on the X-chromosome affecting neurodevelopment. *Neuropsychologia*, 38(5):712–721.

Blackburn, D. G. and A. F. Flemming
2011. Invasive implantation and intimate placental associations in a placentotrophic african lizard, Trachylepis ivensi (scincidae). *Journal of Morphology*, 273(2):137–159.

Blakeley, P., N. M. E. Fogarty, I. del Valle, S. E. Wamaitha, T. X. Hu, K. Elder, P. Snell, L. Christie, P. Robson, and K. K. Niakan
2015. Defining the three cell lineages of the human blastocyst by single-cell RNA-seq. *Development*, 142(20):3613–3613.

Blakeslee, A. F., J. Belling, and M. E. Farnham
1920. Chromosomal duplication and Mendelian phenomena in Datura mutants. *Science*, 52(1347):388–390.

Blank, H. M., J. M. Sheltzer, C. M. Meehl, and A. Amon
2015. Mitotic entry in the presence of DNA damage is a widespread property of aneuploidy in yeast. *Molecular Biology of the Cell*, 26(8):1440–1451.

Blaschke, K., K. T. Ebata, M. M. Karimi, J. A. Zepeda-Martínez, P. Goyal, S. Mahapatra, A. Tam, D. J. Laird, M. Hirst, A. Rao, M. C. Lorincz, and M. Ramalho-Santos
2013. Vitamin C induces Tet-dependent DNA demethylation and a blastocyst-like state in ES cells. *Nature*, 500(7461):222–226.

Blaschke, R. J., A. P. Monaghan, S. Schiller, B. Schechinger, E. Rao, H. Padilla-Nash, T. Ried, and G. A. Rappold
1998. SHOT, a SHOX-related homeobox gene, is implicated in craniofacial, brain, heart, and limb development. *Proceedings of the National Academy of Sciences of the United States of America*, 95(5):2406–2411.

Blekhman, R., J. C. Marioni, P. Zumbo, M. Stephens, and Y. Gilad
2010. Sex-specific and lineage-specific alternative splicing in primates. *Genome Research*, 20(2):180–189.

Blok, L. S., E. Madsen, J. Juusola, C. Gilissen, D. Baralle, M. R. F. Reijnders, H. Venselaar, C. Helsmoortel, M. T. Cho, A. Hoischen, L. E. L. M. Vissers, T. S. Koemans, W. Wissink-Lindhout, E. E. Eichler, C. Romano, H. Van Esch, C. Stumpel, M. Vreeburg, E. Smeets, K. Oberndorff, B. W. M. van Bon, M. Shaw, J. Gecz, E. Haan, M. Bienek, C. Jensen, B. L. Loeys, A. Van Dijck, A. M. Innes, H. Racher, S. Vermeer, N. Di Donato, A. Rump, K. Tatton-Brown, M. J. Parker, A. Henderson, S. A. Lynch, A. Fryer, A. Ross, P. Vasudevan, U. Kini, R. Newbury-Ecob, K. Chandler, A. Male, S. Dijkstra, J. Schieving, J. Giltay, K. L. I. van Gassen, J. Schuurs-Hoeijmakers, P. L. Tan, I. Pediaditakis, S. A. Haas, K. Retterer, P. Reed, K. G. Monaghan, E. Haverfield, M. Natowicz, A. Myers, M. C. Kruer, Q. Stein, K. A. Strauss, K. W. Brigatti, K. Keating, B. K. Burton, K. H. Kim, J. Charrow, J. Norman, A. Foster-Barber, A. D. Kline, A. Kimball, E. Zackai, M. Harr, J. Fox, J. McLaughlin, K. Lindstrom, K. M. Haude, K. van Roozendaal, H. Brunner, W. K. Chung, R. F. Kooy, R. Pfundt, V. Kalscheuer, S. G. Mehta, N. Katsanis, T. Kleefstra, and T. D. Study
2015. Mutations in DDX3X are a common cause of unexplained intellectual disability with gender-specific effects on Wnt signaling. *The American Journal of Human Genetics*, 97(2):343–352.

Bol, G. M., F. Vesuna, M. Xie, J. Zeng, K. Aziz, N. Gandhi, A. Levine, A. Irving, D. Korz, S. Tantravedi, M. R. Heerma van Voss, K. Gabrielson, E. A. Bordt, B. M. Polster, L. Cope, P. van der Groep, A. Kondaskar, M. A. Rudek, R. S. Hosmane, E. van der Wall, P. J. van Diest, P. T. Tran, and V. Raman
2015a. Targeting DDX3 with a small molecule inhibitor for lung cancer therapy. *EMBO Molecular Medicine*, 7(5):1–23.

Bol, G. M., M. Xie, and V. Raman

2015b. DDX3, a potential target for cancer treatment. *Molecular Cancer*, 14(1):188.

Bonomi, M., V. Rochira, D. Pasquali, G. Balercia, E. A. Jannini, A. Ferlin, and Klinefelter ItaliaN Group (KING)

2017. Klinefelter syndrome (KS): genetics, clinical phenotype and hypogonadism. *Journal of endocrinological investigation*, 40(2):123–134.

Borck, G., B.-S. Shin, B. Stiller, A. Mimouni-Bloch, H. Thiele, J.-R. Kim, M. Thakur, C. Skinner, L. Aschenbach, P. Smirin-Yosef, A. Har-Zahav, G. Nürnberg, J. Altmüller, P. Frommolt, K. Hofmann, O. Konen, P. Nürnberg, A. Munnich, C. E. Schwartz, D. Gothelf, L. Colleaux, T. E. Dever, C. Kubisch, and L. Basel-Vanagaite

2012. eIF2γ mutation that disrupts eIF2 complex integrity links intellectual disability to impaired translation initiation. *Molecular Cell*, 48(4):641–646.

Borensztein, M., L. Syx, K. Ancelin, P. Diabangouaya, C. Picard, T. Liu, J.-B. Liang, I. Vassilev, R. Galupa, N. Servant, E. Barillot, A. Surani, C.-J. Chen, and E. Heard

2017. Xist-dependent imprinted X inactivation and the early developmental consequences of its failure. *Nature Structural & Molecular Biology*, 24(3):226–233.

Borsani, G., R. Tonlorenzi, M. C. Simmler, L. Dandolo, D. Arnaud, V. Capra, M. Grompe, A. Pizzuti, D. Muzny, and C. Lawrence

1991. Characterization of a murine gene expressed from the inactive X chromosome. *Nature*, 351(6324):325–329.

Bouma, G. J., Q. J. Hudson, L. L. Washburn, and E. M. Eicher

2010. New Candidate Genes Identified for Controlling Mouse Gonadal Sex Determination and the Early Stages of Granulosa and Sertoli Cell Differentiation. *Biology of Reproduction*, 82(2):380–389.

Branco, M. R., M. King, V. Perez-Garcia, A. B. Bogutz, M. Caley, E. Fineberg, L. Lefebvre, S. J. Cook, W. Dean, M. Hemberger, and W. Reik

2016. Maternal DNA Methylation Regulates Early Trophoblast Development. *Developmental Cell*, 36(2):152–163.

Brandt, J., S. Schrauth, A.-M. Veith, A. Froschauer, T. Haneke, C. Schultheis, M. Gessler, C. Leimeister, and J.-N. Volff

2005a. Transposable elements as a source of genetic innovation: expression and evolution of a family of retrotransposon-derived neogenes in mammals. *Gene*, 345(1):101–111.

Brandt, J., A. M. Veith, and J. N. Volff

2005b. A family of neofunctionalized Ty3/gypsy retrotransposon genes in mammalian genomes. *Cytogenetic and Genome Research*, 110(1-4):307–317.

Brawand, D., M. Soumillon, A. Necsulea, P. Julien, G. Csárdi, P. Harrigan, M. Weier, A. Liechti, A. Aximu-Petri, M. Kircher, F. W. Albert, U. Zeller, P. Khaitovich, F. Grützner, S. Bergmann, R. Nielsen, S. Pääbo, and H. Kaessmann

2011. The evolution of gene expression levels in mammalian organs. *Nature*, 478(7369):343–348.

Bray, N. L., H. Pimentel, P. Melsted, and L. Pachter

2016. Near-optimal probabilistic RNA-seq quantification. *Nature Biotechnology*, 34(5):525–527.

Brockdorff, N., A. Ashworth, G. F. Kay, P. Cooper, S. Smith, V. M. McCabe, D. P. Norris, G. D. Penny, D. Patel, and S. Rastan

1991. Conservation of position and exclusive expression of mouse Xist from the inactive X chromosome. *Nature*, 351(6324):329–331.

Brook, C. G., G. Mürset, M. Zachmann, and A. Prader

1974. Growth in children with 45,XO Turner's syndrome. *Archives of disease in childhood*, 49(10):789–795.

Brown, C. J., A. Ballabio, J. L. Rupert, R. G. Lafreniere, M. Grompe, R. Tonlorenzi, and H. F. Willard

1991. A gene from the region of the human X inactivation centre is expressed exclusively from the inactive X chromosome. *Nature*, 349(6304):38–44.

Bunt, J., N. A. Hasselt, D. A. Zwijnenburg, J. Koster, R. Versteeg, and M. Kool

2012. OTX2 sustains a bivalent-like state of OTX2-bound promoters in medulloblastoma by maintaining their H3K27me3 levels. *Acta Neuropathologica*, 125(3):385–394.

Burgoyne, P. S.

1982. Genetic homology and crossing over in the X and Y chromosomes of Mammals. *Human Genetics*, 61(2):85–90.

Burgoyne, P. S.

1993. A Y-chromosomal effect on blastocyst cell number in mice. *Development*, 117(1):341–345.

Burgoyne, P. S. and A. P. Arnold

2016. A primer on the use of mouse models for identifying direct sex chromosome effects that cause sex differences in non-gonadal tissues. *Biology of Sex Differences*, 7(1):68.

Burgoyne, P. S. and T. G. Baker

1981. Oocyte depletion in XO mice and their XX sibs from 12 to 200 days post partum. *Journal of Reproduction and Fertility*, 61(1):207–212.

Burgoyne, P. S. and T. G. Baker

1985. Perinatal oocyte loss in XO mice and its implications for the aetiology of gonadal dysgenesis in XO women. *Journal of Reproduction and Fertility*, 75(2):633–645.

Burgoyne, P. S. and J. D. Biggers

1976. The consequences of X-dosage deficiency in the germ line: impaired de-

velopment in vitro of preimplantation embryos from XO mice. *Developmental Biology*, 51(1):109–117.

Burgoyne, P. S. and E. P. Evans

2000. A high frequency of XO offspring from X(Paf)Y* male mice: evidence that the Paf mutation involves an inversion spanning the X PAR boundary. *Cytogenetics and Cell Genetics*, 91(1-4):57–61.

Burgoyne, P. S., E. P. Evans, and K. Holland

1983a. XO monosomy is associated with reduced birthweight and lowered weight gain in the mouse. *Journal of Reproduction and Fertility*, 68(2):381–385.

Burgoyne, P. S., S. K. Mahadevaiah, J. Perry, S. J. Palmer, and A. Ashworth

1998. The Y* rearrangement in mice: new insights into a perplexing PAR. *Cytogenetics and Cell Genetics*, 80(1-4):37–40.

Burgoyne, P. S., O. A. Ojarikre, and J. M. A. Turner

2002. Evidence that postnatal growth retardation in XO mice is due to haploinsufficiency for a non-PAR X gene. *Cytogenetic and Genome Research*, 99(1-4):252–256.

Burgoyne, P. S., P. Tam, and E. P. Evans

1983b. Retarded development of XO conceptuses during early pregnancy in the mouse. *Journal of Reproduction and Fertility*, 68(2):387–393.

Burgoyne, P. S., A. R. Thornhill, S. K. Boudrean, S. M. Darling, C. E. Bishop, E. P. Evans, B. Capel, and U. Mittwoch

1995. The Genetic Basis of XX-XY Differences Present before Gonadal Sex Differentiation in the Mouse [and Discussion]. *Philosophical Transactions of the Royal Society B: Biological Sciences*, 350(1333):253–261.

Calabrese, J. M., J. Starmer, M. D. Schertzer, D. Yee, and T. Magnuson

2015. A survey of imprinted gene expression in mouse trophoblast stem cells. *G3*, 5(5):751–759.

Carney, E. W., V. Prideaux, S. J. Lye, and J. Rossant

1993. Progressive expression of trophoblast-specific genes during formation of mouse trophoblast giant cells in vitro. *Molecular Reproduction and Development*, 34(4):357–368.

Carrel, L., P. A. Hunt, and H. F. Willard

1996. Tissue and lineage-specific variation in inactive X chromosome expression of the murine Smcx gene. *Human Molecular Genetics*, 5(9):1361–1366.

Carrel, L. and H. F. Willard

1999. Heterogeneous gene expression from the inactive X chromosome: an X-linked gene that escapes X inactivation in some human cell lines but is inactivated in others. *Proceedings of the National Academy of Sciences of the United States of America*, 96(13):7364–7369.

Carrel, L. and H. F. Willard

2005. X-inactivation profile reveals extensive variability in X-linked gene expression in females. *Nature*, 434(7031):400–404.

Carver, E. A. and L. Stubbs

1997. Zooming in on the human-mouse comparative map: genome conservation re-examined on a high-resolution scale. *Genome Research*, 7(12):1123–1137.

Castagné, R., M. Rotival, T. Zeller, P. S. Wild, V. Truong, D.-A. Trégouët, T. Munzel, A. Ziegler, F. Cambien, S. Blankenberg, and L. Tiret

2011. The choice of the filtering method in microarrays affects the inference regarding dosage compensation of the active X-chromosome. *PLoS ONE*, 6(9):e23956.

Cattanach, B. M.

1961. XXY mice. *Genetical Research*, 2(01):156–158.

Cattanach, B. M.

1962. XO mice. *Genetical Research*, 3(03):487–490.

Chang, P.-C., C.-W. Chi, G.-Y. Chau, F.-Y. Li, Y.-H. Tsai, J.-C. Wu, and Y.-H. Wu Lee

2005. DDX3, a DEAD box RNA helicase, is deregulated in hepatitis virus-associated hepatocellular carcinoma and is involved in cell growth control. *Oncogene*, 25(14):1991–2003.

Chao, C.-H., C.-M. Chen, P.-L. Cheng, J. W. Shih, A.-P. Tsou, and Y.-H. W. Lee

2006. DDX3, a DEAD box RNA helicase with tumor growth-suppressive property and transcriptional regulation activity of the p21waf1/cip1 promoter, is a candidate tumor suppressor. *Cancer Research*, 66(13):6579–6588.

Charlesworth, B.

2006. The evolutionary biology of sex. *Current Biology*, 16(17):R693–5.

Chen, C.-Y., C.-H. Chan, C.-M. Chen, Y.-S. Tsai, T. Y. Tsai, Y. H. Wu Lee, and L.-R. You

2016a. Targeted inactivation of murine Ddx3x: essential roles of Ddx3x in placentation and embryogenesis. *Human Molecular Genetics*, 25(14):2905–2922.

Chen, G., J. P. Schell, J. A. Benitez, S. Petropoulos, M. Yilmaz, B. Reinius, Z. Alekseenko, L. Shi, E. Hedlund, F. Lanner, R. Sandberg, and Q. Deng

2016b. Single-cell analyses of X Chromosome inactivation dynamics and pluripotency during differentiation. *Genome Research*, 26(10):1342–1354.

Chen, H., Z. K. Attieh, T. Su, B. A. Syed, H. Gao, R. M. Alaeddine, T. C. Fox, J. Usta, C. E. Naylor, R. W. Evans, A. T. McKie, G. J. Anderson, and C. D. Vulpe

2004a. Hephaestin is a ferroxidase that maintains partial activity in sex-linked anemia mice. *Blood*, 103(10):3933–3939.

Chen, T.-C., H. Waldmann, and P. J. Fairchild

2004b. Induction of dominant transplantation tolerance by an altered peptide ligand of the male antigen Dby. *Journal of Clinical Investigation*, 113(12):1754–1762.

Chen, Z., Z. Liu, J. Huang, T. Amano, C. Li, S. Cao, C. Wu, B. Liu, L. Zhou, M. G. Carter, D. L. Keefe, X. Yang, and L. Liu
2009. Birth of Parthenote Mice Directly from Parthenogenetic Embryonic Stem Cells. *Stem Cells*, 27(9):2136–2145.

Chen, Z., J. Zang, J. Whetstine, X. Hong, F. Davrazou, T. G. Kutateladze, M. Simpson, Q. Mao, C.-H. Pan, S. Dai, J. Hagman, K. Hansen, Y. Shi, and G. Zhang
2006. Structural insights into histone demethylation by JMJD2 family members. *Cell*, 125(4):691–702.

Cho, Y.-W., T. Hong, S. Hong, H. Guo, H. Yu, D. Kim, T. Guszczynski, G. R. Dressler, T. D. Copeland, M. Kalkum, and K. Ge
2007. PTIP associates with MLL3- and MLL4-containing histone H3 lysine 4 methyltransferase complex. *The Journal of Biological Chemistry*, 282(28):20395–20406.

Chomez, P., O. De Backer, M. Bertrand, E. De Plaen, T. Boon, and S. Lucas
2001. An overview of the MAGE gene family with the identification of all human members of the family. *Cancer Research*, 61(14):5544–5551.

Chow, J. C., C. Ciaudo, M. J. Fazzari, N. Mise, N. Servant, J. L. Glass, M. Attreed, P. Avner, A. Wutz, E. Barillot, J. M. Greally, O. Voinnet, and E. Heard
2010. LINE-1 activity in facultative heterochromatin formation during X chromosome inactivation. *Cell*, 141(6):956–969.

Christensen, J., K. Agger, P. A. C. Cloos, D. Pasini, S. Rose, L. Sennels, J. Rappsilber, K. H. Hansen, A. E. Salcini, and K. Helin
2007. RBP2 Belongs to a Family of Demethylases, Specific for Tri-and Dimethylated Lysine 4 on Histone 3. *Cell*, 128(6):1063–1076.

Chu, D. S., H. Liu, P. Nix, T. F. Wu, E. J. Ralston, J. R. Yates, III, and B. J. Meyer
2006. Sperm chromatin proteomics identifies evolutionarily conserved fertility factors. *Nature*, 443(7107):101–105.

Chureau, C., S. Chantalat, A. Romito, A. Galvani, L. Duret, P. Avner, and C. Rougeulle

2011. Ftx is a non-coding RNA which affects Xist expression and chromatin structure within the X-inactivation center region. *Human Molecular Genetics*, 20(4):705–718.

Chureau, C., M. Prissette, A. Bourdet, V. Barbe, L. Cattolico, L. Jones, A. Eggen, P. Avner, and L. Duret

2002. Comparative sequence analysis of the X-inactivation center region in mouse, human, and bovine. *Genome Research*, 12(6):894–908.

Cleaton, M. A. M., C. A. Edwards, and A. C. Ferguson-Smith

2014. Phenotypic Outcomes of Imprinted Gene Models in Mice: Elucidation of Pre- and Postnatal Functions of Imprinted Genes. *Annual Review of Genomics and Human Genetics*, 15(1):93–126.

Clement-Jones, M., S. Schiller, E. Rao, R. J. Blaschke, A. Zuniga, R. Zeller, S. C. Robson, G. Binder, I. Glass, T. Strachan, S. Lindsay, and G. A. Rappold

2000. The short stature homeobox gene SHOX is involved in skeletal abnormalities in Turner syndrome. *Human Molecular Genetics*, 9(5):695–702.

Coan, P. M., G. J. Burton, and A. C. Ferguson-Smith

2005. Imprinted genes in the placenta – A review. *Placenta*, 26:S10–S20.

Coate, J. E. and J. J. Doyle

2010. Quantifying Whole Transcriptome Size, a Prerequisite for Understanding Transcriptome Evolution Across Species: An Example from a Plant Allopolyploid. *Genome Biology and Evolution*, 2(0):534–546.

Cobb, J., A. Dierich, Y. Huss-Garcia, and D. Duboule

2006. A mouse model for human short-stature syndromes identifies Shox2 as an upstream regulator of Runx2 during long-bone development. *Proceedings of the National Academy of Sciences of the United States of America*, 103(12):4511–4515.

Cockwell, A., M. MacKenzie, S. Youings, and P. Jacobs

1991. A cytogenetic and molecular study of a series of 45,X fetuses and their parents. *Journal of Medical Genetics*, 28(3):151–155.

Conesa, A., P. Madrigal, S. Tarazona, D. Gomez-Cabrero, A. Cervera, A. McPherson, M. W. Szcześniak, D. J. Gaffney, L. L. Elo, X. Zhang, and A. Mortazavi

2016. A survey of best practices for RNA-seq data analysis. *Genome Biology*, 17(1):1–19.

Cong, L., F. A. Ran, D. Cox, S. Lin, R. Barretto, N. Habib, P. D. Hsu, X. Wu, W. Jiang, L. A. Marraffini, and F. Zhang

2013. Multiplex Genome Engineering Using CRISPR/Cas Systems. *Science*, 339(6121):819–823.

Conway, E., E. Healy, and A. P. Bracken

2015. PRC2 mediated H3K27 methylations in cellular identity and cancer. *Current Opinion in Cell Biology*, 37:42–48.

Cooper, D. W., J. L. VandeBerg, G. B. Sharman, and W. E. Poole

1971. Phosphoglycerate kinase polymorphism in kangaroos provides further evidence for paternal X inactivation. *Nature: New Biology*, 230(13):155–157.

Corbel, C., P. Diabangouaya, A.-V. Gendrel, J. C. Chow, and E. Heard

2013. Unusual chromatin status and organization of the inactive X chromosome in murine trophoblast giant cells. *Development*, 140(4):861–872.

Cordin, O., J. Banroques, N. K. Tanner, and P. Linder

2006. The DEAD-box protein family of RNA helicases. *Gene*, 367:17–37.

Correa, S. M., L. L. Washburn, R. S. Kahlon, M. C. Musson, G. J. Bouma, E. M. Eicher, and K. H. Albrecht

2012. Sex Reversal in C57BL/6J XY Mice Caused by Increased Expression of Ovarian Genes and Insufficient Activation of the Testis Determining Pathway. *PLoS Genetics*, 8(4):e1002569–20.

Cortez, D., R. Marin, D. Toledo-Flores, L. Froidevaux, A. Liechti, P. D. Waters, F. Grützner, and H. Kaessmann

2014. Origins and functional evolution of Y chromosomes across mammals. *Nature*, 508(7497):488–493.

Cotton, A. M., C.-Y. Chen, L. L. Lam, W. W. Wasserman, M. S. Kobor, and C. J. Brown

2014. Spread of X-chromosome inactivation into autosomal sequences: role for DNA elements, chromatin features and chromosomal domains. *Human Molecular Genetics*, 23(5):1211–1223.

Cremer, T., M. Cremer, S. Dietzel, S. Müller, I. Solovei, and S. Fakan

2006. Chromosome territories – a functional nuclear landscape. *Current Opinion in Cell Biology*, 18(3):307–316.

Cross, J. C., Z. Werb, and S. J. Fisher

1994. Implantation and the placenta: key pieces of the development puzzle. *Science*, 266(5190):1508–1518.

Curry, C. J., R. E. Magenis, M. Brown, J. T. Lanman, J. Tsai, P. O'Lague, P. Goodfellow, T. Mohandas, E. A. Bergner, and L. J. Shapiro

1984. Inherited chondrodysplasia punctata due to a deletion of the terminal short arm of an X chromosome. *New England Journal of Medicine*, 311(16):1010–1015.

Dalgliesh, G. L., K. Furge, C. Greenman, L. Chen, G. Bignell, A. Butler, H. Davies, S. Edkins, C. Hardy, C. Latimer, J. Teague, J. Andrews, S. Barthorpe, D. Beare, G. Buck, P. J. Campbell, S. Forbes, M. Jia, D. Jones, H. Knott, C. Y. Kok, K. W. Lau, C. Leroy, M.-L. Lin, D. J. McBride, M. Maddison, S. Maguire, K. McLay, A. Menzies, T. Mironenko, L. Mulderrig, L. Mudie, S. O'Meara, E. Pleasance, A. Rajasingham, R. Shepherd, R. Smith, L. Stebbings, P. Stephens, G. Tang, P. S. Tarpey, K. Turrell, K. J. Dykema, S. K. Khoo, D. Petillo, B. Wondergem,

J. Anema, R. J. Kahnoski, B. T. Teh, M. R. Stratton, and P. A. Futreal
2010. Systematic sequencing of renal carcinoma reveals inactivation of histone modifying genes. *Nature*, 463(7279):360–363.

Davies, W., A. Isles, R. Smith, D. Karunadasa, D. Burrmann, T. Humby, O. Ojarikre, C. Biggin, D. Skuse, P. Burgoyne, and L. Wilkinson
2005. Xlr3b is a new imprinted candidate for X-linked parent-of-origin effects on cognitive function in mice. *Nature Genetics*, 37(6):625–629.

De Plaen, E., O. De Backer, D. Arnaud, B. Bonjean, P. Chomez, V. Martelange, P. Avner, P. Baldacci, C. Babinet, S. Y. Hwang, B. Knowles, and T. Boon
1999. A new family of mouse genes homologous to the human MAGE genes. *Genomics*, 55(2):176–184.

de Sousa Abreu, R., L. O. Penalva, E. M. Marcotte, and C. Vogel
2009. Global signatures of protein and mRNA expression levels. *Molecular bioSystems*, 5(12):1512–1526.

DeCarlo, K., A. Emley, O. E. Dadzie, and M. Mahalingam
2011. Laser Capture Microdissection: Methods and Applications. In *Laser Capture Microdissection*, G. I. Murray, ed., Pp. 1–15. Totowa, NJ: Humana Press.

DeChiara, T. M., E. J. Robertson, and A. Efstratiadis
1991. Parental imprinting of the mouse insulin-like growth factor II gene. *Cell*, 64(4):849–859.

Deckers, J. F. M. and P. H. W. Van der Kroon
1981. Some characteristics of the XO mouse (Mus musculus L.) I. Vitality: Growth and metabolism. *Genetica*, 55(3):179–185.

Deckert, J., K. Hartmuth, D. Boehringer, N. Behzadnia, C. L. Will, B. Kastner, H. Stark, H. Urlaub, and R. Lührmann
2006. Protein composition and electron microscopy structure of affinity-purified human spliceosomal B complexes isolated under physiological conditions. *Molecular and Cellular Biology*, 26(14):5528–5543.

Dekker, J. and E. Heard

2015. Structural and functional diversity of Topologically Associating Domains. *FEBS Letters*, 589(20 Pt A):2877–2884.

Deng, Q., D. Ramskold, B. Reinius, and R. Sandberg

2014. Single-Cell RNA-Seq Reveals Dynamic, Random Monoallelic Gene Expression in Mammalian Cells. *Science*, 343(6167):193–196.

Deng, X., J. B. Hiatt, D. K. Nguyen, S. Ercan, D. Sturgill, L. W. Hillier, F. Schlesinger, C. A. Davis, V. J. Reinke, T. R. Gingeras, J. Shendure, R. H. Waterston, B. Oliver, J. D. Lieb, and C. M. Disteche

2011. Evidence for compensatory upregulation of expressed X-linked genes in mammals, Caenorhabditis elegans and Drosophila melanogaster. *Nature Reviews Genetics*, 43(12):1179–1185.

Diez-Roux, G., S. Banfi, M. Sultan, L. Geffers, S. Anand, D. Rozado, A. Magen, E. Canidio, M. Pagani, I. Peluso, N. Lin-Marq, M. Koch, M. Bilio, I. Cantiello, R. Verde, C. De Masi, S. A. Bianchi, J. Cicchini, E. Perroud, S. Mehmeti, E. Dagand, S. Schrinner, A. Nürnberger, K. Schmidt, K. Metz, C. Zwingmann, N. Brieske, C. Springer, A. M. Hernandez, S. Herzog, F. Grabbe, C. Sieverding, B. Fischer, K. Schrader, M. Brockmeyer, S. Dettmer, C. Helbig, V. Alunni, M.-A. Battaini, C. Mura, C. N. Henrichsen, R. Garcia-Lopez, D. Echevarria, E. Puelles, E. Garcia-Calero, S. Kruse, M. Uhr, C. Kauck, G. Feng, N. Milyaev, C. K. Ong, L. Kumar, M. Lam, C. A. Semple, A. Gyenesei, S. Mundlos, U. Radelof, H. Lehrach, P. Sarmientos, A. Reymond, D. R. Davidson, P. Dollé, S. E. Antonarakis, M.-L. Yaspo, S. Martinez, R. A. Baldock, G. Eichele, and A. Ballabio

2011. A high-resolution anatomical atlas of the transcriptome in the mouse embryo. *PLoS Biology*, 9(1):e1000582.

Disteche, C. M.

2012. Dosage compensation of the sex chromosomes. *Annual Review of Genetics*, 46(1):537–560.

Disteche, C. M.

2016. Dosage compensation of the sex chromosomes and autosomes. *Seminars in Cell & Developmental Biology*, 56:9–18.

Disteche, C. M., G. N. Filippova, and K. D. Tsuchiya

2002. Escape from X inactivation. *Cytogenetic and Genome Research*, 99(1-4):36–43.

Ditton, H. J., J. Zimmer, C. Kamp, E. Rajpert-De Meyts, and P. H. Vogt

2004. The AZFa gene DBY (DDX3Y) is widely transcribed but the protein is limited to the male germ cells by translation control. *Human Molecular Genetics*, 13(19):2333–2341.

Dixon, J. R., S. Selvaraj, F. Yue, A. Kim, Y. Li, Y. Shen, M. Hu, J. S. Liu, and B. Ren

2012. Topological domains in mammalian genomes identified by analysis of chromatin interactions. *Nature*, 485(7398):376–380.

Donohoe, M. E., S. S. Silva, S. F. Pinter, N. Xu, and J. T. Lee

2009. The pluripotency factor Oct4 interacts with Ctcf and also controls X-chromosome pairing and counting. *Nature*, 460(7251):128–132.

Du, S., N. Itoh, S. Askarinam, H. Hill, A. P. Arnold, and R. R. Voskuhl

2014. XY sex chromosome complement, compared with XX, in the CNS confers greater neurodegeneration during experimental autoimmune encephalomyelitis. *Proceedings of the National Academy of Sciences of the United States of America*, 111(7):2806–2811.

Dubois, A., J. L. Deuve, P. Navarro, S. Merzouk, S. Pichard, P.-H. Commere, A. Louise, D. Arnaud, P. Avner, and C. Morey

2014. Spontaneous reactivation of clusters of X-linked genes is associated with the plasticity of X-inactivation in mouse trophoblast stem cells. *Stem Cells*, 32(2):377–390.

Dubuc, A. M., M. Remke, A. Korshunov, P. A. Northcott, S. H. Zhan, M. Mendez-Lago, M. Kool, D. T. W. Jones, A. Unterberger, A. S. Morrissy, D. Shih, J. Peacock, V. Ramaswamy, A. Rolider, X. Wang, H. Witt, T. Hielscher, C. Hawkins, R. Vibhakar, S. Croul, J. T. Rutka, W. A. Weiss, S. J. M. Jones, C. G. Eberhart, M. A. Marra, S. M. Pfister, and M. D. Taylor

2012. Aberrant patterns of H3K4 and H3K27 histone lysine methylation occur across subgroups in medulloblastoma. *Acta Neuropathologica*, 125(3):373–384.

Dupont, C., F. Loos, J. Kong-A-San, and J. Gribnau

2017. FGF treatment of host embryos injected with ES cells increases rates of chimaerism. *Transgenic Research*, 26(2):237–246.

Eggan, K., A. Rode, I. Jentsch, C. Samuel, T. Hennek, H. Tintrup, B. Zevnik, J. Erwin, J. Loring, L. Jackson-Grusby, M. R. Speicher, R. Kuehn, and R. Jaenisch

2002. Male and female mice derived from the same embryonic stem cell clone by tetraploid embryo complementation. *Nature Biotechnology*, 20(5):455–459.

Ehrmann, I. E., P. S. Ellis, S. Mazeyrat, S. Duthie, N. Brockdorff, M. G. Mattei, M. A. Gavin, N. A. Affara, G. M. Brown, and E. Simpson

1998. Characterization of genes encoding translation initiation factor eIF-2γ in mouse and human: Sex chromosome localization, escape from X-inactivation and evolution. *Human Molecular Genetics*, 7(11):1725–1737.

Eicher, E. M., D. W. Hale, P. A. Hunt, B. K. Lee, P. K. Tucker, T. R. King, J. T. Eppig, and L. L. Washburn

1991. The mouse Y* chromosome involves a complex rearrangement, including interstitial positioning of the pseudoautosomal region. *Cytogenetics and Cell Genetics*, 57(4):221–230.

Eissenberg, J. C., M. G. Lee, J. Schneider, A. Ilvarsonn, R. Shiekhattar, and A. Shilatifard

2007. The trithorax-group gene in Drosophila little imaginal discs encodes a

trimethylated histone H3 Lys4 demethylase. *Nature Structural & Molecular Biology*, 14(4):344–346.

Elliott, D. J.

2004. The role of potential splicing factors including RBMY, RBMX, hnRNPG-T and STAR proteins in spermatogenesis. *International Journal of Andrology*, 27(6):328–334.

Ellis, N. and P. N. Goodfellow

1989. The mammalian pseudoautosomal region. *Trends in Genetics*, 5(12):406–410.

Ellison, J. W., Z. Wardak, M. F. Young, P. G. Robey, M. Laig-Webster, and W. Chiong

1997. PHOG, a candidate gene for involvement in the short stature of Turner syndrome. *Human Molecular Genetics*, 6(8):1341–1347.

Emerson, J. J., H. Kaessmann, E. Betrán, and M. Long

2004. Extensive gene traffic on the mammalian X chromosome. *Science*, 303(5657):537–540.

Evans, E. P. and R. J. Phillips

1975. Inversion heterozygosity and the origin of XO daughters of Bpa/+female mice. *Nature*, 256(5512):40–41.

Federici, F., A. Magaraki, E. Wassenaar, C. J. H. van Veen-Buurman, C. van de Werken, E. B. Baart, J. S. E. Laven, J. A. Grootegoed, J. Gribnau, and W. M. Baarends

2016. Round Spermatid Injection Rescues Female Lethality of a Paternally Inherited Xist Deletion in Mouse. *PLoS Genetics*, 12(10):e1006358–24.

Ferguson-Smith, M. A.

1965. Karyotype-phenotype Correlations in Gonadal Dysgenesis and Their Bearing on the Pathogenesis of Malformations. *Journal of Medical Genetics*, 2(2):142–155.

Ficz, G., T. A. Hore, F. Santos, H. J. Lee, W. Dean, J. Arand, F. Krueger, D. Oxley, Y.-L. Paul, J. Walter, S. J. Cook, S. Andrews, M. R. Branco, and W. Reik

2013. FGF signaling inhibition in ESCs drives rapid genome-wide demethylation to the epigenetic ground state of pluripotency. *Cell Stem Cell*, 13(3):351–359.

Fieremans, N., H. Van Esch, T. de Ravel, J. Van Driessche, S. Belet, M. Bauters, and G. Froyen

2015. Microdeletion of the escape genes KDM5C and IQSEC2 in a girl with severe intellectual disability and autistic features. *European Journal of Medical Genetics*, 58(5):324–327.

Ford, C. E., K. W. Jones, and P. E. Polani

1959a. A sex-chromosome anomaly in a case of gonadal dysgenesis (Turner's syndrome). *Lancet*, 1(7075):711–713.

Ford, C. E., P. E. Polani, J. H. Briggs, and P. M. Bishop

1959b. A presumptive human XXY/XX mosaic. *Nature*, 183(4667):1030–1032.

Foresta, C., A. Ferlin, and E. Moro

2000. Deletion and expression analysis of AZFa genes on the human Y chromosome revealed a major role for DBY in male infertility. *Human Molecular Genetics*, 9(8):1161–1169.

Freriks, K., H. J. L. M. Timmers, R. T. Netea-Maier, C. C. M. Beerendonk, B. J. Otten, J. A. E. M. van Alfen-van der Velden, M. A. F. Traas, H. Mieloo, G. W. H. J. F. L. van de Zande, L. H. Hoefsloot, A. R. M. M. Hermus, and D. F. C. M. Smeets

2013. Buccal cell FISH and blood PCR-Y detect high rates of X chromosomal mosaicism and Y chromosomal derivatives in patients with Turner syndrome. *European Journal of Medical Genetics*, 56(9):497–501.

Fudenberg, G. and M. Imakaev

2017. FISH-ing for captured contacts: towards reconciling FISH and 3C. *Nature Methods*, 14(7):673–678.

Fukami, M., A. Seki, and T. Ogata

2016. SHOX Haploinsufficiency as a Cause of Syndromic and Nonsyndromic Short Stature. *Molecular Syndromology*, 7(1):3–11.

Fukuda, A., A. Mitani, T. Miyashita, T. Sado, A. Umezawa, and H. Akutsu

2016. Maintenance of Xist Imprinting Depends on Chromatin Condensation State and Rnf12 Dosage in Mice. *PLoS Genetics*, 12(10):e1006375–24.

Fukuda, A., M. Tanino, R. Matoba, A. Umezawa, and H. Akutsu

2015. Imbalance between the expression dosages of X-chromosome and autosomal genes in mammalian oocytes. *Scientific Reports*, 5:14101.

Fukuda, A., J. Tomikawa, T. Miura, K. Hata, K. Nakabayashi, K. Eggan, A. Umezawa, and H. Akutsu

2014. The role of maternal-specific H3K9me3 modification in establishing imprinted X-chromosome inactivation and embryogenesis in mice. *Nature Communications*, 5:1–14.

Garbelli, A., S. Beermann, G. Di Cicco, U. Dietrich, and G. Maga

2011. A Motif Unique to the Human Dead-Box Protein DDX3 Is Important for Nucleic Acid Binding, ATP Hydrolysis, RNA/DNA Unwinding and HIV-1 Replication. *PLoS ONE*, 6(5):e19810.

Gardner, R. L., V. E. Papaioannou, and S. C. Barton

1973. Origin of the ectoplacental cone and secondary giant cells in mouse blastocysts reconstituted from isolated trophoblast and inner cell mass. *Journal of Embryology and Experimental Morphology*, 30(3):561–572.

Gaspar, N. J., T. G. Kinzy, B. J. Scherer, M. Hümbelin, J. W. Hershey, and W. C. Merrick

1994. Translation initiation factor eIF-2. Cloning and expression of the human cDNA encoding the gamma-subunit. *The Journal of Biological Chemistry*, 269(5):3415–3422.

Gayen, S., E. Maclary, E. Buttigieg, M. Hinten, and S. Kalantry

2015. A Primary Role for the Tsix lncRNA in Maintaining Random X-Chromosome Inactivation. *Cell Reports*, 11(8):1251–1265.

Gaztelumendi, N. and C. Nogués

2014. Chromosome Instability in mouse Embryonic Stem Cells. *Scientific Reports*, 4(1):154–8.

Gee, S. L. and J. G. Conboy

1994. Mouse erythroid cells express multiple putative RNA helicase genes exhibiting high sequence conservation from yeast to mammals. *Gene*, 140(2):171–177.

Glynn, L. M. and C. A. Sandman

2011. Prenatal Origins of Neurological Development. *Current Directions in Psychological Science*, 20(6):384–389.

Gontan, C., E. M. Achame, J. Demmers, T. S. Barakat, E. Rentmeester, W. van Ijcken, J. A. Grootegoed, and J. Gribnau

2012. RNF12 initiates X-chromosome inactivation by targeting REX1 for degradation. *Nature*, 485(7398):386–390.

Goto, Y. and N. Takagi

1998. Tetraploid embryos rescue embryonic lethality caused by an additional maternally inherited X chromosome in the mouse. *Development*, 125(17):3353–3363.

Goto, Y. and N. Takagi

2000. Maternally inherited X chromosome is not inactivated in mouse blastocysts due to parental imprinting. *Chromosome Research*, 8(2):101–109.

Grafodatskaya, D., B. H. Chung, D. T. Butcher, A. L. Turinsky, S. J. Goodman, S. Choufani, Y.-A. Chen, Y. Lou, C. Zhao, R. Rajendram, F. E. Abidi, C. Skinner, J. Stavropoulos, C. A. Bondy, J. Hamilton, S. Wodak, S. W. Scherer, C. E.

Schwartz, and R. Weksberg

2013. Multilocus loss of DNA methylation in individuals with mutations in the histone H3 Lysine 4 Demethylase KDM5C. *BMC Medical Genomics*, 6(1):1–1.

Grant, J., S. K. Mahadevaiah, P. Khil, M. N. Sangrithi, H. Royo, J. Duckworth, J. R. McCarrey, J. L. VandeBerg, M. B. Renfree, W. Taylor, G. Elgar, R. D. Camerini-Otero, M. J. Gilchrist, and J. M. A. Turner

2012. Rsx is a metatherian RNA with Xist-like properties in X-chromosome inactivation. *Nature*, 487(7406):254–258.

Greenberg, M. V. C., J. Glaser, M. Borsos, F. E. Marjou, M. Walter, A. Teissandier, and D. Bourc'his

2017. Transient transcription in the early embryo sets an epigenetic state that programs postnatal growth. *Nature Genetics*, 49(1):110–118.

Greene, M. E., G. Mundschau, J. Wechsler, M. McDevitt, A. Gamis, J. Karp, S. Gurbuxani, R. Arceci, and J. D. Crispino

2003. Mutations in GATA1 in both transient myeloproliferative disorder and acute megakaryoblastic leukemia of Down syndrome. *Blood Cells, Molecules & Diseases*, 31(3):351–356.

Greenfield, A., L. Carrel, D. Pennisi, C. Philippe, N. Quaderi, P. Siggers, K. Steiner, P. P. Tam, A. P. Monaco, and H. F. Willard

1998. The UTX gene escapes X inactivation in mice and humans. *Human Molecular Genetics*, 7(4):737–742.

Greenfield, A., D. Scott, D. Pennisi, I. Ehrmann, P. Ellis, L. Cooper, E. Simpson, and P. Koopman

1996. An H–YDb epitope is encoded by a novel mouse Y chromosome gene. *Nature Genetics*, 14(4):474–478.

Gubbay, J., J. Collignon, P. Koopman, B. Capel, A. Economou, A. Münsterberg, N. Vivian, P. Goodfellow, and R. Lovell-Badge

1990. A gene mapping to the sex-determining region of the mouse Y chromo-

some is a member of a novel family of embryonically expressed genes. *Nature*, 346(6281):245–250.

Gubbay, J., N. Vivian, A. Economou, D. Jackson, P. Goodfellow, and R. Lovell-Badge

1992. Inverted repeat structure of the Sry locus in mice. *Proceedings of the National Academy of Sciences of the United States of America*, 89(17):7953–7957.

Guillemot, F., T. Caspary, S. M. Tilghman, N. G. Copeland, D. J. Gilbert, N. A. Jenkins, D. J. Anderson, A. L. Joyner, J. Rossant, and A. Nagy

1995. Genomic imprinting of Mash2, a mouse gene required for trophoblast development. *Nature Genetics*, 9(3):235–242.

Guillemot, F., A. Nagy, A. Auerbach, J. Rossant, and A. L. Joyner

1994. Essential role of Mash-2 in extraembryonic development. *Nature*, 371(6495):333–336.

Guo, J., P. Zhu, C. Wu, L. Yu, S. Zhao, and X. Gu

2003. In silico analysis indicates a similar gene expression pattern between human brain and testis. *Cytogenetic and Genome Research*, 103(1-2):58–62.

Guo, J. H., Q. Huang, D. J. Studholme, C. Q. Wu, and Z. Zhao

2005. Transcriptomic analyses support the similarity of gene expression between brain and testis in human as well as mouse. *Cytogenetic and Genome Research*, 111(2):107–109.

Gupta, V., M. Parisi, D. Sturgill, R. Nuttall, M. Doctolero, O. K. Dudko, J. D. Malley, P. S. Eastman, and B. Oliver

2006. Global analysis of X-chromosome dosage compensation. *Journal of Biology*, 5(1):3.

Habibi, E., A. B. Brinkman, J. Arand, L. I. Kroeze, H. H. D. Kerstens, F. Matarese, K. Lepikhov, M. Gut, I. Brun-Heath, N. C. Hubner, R. Benedetti, L. Altucci, J. H.

Jansen, J. Walter, I. G. Gut, H. Marks, and H. G. Stunnenberg
2013. Short Article. *Cell Stem Cell*, 13(3):360–369.

Habuchi, H., N. Nagai, N. Sugaya, F. Atsumi, R. L. Stevens, and K. Kimata
2007. Mice Deficient in Heparan Sulfate 6- O-Sulfotransferase-1 Exhibit Defective Heparan Sulfate Biosynthesis, Abnormal Placentation, and Late Embryonic Lethality. *The Journal of Biological Chemistry*, 282(21):15578–15588.

Habuchi, H., M. Tanaka, O. Habuchi, K. Yoshida, H. Suzuki, K. Ban, and K. Kimata
2000. The occurrence of three isoforms of heparan sulfate 6-O-sulfotransferase having different specificities for hexuronic acid adjacent to the targeted N-sulfoglucosamine. *The Journal of Biological Chemistry*, 275(4):2859–2868.

Hadjantonakis, A. K., L. L. Cox, P. P. Tam, and A. Nagy
2001. An X-linked GFP transgene reveals unexpected paternal X-chromosome activity in trophoblastic giant cells of the mouse placenta. *genesis*, 29(3):133–140.

Haeussler, M., K. Schönig, H. Eckert, A. Eschstruth, J. Mianné, J.-B. Renaud, S. Schneider-Maunoury, A. Shkumatava, L. Teboul, J. Kent, J.-S. Joly, and J.-P. Concordet
2016. Evaluation of off-target and on-target scoring algorithms and integration into the guide RNA selection tool CRISPOR. *Genome Biology*, Pp. 1–12.

Haig, D. and M. Westoby
1989. Parent-specific gene expression and the triploid endosperm. *The American Naturalist*, 134(1):147–155.

Hamlett, W. C.
1989. Evolution and morphogenesis of the placenta in sharks. *Journal of Experimental Zoology Part A: Ecological Genetics and Physiology*, 252(S2):35–52.

Hassold, T., F. Benham, and M. Leppert

1988. Cytogenetic and molecular analysis of sex-chromosome monosomy. *American Journal of Human Genetics*, 42(4):534–541.

Hassold, T., E. Kumlin, N. Takaesu, and M. Leppert

1985. Determination of the parental origin of sex-chromosome monosomy using restriction fragment length polymorphisms. *American Journal of Human Genetics*, 37(5):965–972.

Hassold, T., D. Pettay, A. Robinson, and I. Uchida

1992. Molecular studies of parental origin and mosaicism in 45,X conceptuses. *Human Genetics*, 89(6):647–652.

Hayashi, K., H. Ohta, K. Kurimoto, S. Aramaki, and M. Saitou

2011a. Reconstitution of the mouse germ cell specification pathway in culture by pluripotent stem cells. *Cell*, 146(4):519–532.

Hayashi, K., H. Ohta, K. Kurimoto, S. Aramaki, and M. Saitou

2011b. Reconstitution of the Mouse Germ Cell Specification Pathway in Culture by Pluripotent Stem Cells. *Cell*, 146(4):519–532.

Hayashi, K. and M. Saitou

2013. Generation of eggs from mouse embryonic stem cells and induced pluripotent stem cells. *Nature Protocols*, 8(8):1513–1524.

Heard, E., C. Kress, F. Mongelard, B. Courtier, C. Rougeulle, A. Ashworth, C. Vourc'h, C. Babinet, and P. Avner

1996. Transgenic mice carrying an Xist-containing YAC. *Human Molecular Genetics*, 5(4):441–450.

Heard, E., F. Mongelard, D. Arnaud, and P. Avner

1999a. Xist yeast artificial chromosome transgenes function as X-inactivation centers only in multicopy arrays and not as single copies. *Molecular and Cellular Biology*, 19(4):3156–3166.

Heard, E., F. Mongelard, D. Arnaud, C. Chureau, C. Vourc'h, and P. Avner
1999b. Human XIST yeast artificial chromosome transgenes show partial X inactivation center function in mouse embryonic stem cells. *Proceedings of the National Academy of Sciences of the United States of America*, 96(12):6841–6846.

Hemberger, M.
2002. The role of the X chromosome in mammalian extra embryonic development. *Cytogenetic and Genome Research*, 99(1-4):210–217.

Hemmi, H., T. Kaisho, O. Takeuchi, S. Sato, H. Sanjo, K. Hoshino, T. Horiuchi, H. Tomizawa, K. Takeda, and S. Akira
2002. Small anti-viral compounds activate immune cells via the TLR7 MyD88–dependent signaling pathway. *Nature Immunology*, 3(2):196–200.

Henery, C. C., J. B. Bard, and M. H. Kaufman
1992. Tetraploidy in mice, embryonic cell number, and the grain of the developmental map. *Developmental Biology*, 152(2):233–241.

Herz, H. M., L. D. Madden, Z. Chen, C. Bolduc, E. Buff, R. Gupta, R. Davuluri, A. Shilatifard, I. K. Hariharan, and A. Bergmann
2010. The H3K27me3 Demethylase dUTX Is a Suppressor of Notch- and Rb-Dependent Tumors in Drosophila. *Molecular and Cellular Biology*, 30(10):2485–2497.

Himeno, E., S. Tanaka, and T. Kunath
2008. Isolation and manipulation of mouse trophoblast stem cells. *Current Protocols in Stem Cell Biology*, Chapter 1:Unit 1E.4.

Hofstetter, C., J. M. Kampka, S. Huppertz, H. Weber, A. Schlosser, A. M. Mu ller, and M. Becker
2016. Inhibition of KDM6 activity during murine ESC differentiation induces DNA damage. *Journal of Cell Science*, 129(4):788–803.

Holm, S.

1979. A simple sequentially rejective multiple test procedure. *Scandinavian journal of statistics*, 6(2):65–70.

Hong, S., Y.-W. Cho, L.-R. Yu, H. Yu, T. D. Veenstra, and K. Ge

2007. Identification of JmjC domain-containing UTX and JMJD3 as histone H3 lysine 27 demethylases. *Proceedings of the National Academy of Sciences of the United States of America*, 104(47):18439–18444.

Hook, E. B. and D. Warburton

1983. The distribution of chromosomal genotypes associated with Turner's syndrome: livebirth prevalence rates and evidence for diminished fetal mortality and severity in genotypes associated with structural X abnormalities or mosaicism. *Human Genetics*, 64(1):24–27.

Hook, E. B. and D. Warburton

2014. Turner syndrome revisited: review of new data supports the hypothesis that all viable 45,X cases are cryptic mosaics with a rescue cell line, implying an origin by mitotic loss. *Human Genetics*, 133(4):417–424.

Horton, J. R., A. K. Upadhyay, H. H. Qi, X. Zhang, Y. Shi, and X. Cheng

2009. Enzymatic and structural insights for substrate specificity of a family of jumonji histone lysine demethylases. *Nature Structural & Molecular Biology*, 17(1):38–43.

Horvath, L. M., N. Li, and L. Carrel

2013. Deletion of an X-inactivation boundary disrupts adjacent gene silencing. *PLoS Genetics*, 9(11):e1003952.

Hu, D. and J. C. Cross

2010. Development and function of trophoblast giant cells in the rodent placenta. *The International Journal of Developmental Biology*, 54(2-3):341–354.

Huang, J.-S., C.-C. Chao, T.-L. Su, S.-H. Yeh, D.-S. Chen, C.-T. Chen, P.-J. Chen, and Y.-S. Jou

2004. Diverse cellular transformation capability of overexpressed genes in human hepatocellular carcinoma. *Biochemical and Biophysical Research Communications*, 315(4):950–958.

Hughes, J. F., H. Skaletsky, L. G. Brown, T. Pyntikova, T. Graves, R. S. Fulton, S. Dugan, Y. Ding, C. J. Buhay, C. Kremitzki, Q. Wang, H. Shen, M. Holder, D. Villasana, L. V. Nazareth, A. Cree, L. Courtney, J. Veizer, H. Kotkiewicz, T.-J. Cho, N. Koutseva, S. Rozen, D. M. Muzny, W. C. Warren, R. A. Gibbs, R. K. Wilson, and D. C. Page

2012. Strict evolutionary conservation followed rapid gene loss on human and rhesus Y chromosomes. *Nature*, 483(7387):82–86.

Hughes, J. F., H. Skaletsky, N. Koutseva, T. Pyntikova, and D. C. Page

2015. Sex chromosome-to-autosome transposition events counter Y-chromosome gene loss in mammals. *Genome Biology*, 16(1):104.

Hughes, J. F., H. Skaletsky, T. Pyntikova, T. A. Graves, S. K. M. van Daalen, P. J. Minx, R. S. Fulton, S. D. McGrath, D. P. Locke, C. Friedman, B. J. Trask, E. R. Mardis, W. C. Warren, S. Repping, S. Rozen, R. K. Wilson, and D. C. Page

2010. Chimpanzee and human Y chromosomes are remarkably divergent in structure and gene content. *Nature*, 463(7280):536–539.

Hughes, J. F., H. Skaletsky, T. Pyntikova, P. J. Minx, T. Graves, S. Rozen, R. K. Wilson, and D. C. Page

2005. Conservation of Y-linked genes during human evolution revealed by comparative sequencing in chimpanzee. *Nature*, 437(7055):100–103.

Hunt, P. A.

1991. Survival of XO mouse fetuses: effect of parental origin of the X chromosome or uterine environment? *Development*, 111(4):1137–1141.

Huynh, K. D. and J. T. Lee

2003. Inheritance of a pre-inactivated paternal X chromosome in early mouse embryos. *Nature*, 426(6968):857–862.

Inoue, A., L. Jiang, F. Lu, T. Suzuki, and Y. Zhang

2017. Maternal H3K27me3 controls DNA methylation-independent imprinting. *Nature*, 547(7664):419–424.

Isensee, J., H. Witt, R. Pregla, R. Hetzer, V. Regitz-Zagrosek, and P. Ruiz Noppinger

2007. Sexually dimorphic gene expression in the heart of mice and men. *Journal of Molecular Medicine*, 86(1):61–74.

Ishikawa, H., M. Banzai, and T. Yamauchi

1999. Developmental retardation of XO mouse embryos at mid-gestation. *Journal of Reproduction and Fertility*, 115(2):263–267.

Ishikawa, H., Á. Rattigan, R. Fundele, R. Fundele, P. S. Burgoyne, and P. S. Burgoyne

2003. Effects of sex chromosome dosage on placental size in mice. *Biology of Reproduction*, 69(2):483–488.

Issaeva, I., Y. Zonis, T. Rozovskaia, K. Orlovsky, C. M. Croce, T. Nakamura, A. Mazo, L. Eisenbach, and E. Canaani

2007. Knockdown of ALR (MLL2) Reveals ALR Target Genes and Leads to Alterations in Cell Adhesion and Growth. *Molecular and Cellular Biology*, 27(5):1889–1903.

Iurlaro, M., F. von Meyenn, and W. Reik

2017. DNA methylation homeostasis in human and mouse development. *Current Opinion in Genetics & Development*, 43:101–109.

Ivanov, R., S. Hol, T. Aarts, A. Hagenbeek, E. H. Slager, and S. Ebeling

2005. UTY-specific TCR-transfer generates potential graft-versus-leukaemia effector T cells. *British Journal of Haematology*, 129(3):392–402.

Iwase, S., F. Lan, P. Bayliss, L. de la Torre-Ubieta, M. Huarte, H. H. Qi, J. R. Whetstine, A. Bonni, T. M. Roberts, and Y. Shi

2007. The X-Linked Mental Retardation Gene SMCX/JARID1C Defines a Family of Histone H3 Lysine 4 Demethylases. *Cell*, 128(6):1077–1088.

Iyer, V., B. Shen, W. Zhang, A. Hodgkins, T. Keane, X. Huang, and W. C. Skarnes

2015. Off-target mutations are rare in Cas9-modified mice. *Nature Methods*, 12(6):479–479.

Jackman, S. M., X. Kong, and M. E. Fant

2012. Plac1 (placenta-specific 1) is essential for normal placental and embryonic development. *Molecular Reproduction and Development*, 79(8):564–572.

Jacobs, P., P. Dalton, R. James, K. Mosse, M. Power, D. Robinson, and D. Skuse

1997. Turner syndrome: a cytogenetic and molecular study. *Annals of Human Genetics*, 61(Pt 6):471–483.

Jacobs, P. A.

1990. The role of chromosome abnormalities in reproductive failure. *Reproduction, nutrition, development*, Suppl 1:63s–74s.

Jacobs, P. A., A. G. Baikie, W. M. Brown, T. N. Macgregor, N. Maclean, and D. G. Harnden

1959. Evidence for the existence of the human "super female". *Lancet*, 2(7100):423–425.

Jacobs, P. A., P. R. Betts, A. E. Cockwell, J. A. Crolla, M. J. Mackenzie, D. O. Robinson, and S. A. Youings

1990. A cytogenetic and molecular reappraisal of a series of patients with Turner's syndrome. *Annals of Human Genetics*, 54(Pt 3):209–223.

Jacobs, P. A. and J. A. Strong

1959. A case of human intersexuality having a possible XXY sex-determining mechanism. *Nature*, 183(4657):302–303.

Jamieson, R. V., P. P. Tam, and M. Gardiner-Garden

1996. X-chromosome activity: impact of imprinting and chromatin structure. *The International Journal of Developmental Biology*, 40(6):1065–1080.

Jamieson, R. V., S. S. Tan, and P. Tam

1998. Retarded postimplantation development of X0 mouse embryos: impact of the parental origin of the monosomic X chromosome. *Developmental Biology*.

Jankowska, A. M., H. Makishima, R. V. Tiu, H. Szpurka, Y. Huang, F. Traina, V. Visconte, Y. Sugimoto, C. Prince, C. O'Keefe, E. D. Hsi, A. List, M. A. Sekeres, A. Rao, M. A. McDevitt, and J. P. Maciejewski

2011. Mutational spectrum analysis of chronic myelomonocytic leukemia includes genes associated with epigenetic regulation: UTX, EZH2, and DNMT3A. *Blood*, 118(14):3932–3941.

Jensen, L. R., M. Amende, U. Gurok, B. Moser, V. Gimmel, A. Tzschach, A. R. Janecke, G. Tariverdian, J. Chelly, J.-P. Fryns, H. Van Esch, T. Kleefstra, B. Hamel, C. Moraine, J. Gecz, G. Turner, R. Reinhardt, V. M. Kalscheuer, H.-H. Ropers, and S. Lenzner

2005. Mutations in the JARID1C gene, which is involved in transcriptional regulation and chromatin remodeling, cause X-linked mental retardation. *American Journal of Human Genetics*, 76(2):227–236.

Ji, X., S. Jin, X. Qu, K. Li, H. Wang, H. He, F. Guo, and L. Dong

2015. Lysine-specific demethylase 5C promotes hepatocellular carcinoma cell invasion through inhibition BMP7 expression. *BMC Cancer*, 15(1):801.

Jiang, L., F. Schlesinger, C. A. Davis, Y. Zhang, R. Li, M. Salit, T. R. Gingeras, and B. Oliver

2011. Synthetic spike-in standards for RNA-seq experiments. *Genome Research*, 21(9):1543–1551.

Jiang, R., C. Hua, Y. Wan, B. Jiang, H. Hu, J. Zheng, B. K. Fuqua, J. L. Dunaief, G. J. Anderson, S. David, C. D. Vulpe, and H. Chen

2015. Hephaestin and Ceruloplasmin Play Distinct but Interrelated Roles in Iron Homeostasis in Mouse Brain. *Journal of Nutrition*, 145(5):1003–1009.

Jiang, W., J. Wang, and Y. Zhang

2013. Histone H3K27me3 demethylases KDM6A and KDM6B modulate definitive endoderm differentiation from human ESCs by regulating WNT signaling pathway. *Cell Research*, 23(1):122–130.

Jimenez-Chillaron, J. C., M. Hernandez-Valencia, C. Reamer, S. Fisher, A. Joszi, M. Hirshman, A. Oge, S. Walrond, R. Przybyla, C. Boozer, L. J. Goodyear, and M.-E. Patti

2005. Beta-cell secretory dysfunction in the pathogenesis of low birth weight-associated diabetes: a murine model. *Diabetes*, 54(3):702–711.

Jin, C., J. Li, C. D. Green, X. Yu, X. Tang, D. Han, B. Xian, D. Wang, X. Huang, X. Cao, Z. Yan, L. Hou, J. Liu, N. Shukeir, P. Khaitovich, C. D. Chen, H. Zhang, T. Jenuwein, and J.-D. J. Han

2011. Histone demethylase UTX-1 regulates C. elegans life span by targeting the insulin/IGF-1 signaling pathway. *Cell Metabolism*, 14(2):161–172.

Jinek, M., K. Chylinski, I. Fonfara, M. Hauer, J. A. Doudna, and E. Charpentier

2012. A programmable dual-RNA-guided DNA endonuclease in adaptive bacterial immunity. *Science*, 337(6096):816–821.

John, R. and M. Hemberger

2012. A placenta for life. *Reproductive BioMedicine Online*, 25(1):5–11.

Johnson, M. A., I. Hernandez, Y. Wei, and N. Greenberg

2000. Isolation and characterization of mouse probasin: An androgen-regulated protein specifically expressed in the differentiated prostate. *The Prostate*, 43(4):255–262.

Jones, D. T. W., N. Jäger, M. Kool, T. Zichner, B. Hutter, M. Sultan, Y.-J. Cho, T. J. Pugh, V. Hovestadt, A. M. Stütz, T. Rausch, H.-J. Warnatz, M. Ryzhova, S. Bender, D. Sturm, S. Pleier, H. Cin, E. Pfaff, L. Sieber, A. Wittmann, M. Remke, H. Witt, S. Hutter, T. Tzaridis, J. Weischenfeldt, B. Raeder, M. Avci, V. Amstislavskiy, M. Zapatka, U. D. Weber, Q. Wang, B. Lasitschka, C. C. Bartholomae, M. Schmidt, C. von Kalle, V. Ast, C. Lawerenz, J. Eils, R. Kabbe, V. Benes, P. van Sluis, J. Koster, R. Volckmann, D. Shih, M. J. Betts, R. B. Russell, S. Coco, G. Paolo Tonini, U. Schüller, V. Hans, N. Graf, Y.-J. Kim, C. Monoranu, W. Roggendorf, A. Unterberg, C. Herold-Mende, T. Milde, A. E. Kulozik, A. von Deimling, O. Witt, E. Maass, J. Rössler, M. Ebinger, M. U. Schuhmann, M. C. Frühwald, M. Hasselblatt, N. Jabado, S. Rutkowski, A. O. von Bueren, D. Williamson, S. C. Clifford, M. G. McCabe, V. Peter Collins, S. Wolf, S. Wiemann, H. Lehrach, B. Brors, W. Scheurlen, J. Felsberg, G. Reifenberger, P. A. Northcott, M. D. Taylor, M. Meyerson, S. L. Pomeroy, M.-L. Yaspo, J. O. Korbel, A. Korshunov, R. Eils, S. M. Pfister, and P. Lichter

2012. Dissecting the genomic complexity underlying medulloblastoma. *Nature*, 488(7409):100–105.

Jonkers, I., T. S. Barakat, E. M. Achame, K. Monkhorst, A. Kenter, E. Rentmeester, F. Grosveld, J. A. Grootegoed, and J. Gribnau

2009. RNF12 Is an X-Encoded Dose-Dependent Activator of X Chromosome Inactivation. *Cell*, 139(5):999–1011.

Jue, N. K., M. B. Murphy, S. D. Kasowitz, S. M. Qureshi, C. J. Obergfell, S. Elsisi, R. J. Foley, R. J. O. Neill, and M. J. O. Neill

2013. Determination of dosage compensation of the mammalian X chromosome by RNA-seq is dependent on analytical approach. *BMC Genomics*, 14(1):1–1.

Julien, P., D. Brawand, M. Soumillon, A. Necsulea, A. Liechti, F. Schütz, T. Daish, F. Grützner, and H. Kaessmann

2012. Mechanisms and evolutionary patterns of mammalian and avian dosage compensation. *PLoS Biology*, 10(5):e1001328.

Kanai, Y., N. Dohmae, and N. Hirokawa

2004. Kinesin transports RNA: isolation and characterization of an RNA-transporting granule. *Neuron*, 43(4):513–525.

Kapahnke, M., A. Banning, and R. Tikkanen

2016. Random Splicing of Several Exons Caused by a Single Base Change in the Target Exon of CRISPR/Cas9 Mediated Gene Knockout. *Cells*, 5(4):45–12.

Kappelgaard, A.-M. and T. Laursen

2011. The benefits of growth hormone therapy in patients with Turner syndrome, Noonan syndrome and children born small for gestational age. *YGHIR*, 21(6):305–313.

Kaufman, M. H., S. C. Barton, and M. A. Surani

1977. Normal postimplantation development of mouse parthenogenetic embryos to the forelimb bud stage. *Nature*, 265(5589):53–55.

Kaufman, M. H. and S. Webb

1990. Postimplantation development of tetraploid mouse embryos produced by electrofusion. *Development*, 110(4):1121–1132.

Keverne, E. B.

2015. Genomic imprinting, action, and interaction of maternal and fetal genomes. *Proceedings of the National Academy of Sciences of the United States of America*, 112(22):6834–6840.

Khil, P. P., N. A. Smirnova, P. J. Romanienko, and R. D. Camerini-Otero

2004. The mouse X chromosome is enriched for sex-biased genes not subject to selection by meiotic sex chromosome inactivation. *Nature Genetics*, 36(6):642–646.

Kim, D., B. Langmead, and S. L. Salzberg

2015. HISAT: a fast spliced aligner with low memory requirements. *Nature Methods*, 12(4):357–360.

Kim, I. W., A. C. Khadilkar, E. Y. Ko, and E. S. Sabanegh

2013. 47,XYY Syndrome and Male Infertility. *Reviews in Urology*, 15(4):188–196.

King, M. C. and A. C. Wilson

1975. Evolution at two levels in humans and chimpanzees. *Science*, 188(4184):107–116.

Klinefelter, H. F., E. C. Reifenstein Jr, and F. A. Jr

1942. Syndrome characterized by gynecomastia, aspermatogenesis without A-Leydigism, and increased excretion of follicle-stimulating hormone 1. *The Journal of Clinical Endocrinology*, 2(11):615–627.

Klose, R. J., E. M. Kallin, and Y. Zhang

2006. JmjC-domain-containing proteins and histone demethylation. *Nature Reviews Genetics*, 7(9):715–727.

Kobayashi, S., Y. Fujihara, N. Mise, K. Kaseda, K. Abe, F. Ishino, and M. Okabe

2010. The X-linked imprinted gene family Fthl17 shows predominantly female expression following the two-cell stage in mouse embryos. *Nucleic Acids Research*, 38(11):3672–3681.

Kobayashi, S., A. Isotani, N. Mise, M. Yamamoto, Y. Fujihara, K. Kaseda, T. Nakanishi, M. Ikawa, H. Hamada, K. Abe, and M. Okabe

2006. Comparison of Gene Expression in Male and Female Mouse Blastocysts Revealed Imprinting of the X-Linked Gene, Rhox5/Pem, at Preimplantation Stages. *Current Biology*, 16(2):166–172.

Kobayashi, S., Y. Totoki, M. Soma, K. Matsumoto, Y. Fujihara, A. Toyoda, Y. Sakaki, M. Okabe, and F. Ishino

2013. Identification of an Imprinted Gene Cluster in the X-Inactivation Center. *PLoS ONE*, 8(8):e71222.

Koehler, K. E., E. A. Millie, J. P. Cherry, P. S. Burgoyne, E. P. Evans, P. A. Hunt, and T. J. Hassold

2002. Sex-specific differences in meiotic chromosome segregation revealed by dicentric bridge resolution in mice. *Genetics*, 162(3):1367–1379.

Koller, P. C. and C. D. Darlington

1934. The genetical and mechanical properties of the sex-chromosomes. *Journal of Genetics*, 29(2):159–173.

Koo, G. C., S. S. Wachtel, K. Krupen-Brown, L. R. Mittl, W. R. Breg, M. Genel, I. M. Rosenthal, D. S. Borgaonkar, A. D. Miller, and R. Tantravahi

1977. Mapping the locus of the HY gene on the human Y chromosome. *Science*, 198(4320):940.

Koopman, P., J. Gubbay, N. Vivian, P. Goodfellow, and R. Lovell-Badge

1991. Male development of chromosomally female mice transgenic for Sry. *Nature*, 351(6322):117–121.

Kortschak, R. D., P. W. Tucker, and R. Saint

2000. ARID proteins come in from the desert. *Trends in Biochemical Sciences*, 25(6):294–299.

Koshio, J., H. Kagamu, K. Nozaki, Y. Saida, T. Tanaka, S. Shoji, N. Igarashi, S. Miura, M. Okajima, S. Watanabe, H. Yoshizawa, and I. Narita

2013. DEAD/H (Asp–Glu–Ala–Asp/His) box polypeptide 3, X-linked is an immunogenic target of cancer stem cells. *Cancer Immunology, Immunotherapy*, 62(10):1619–1628.

Kozak, M.

1984. Compilation and analysis of sequences upstream from the translational start site in eukaryotic mRNAs. *Nucleic Acids Research*, 12(2):857–872.

Kubaczka, C., C. Senner, M. J. Araúzo-Bravo, N. Sharma, P. Kuckenberg, A. Becker, A. Zimmer, O. Brüstle, M. Peitz, M. Hemberger, and H. Schorle
2014. Derivation and Maintenance of Murine Trophoblast Stem Cells under Defined Conditions. *Stem Cell Reports*, 2(2):232–242.

Kubaczka, C., C. E. Senner, M. Cierlitza, M. J. Araúzo-Bravo, P. Kuckenberg, M. Peitz, M. Hemberger, and H. Schorle
2015. Direct Induction of Trophoblast Stem Cells from Murine Fibroblasts. *Cell Stem Cell*, 17(5):557–568.

Kunath, T., D. Arnaud, G. D. Uy, I. Okamoto, C. Chureau, Y. Yamanaka, E. Heard, R. L. Gardner, P. Avner, and J. Rossant
2005. Imprinted X-inactivation in extra-embryonic endoderm cell lines from mouse blastocysts. *Development*, 132(7):1649–1661.

Lahn, B. T.
1997. Functional Coherence of the Human Y Chromosome. *Science*, 278(5338):675–680.

Lahn, B. T. and D. C. Page
1997. Functional coherence of the human Y chromosome. *Science*, 278(5338):675–680.

Lahn, B. T. and D. C. Page
1999. Four evolutionary strata on the human X chromosome. *Science*, 286(5441):964–967.

Lan, F., P. E. Bayliss, J. L. Rinn, J. R. Whetstine, J. K. Wang, S. Chen, S. Iwase, R. Alpatov, I. Issaeva, E. Canaani, T. M. Roberts, H. Y. Chang, and Y. Shi
2007. A histone H3 lysine 27 demethylase regulates animal posterior development. *Nature*, 449(7163):689–694.

Lanfranco, F., A. Kamischke, M. Zitzmann, and E. Nieschlag
2004. Klinefelter's syndrome. *Lancet*, 364(9430):273–283.

Larizza, D., M. Martinetti, J. M. Dugoujon, C. Tinelli, V. Calcaterra, M. Cuccia, L. Salvaneschi, and F. Severi

2002. Parental GM and HLA genotypes and reduced birth weight in patients with Turner's syndrome. *Journal of Pediatric Endocrinology & Metabolism*, 15(8):1183–1190.

Latham, K. E.

1994. Strain-specific differences in mouse oocytes and their contributions to epigenetic inheritance. *Development*, 120(12):3419–3426.

Latham, K. E., B. Patel, F. D. Bautista, and S. M. Hawes

2000. Effects of X chromosome number and parental origin on X-linked gene expression in preimplantation mouse embryos. *Biology of Reproduction*, 63(1):64–73.

Latham, K. E. and L. Rambhatla

1995. Expression of X-linked genes in androgenetic, gynogenetic, and normal mouse preimplantation embryos. *Developmental Genetics*, 17(3):212–222.

Lazic, S. E. and L. Essioux

2013. Improving basic and translational science by accounting for litter-to-litter variation in animal models. *BMC Neuroscience*, 14(1):37.

Lederer, D., B. Grisart, M. C. Digilio, V. Benoit, M. Crespin, S. C. Ghariani, I. Maystadt, B. Dallapiccola, and C. Verellen-Dumoulin

2012. Deletion of KDM6A, a Histone Demethylase Interacting with MLL2, in Three Patients with Kabuki Syndrome. *American Journal of Human Genetics*, 90(1):119–124.

Lee, J. T.

2002. Homozygous Tsix mutant mice reveal a sex-ratio distortion and revert to random X-inactivation. *Nature Genetics*, 32(1):195–200.

Lee, J. T., L. S. Davidow, and D. Warshawsky

1999. Tsix, a gene antisense to Xist at the X-inactivation centre. *Nature Genetics*, 21(4):400–404.

Lee, J. T. and N. Lu

1999. Targeted mutagenesis of Tsix leads to nonrandom X inactivation. *Cell*, 99(1):47–57.

Lee, J. T., W. M. Strauss, J. A. Dausman, and R. Jaenisch

1996. A 450 kb transgene displays properties of the mammalian X-inactivation center. *Cell*, 86(1):83–94.

Lee, M. C. and G. S. Conway

2014. Turner's syndrome: challenges of late diagnosis. *The Lancet Diabetes & Endocrinology*.

Lee, M. G., J. Norman, A. Shilatifard, and R. Shiekhattar

2007a. Physical and functional association of a trimethyl H3K4 demethylase and Ring6a/MBLR, a polycomb-like protein. *Cell*, 128(5):877–887.

Lee, N., J. Zhang, R. J. Klose, H. Erdjument-Bromage, P. Tempst, R. S. Jones, and Y. Zhang

2007b. The trithorax-group protein Lid is a histone H3 trimethyl-Lys4 demethylase. *Nature Structural & Molecular Biology*, 14(4):341–343.

Lee, S., M. K. Leach, S. A. Redmond, S. Y. C. Chong, S. H. Mellon, S. J. Tuck, Z.-Q. Feng, J. M. Corey, and J. R. Chan

2012. A culture system to study oligodendrocyte myelination processes using engineered nanofibers. *Nature Methods*, 9(9):917–922.

Lefebvre, L., S. Viville, S. C. Barton, F. Ishino, E. B. Keverne, and M. A. Surani

1998. Abnormal maternal behaviour and growth retardation associated with loss of the imprinted gene Mest. *Nature Genetics*, 20(2):163–169.

Leighton, P. A., R. S. Ingram, J. Eggenschwiler, A. Efstratiadis, and S. M. Tilghman
1995. Disruption of imprinting caused by deletion of the H19 gene region in mice. *Nature*, 375(6526):34–39.

Leitch, H. G., K. R. McEwen, A. Turp, V. Encheva, T. Carroll, N. Grabole, W. Mansfield, B. Nashun, J. G. Knezovich, A. Smith, M. A. Surani, and P. Hajkova
2013. Naive pluripotency is associated with global DNA hypomethylation. *Nature Structural & Molecular Biology*, 20(3):311–316.

Lewis, A., K. Green, C. Dawson, L. Redrup, K. D. Huynh, J. T. Lee, M. Hemberger, and W. Reik
2006. Epigenetic dynamics of the Kcnq1 imprinted domain in the early embryo. *Development*, 133(21):4203–4210.

Lewis, A., K. Mitsuya, D. Umlauf, P. Smith, W. Dean, J. Walter, M. J. Higgins, R. Feil, and W. Reik
2004. Imprinting on distal chromosome 7 in the placenta involves repressive histone methylation independent of DNA methylation. *Nature Genetics*, 36(12):1291–1295.

Li, B., V. Ruotti, R. M. Stewart, J. A. Thomson, and C. N. Dewey
2009a. RNA-Seq gene expression estimation with read mapping uncertainty. *Bioinformatics (Oxford, England)*, 26(4):493–500.

Li, H. L., P. Gee, K. Ishida, and A. Hotta
2016. Efficient genomic correction methods in human iPS cells using CRISPR-Cas9 system. *Methods*, 101:27–35.

Li, L., E. B. Keverne, S. A. Aparicio, F. Ishino, S. C. Barton, and M. A. Surani
1999. Regulation of maternal behavior and offspring growth by paternally expressed Peg3. *Science*, 284(5412):330–333.

Li, N. and L. Carrel
2008. Escape from X chromosome inactivation is an intrinsic property of the

Jarid1c locus. *Proceedings of the National Academy of Sciences of the United States of America*, 105(44):17055–17060.

Li, Q., A. L. Brass, A. Ng, Z. Hu, R. J. Xavier, T. J. Liang, and S. J. Elledge

2009b. A genome-wide genetic screen for host factors required for hepatitis C virus propagation. *Proceedings of the National Academy of Sciences of the United States of America*, 106(38):16410–16415.

Li, Q., P. Zhang, C. Zhang, Y. Wang, R. Wan, Y. Yang, X. Guo, R. Huo, M. Lin, Z. Zhou, and J. Sha

2014. DDX3X regulates cell survival and cell cycle during mouse early embryonic development. *Journal of Biomedical Research*, 28(4):282–291.

Li, Y. and R. R. Behringer

1998. Esx1 is an X-chromosome-imprinted regulator of placental development and fetal growth. *Nature Genetics*, 20(3):309–311.

Lin, F., K. Xing, J. Zhang, and X. He

2012a. Expression reduction in mammalian X chromosome evolution refutes Ohno's hypothesis of dosage compensation. *Proceedings of the National Academy of Sciences of the United States of America*, 109(29):11752–11757.

Lin, H., V. Gupta, M. D. VerMilyea, F. Falciani, J. T. Lee, L. P. O'Neill, and B. M. Turner

2007. Dosage Compensation in the Mouse Balances Up-Regulation and Silencing of X-Linked Genes. *PLoS Biology*, 5(12):e326.

Lin, Y., T. Wen, X. Meng, Z. Wu, L. Zhao, P. Wang, Z. Hong, and Z. Yin

2012b. The mouse Mageb18 gene encodes a ubiquitously expressed type I MAGE protein and regulates cell proliferation and apoptosis in melanoma B16-F0 cells. *Biochemical Journal*, 443(3):779–788.

Linder, P.

2006. Dead-box proteins: a family affair–active and passive players in RNP-remodeling. *Nucleic Acids Research*, 34(15):4168–4180.

Linder, P., P. F. Lasko, M. Ashburner, P. Leroy, P. J. Nielsen, K. Nishi, J. Schnier, and P. P. Slonimski

1989. Birth of the D-E-A-D box. *Nature*, 337(6203):121–122.

Lingenfelter, P. A., D. A. Adler, D. Poslinski, S. Thomas, R. W. Elliott, V. M. Chapman, and C. M. Disteche

1998. Escape from X inactivation of Smcx is preceded by silencing during mouse development. *Nature Genetics*, 18(3):212–213.

Liu, J., J. Henao-Mejia, H. Liu, Y. Zhao, and J. J. He

2011. Translational Regulation of HIV-1 Replication by HIV-1 Rev Cellular Cofactors Sam68, eIF5A, hRIP, and DDX3. *Journal of Neuroimmune Pharmacology*, 6(2):308–321.

Liu, N., S. A. Enkemann, P. Liang, R. Hersmus, C. Zanazzi, J. Huang, C. Wu, Z. Chen, L. H. J. Looijenga, D. L. Keefe, and L. Liu

2010. Genome-wide gene expression profiling reveals aberrant MAPK and Wnt signaling pathways associated with early parthenogenesis. *Journal of Molecular Cell Biology*, 2(6):333–344.

Livak, K. J. and T. D. Schmittgen

2001. Analysis of Relative Gene Expression Data Using Real-Time Quantitative PCR and the $2^{-\Delta\Delta CT}$ Method. *Methods*, 25(4):402–408.

Liyanage, M., A. Coleman, S. du Manoir, T. Veldman, S. McCormack, R. B. Dickson, C. Barlow, A. Wynshaw-Boris, S. Janz, J. Wienberg, M. A. Ferguson-Smith, E. Schrock, and T. Ried

1996. Multicolour spectral karyotyping of mouse chromosomes. *Nature Genetics*, 14(3):312–315.

Lovell-Badge, R. and E. Robertson

1990. XY female mice resulting from a heritable mutation in the primary testis-determining gene, Tdy. *Development*, 109(3):635–646.

Lovén, J., D. A. Orlando, A. A. Sigova, C. Y. Lin, P. B. Rahl, C. B. Burge, D. L. Levens, T. I. Lee, and R. A. Young

2012. Revisiting Global Gene Expression Analysis. *Cell*, 151(3):476–482.

Lyon, M. F.

1961. Gene action in the X-chromosome of the mouse (Mus musculus L.). *Nature*, 190(4773):372–373.

Maclary, E., E. Buttigieg, M. Hinten, S. Gayen, C. Harris, M. K. Sarkar, S. Purushothaman, and S. Kalantry

2014. Differentiation-dependent requirement of Tsix long non-coding RNA in imprinted X-chromosome inactivation. *Nature Communications*, 5:4209.

Maclean, J. A., A. Bettegowda, B. J. Kim, C.-H. Lou, S.-M. Yang, A. Bhardwaj, S. Shanker, Z. Hu, Y. Fan, S. Eckardt, K. J. McLaughlin, A. I. Skoultchi, and M. F. Wilkinson

2011. The rhox homeobox gene cluster is imprinted and selectively targeted for regulation by histone h1 and DNA methylation. *Molecular and Cellular Biology*, 31(6):1275–1287.

MacLean, J. A., M. A. Chen, C. M. Wayne, S. R. Bruce, M. Rao, M. L. Meistrich, C. Macleod, and M. F. Wilkinson

2005. Rhox: A New Homeobox Gene Cluster. *Cell*, 120(3):369–382.

Maclean, J. A., D. Lorenzetti, Z. Hu, W. J. Salerno, J. Miller, and M. F. Wilkinson

2006. Rhox homeobox gene cluster: recent duplication of three family members. *genesis*, 44(3):122–129.

Mahadevaiah, S. K., T. Odorisio, D. J. Elliott, A. Rattigan, M. Szot, S. H. Laval, L. L. Washburn, J. R. McCarrey, B. M. Cattanach, R. Lovell-Badge, and P. S. Burgoyne

1998. Mouse homologues of the human AZF candidate gene RBM are expressed in spermatogonia and spermatids, and map to a Y chromosome deletion inter-

val associated with a high incidence of sperm abnormalities. *Human Molecular Genetics*, 7(4):715–727.

Maier, T., M. Güell, and L. Serrano

2009. Correlation of mRNA and protein in complex biological samples. *FEBS Letters*, 583(24):3966–3973.

Mak, W., J. Baxter, J. Silva, A. E. Newall, A. P. Otte, and N. Brockdorff

2002. Mitotically stable association of polycomb group proteins eed and enx1 with the inactive x chromosome in trophoblast stem cells. *Current Biology*, 12(12):1016–1020.

Mak, W., T. B. Nesterova, M. de Napoles, R. Appanah, S. Yamanaka, A. P. Otte, and N. Brockdorff

2004. Reactivation of the paternal X chromosome in early mouse embryos. *Science*, 303(5658):666–669.

Mamiya, N. and H. J. Worman

1999. Hepatitis C virus core protein binds to a DEAD box RNA helicase. *The Journal of Biological Chemistry*, 274(22):15751–15756.

Manes, C. and P. Menzel

1981. Demethylation of CpG sites in DNA of early rabbit trophoblast. *Nature*, 293(5833):589–590.

Mansour, A. A., O. Gafni, L. Weinberger, A. Zviran, M. Ayyash, Y. Rais, V. Krupalnik, M. Zerbib, D. Amann-Zalcenstein, I. Maza, S. Geula, S. Viukov, L. Holtzman, A. Pribluda, E. Canaani, S. Horn-Saban, I. Amit, N. Novershtern, and J. H. Hanna

2012. The H3K27 demethylase Utx regulates somatic and germ cell epigenetic reprogramming. *Nature*, 488(7411):409–413.

Marahrens, Y., B. Panning, J. Dausman, W. Strauss, and R. Jaenisch

1997. Xist-deficient mice are defective in dosage compensation but not spermatogenesis. *Genes & Development*, 11(2):156–166.

Marks, H., H. H. D. Kerstens, T. S. Barakat, E. Splinter, R. A. M. Dirks, G. van Mierlo, O. Joshi, S.-Y. Wang, T. Babak, C. A. Albers, T. Kalkan, A. Smith, A. Jouneau, W. de Laat, J. Gribnau, and H. G. Stunnenberg

2015. Dynamics of gene silencing during X inactivation using allele-specific RNA-seq. *Genome Biology*, 16(1):1–20.

Marstrand-Joergensen, M. R., R. B. Jensen, L. Aksglaede, M. Duno, and A. Juul

2016. Prevalence of SHOX haploinsufficiency among short statured children. *Pediatric Research*, 81(2):335–341.

Martin, G. R., C. J. Epstein, B. Travis, G. Tucker, S. Yatziv, D. W. Martin, S. Clift, and S. Cohen

1978. X-chromosome inactivation during differentiation of female teratocarcinoma stem cells in vitro. *Nature*, 271(5643):329–333.

Matsui, J., Y. Goto, and N. Takagi

2001. Control of Xist expression for imprinted and random X chromosome inactivation in mice. *Human Molecular Genetics*, 10(13):1393–1401.

Mazeyrat, S. and M. J. Mitchell

1998. Rodent Y chromosome TSPY gene is functional in rat and non-functional in mouse. *Human Molecular Genetics*, 7(3):557–562.

Mazeyrat, S., N. Saut, V. Grigoriev, S. K. Mahadevaiah, O. A. Ojarikre, A. Rattigan, C. Bishop, E. M. Eicher, M. J. Mitchell, and P. S. Burgoyne

2001. A Y-encoded subunit of the translation initiation factor Eif2 is essential for mouse spermatogenesis. *Nature Genetics*, 29(1):49–53.

Mazeyrat, S., N. Saut, M. G. Mattei, and M. J. Mitchell

1999. RBMY evolved on the Y chromosome from a ubiquitously transcribed X-Y identical gene. *Nature Genetics*, 22(3):224–226.

McDonald, L. E., C. A. Paterson, and G. F. Kay

1998. Bisulfite genomic sequencing-derived methylation profile of the xist gene throughout early mouse development. *Genomics*, 54(3):379–386.

McGrath, J. and D. Solter

1984. Completion of mouse embryogenesis requires both the maternal and paternal genomes. *Cell*, 37(1):179–183.

Meaburn, K. J. and T. Misteli

2008. Locus-specific and activity-independent gene repositioning during early tumorigenesis. *The Journal of Cell Biology*, 180(1):39–50.

Menke, D. B. and D. C. Page

2002. Sexually dimorphic gene expression in the developing mouse gonad. *Gene Expression Patterns*, 2(3-4):359–367.

Merkin, J., C. Russell, P. Chen, and C. B. Burge

2012. Evolutionary dynamics of gene and isoform regulation in Mammalian tissues. *Science*, 338(6114):1593–1599.

Merrick, W. C.

1992. Mechanism and regulation of eukaryotic protein synthesis. *Microbiological Reviews*, 56(2):291–315.

Miller, J. R., S. Koren, and G. Sutton

2010. Assembly algorithms for next-generation sequencing data. *Genomics*, 95(6):315–327.

Minkovsky, A., T. S. Barakat, N. Sellami, M. H. Chin, N. Gunhanlar, J. Gribnau, and K. Plath

2013. The pluripotency factor-bound intron 1 of Xist is dispensable for X chromosome inactivation and reactivation in vitro and in vivo. *Cell Reports*, 3(3):905–918.

Minkovsky, A., S. Patel, and K. Plath

2012. Concise review: Pluripotency and the transcriptional inactivation of the female Mammalian X chromosome. *Stem Cells*, 30(1):48–54.

Miyake, N., S. Mizuno, N. Okamoto, H. Ohashi, M. Shiina, K. Ogata, Y. Tsurusaki, M. Nakashima, H. Saitsu, N. Niikawa, and N. Matsumoto

2012. KDM6A Point Mutations Cause Kabuki Syndrome. *Human Mutation*, 34(1):108–110.

Mohan, M., H.-M. Herz, and A. Shilatifard

2012. SnapShot: Histone lysine methylase complexes. *Cell*, 149(2):498–498.e1.

Monk, M. and M. I. Harper

1979. Sequential X chromosome inactivation coupled with cellular differentiation in early mouse embryos. *Nature*, 281(5729):311–313.

Morales Torres, C., A. Laugesen, and K. Helin

2013. Utx is required for proper induction of ectoderm and mesoderm during differentiation of embryonic stem cells. *PLoS ONE*, 8(4):e60020.

Morris, T.

1968a. The XO and OY chromosome constitutions in the mouse. *Genetical Research*, 12(2):125–137.

Morris, T.

1968b. The XO and OY chromosome constitutions in the mouse. *Genetics Research*, 12(2):125–137.

Moses, M. J., S. J. Counce, and D. F. Paulson

1975. Synaptonemal complex complement of man in spreads of spermatocytes, with details of the sex chromosome pair. *Science*, 187(4174):363–365.

Motomura, K., M. Oikawa, M. Hirose, A. Honda, S. Togayachi, H. Miyoshi, Y. Ohinata, M. Sugimoto, K. Abe, K. Inoue, and A. Ogura

2016. Cellular Dynamics of Mouse Trophoblast Stem Cells: Identification of a Persistent Stem Cell Type1. *Biology of Reproduction*, 94(6):1–14.

Mou, H., J. L. Smith, L. Peng, H. Yin, J. Moore, X.-O. Zhang, C.-Q. Song, A. Sheel, Q. Wu, D. M. Ozata, Y. Li, D. G. Anderson, C. P. Emerson, E. J. Sontheimer, M. J.

Moore, Z. Weng, and W. Xue

2017. CRISPR/Cas9-mediated genome editing induces exon skipping by alternative splicing or exon deletion. *Genome Biology*, 18(108):1–8.

Mueller, F., A. Senecal, K. Tantale, H. Marie-Nelly, N. Ly, O. Collin, E. Basyuk, E. Bertrand, X. Darzacq, and C. Zimmer

2013. FISH-quant: automatic counting of transcripts in 3D FISH images. *Nature Methods*, 10(4):277–278.

Muller, H. J.

1914. A factor for the fourth chromosome in Drosophila. *Science*, 39(1016):906.

Nagano, T., J. A. Mitchell, L. A. Sanz, F. M. Pauler, A. C. Ferguson-Smith, R. Feil, and P. Fraser

2008. The Air noncoding RNA epigenetically silences transcription by targeting G9a to chromatin. *Science*, 322(5908):1717–1720.

Nagy, A., E. Gócza, E. M. Diaz, V. R. Prideaux, E. Iványi, M. Markkula, and J. Rossant

1990. Embryonic stem cells alone are able to support fetal development in the mouse. *Development*, 110(3):815–821.

Nagy, A., J. Rossant, R. Nagy, W. Abramow-Newerly, and J. C. Roder

1993. Derivation of completely cell culture-derived mice from early-passage embryonic stem cells. *Proceedings of the National Academy of Sciences of the United States of America*, 90(18):8424–8428.

Nakagawa, O., M. Arnold, M. Nakagawa, H. Hamada, J. M. Shelton, H. Kusano, T. M. Harris, G. Childs, K. P. Campbell, J. A. Richardson, I. Nishino, and E. N. Olson

2005. Centronuclear myopathy in mice lacking a novel muscle-specific protein kinase transcriptionally regulated by MEF2. *Genes & Development*, 19(17):2066–2077.

Nakamura, T., Y. Yabuta, I. Okamoto, S. Aramaki, S. Yokobayashi, K. Kurimoto, K. Sekiguchi, M. Nakagawa, T. Yamamoto, and M. Saitou

2015. SC3-seq: a method for highly parallel and quantitative measurement of single-cell gene expression. *Nucleic Acids Research*, 43(9):e60–e60.

Nakayama, N., C.-y. E. Han, S. Scully, R. Nishinakamura, C. He, L. Zeni, H. Yamane, D. Chang, D. Yu, T. Yokota, and D. Wen

2001. A Novel Chordin-like Protein Inhibitor for Bone Morphogenetic Proteins Expressed Preferentially in Mesenchymal Cell Lineages. *Developmental Biology*, 232(2):372–387.

Namekawa, S. H., B. Payer, K. D. Huynh, R. Jaenisch, and J. T. Lee

2010. Two-Step Imprinted X Inactivation: Repeat versus Genic Silencing in the Mouse. *Molecular and Cellular Biology*, 30(13):3187–3205.

Naumova, A. K., M. Leppert, D. F. Barker, K. Morgan, and C. Sapienza

1998. Parental origin-dependent, male offspring-specific transmission-ratio distortion at loci on the human X chromosome. *American Journal of Human Genetics*, 62(6):1493–1499.

Navarro, P., I. Chambers, V. Karwacki-Neisius, C. Chureau, C. Morey, C. Rougeulle, and P. Avner

2008. Molecular Coupling of Xist Regulation and Pluripotency. *Science*, 321(5896):1693–1695.

Nesterova, T. B., C. E. Senner, J. Schneider, T. Alcayna-Stevens, A. Tattermusch, M. Hemberger, and N. Brockdorff

2011. Pluripotency factor binding and Tsix expression act synergistically to repress Xist in undifferentiated embryonic stem cells. *Epigenetics & Chromatin*, 4(1):17.

Nguyen, D. K. and C. M. Disteche

2006. High expression of the mammalian X chromosome in brain. *Brain Research*, 1126(1):46–49.

Nicholson, J. M., J. C. Macedo, A. J. Mattingly, D. Wangsa, J. Camps, V. Lima, A. M. Gomes, S. Dória, T. Ried, E. Logarinho, and D. Cimini

2015. Chromosome mis-segregation and cytokinesis failure in trisomic human cells. *eLife*, 4:1315.

Niu, X., T. Zhang, L. Liao, L. Zhou, D. J. Lindner, M. Zhou, B. Rini, Q. Yan, and H. Yang

2012. The von Hippel-Lindau tumor suppressor protein regulates gene expression and tumor growth through histone demethylase JARID1C. *Oncogene*, 31(6):776–786.

Niwa, H., Y. Toyooka, D. Shimosato, D. Strumpf, K. Takahashi, R. Yagi, and J. Rossant

2005. Interaction between Oct3/4 and Cdx2 Determines Trophectoderm Differentiation. *Cell*, 123(5):917–929.

Norris, D. P., N. Brockdorff, and S. Rastan

1991. Methylation status of CpG-rich islands on active and inactive mouse X chromosomes. *Mammalian Genome*, 1(2):78–83.

Nowell, C. S., N. Bredenkamp, S. Tetélin, X. Jin, C. Tischner, H. Vaidya, J. M. Sheridan, F. H. Stenhouse, R. Heussen, A. J. H. Smith, and C. C. Blackburn

2011. Foxn1 Regulates Lineage Progression in Cortical and Medullary Thymic Epithelial Cells But Is Dispensable for Medullary Sublineage Divergence. *PLoS Genetics*, 7(11):e1002348–16.

Odorisio, T., T. A. Rodriguez, E. P. Evans, A. R. Clarke, and P. S. Burgoyne

1998. The meiotic checkpoint monitoring synapsis eliminates spermatocytes via p53-independent apoptosis. *Nature Genetics*, 18(3):257–261.

Ohno, S. and T. S. Hauschka

1960. Allocycly of the X-chromosome in tumors and normal tissues. *Cancer Research*, 20:541–545.

Okamoto, I., D. Arnaud, P. Le Baccon, A. P. Otte, C. M. Disteche, P. Avner, and E. Heard

2005. Evidence for de novo imprinted X-chromosome inactivation independent of meiotic inactivation in mice. *Nature*, 438(7066):369–373.

Okamoto, I., A. P. Otte, C. D. Allis, D. Reinberg, and E. Heard

2004. Epigenetic dynamics of imprinted X inactivation during early mouse development. *Science*, 303(5658):644–649.

Okamoto, I., C. Patrat, D. Thépot, N. Peynot, P. Fauque, N. Daniel, P. Diabangouaya, J.-P. Wolf, J.-P. Renard, V. Duranthon, and E. Heard

2011. Eutherian mammals use diverse strategies to initiate X-chromosome inactivation during development. *Nature*, 472(7343):370–374.

Okamoto, I., S. Tan, and N. Takagi

2000. X-chromosome inactivation in XX androgenetic mouse embryos surviving implantation. *Development*, 127(19):4137–4145.

Ooi, S. K., D. Wolf, O. Hartung, S. Agarwal, G. Q. Daley, S. P. Goff, and T. H. Bestor

2010. Dynamic instability of genomic methylation patterns in pluripotent stem cells. *Epigenetics & Chromatin*, 3(1):17.

Otter, M., C. T. Schrander-Stumpel, and L. M. Curfs

2009. Triple X syndrome: a review of the literature. *European Journal of Human Genetics*, 18(3):265–271.

Õunap, K., H. Puusepp-Benazzouz, M. Peters, U. Vaher, R. Rein, A. Proos, M. Field, and T. Reimand

2012. A novel c.2T > C mutation of the KDM5C/JARID1C gene in one large family with X-linked intellectual disability. *European Journal of Medical Genetics*, 55(3):178–184.

Owsianka, A. M. and A. H. Patel

1999. Hepatitis C virus core protein interacts with a human DEAD box protein DDX3. *Virology*, 257(2):330–340.

Pal Bhadra, M.

2005. Gene Expression Analysis of the Function of the Male-Specific Lethal Complex in Drosophila. *Genetics*, 169(4):2061–2074.

Palmer, S., J. Perry, D. Kipling, and A. Ashworth

1997. A gene spans the pseudoautosomal boundary in mice. *Proceedings of the National Academy of Sciences of the United States of America*, 94(22):12030–12035.

Park, C., L. Carrel, and K. D. Makova

2010. Strong purifying selection at genes escaping X chromosome inactivation. *Molecular Biology and Evolution*, 27(11):2446–2450.

Park, S. H., S. G. Lee, Y. Kim, and K. Song

1998. Assignment of a human putative RNA helicase gene, DDX3, to human X chromosome bands p11.3–>p11.23. *Cytogenetics and Cell Genetics*, 81(3-4):178–179.

Park, S. H., Y. K. Shin, Y. H. Suh, W. S. Park, Y. L. Ban, H.-S. Choi, H. J. Park, and K. C. Jung

2005. Rapid divergency of rodent CD99 orthologs: implications for the evolution of the pseudoautosomal region. *Gene*, 353(2):177–188.

Passerini, V., E. Ozeri-Galai, M. S. de Pagter, N. Donnelly, S. Schmalbrock, W. P. Kloosterman, B. Kerem, and Z. S. aacute

2016. The presence of extra chromosomes leads to genomic instability. *Nature Communications*, 7:1–12.

Patrat, C., I. Okamoto, P. Diabangouaya, V. Vialon, P. Le Baccon, J. Chow, and E. Heard

2009. Dynamic changes in paternal X-chromosome activity during imprinted

X-chromosome inactivation in mice. *Proceedings of the National Academy of Sciences of the United States of America*, 106(13):5198–5203.

Patro, R., G. Duggal, M. I. Love, R. A. Irizarry, and C. Kingsford

2017. Salmon provides fast and bias-aware quantification of transcript expression. *Nature Methods*, 14(4):417–419.

Payer, B.

2016. Developmental regulation of X-chromosome inactivation. *Seminars in Cell & Developmental Biology*, 56:88–99.

Payer, B., M. Rosenberg, M. Yamaji, Y. Yabuta, M. Koyanagi-Aoi, K. Hayashi, S. Yamanaka, M. Saitou, and J. T. Lee

2013. Tsix RNA and the germline factor, PRDM14, link X reactivation and stem cell reprogramming. *Molecular Cell*, 52(6):805–818.

Peng, Y., J. Suryadi, Y. Yang, T. G. Kucukkal, W. Cao, and E. Alexov

2015. Mutations in the KDM5C ARID Domain and Their Plausible Association with Syndromic Claes-Jensen-Type Disease. *International Journal of Molecular Sciences*, 16(11):27270–27287.

Perinchery, G., M. Sasaki, A. Angan, V. Kumar, P. Carroll, and R. Dahiya

2000. Deletion of Y-chromosome specific genes in human prostate cancer. *The Journal of Urology*, 163(4):1339–1342.

Pessia, E., T. Makino, M. Bailly-Bechet, A. McLysaght, and G. A. B. Marais

2012. Mammalian X chromosome inactivation evolved as a dosage-compensation mechanism for dosage-sensitive genes on the X chromosome. *Proceedings of the National Academy of Sciences of the United States of America*, 109(14):5346–5351.

Petropoulos, S., D. Edsgärd, B. Reinius, Q. Deng, S. P. Panula, S. Codeluppi, A. P. Reyes, S. Linnarsson, R. Sandberg, and F. Lanner

2016. Single-Cell RNA-Seq Reveals Lineage and X Chromosome Dynamics in Human Preimplantation Embryos. *Cell*, 165(4):1–33.

Pfeifer, G. P., S. D. Steigerwald, R. S. Hansen, S. M. Gartler, and A. D. Riggs
1990a. Polymerase chain reaction-aided genomic sequencing of an X chromosome-linked CpG island: methylation patterns suggest clonal inheritance, CpG site autonomy, and an explanation of activity state stability. *Proceedings of the National Academy of Sciences of the United States of America*, 87(21):8252–8256.

Pfeifer, G. P., R. L. Tanguay, S. D. Steigerwald, and A. D. Riggs
1990b. In vivo footprint and methylation analysis by PCR-aided genomic sequencing: comparison of active and inactive X chromosomal DNA at the CpG island and promoter of human PGK-1. *Genes & Development*, 4(8):1277–1287.

Phillips, R. J. and M. H. Kaufman
1974. Bare-patches, a new sex-linked gene in the mouse, associated with a high production of XO females: II. Investigations into the nature and mechanism of the XO production. *Genetical Research*, 24(1):27–41.

Pimentel, H., N. L. Bray, S. Puente, P. Melsted, and L. Pachter
2017. Differential analysis of RNA-seq incorporating quantification uncertainty. *Nature Methods*, 14(7):687–690.

Plass, C., S. M. Pfister, A. M. Lindroth, O. Bogatyrova, R. Claus, and P. Lichter
2013. Mutations in regulators of the epigenome and their connections to global chromatin patterns in cancer. *Nature Reviews Genetics*, 14(11):765–780.

Plath, K., J. Fang, S. K. Mlynarczyk-Evans, R. Cao, K. A. Worringer, H. Wang, C. C. de la Cruz, A. P. Otte, B. Panning, and Y. Zhang
2003. Role of histone H3 lysine 27 methylation in X inactivation. *Science*, 300(5616):131–135.

Poupon, V., B. Bègue, J. Gagnon, A. Dautry-Varsat, N. Cerf-Bensussan, and A. Benmerah
1999. Molecular cloning and characterization of MT-ACT48, a novel mi-

tochondrial acyl-CoA thioesterase. *The Journal of Biological Chemistry*, 274(27):19188–19194.

Power, M. A. and P. P. L. Tam

1993. Onset of gastrulation, morphogenesis and somitogenesis in mouse embryos displaying compensatory growth. *Anatomy and Embryology*, 187(5):493–504.

Priolo, M., L. Micale, B. Augello, C. Fusco, F. Zucchetti, P. Prontera, V. Paduano, E. Biamino, A. Selicorni, C. Mammì, C. Laganà, L. Zelante, and G. Merla

2012. Absence of deletion and duplication of MLL2 and KDM6A genes in a large cohort of patients with Kabuki syndrome. *Molecular Genetics and Metabolism*, 107(3):627–629.

Prudhomme, J., A. Dubois, P. Navarro, D. Arnaud, P. Avner, and C. Morey

2015. A rapid passage through a two-active-X-chromosome state accompanies the switch of imprinted X-inactivation patterns in mouse trophoblast stem cells. *Epigenetics & Chromatin*, 8(1):52.

Prudhomme, J. and C. Morey

2015. Epigenesis and plasticity of mouse trophoblast stem cells. *Cellular and Molecular Life Sciences*, 73(4):757–774.

Prykhozhij, S. V., S. L. Steele, B. Razaghi, and J. N. Berman

2017. A rapid and effective method for screening, sequencing and reporter verification of engineered frameshift mutations in zebrafish. *Disease Models & Mechanisms*, 10(6):811–822.

Pugh, T. J., S. D. Weeraratne, T. C. Archer, D. A. P. Krummel, D. Auclair, J. Bochicchio, M. O. Carneiro, S. L. Carter, K. Cibulskis, R. L. Erlich, H. Greulich, M. S. Lawrence, N. J. Lennon, A. McKenna, J. Meldrim, A. H. Ramos, M. G. Ross, C. Russ, E. Shefler, A. Sivachenko, B. Sogoloff, P. Stojanov, P. Tamayo, J. P. Mesirov, V. Amani, N. Teider, S. Sengupta, J. P. Francois, P. A. Northcott, M. D. Taylor, F. Yu, G. R. Crabtree, A. G. Kautzman, S. B. Gabriel, G. Getz, N. Jäger, D. T. W. Jones, P. Lichter, S. M. Pfister, T. M. Roberts, M. Meyerson, S. L.

Pomeroy, and Y.-J. Cho

2012. Medulloblastoma exome sequencing uncovers subtype-specific somatic mutations. *Nature*, 488(7409):106–110.

Radford, E. J., S. R. Ferrón, and A. C. Ferguson-Smith

2011. Genomic imprinting as an adaptative model of developmental plasticity. *FEBS Letters*, 585(13):2059–2066.

Raefski, A. S. and M. J. O'Neill

2005. Identification of a cluster of X-linked imprinted genes in mice. *Nature Genetics*, 37(6):620–624.

Ramathal, C., B. Angulo, M. Sukhwani, J. Cui, J. Durruthy-Durruthy, F. Fang, P. Schanes, P. J. Turek, K. E. Orwig, and R. R. Pera

2015. DDX3Y gene rescue of a Y chromosome AZFa deletion restores germ cell formation and transcriptional programs. *Scientific Reports*, 5:1–13.

Ran, F. A., P. D. Hsu, J. Wright, V. Agarwala, D. A. Scott, and F. Zhang

2013. Genome engineering using the CRISPR-Cas9 system. *Nature Protocols*, 8(11):2281–2308.

Ranke, M. B. and P. Saenger

2001. Turner's syndrome. *The Lancet*, 358(9278):309–314.

Rao, E., R. J. Blaschke, A. Marchini, B. Niesler, M. Burnett, and G. A. Rappold

2001. The Leri-Weill and Turner syndrome homeobox gene SHOX encodes a cell-type specific transcriptional activator. *Human Molecular Genetics*, 10(26):3083–3091.

Rao, E., B. Weiss, M. Fukami, A. Rump, B. Niesler, A. Mertz, K. Muroya, G. Binder, S. Kirsch, M. Winkelmann, G. Nordsiek, U. Heinrich, M. H. Breuning, M. B. Ranke, A. Rosenthal, T. Ogata, and G. A. Rappold

1997. Pseudoautosomal deletions encompassing a novel homeobox gene cause growth failure in idiopathic short stature and Turner syndrome. *Nature Genetics*, 16(1):54–63.

Rastan, S.

1982. Timing of X-chromosome inactivation in postimplantation mouse embryos. *Journal of Embryology and Experimental Morphology*, 71:11–24.

Rebuzzini, P., T. Neri, G. Mazzini, M. Zuccotti, C. A. Redi, and S. Garagna

2008. Karyotype analysis of the euploid cell population of a mouse embryonic stem cell line revealed a high incidence of chromosome abnormalities that varied during culture. *Cytogenetic and Genome Research*, 121(1):18–24.

Rebuzzini, P., M. Zuccotti, C. A. Redi, and S. Garagna

2016. Chromosomal Abnormalities in Embryonic and Somatic Stem Cells. *Cytogenetic and Genome Research*, 147(1):1–9.

Reik, W., M. Constancia, A. Fowden, N. Anderson, W. Dean, A. Ferguson-Smith, B. Tycko, and C. Sibley

2003. Regulation of supply and demand for maternal nutrients in mammals by imprinted genes. *The Journal of Physiology*, 547(1):35–44.

Reinius, B., M. M. Johansson, K. J. Radomska, E. H. Morrow, G. K. Pandey, C. Kanduri, R. Sandberg, R. W. Williams, and E. Jazin

2012. Abundance of female-biased and paucity of male-biased somatically expressed genes on the mouse X-chromosome. *BMC Genomics*, 13(1):607.

Renfree, M. B., S. Suzuki, and T. Kaneko-Ishino

2013. The origin and evolution of genomic imprinting and viviparity in mammals. *Philosophical transactions of the Royal Society of London. Series B, Biological sciences*, 368(1609):20120151–20120151.

Richardson, B. J., A. B. Czuppon, and G. B. Sharman

1971. Inheritance of glucose-6-phosphate dehydrogenase variation in kangaroos. *Nature: New Biology*, 230(13):154–155.

Riddell, S. R., M. Murata, S. Bryant, and E. H. Warren

2002. Minor histocompatibility antigens–targets of graft versus leukemia responses. *International Journal of Hematology*, 76 Suppl 2:155–161.

Ritchie, M. E., B. Phipson, D. Wu, Y. Hu, C. W. Law, W. Shi, and G. K. Smyth
2015. limma powers differential expression analyses for RNA-sequencing and microarray studies. *Nucleic Acids Research*, 43(7):e47–e47.

Robertson, E. J., M. J. Evans, and M. H. Kaufman
1983. X-chromosome instability in pluripotential stem cell lines derived from parthenogenetic embryos. *Journal of Embryology and Experimental Morphology*, 74:297–309.

Robinson, G., M. Parker, T. A. Kranenburg, C. Lu, X. Chen, L. Ding, T. N. Phoenix, E. Hedlund, L. Wei, X. Zhu, N. Chalhoub, S. J. Baker, R. Huether, R. Kriwacki, N. Curley, R. Thiruvenkatam, J. Wang, G. Wu, M. Rusch, X. Hong, J. Becksfort, P. Gupta, J. Ma, J. Easton, B. Vadodaria, A. Onar-Thomas, T. Lin, S. Li, S. Pounds, S. Paugh, D. Zhao, D. Kawauchi, M. F. Roussel, D. Finkelstein, D. W. Ellison, C. C. Lau, E. Bouffet, T. Hassall, S. Gururangan, R. Cohn, R. S. Fulton, L. L. Fulton, D. J. Dooling, K. Ochoa, A. Gajjar, E. R. Mardis, R. K. Wilson, J. R. Downing, J. Zhang, and R. J. Gilbertson
2012. Novel mutations target distinct subgroups of medulloblastoma. *Nature*, 488(7409):43–48.

Robles Valdés, C., V. del Castillo Ruiz, J. Oyoqui, N. Altamirano Bustamante, M. de la Luz Ruiz Reyes, and R. Calzada León
2003. Growth, growth velocity and adult height in Mexican girls with Turner's syndrome. *Journal of Pediatric Endocrinology & Metabolism*, 16(8):1165–1173.

Rodriguez, T. A., D. B. Sparrow, A. N. Scott, S. L. Withington, J. I. Preis, J. Michalicek, M. Clements, T. E. Tsang, T. Shioda, R. S. P. Beddington, and S. L. Dunwoodie
2004. Cited1 is required in trophoblasts for placental development and for embryo growth and survival. *Molecular and Cellular Biology*, 24(1):228–244.

Roeleveld, N., G. A. Zielhuis, and F. Gabreëls

1997. The prevalence of mental retardation: a critical review of recent literature. *Developmental Medicine and Child Neurology*, 39(2):125–132.

Ross, J. L., C. Scott, P. Marttila, K. Kowal, A. Nass, P. Papenhausen, J. Abboudi, L. Osterman, H. Kushner, P. Carter, M. Ezaki, F. Elder, F. Wei, H. Chen, and A. R. Zinn

2001. Phenotypes Associated with SHOX Deficiency. *The Journal of Clinical Endocrinology and Metabolism*, 86(12):5674–5680.

Ross, M. T., D. V. Grafham, A. J. Coffey, S. Scherer, K. McLay, D. Muzny, M. Platzer, G. R. Howell, C. Burrows, and C. P. Bird

2005. The DNA sequence of the human X chromosome. *Nature*, 434(7031):325–337.

Rossant, J. and J. C. Cross

2001. Placental development: lessons from mouse mutants. *Nature Reviews Genetics*, 2(7):538–548.

Rossant, J., J. P. Sanford, V. M. Chapman, and G. K. Andrews

1986. Undermethylation of structural gene sequences in extraembryonic lineages of the mouse. *Developmental Biology*, 117(2):567–573.

Rovescalli, A. C., S. Asoh, and M. Nirenberg

1996. Cloning and characterization of four murine homeobox genes. *Proceedings of the National Academy of Sciences of the United States of America*, 93(20):10691–10696.

Royo, H., G. Polikiewicz, S. K. Mahadevaiah, H. Prosser, M. Mitchell, A. Bradley, D. G. de Rooij, P. S. Burgoyne, and J. M. A. Turner

2010. Evidence that meiotic sex chromosome inactivation is essential for male fertility. *Current Biology*, 20(23):2117–2123.

Rozen, S., H. Skaletsky, J. D. Marszalek, P. J. Minx, H. S. Cordum, R. H. Waterston, R. K. Wilson, and D. C. Page

2003. Abundant gene conversion between arms of palindromes in human and ape Y chromosomes. *Nature*, 423(6942):873–876.

Rugarli, E. I., D. A. Adler, G. Borsani, K. Tsuchiya, B. Franco, X. Hauge, C. Disteche, V. Chapman, and A. Ballabio

1995. Different chromosomal localization of the Clcn4 gene in Mus spretus and C57BL/6J mice. *Nature Genetics*, 10(4):466–471.

Rujirabanjerd, S., J. Nelson, P. S. Tarpey, A. Hackett, S. Edkins, F. L. Raymond, C. E. Schwartz, G. Turner, S. Iwase, Y. Shi, P. A. Futreal, M. R. Stratton, and J. Gecz

2010. Identification and characterization of two novel JARID1C mutations: suggestion of an emerging genotype-phenotype correlation. *European Journal of Human Genetics : EJHG*, 18(3):330–335.

Russell, L. B.

1961. Genetics of mammalian sex chromosomes. *Science*, 133(3467):1795–1803.

Sado, T., M. H. Fenner, S.-S. Tan, P. Tam, T. Shioda, and E. Li

2000. X Inactivation in the Mouse Embryo Deficient for Dnmt1: Distinct Effect of Hypomethylation on Imprinted and Random X Inactivation. *Developmental Biology*, 225(2):294–303.

Sado, T., Y. Hoki, and H. Sasaki

2006. Tsix defective in splicing is competent to establish Xist silencing. *Development*, 133(24):4925–4931.

Sado, T., Z. Wang, H. Sasaki, and E. LI

2001. Regulation of imprinted X-chromosome inactivation in mice by Tsix. *Development*, 128(8):1275–1286.

Sakaue, M., H. Ohta, Y. Kumaki, M. Oda, Y. Sakaide, C. Matsuoka, A. Yamagiwa, H. Niwa, T. Wakayama, and M. Okano
2010. DNA Methylation Is Dispensable for the Growth and Survival of the Extraembryonic Lineages. *Current Biology*, 20(16):1452–1457.

Saldarriaga, W., H. Andrés García-Perdomo, J. Arango-Pineda, and J. Fonseca
2015. Karyotype versus genomic hybridization for the prenatal diagnosis of chromosomal abnormalities: a metaanalysis. *The American Journal of Obstetrics & Gynecology*, 212(3):330.e1–330.e10.

Samal, S. K., S. Routray, G. K. Veeramachaneni, R. Dash, and M. Botlagunta
2015. Ketorolac salt is a newly discovered DDX3 inhibitor to treat oral cancer. *Scientific Reports*, 5:9982.

Sanger, R., P. Tippett, J. Gavin, P. Teesdale, and G. L. Daniels
1977. Xg groups and sex chromosome abnormalities in people of northern European ancestry: an addendum. *Journal of Medical Genetics*, 14(3):210–211.

Sangrithi, M. N., H. Royo, S. K. Mahadevaiah, O. Ojarikre, L. Bhaw, A. Sesay, A. H. F. M. Peters, M. Stadler, and J. M. A. Turner
2017. Non-Canonical and Sexually Dimorphic X Dosage Compensation States in the Mouse and Human Germline. *Developmental Cell*, 40(3):289–301.e3.

Santos, C., L. Rodriguez-Revenga, I. Madrigal, C. Badenas, M. Pineda, and M. Milà
2006. A novel mutation in JARID1C gene associated with mental retardation. *European Journal of Human Genetics*, 14(5):583–586.

Santos-Reboucas, C. B., N. Fintelman-Rodrigues, L. R. Jensen, A. W. Kuss, M. G. Ribeiro, M. Campos, Jr, J. M. Santos, and M. M. G. Pimentel
2011. A novel nonsense mutation in KDM5C/JARID1C gene causing intellectual disability, short stature and speech delay. *Neuroscience Letters*, 498(1):67–71.

Schaefer, K. A., W.-H. Wu, D. F. Colgan, S. H. Tsang, A. G. Bassuk, and V. B. Mahajan

2017. Unexpected mutations after CRISPR–Cas9 editing in vivo. *Nature Methods*, 14(6):1–2.

Schoeftner, S., A. K. Sengupta, S. Kubicek, K. Mechtler, L. Spahn, H. Koseki, T. Jenuwein, and A. Wutz

2006. Recruitment of PRC1 function at the initiation of X inactivation independent of PRC2 and silencing. *The EMBO Journal*, 25(13):3110–3122.

Schultz, M. D., Y. He, J. W. Whitaker, M. Hariharan, E. A. Mukamel, D. Leung, N. Rajagopal, J. R. Nery, M. A. Urich, H. Chen, S. Lin, Y. Lin, I. Jung, A. D. Schmitt, S. Selvaraj, B. Ren, T. J. Sejnowski, W. Wang, and J. R. Ecker

2015. Human body epigenome maps reveal noncanonical DNA methylation variation. *Nature*, 523(7559):212–216.

Schulz, E. G., J. Meisig, T. Nakamura, I. Okamoto, A. Sieber, C. Picard, M. Borensztein, M. Saitou, N. Blüthgen, and E. Heard

2014. The two active X chromosomes in female ESCs block exit from the pluripotent state by modulating the ESC signaling network. *Cell Stem Cell*, 14(2):203–216.

Scott, D. M., I. E. Ehrmann, P. S. Ellis, C. E. Bishop, A. I. Agulnik, E. Simpson, and M. J. Mitchell

1995. Identification of a mouse male-specific transplantation antigen, H-Y. *Nature*, 376(6542):695–698.

Scott, I. C., L. Anson-Cartwright, P. Riley, D. Reda, and J. C. Cross

2000. The HAND1 Basic Helix-Loop-Helix Transcription Factor Regulates Trophoblast Differentiation via Multiple Mechanisms. *Molecular and Cellular Biology*, 20(2):530–541.

Sekiguchi, T., H. Iida, J. Fukumura, and T. Nishimoto

2004. Human DDX3Y, the Y-encoded isoform of RNA helicase DDX3, rescues

a hamster temperature-sensitive ET24 mutant cell line with a DDX3X mutation. *Experimental Cell Research*, 300(1):213–222.

Sekiguchi, T., Y. Kurihara, and J. Fukumura

2007. Phosphorylation of threonine 204 of DEAD-box RNA helicase DDX3 by cyclin B/cdc2 in vitro. *Biochemical and Biophysical Research Communications*, 356(3):668–673.

Semina, E. V., R. S. Reiter, and J. C. Murray

1998. A new human homeobox gene OGI2X is a member of the most conserved homeobox gene family and is expressed during heart development in mouse. *Human Molecular Genetics*, 7(3):415–422.

Sengoku, T. and S. Yokoyama

2011. Structural basis for histone H3 Lys 27 demethylation by UTX/KDM6A. *Genes & Development*, 25(21):2266–2277.

Senner, C. E., F. Krueger, D. Oxley, S. Andrews, and M. Hemberger

2012. DNA methylation profiles define stem cell identity and reveal a tight embryonic-extraembryonic lineage boundary. *Stem Cells*, 30(12):2732–2745.

Shao, C. and N. Takagi

1990. An extra maternally derived X chromosome is deleterious to early mouse development. *Development*, 110(3):969–975.

Sharma, D. and J. Bhattacharya

2010. Evolutionary Constraints Acting on DDX3X Protein Potentially Interferes with Rev-Mediated Nuclear Export of HIV-1 RNA. *PLoS ONE*, 5(3):e9613.

Sharman, G. B.

1971. Late DNA replication in the paternally derived X chromosome of female kangaroos. *Nature*, 230(5291):231–232.

Sheardown, S., D. Norris, A. Fisher, and N. Brockdorff

1996. The mouse Smcx gene exhibits developmental and tissue specific variation

in degree of escape from X inactivation. *Human Molecular Genetics*, 5(9):1355–1360.

Shi, W., J. A. J. M. van den Hurk, V. Alamo-Bethencourt, W. Mayer, H. J. Winkens, H.-H. Ropers, F. P. M. Cremers, and R. Fundele
2004. Choroideremia gene product affects trophoblast development and vascularization in mouse extra-embryonic tissues. *Developmental Biology*, 272(1):53–65.

Shi, X., T. Hong, K. L. Walter, M. Ewalt, E. Michishita, T. Hung, D. Carney, P. Peña, F. Lan, M. R. Kaadige, N. Lacoste, C. Cayrou, F. Davrazou, A. Saha, B. R. Cairns, D. E. Ayer, T. G. Kutateladze, Y. Shi, J. Côté, K. F. Chua, and O. Gozani
2006. ING2 PHD domain links histone H3 lysine 4 methylation to active gene repression. *Nature*, 442(7098):96–99.

Shibata, S. and J. T. Lee
2004. Tsix Transcription- versus RNA-Based Mechanisms in Xist Repression and Epigenetic Choice. *Current Biology*, 14(19):1747–1754.

Shih, J.-W., T.-Y. Tsai, C.-H. Chao, and Y.-H. Wu Lee
2008. Candidate tumor suppressor DDX3 RNA helicase specifically represses cap-dependent translation by acting as an eIF4E inhibitory protein. *Oncogene*, 27(5):700–714.

Shin, J., M. Bossenz, Y. Chung, H. Ma, M. Byron, N. Taniguchi-Ishigaki, X. Zhu, B. Jiao, L. L. Hall, M. R. Green, S. N. Jones, I. Hermans-Borgmeyer, J. B. Lawrence, and I. Bach
2010. Maternal Rnf12/RLIM is required for imprinted X-chromosome inactivation in mice. *Nature*, 467(7318):977–981.

Shin, J., M. C. Wallingford, J. Gallant, C. Marcho, B. Jiao, M. Byron, M. Bossenz, J. B. Lawrence, S. N. Jones, J. Mager, and I. Bach
2014. RLIM is dispensable for X-chromosome inactivation in the mouse embryonic epiblast. *Nature*, 511(7507):1–10.

Shpargel, K. B., T. Sengoku, S. Yokoyama, and T. Magnuson
2012. UTX and UTY Demonstrate Histone Demethylase-Independent Function in Mouse Embryonic Development. *PLoS Genetics*, 8(9):e1002964.

Silva, J., W. Mak, I. Zvetkova, R. Appanah, T. B. Nesterova, Z. Webster, A. H. F. M. Peters, T. Jenuwein, A. P. Otte, and N. Brockdorff
2003. Establishment of histone h3 methylation on the inactive X chromosome requires transient recruitment of Eed-Enx1 polycomb group complexes. *Developmental Cell*, 4(4):481–495.

Simmons, D. G., A. L. Fortier, and J. C. Cross
2007. Diverse subtypes and developmental origins of trophoblast giant cells in the mouse placenta. *Developmental Biology*, 304(2):567–578.

Simmons, D. G., D. R. C. Natale, V. Begay, M. Hughes, A. Leutz, and J. C. Cross
2008. Early patterning of the chorion leads to the trilaminar trophoblast cell structure in the placental labyrinth. *Development*, 135(12):2083–2091.

Simon, M. D., S. F. Pinter, R. Fang, K. Sarma, M. Rutenberg-Schoenberg, S. K. Bowman, B. A. Kesner, V. K. Maier, R. E. Kingston, and J. T. Lee
2014. High-resolution Xist binding maps reveal two-step spreading during X-chromosome inactivation. *Nature*, 504(7480):465–469.

Simpson, A. J. G., O. L. Caballero, A. Jungbluth, Y.-T. Chen, and L. J. Old
2005. Cancer/testis antigens, gametogenesis and cancer. *Nature Reviews Cancer*, 5(8):615–625.

Simpson, E.
1986. The HY antigen and sex reversal. *Cell*, 44(6):813–814.

Simpson, E., P. Chandler, E. Goulmy, C. M. Disteche, M. A. Ferguson-Smith, and D. C. Page
1987. Separation of the genetic loci for the H-Y antigen and for testis determination on human Y chromosome. *Nature*, 326(6116):876–878.

Sinclair, A., P. Berta, M. Palmer, J. Hawkins, B. Griffiths, and M. S. Palmer
1990. A gene from the human sex-determining region encodes a protein with. *Nature*, 346(6281):240–244.

Skaletsky, H., T. Kuroda-Kawaguchi, P. J. Minx, H. S. Cordum, L. Hillier, L. G. Brown, S. Repping, T. Pyntikova, J. Ali, T. Bieri, A. Chinwalla, A. Delehaunty, K. Delehaunty, H. Du, G. Fewell, L. Fulton, R. Fulton, T. Graves, S.-F. Hou, P. Latrielle, S. Leonard, E. Mardis, R. Maupin, J. McPherson, T. Miner, W. Nash, C. Nguyen, P. Ozersky, K. Pepin, S. Rock, T. Rohlfing, K. Scott, B. Schultz, C. Strong, A. Tin-Wollam, S.-P. Yang, R. H. Waterston, R. K. Wilson, S. Rozen, and D. C. Page
2003. The male-specific region of the human Y chromosome is a mosaic of discrete sequence classes. *Nature*, 423(6942):825–837.

Skuse, D. H., R. S. James, D. V. Bishop, B. Coppin, P. Dalton, G. Aamodt-Leeper, M. Bacarese-Hamilton, C. Creswell, R. McGurk, and P. A. Jacobs
1997. Evidence from Turner's syndrome of an imprinted X-linked locus affecting cognitive function. *Nature*, 387(6634):705–708.

Slavney, A., L. Arbiza, A. G. Clark, and A. Keinan
2016. Strong Constraint on Human Genes Escaping X-Inactivation Is Modulated by their Expression Level and Breadth in Both Sexes. *Molecular Biology and Evolution*, 33(2):384–393.

Smith, E. Y., C. R. Futtner, S. J. Chamberlain, K. A. Johnstone, and J. L. Resnick
2011. Transcription Is Required to Establish Maternal Imprinting at the Prader-Willi Syndrome and Angelman Syndrome Locus. *PLoS Genetics*, 7(12):e1002422.

Soejima, H. and K. Higashimoto
2013. Epigenetic and genetic alterations of the imprinting disorder Beckwith-Wiedemann syndrome and related disorders. *Journal of Human Genetics*, 58(7):402–409.

Soh, Y. Q. S., J. Alföldi, T. Pyntikova, L. G. Brown, T. Graves, P. J. Minx, R. S. Fulton, C. Kremitzki, N. Koutseva, J. L. Mueller, S. Rozen, J. F. Hughes, E. Owens, J. E. Womack, W. J. Murphy, Q. Cao, P. de Jong, W. C. Warren, R. K. Wilson, H. Skaletsky, and D. C. Page

2014. Sequencing the Mouse Y Chromosome Reveals Convergent Gene Acquisition and Amplification on Both Sex Chromosomes. *Cell*, 159(4):800–813.

Solari, A. J.

1974. The behavior of the XY pair in mammals. *International Review of Cytology*, 38(0):273–317.

Soma, M., Y. Fujihara, M. Okabe, F. Ishino, and S. Kobayashi

2014. Ftx is dispensable for imprinted X-chromosome inactivation in preimplantation mouse embryos. *Scientific Reports*, 4:5181.

Soneson, C., M. I. Love, and M. D. Robinson

2015. Differential analyses for RNA-seq: transcript-level estimates improve gene-level inferences. *F1000 Research*, 4:1521–19.

Soulat, D., T. Bürckstümmer, S. Westermayer, A. Goncalves, A. Bauch, A. Stefanovic, O. Hantschel, K. L. Bennett, T. Decker, and G. Superti-Furga

2008. The DEAD-box helicase DDX3X is a critical component of the TANK-binding kinase 1-dependent innate immune response. *The EMBO Journal*, 27(15):2135–2146.

Stavropoulos, N., N. Lu, and J. T. Lee

2001. A functional role for Tsix transcription in blocking Xist RNA accumulation but not in X-chromosome choice. *Proceedings of the National Academy of Sciences of the United States of America*, 98(18):10232–10237.

Stern, C.

1957. The Problem of Complete Y-Linkage in Man. *American Journal of Human Genetics*, 9(3):147–166.

Stransky, N., A. M. Egloff, A. D. Tward, A. D. Kostic, K. Cibulskis, A. Sivachenko, G. V. Kryukov, M. S. Lawrence, C. Sougnez, A. McKenna, E. Shefler, A. H. Ramos, P. Stojanov, S. L. Carter, D. Voet, M. L. Cortés, D. Auclair, M. F. Berger, G. Saksena, C. Guiducci, R. C. Onofrio, M. Parkin, M. Romkes, J. L. Weissfeld, R. R. Seethala, L. Wang, C. Rangel-Escareño, J. C. Fernandez-Lopez, A. Hidalgo-Miranda, J. Melendez-Zajgla, W. Winckler, K. Ardlie, S. B. Gabriel, M. Meyerson, E. S. Lander, G. Getz, T. R. Golub, L. A. Garraway, and J. R. Grandis

2011. The mutational landscape of head and neck squamous cell carcinoma. *Science*, 333(6046):1157–1160.

Su, C.-Y., T.-C. Lin, Y.-F. Lin, M.-H. Chen, C.-H. Lee, H.-Y. Wang, Y.-C. Lee, Y.-P. Liu, C.-L. Chen, and M. Hsiao

2015. DDX3 as a strongest prognosis marker and its downregulation promotes metastasis in colorectal cancer. *Oncotarget*, 6(21):18602–18612.

Sugawara, A., K. Goto, Y. Sotomaru, T. Sofuni, and T. Ito

2006. Current status of chromosomal abnormalities in mouse embryonic stem cell lines used in Japan. *Comparative medicine*, 56(1):31–34.

Sugawara, O., N. Takagi, and M. Sasaki

1983. Allocyclic early replicating X chromosome in mice: Genetic inactivity and shift into a late replicator in early embryogenesis. *Chromosoma*, 88(2):133–138.

Sun, C., C. T. Pager, G. Luo, P. Sarnow, and J. H. D. Cate

2010. Hepatitis C Virus Core-Derived Peptides Inhibit Genotype 1b Viral Genome Replication via Interaction with DDX3X. *PLoS ONE*, 5(9):e12826.

Sun, M., L. Song, Y. Li, T. Zhou, and R. S. Jope

2008. Identification of an antiapoptotic protein complex at death receptors. *Cell death and differentiation*, 15(12):1887–1900.

Sun, M., T. Zhou, E. Jonasch, and R. S. Jope

2013a. Biochimica et Biophysica Acta. *BBA - Molecular Cell Research*, 1833(6):1489–1497.

Sun, S., B. C. Del Rosario, A. Szanto, Y. Ogawa, Y. Jeon, and J. T. Lee

2013b. Jpx RNA Activates Xist by Evicting CTCF. *Cell*, 153(7):1537–1551.

Sun, S., B. Payer, S. Namekawa, J. Y. An, W. Press, J. Catalan-Dibene, H. Sunwoo, and J. T. Lee

2015. Xist imprinting is promoted by the hemizygous (unpaired) state in the male germ line. *Proceedings of the National Academy of Sciences of the United States of America*, 112(47):14415–14422.

Surani, M. A. and S. C. Barton

1983. Development of gynogenetic eggs in the mouse: implications for parthenogenetic embryos. *Science*, 222(4627):1034–1036.

Surani, M. A., S. C. Barton, and M. L. Norris

1984. Development of reconstituted mouse eggs suggests imprinting of the genome during gametogenesis. *Nature*, 308(5959):548–550.

Tada, T., Y. Obata, M. Tada, Y. Goto, N. Nakatsuji, S. Tan, T. Kono, and N. Takagi

2000. Imprint switching for non-random X-chromosome inactivation during mouse oocyte growth. *Development*, 127(14):3101–3105.

Tahiliani, M., P. Mei, R. Fang, T. Leonor, M. Rutenberg, F. Shimizu, J. Li, A. Rao, and Y. Shi

2007. The histone H3K4 demethylase SMCX links REST target genes to X-linked mental retardation. *Nature*, 447(7144):601–605.

Takagi, N. and G. R. Martin

1984. Studies of the temporal relationship between the cytogenetic and biochemical manifestations of X-chromosome inactivation during the differentiation of LT-1 teratocarcinoma stem cells. *Developmental Biology*, 103(2):425–433.

Takagi, N. and M. Sasaki

1975. Preferential inactivation of the paternally derived X chromosome in the extraembryonic membranes of the mouse. *Nature*, 256(5519):640–642.

Takagi, N., O. Sugawara, and M. Sasaki

1982. Regional and temporal changes in the pattern of X-chromosome replication during the early post-implantation development of the female mouse. *Chromosoma*, 85(2):275–286.

Tam, P. P.

1981. The control of somitogenesis in mouse embryos. *Journal of Embryology and Experimental Morphology*, 65 Suppl:103–128.

Tam, P. P. L.

2003. Mouse embryonic chimeras: tools for studying mammalian development. *Development*, 130(25):6155–6163.

Tanaka, S., T. Kunath, A. K. Hadjantonakis, A. Nagy, and J. Rossant

1998. Promotion of trophoblast stem cell proliferation by FGF4. *Science*, 282(5396):2072–2075.

Tavares, L., E. Dimitrova, D. Oxley, J. Webster, R. Poot, J. Demmers, K. Bezstarosti, S. Taylor, H. Ura, H. Koide, A. Wutz, M. Vidal, S. Elderkin, and N. Brockdorff

2012. RYBP-PRC1 complexes mediate H2A ubiquitylation at polycomb target sites independently of PRC2 and H3K27me3. *Cell*, 148(4):664–678.

Tease, C. and B. M. Cattanach

1989. Sex chromosome pairing patterns in male mice of novel Sxr genotypes. *Chromosoma*, 97(5):390–395.

Thieme, S., T. Gyarfas, C. Richter, G. Ozhan, J. Fu, D. Alexopulou, M. H. Muders, I. Michalk, C. Jakob, A. Dahl, B. Klink, J. Bandola, M. Bachmann, E. Schrock,

F. Buchholz, A. F. Stewart, G. Weidinger, K. Anastassiadis, and S. Brenner
2013. The histone demethylase UTX regulates stem cell migration and hematopoiesis. *Blood*, 121(13):2462–2473.

Thornhill, A. R. and P. S. Burgoyne
1993. A paternally imprinted X chromosome retards the development of the early mouse embryo. *Development*, 118(1):171–174.

Tian, D., S. Sun, and J. T. Lee
2010. The long noncoding RNA, Jpx, is a molecular switch for X chromosome inactivation. *Cell*, 143(3):390–403.

Tian, G., U. Singh, Y. Yu, B. S. Ellsworth, M. Hemberger, R. Geyer, M. D. Stewart, R. R. Behringer, and R. Fundele
2008. Expression and function of the LIM homeobox containing genes Lhx3 and Lhx4 in the mouse placenta. *Developmental Dynamics*, 237(5):1517–1525.

Tie, F., R. Banerjee, P. A. Conrad, P. C. Scacheri, and P. J. Harte
2012. Histone Demethylase UTX and Chromatin Remodeler BRM Bind Directly to CBP and Modulate Acetylation of Histone H3 Lysine 27. *Molecular and Cellular Biology*, 32(12):2323–2334.

Traub, S., O. Demaria, L. Chasson, F. Serra, B. Desnues, and L. Alexopoulou
2012. Sex Bias in Susceptibility to MCMV Infection: Implication of TLR9. *PLoS ONE*, 7(9):e45171–13.

Trent, S., A. Dennehy, H. Richardson, O. A. Ojarikre, P. S. Burgoyne, T. Humby, and W. Davies
2012. Steroid sulfatase-deficient mice exhibit endophenotypes relevant to attention deficit hyperactivity disorder. *Psychoneuroendocrinology*, 37(2):221–229.

Tsai, C.-L., R. K. Rowntree, D. E. Cohen, and J. T. Lee
2008. Higher order chromatin structure at the X-inactivation center via looping DNA. *Developmental Biology*, 319(2):416–425.

Tsunoda, Y., T. Tokunaga, and T. Sugie

1985. Altered sex ratio of live young after transfer of fast- and slow-developing mouse embryos. *Molecular Reproduction and Development*, 12(3):301–304.

Tucker, K. L., C. Beard, J. Dausmann, L. Jackson-Grusby, P. W. Laird, H. Lei, E. LI, and R. Jaenisch

1996. Germ-line passage is required for establishment of methylation and expression patterns of imprinted but not of nonimprinted genes. *Genes & Development*, 10(8):1008–1020.

Tunster, S. J., A. B. Jensen, and R. M. John

2013. Imprinted genes in mouse placental development and the regulation of fetal energy stores. *Reproduction*, 145(5):R117–R137.

Turner, H. H.

1938. A syndrome of infantilism, congenital webbed neck, and cubitus valgus. *Endocrinology*, 23(5):566–574.

Turner, J. M. A.

2007. Meiotic sex chromosome inactivation. *Development*, 134(10):1823–1831.

Tybulewicz, V. L. J.

2006. New techniques to understand chromosome dosage: mouse models of aneuploidy. *Human Molecular Genetics*, 15(Review Issue 2):R103–R109.

Tzschach, A., S. Lenzner, B. Moser, R. Reinhardt, J. Chelly, J.-P. Fryns, T. Kleefstra, M. Raynaud, G. Turner, H.-H. Ropers, A. Kuss, and L. R. Jensen

2006. Novel JARID1C/SMCX mutations in patients with X-linked mental retardation. *Human Mutation*, 27(4):389–389.

Ullrich, O.

1930. Typical features and multiple malformations. *European Journal of Pediatrics*, 49:271–276.

Umlauf, D., Y. Goto, R. Cao, F. Cerqueira, A. Wagschal, Y. Zhang, and R. Feil
2004. Imprinting along the Kcnq1 domain on mouse chromosome 7 involves repressive histone methylation and recruitment of Polycomb group complexes. *Nature Genetics*, 36(12):1296–1300.

Untergasser, A., H. Nijveen, X. Rao, T. Bisseling, R. Geurts, and J. A. M. Leunissen
2007. Primer3Plus, an enhanced web interface to Primer3. *Nucleic Acids Research*, 35(Web Server issue):W71–4.

Urbach, A. and N. Benvenisty
2009. Studying Early Lethality of 45,XO (Turner's Syndrome) Embryos Using Human Embryonic Stem Cells. *PLoS ONE*, 4(1):e4175.

Vakilian, H., M. Mirzaei, M. Sharifi Tabar, P. Pooyan, L. Habibi Rezaee, L. Parker, P. A. Haynes, H. Gourabi, H. Baharvand, and G. H. Salekdeh
2015. DDX3Y, a Male-Specific Region of Y Chromosome Gene, May Modulate Neuronal Differentiation. *Journal of Proteome Research*, 14(9):150722163029001–10.

Van der Meulen, J., V. Sanghvi, K. Mavrakis, K. Durinck, F. Fang, F. Matthijssens, P. Rondou, M. Rosen, T. Pieters, P. Vandenberghe, E. Delabesse, T. Lammens, B. De Moerloose, B. Menten, N. Van Roy, B. Verhasselt, B. Poppe, Y. Benoit, T. Taghon, A. M. Melnick, F. Speleman, H.-G. Wendel, and P. Van Vlierberghe
2015. The H3K27me3 demethylase UTX is a gender-specific tumor suppressor in T-cell acute lymphoblastic leukemia. *Blood*, 125(1):13–21.

van Haaften, G., G. L. Dalgliesh, H. Davies, L. Chen, G. Bignell, C. Greenman, S. Edkins, C. Hardy, S. O'Meara, J. Teague, A. Butler, J. Hinton, C. Latimer, J. Andrews, S. Barthorpe, D. Beare, G. Buck, P. J. Campbell, J. Cole, S. Forbes, M. Jia, D. Jones, C. Y. Kok, C. Leroy, M.-L. Lin, D. J. McBride, M. Maddison, S. Maquire, K. McLay, A. Menzies, T. Mironenko, L. Mulderrig, L. Mudie, E. Pleasance, R. Shepherd, R. Smith, L. Stebbings, P. Stephens, G. Tang, P. S.

Tarpey, R. Turner, K. Turrell, J. Varian, S. West, S. Widaa, P. Wray, V. P. Collins, K. Ichimura, S. Law, J. Wong, S. T. Yuen, S. Y. Leung, G. Tonon, R. A. DePinho, Y.-T. Tai, K. C. Anderson, R. J. Kahnoski, A. Massie, S. K. Khoo, B. T. Teh, M. R. Stratton, and P. A. Futreal

2009. Somatic mutations of the histone H3K27 demethylase gene UTX in human cancer. *Nature Genetics*, 41(5):521–523.

Vandamme, J., G. Lettier, S. Sidoli, E. Di Schiavi, O. Nørregaard Jensen, and A. E. Salcini

2012. The C. elegans H3K27 Demethylase UTX-1 Is Essential for Normal Development, Independent of Its Enzymatic Activity. *PLoS Genetics*, 8(5):e1002647.

Veith, A.-M., J. Klattig, A. Dettai, C. Schmidt, C. Englert, and J.-N. Volff

2006. Male-biased expression of X-chromosomal DM domain-less Dmrt8 genes in the mouse. *Genomics*, 88(2):185–195.

Veitia, R. A. and J. A. Birchler

2010. Dominance and gene dosage balance in health and disease: why levels matter! *The Journal of Pathology*, 220(2):174–185.

Vicoso, B. and B. Charlesworth

2006. Evolution on the X chromosome: unusual patterns and processes. *Nature Reviews Genetics*, 7(8):645–653.

Vogel, C. and E. M. Marcotte

2012. Insights into the regulation of protein abundance from proteomic and transcriptomic analyses. *Nature Reviews Genetics*, 5:1512–13.

Vogt, M. H., E. Goulmy, F. M. Kloosterboer, E. Blokland, R. A. de Paus, R. Willemze, and J. H. Falkenburg

2000. UTY gene codes for an HLA-B60-restricted human male-specific minor histocompatibility antigen involved in stem cell graft rejection: characterization of the critical polymorphic amino acid residues for T-cell recognition. *Blood*, 96(9):3126–3132.

Vulpe, C. D., Y. M. Kuo, T. L. Murphy, L. Cowley, C. Askwith, N. Libina, J. Gitschier, and G. J. Anderson

1999. Hephaestin, a ceruloplasmin homologue implicated in intestinal iron transport, is defective in the sla mouse. *Nature Genetics*, 21(2):195–199.

Walport, L. J., R. J. Hopkinson, M. Vollmar, S. K. Madden, C. Gileadi, U. Oppermann, C. J. Schofield, and C. Johansson

2014. Human UTY(KDM6C) is a male-specific Nε-methyl lysyl demethylase. *Journal of Biological Chemistry*, 289(26):18302–18313.

Wang, C., J.-E. Lee, Y.-W. Cho, Y. Xiao, Q. Jin, C. Liu, and K. Ge

2012. UTX regulates mesoderm differentiation of embryonic stem cells independent of H3K27 demethylase activity. *Proceedings of the National Academy of Sciences of the United States of America*, 109(38):15324–15329.

Wang, F., J. Shin, J. M. Shea, J. Yu, A. Bošković, M. Byron, X. Zhu, A. K. Shalek, A. Regev, J. B. Lawrence, E. M. Torres, L. J. Zhu, O. J. Rando, and I. Bach

2016. Regulation of X-linked gene expression during early mouse development by Rlim. *eLife*, 5:1765.

Wang, J., J. Mager, Y. Chen, E. Schneider, J. C. Cross, A. Nagy, and T. Magnuson

2001a. Imprinted X inactivation maintained by a mouse Polycomb group gene. *Nature Genetics*, 28(4):371–375.

Wang, J., S. Vasaikar, Z. Shi, M. Greer, and B. Zhang

2017. WebGestalt 2017: a more comprehensive, powerful, flexible and interactive gene set enrichment analysis toolkit. *Nucleic Acids Research*, Pp. 1–8.

Wang, P. J., J. R. McCarrey, F. Yang, and D. C. Page

2001b. An abundance of X-linked genes expressed in spermatogonia. *Nature Genetics*, 27(4):422–426.

Wang, Q., J. Wei, P. Su, and P. Gao

2015. Histone demethylase JARID1C promotes breast cancer metastasis cells

via down regulating BRMS1 expression. *Biochemical and Biophysical Research Communications*, 464(2):659–666.

Wang, X., K. C. Douglas, J. L. VandeBerg, A. G. Clark, and P. B. Samollow
2014. Chromosome-wide profiling of X-chromosome inactivation and epigenetic states in fetal brain and placenta of the opossum, Monodelphis domestica. *Genome Research*, 24(1):70–83.

Wang, Z. Q., M. R. Fung, D. P. Barlow, and E. F. Wagner
1994. Regulation of embryonic growth and lysosomal targeting by the imprinted Igf2/Mpr gene. *Nature*, 372(6505):464–467.

Warburton, P. E., J. Giordano, F. Cheung, Y. Gelfand, and G. Benson
2004. Inverted repeat structure of the human genome: the X-chromosome contains a preponderance of large, highly homologous inverted repeats that contain testes genes. *Genome Research*, 14(10A):1861–1869.

Warren, E. H., M. A. Gavin, E. Simpson, P. Chandler, D. C. Page, C. Disteche, K. A. Stankey, P. D. Greenberg, and S. R. Riddell
2000. The human UTY gene encodes a novel HLA-B8-restricted H-Y antigen. *Journal of Immunology*, 164(5):2807–2814.

Waters, P. D., M. C. Wallis, and J. A. M. Graves
2007. Mammalian sex—Origin and evolution of the Y chromosome and SRY. *Seminars in Cell & Developmental Biology*, 18(3):389–400.

Watson, E. D., M. Hughes, D. G. Simmons, D. R. C. Natale, A. E. Sutherland, and J. C. Cross
2011. Cell-cell adhesion defects in Mrj mutant trophoblast cells are associated with failure to pattern the chorion during early placental development. *Developmental Dynamics*, 240(11):2505–2519.

Welshons, W. J. and L. B. Russell
1959. The Y-chromosome as the bearer of male determining factors in the mouse.

Proceedings of the National Academy of Sciences of the United States of America, 45(4):560–566.

Welstead, G. G., M. P. Creyghton, S. Bilodeau, A. W. Cheng, S. Markoulaki, R. A. Young, and R. Jaenisch

2012. X-linked H3K27me3 demethylase Utx is required for embryonic development in a sex-specific manner. *Proceedings of the National Academy of Sciences of the United States of America*, 109(32):13004–13009.

West, J. D., W. I. Frels, V. M. Chapman, and V. E. Papaioannou

1977. Preferential expression of the maternally derived X chromosome in the mouse yolk sac. *Cell*, 12(4):873–882.

Wilsker, D., A. Patsialou, P. B. Dallas, and E. Moran

2002. ARID proteins: a diverse family of DNA binding proteins implicated in the control of cell growth, differentiation, and development. *Cell Growth & Differentiation*, 13(3):95–106.

Wisniewski, A., K. Milde, R. Stupnicki, and J. Szufladowicz-Wozniak

2007. Weight deficit at birth and Turner's syndrome. *Journal of Pediatric Endocrinology & Metabolism*, 20(5):607–613.

Wladimiroff, J. W., W. R. Bhaggoe, M. Kristelijn, T. E. Cohen-Overbeek, N. S. Den Hollander, H. Brandenburg, and F. J. Los

1995. Sonographically determined anomalies and outcome in 170 chromosomally abnormal fetuses. *Prenatal Diagnosis*, 15(5):431–438.

Wolf, J. B. and R. Hager

2006. A Maternal–Offspring Coadaptation Theory for the Evolution of Genomic Imprinting. *PLoS Biology*, 4(12):e380–6.

Wright, A. E., R. Dean, F. Zimmer, and J. E. Mank

2016. How to make a sex chromosome. *Nature Communications*, 7:1–8.

Wu, J., J. Ellison, E. Salido, P. Yen, T. Mohandas, and L. J. Shapiro

1994. Isolation and characterization of XE169, a novel human gene that escapes X-inactivation. *Human Molecular Genetics*, 3(1):153–160.

Wu, J. A., B. L. Johnson, Y. Chen, C. T. Ha, and G. S. Dveksler

2008. Murine Pregnancy-Specific Glycoprotein 23 Induces the Proangiogenic Factors Transforming-Growth Factor Beta 1 and Vascular Endothelial Growth Factor A in Cell Types Involved in Vascular Remodeling in Pregnancy1. *Biology of Reproduction*, 79(6):1054–1061.

Wutz, A., T. P. Rasmussen, and R. Jaenisch

2002. Chromosomal silencing and localization are mediated by different domains of Xist RNA. *Nature Genetics*, 30(2):167–174.

Wysocka, J., T. Swigut, H. Xiao, T. A. Milne, S. Y. Kwon, J. Landry, M. Kauer, A. J. Tackett, B. T. Chait, P. Badenhorst, C. Wu, and C. D. Allis

2006. A PHD finger of NURF couples histone H3 lysine 4 trimethylation with chromatin remodelling. *Nature*, 442(7098):86–90.

Xiong, Y., X. Chen, Z. Chen, X. Wang, S. Shi, X. Wang, J. Zhang, and X. He

2010. RNA sequencing shows no dosage compensation of the active X-chromosome. *Nature Genetics*, 42(12):1043–1047.

Xu, J.

2005. Preparation, culture, and immortalization of mouse embryonic fibroblasts. *Current Protocols in Molecular Biology*, Chapter 28:Unit 28.1.

Xu, J., P. S. Burgoyne, and A. P. Arnold

2002. Sex differences in sex chromosome gene expression in mouse brain. *Human Molecular Genetics*, 11(12):1409–1419.

Xu, J., X. Deng, and C. M. Disteche

2008a. Sex-specific expression of the X-linked histone demethylase gene Jarid1c in brain. *PLoS ONE*, 3(7):e2553.

Xu, J., X. Deng, R. Watkins, and C. M. Disteche

2008b. Sex-specific differences in expression of histone demethylases Utx and Uty in mouse brain and neurons. *The Journal of Neuroscience*, 28(17):4521–4527.

Xu, J., R. Watkins, and A. P. Arnold

2006. Sexually dimorphic expression of the X-linked gene Eif2s3x mRNA but not protein in mouse brain. *Gene Expression Patterns*, 6(2):146–155.

Xu, N., M. E. Donohoe, S. S. Silva, and J. T. Lee

2007. Evidence that homologous X-chromosome pairing requires transcription and Ctcf protein. *Nature Genetics*, 39(11):1390–1396.

Xue, F., X. C. Tian, F. Du, C. Kubota, M. Taneja, A. Dinnyes, Y. Dai, H. Levine, L. V. Pereira, and X. Yang

2002. Aberrant patterns of X chromosome inactivation in bovine clones. *Nature Genetics*, 31(2):216–220.

Yamanaka, Y., F. Lanner, and J. Rossant

2010. FGF signal-dependent segregation of primitive endoderm and epiblast in the mouse blastocyst. *Development*, 137(5):715–724.

Yamauchi, Y., J. M. Riel, V. Ruthig, and M. A. Ward

2015. Mouse Y-Encoded Transcription Factor Zfy2 Is Essential for Sperm Formation and Function in Assisted Fertilization. *PLoS Genetics*, 11(12):e1005476.

Yamauchi, Y., J. M. Riel, V. A. Ruthig, E. A. Ortega, M. J. Mitchell, and M. A. Ward

2016. Two genes substitute for the mouse Y chromosome for spermatogenesis and reproduction. *Science*, 351(6272):514–516.

Yang, F., T. Babak, J. Shendure, and C. M. Disteche

2010. Global survey of escape from X inactivation by RNA-sequencing in mouse. *Genome Research*, 20(5):614–622.

Yang, H., H. Wang, C. S. Shivalila, A. W. Cheng, L. Shi, and R. Jaenisch
2013. One-Step Generation of Mice Carrying Reporter and Conditional Alleles by CRISPR/Cas-Mediated Genome Engineering. *Cell*, 154(6):1–14.

Yedavalli, V. S. R. K., C. Neuveut, Y.-H. Chi, L. Kleiman, and K.-T. Jeang
2004. Requirement of DDX3 DEAD box RNA helicase for HIV-1 Rev-RRE export function. *Cell*, 119(3):381–392.

Ying, Q.-L., J. Wray, J. Nichols, L. Batlle-Morera, B. Doble, J. Woodgett, P. Cohen, and A. Smith
2008. The ground state of embryonic stem cell self-renewal. *Nature*, 453(7194):519–523.

Yoshimi, K., Y. Kunihiro, T. Kaneko, H. Nagahora, B. Voigt, and T. Mashimo
2016. ssODN-mediated knock-in with CRISPR-Cas for large genomic regions in zygotes. *Nature Communications*, 7:1–10.

Yu, L.
2005. Shox2-deficient mice exhibit a rare type of incomplete clefting of the secondary palate. *Development*, 132(19):4397–4406.

Zechner, U., M. Hemberger, M. Constância, A. Orth, I. Dragatsis, A. Lüttges, H. Hameister, and R. Fundele
2002. Proliferation and growth factor expression in abnormally enlarged placentas of mouse interspecific hybrids. *Developmental Dynamics*, 224(2):125–134.

Zechner, U., M. Reule, A. Orth, F. Bonhomme, B. Strack, Guénet, H. Hameister, and R. Fundele
1996. An X-chromosome linked locus contributes to abnormal placental development in mouse interspecific hybrid. *Nature Genetics*, 12(4):398–403.

Zechner, U., M. Wilda, H. Kehrer-Sawatzki, W. Vogel, R. Fundele, and H. Hameister
2001. A high density of X-linked genes for general cognitive ability: a run-away process shaping human evolution? *Trends in Genetics*, 17(12):697–701.

Zhang, B., S. Kirov, and J. Snoddy

2005. WebGestalt: an integrated system for exploring gene sets in various biological contexts. *Nucleic Acids Research*, 33(Web Server issue):W741–8.

Zhang, B., J. Wang, XiaojingWang, J. Zhu, Q. Liu, Z. Shi, M. C. Chambers, L. J. Zimmerman, K. F. Shaddox, S. Kim, S. R. Davies, S. Wang, PeiWang, C. R. Kinsinger, R. C. Rivers, H. Rodriguez, R. R. Townsend, M. J. C. Ellis, S. A. Carr, D. L. Tabb, R. J. Coffey, R. J. C. Slebos, D. C. Liebler, and t. N. CPTAC

2014. Proteogenomic characterization of human colon and rectal cancer. *Nature*, 513(7518):382–387.

Zhao, J., B. K. Sun, J. A. Erwin, J. J. Song, and J. T. Lee

2008. Polycomb proteins targeted by a short repeat RNA to the mouse X chromosome. *Science*, 322(5902):750–756.

Zhao, L., T. Svingen, E. T. Ng, and P. Koopman

2015. Female-to-male sex reversal in mice caused by transgenic overexpression of Dmrt1. *Development*, 142(6):1083–1088.

Zhou, J., E. M. Goldberg, N. A. Leu, L. Zhou, D. A. Coulter, and P. J. Wang

2014. Respiratory failure, cleft palate and epilepsy in the mouse model of human Xq22.1 deletion syndrome. *Human Molecular Genetics*, 23(14):3823–3829.

Zhou, J., J. R. McCarrey, and P. J. Wang

2013. A 1.1-Mb Segmental Deletion on the X Chromosome Causes Meiotic Failure in Male Mice. *Biology of Reproduction*, 88(6):159–159.

Zinn, A. R. and J. L. Ross

1998. Turner syndrome and haploinsufficiency. *Current Opinion in Genetics & Development*, 8(3):322–327.

Zuffardi, O., P. Maraschio, F. Lo Curto, U. Müller, A. Giarola, and L. Perotti

1982. The role of Yp in sex determination: new evidence from X/Y translocations. *American Journal of Medical Genetics*, 12(2):175–184.

Zvetkova, I., A. Apedaile, B. Ramsahoye, J. E. Mermoud, L. A. Crompton, R. John, R. Feil, and N. Brockdorff

2005. Global hypomethylation of the genome in XX embryonic stem cells. *Nature Genetics*, 37(11):1274–1279.